

Fundamental Problems in the Application of
Structural Identification Procedures to
Damage Detection

Thesis by

Robert Teran Beck

In partial Fulfillment of the Requirements

for the Degree of

Doctor of Philosophy

California Institute of Technology

Pasadena, California

1991

(Submitted April 29, 1991)

To Biggi

Acknowledgments

I am most grateful to my advisor, Jim Beck, for enabling me to pursue graduate studies at this great institution. His enthusiasm has always provided me with the energy required to overcome difficult moments, even in this often-frustrating field of study. I am also very grateful to very many professors, especially Ronald Scott. They have oftentimes inspired me, not only professionally, but because of their fine attention to the human side, thereby allowing me to maintain a better perspective.

Thanks go to the many fellow students and colleagues with whom I have had the chance to share the 'ups' and 'downs' of graduate life. In particular, thanks go to Francisco Avila, Agnes Allard, Eric Majani, Adiel Guinzburg, Jorge and Alejandra Kittl, Al Moser, Liping Yan, Ares and Phoebus Rosakis, Pascal Yvon, Olivier Goldberg, Costas Papadimitriou, and to my ex-officemates, Karl Rubenacker and Sunil Malhotra, and also the members of the 'old' SOPS frisbee club, especially Bill Donlon, John Hall, George Yates, Garrett Yeong, Nick Jones, Paul and Linda Nowak, and John Lee, without whom I would not have achieved the high levels of fitness those many Saturday mornings. I am also very fortunate to have Gunnar Klinkhammer, Karim El Barkawi, Karl and Lotta Linde, John Coanda, Annika Lyrevik, and Ki Nilsson as friends and with whom I have had an opportunity to discover and enjoy L.A.

In Thomas Building, many thanks go to Tom Welmers who has, perhaps unknowingly, steered my future into new directions by kindly exposing me to lots of megabytes of computer information; to Cecilia Lin, who has taken me very warmly as her "foster nephew"; to Donna Covarrubias, Sharon Beckenbach and Jackie Beard who, indeed, are the ones that take care of all of those invisible goods and services that make graduate life a bit more tolerable.

Lastly, and most importantly, to my parents and my wife who, to this day, have done so much especially in supporting me in all ways and in helping me make this career decision worth it; to my wife Biggi: thanks for offering me the two most important 'ups' in my life and for bearing with me what could be the longest graduation process in recent history!

Abstract

There are fundamental problems in the application of structural identification procedures to damage detection which still need to be resolved. The present study investigates the underlying issues and then provides a number of techniques which solve a series of unresolved problems. The techniques developed range from extensions and refinements of previous methods to the adaptation of novel homotopy methods.

The results from simulated data show that ill-conditioning, non-uniqueness and temporal synchronization of the data are the most serious problems encountered. Criteria to resolve these are then put forth. From the experimental studies, however, it becomes evident that modeling error is the most serious issue. The experimental results show, nonetheless, that even with large model errors, it is possible to localize the area of damage to within a sub-structure.

The techniques are then applied to data obtained from a ten-story steel frame building. Previous studies on such structures have indicated large changes in the natural frequencies, especially during the San Fernando earthquake of February 9, 1971. The present study shows how changes in the natural frequencies and in the modeshapes are related to the degradation of the inter-story stiffness along the height of the building. Low amplitude forced vibration and ambient vibration test data yield one set of results: at these levels of motion the structure seems to retain much of its original uniform stiffness. This is true even after strong motion, leading to the notion that the building "has healed" with time. It is clear from the studies how this apparent stiffness is lost immediately once the strong motion of even moderate earthquakes has begun and it is thought that this is due to a combinations of effects. Results show that for the 1971 San Fernando earthquake, stiffness losses in the order of 50% occurred in the middle stories towards the end of the strong motion part of the seismic motion.

Table of Contents

	Acknowledgments	iii
	Abstract	iv
1	Introduction	1
1.1	Prior Work in Structural Identification	2
1.2	Outline of this Work	5
	References	7
2	Models	12
2.1	Classification of Models	12
2.1.1	Modal Models	12
2.1.2	Physical Parametric Models	13
2.2	A Class of Mechanical Models	15
2.2.1	Structural Model	15
2.2.2	Reduced Models	18
2.2.3	Numerical Algorithms	18
	References	21
3	Parameter Estimation	22
3.1	Formulation	22
3.2	Method of Successive Substitutions	23
3.3	Generalized Least-Squares Approach	26
3.3.1	Output Error	27
3.3.2	Modal Output Error	28
3.3.3	Minimization Problem	29
3.3.4	Uniqueness via Minimization	34
3.4	Bayesian Model Identification	34
3.5	Homotopy-based Parameter Estimation	39
	References	42
4	Simulated Data	43
4.1	Chain Model Simulations	44
4.1.1	Simulation with a 2-DOF Chain System	45
4.1.1.1	Characteristics of the Two-Degree-of-Freedom Chain System	45
4.1.1.2	Method of Successive Substitutions	47
4.1.1.3	Generalized Least-Squares, Output Error, Modal Domain	49
4.1.1.4	Generalized Least-Squares, Output Error, Time Domain	49
4.1.1.5	Bayesian Approach	50
4.1.1.6	Homotopy Method	52
4.1.1.7	Summary for the 2-DOF Chain System	53
4.1.2	Simulation with a 10-DOF Chain Model	53
4.1.2.1	Frequency Content of the Excitation	54
4.1.2.2	Duration of the Excitation	56
4.1.2.3	Selection of Monitored Degrees of Freedom	56
4.1.2.4	Response Quantity to Monitor	57

4.1.2.5	Noise in the Excitation and Response Signals	57
4.1.2.6	Type of Damage Present in the Structure	58
4.1.2.7	Signal Synchronization	58
4.1.2.8	Miscalibration of the Signals	59
4.1.2.9	Summary for the 10-DOF Chain System	59
4.2	Beam-Column Model Simulations	60
4.2.1	Frequency Content of the Excitation	61
4.2.2	Selection of Monitored Degrees of Freedom	61
4.2.3	Noise in the Excitation and Response Signals	62
4.2.4	Summary of the 20-DOF Beam-Column System	63
	References	64
	Tables	65
	Figures	75
5	Data from a Model Structure	91
5.1	Experimental Setup and Procedures	91
5.2	SUB-ID Results	93
5.2.1	Preliminary Simulation Results	93
5.2.1.1	3-DOF Chain Model of System	95
5.2.1.2	18-DOF Frame Model of System	97
5.2.2	Experimental Results	100
5.2.2.1	3-DOF Chain Model of Test Structure	100
5.2.2.2	18-DOF Frame Model of Test Structure	101
5.3	Summary	102
	References	104
	Tables	105
	Figures	115
6	Data from a Real Building	122
6.1	Available Data for Building 180	123
6.1.1	Nielsen's Tests of 1963-1964	123
6.1.2	1970 Lytle Creek Earthquake Records	123
6.1.3	1971 San Fernando Earthquake Records	124
6.1.4	Teledyne's Tests of November, 1971	124
6.1.5	Nielsen's Tests of February, 1972	124
6.2	Previous Dynamic Analyses of Building 180	125
6.2.1	Nielsen's Analysis of 1964	125
6.2.2	Brandow and Johnston Associates Analysis of 1971	125
6.2.3	Wood's Analysis of October, 1972	125
6.2.4	McVerry and Beck's Analysis of 1983	126
6.2.5	Teledyne's Analysis of November, 1971	127
6.3	SUB-ID Results for Building 180	127
6.3.1	Results from Nielsen's Data	128
6.3.2	Results from the 1970 Lytle Creek Records	129
6.3.3	Results from the 1971 San Fernando Records	130
6.3.4	Results from Teledyne's Data	131
6.4	Discussion	132
	References	134
	Tables	135
	Figures	141

7	Discussion and Conclusions	150
7.1	Problems in Structural Identification	150
7.2	Rules of Thumb	142
7.3	Future Research	154
7.4	Conclusions	154

Chapter 1 : Introduction

The decision of whether a damaged structure should be repaired can have considerable economic repercussions for the owner. Moral issues, aside from purely economic, arise in the case of structures normally inhabited by humans. It may not be clear whether these structures will be able to withstand their future loads. Therefore, engineers should attempt to *precisely* evaluate the amount of damage incurred by the structure before making any far-reaching decisions. In the absence of precise data, poor decisions may be made. The importance of reliable system identification/damage detection techniques is that they can help produce a more accurate assessment of the damage state of a structure.

The field of damage detection in structures has been approached from various view points. Among these, the most notable ones are those which emphasize (1) visual signs of “damage” (cracks, pulled bars, etc.); (2) ultrasound techniques; and (3) vibration monitoring. The conveniences and disadvantages of each method are numerous and, in principle, all of them should be employed for the stated purpose. Visual inspections, however, are often the only or most common practice.

This study uses the third approach, that is, vibration monitoring. Vibration monitoring aims at determining the state of a structure by studying its dynamic behavior. Due to the difficulty of determining the *ultimate strength* of a sub-structure, damage detection techniques have emphasized the less complex problem of determining the loss of elastic stiffness within the structure. This approach has limitations but can be useful when the damage/stiffness-loss relationship can be justified. Empirical observations and analytical studies [1.1,1.2] often indicate that such a relationship is justified.

A number of researchers have pursued damage detection by vibration monitoring but there are still fundamental issues which need to be resolved. In this study, the goal is to define the fundamental problems when trying to determine the changes in the elastic stiffness of members within a structure. The next section describes some of the approaches taken by other researchers, and in the last section of this chapter an outline of this study is given.

Section 1.1 - Prior Work in Structural Identification

Dynamic models of complex structures are usually tested or validated based on a subjective evaluation of the predicted and measured natural frequencies and normal mode shapes. System identification provides a more sophisticated approach for validation and, to this end, much research effort has been expended on this topic in almost all fields of engineering. This section describes those procedures which researchers have developed to obtain better knowledge of the physical (mass, stiffness, damping) properties of dynamical systems.

Structural identification methods can be characterized according to whether they are: (a) “batch” or sequential, with complete (all degrees of freedom) or incomplete data; (b) time, frequency, or modal based; (c) input-error, output-error, equation-error, or instrumental variable; (d) global (full, banded, or reduced) or local; (e) statistical (classical or Bayesian) or deterministic; (f) direct or iterative. Consideration is given only to linear elastic dynamic systems in most structural identification research.

Batch methods employ all information at once while sequential methods continuously update the structural parameter estimates as more information is accrued. By and large, most researchers in this field employ batch methods although sequential methods may be more convenient for on-line situations or with methods which stress filtering techniques such as those presented by Mottershead and Foster [1.3-1.4].

The time and frequency domain approaches make use of the response and excitation data directly from the observed time records and from the FFT-based Fourier spectra, respectively. Previous conditioning (including filtering, integration, etc.) may be performed on the signals. Udawadia and Shah [1.7], Kaya and McNiven [1.5], Dimsdale [1.6], Agbabian et al. [1.8-1.9], Matzen [1.10], Banks et al. [1.11], and Beck and Beck [1.12] have employed time domain approaches while Cottin et al. [1.13-1.15], Fritzen [1.16], Hoff [1.17,1.18], and Mottershead and Foster [1.3,1.4,1.19] have used the frequency domain in the way of Fourier spectra or frequency response functions (“FRFs”). Modal domain methods, on the other hand, make use of previously determined modal parameters. Any of the large number of modal parameter estimation techniques, not all of these being systematic “identification” techniques, may be used for this purpose although few of these estimate the modal effective participation factors as in Beck [1.82]. Modal based techniques have been much more widely used in structural identification perhaps due to the widespread availability of structural modal data. Perhaps the first attempt to make use of this data is that of Kanai [1.20], followed later by Berg [1.21], Nielsen [1.22], Rodden [1.23], Hall et al. [1.24], Berman and Flannelly [1.25], and Ross [1.33]. A list of later authors includes Berman and Fuh [1.28,1.29], Caesar [1.30], Wei [1.31,1.32], Collins et al. [1.34], Thoren [1.35], Schiff et al. [1.36], Udawadia et al. [1.37], Vandiver [1.38], Wojnarowski et al. [1.39], Caravani et al. [1.40], Garba and Wada [1.41], Baruch [1.42-1.45],

Chen et al. [1.46-1.49], Coppolino and Rubin [1.50,1.51], Heylen [1.52], Natke et al. [1.53-1.55], Lallement and Zhang [1.56-1.59], Zak [1.60], Kabe [1.61], Stubbs and Osegueda [1.62-1.64], Fritzen [1.16], Hanagud et al. [1.65], Thomas et al. [1.66], Beliveau [1.67], Flanigan [1.68,1.69], Gray and Starke [1.70,1.71], Ojalvo et al. [1.80,1.81], Kammer [1.72], Eiber [1.73], Inman [1.74], Waller and Schmidt [1.75], and Waqfi [1.76]. Much of this research was done with a focus on structural health monitoring.

Output-error approaches consider errors between the observed and predicted output quantities such as accelerations, displacements, stresses, etc. Accelerations are the most common quantities. Displacements are not used as often although recent progress in the field [1.77] might change this trend. The predicted output quantities are calculated according to the model in hand and if these correspond “identically” to the observed quantities, then no (output) error exists. Equation-error methods, however, correspond to the cases where errors arise in the governing equations once all the kinetic and kinematic quantities are replaced by the observed quantities. In either case, a least-squares approach can then be taken to incorporate these error vectors into a single scalar “error functional”. Input-error methods are generally equivalent to equation-error approaches since for linearly elastic systems the forcing function, i.e., input to the system, is placed alone on one side of the governing equation. The aim of these error approaches is to minimize a measure of the error. Since the output quantities in dynamical systems are almost never linear with respect to the parameters of interest, the output-error minimization procedure is generally iterative. When noisy data is employed, or when there is model error in the identification procedure, minimizing the output error does not necessarily lead to a minimization of the equation error. Equation-error approaches often allow the error to be linear in the unknown parameters, leading to direct methods of solution. When employed in a least-squares context, however, equation-error methods are known to suffer from “inherent, noise-induced asymptotic bias in the parameter estimates” [1.4] As mentioned by Mottershead and Foster, “this arises because the EE [equation error] model is not a ‘regression model’, as required for linear least-squares analysis, but a ‘structural model’ ” [1.80]. The Instrumental Variable technique described by these authors is a modification of the equation error approach whose objective is to minimize the bias.

Global methods are those that modify most of the components of the mass, damping, or stiffness matrices. The matrix modifications or “updates” are generally not intuitive to an engineer since a very large number (or even all) elements in the matrices are allowed to be modified. The modification of global matrices, however, can often be accomplished in a direct manner. Parametric methods, on the other hand, are those in which the governing equations depend directly on the values of a pre-determined number of structural/FEM (design) parameters. Kaya and McNiven [1.5] and Dimsdale [1.6], for example, have studied the influence of effective beam lengths and joint stiffnesses on the response of a frame structure and identified those values which offer best match of the model prediction with experimental data. The structure, in general, can be decomposed into local structural

regions (also called modules or sub-structures). In the mathematical representation, each of the sub-structure stiffnesses can be modified easily by just scaling the original sub-structure stiffness with a “stiffness coefficient or parameter” as proposed by Natke and Schulze [1.53], Lallement et al. [1.56], Beck and Beck [1.12]. There are some discrepancies in views expressed in the literature as to the usefulness of global methods. The view taken in this study belongs to the parametrized group. Authors supporting the parametrized approach claim that modifying all coefficients of the different matrices as done by the global approach is highly undesirable (Kabe[1.61]) since, in general, no clear interpretation of the state of the structure can be deduced from the resulting matrix coefficients. Furthermore, in general, there are an infinite number of possible values which the matrix coefficients can take that yield the same observed data. Often, the solution which yields the least deviation from the original values is chosen. From a damage detection point of view, this choice does not seem particularly useful. The global approach, however, is closer to predicting exactly the *observed* data and to not violating the governing equations. On the other hand, the response predicted by the optimized global model at the other degrees of freedom of the structure will be, in general, incorrect. The optimal parameter model will not predict the observed response so closely as the global model will. But it is generally the case that the parameter model will predict the response at the other degrees of freedom more closely than the global model. In addition, the parameter model allows the user to monitor through time the estimation of mechanical quantities with clear meaning in order to ascertain the good health of the structure.

Statistical (stochastic) approaches consider the probabilistic aspects of the output or equation errors. Classical statistics are based on well-known, maximum likelihood estimation techniques. Application of classical statistics has been implemented by Friswell [1.78], Stubbs and Osegueda [1.62-1.64], Thomas et al. [1.66], Agbabian et al. [1.8-1.10], Mottershead and Foster [1.3-1.4,1.21]. Bayesian statistical approaches differ from classical in that they associate a probability distribution with each parameter. A prior probability distribution for the parameter and the data obtained from experiments are combined to yield a posterior probability distribution. Bayesian probability distributions convey the plausibility of each parameter taking a certain value. Prior distributions are important in Bayesian statistics since the user can then emphasize prior information based on previous experience or on theoretical grounds. The prior distributions are clearly reflected in the posterior distribution when there is little data available. Although the underlying interpretation is different, classical and Bayesian statistics may give similar results when the prior distribution is assumed to be local and non-informative. Collins et al. [1.34] have employed the Bayesian formulation with different prior distributions. Beck [1.79] has recently formulated the general Bayesian structural identification problem. Deterministic approaches, on the other hand, aim to obtain the parameters which yield a solution without explicit consideration of the uncertainty in the observed data. The usual least-square methods fall in this category. In general, most successful deterministic techniques can be given a statistical interpretation.

Methods can be either direct or iterative. Direct methods estimate the optimal parameters in a fixed number of calculations and thus are typically many times more computationally-efficient than iterative methods where the number of calculations is not known beforehand. Direct methods are usually found in global equation-error formulations which assume that the whole state vector and its derivative are known. Under these circumstances, a least-squares formulation for equation error leads to a set of linear simultaneous equations; the solution method for these does not require an iterative method. Many authors reduce or condense a large system of equations to a smaller one whose order is equal to the number of observed degrees of freedom. In this way, the assumption stated above, that the whole state vector and its derivative are known, is satisfied. Iterative solutions are usually found in output-error formulations since the output quantities are almost always non-linear functions of parameters or matrix coefficients. Iterations are also required in equation-error formulations when the number of observed degrees of freedom is less than the number of total degrees of freedom. Iterative methods often require optimization techniques of which the Gauss-Newton is the most frequently employed.

Section 1.2 - Outline of this Work

A family of methodologies is presented in this study to confront the problems in structural identification which are described in detail in later chapters.

An identification methodology consists of the following components: (1) a structural model with associated structural parameters; (2) a parameter estimation procedure; (3) a data processing and reduction procedure; (4) a reliability/model appraisal procedure. Unfortunately, the most appropriate choice for each component cannot be made independently of the rest of the components. A full description of the methodology requires a thorough explanation of their interaction.

Chapter 2 presents a description of parametric models and, in particular, the fundamental mechanical model on which this study is based.

The various methods employed for parameter estimation are described in Chapter 3. More than one technique is considered since some combinations of model and parameter-estimation-methods yield more efficient computational algorithms, while others might provide more information to the engineer. Both the nature of the structural parameters to be identified and the available data determine which model/technique combination is to be preferred. Factors influencing the efficiency are taken into account.

Chapters 4, 5, and 6 apply the methodologies developed in earlier chapters to different kinds of data. Chapter 4 uses simulated data to test each methodology under controlled conditions. The error characteristics of each methodology are also discussed. Chapter 5 discusses the results

obtained from a specific experimental set up. This set up addresses the issue of employing real data instead of artificial data in an effort to validate the methodologies. Stiffnesses and modal dampings are evaluated and compared to those obtained by other existing methods. Chapter 6 applies one of the methodologies to Building 180 on the campus of the Jet Propulsion Laboratory, California Institute of Technology, Pasadena, California. The data available for JPL Building 180 makes it possible to determine a stiffness distribution prior to, during and after the February 9, 1971, San Fernando earthquake. This structure, and many others, present significantly different dynamic behavior during strong motion than in ambient vibration, man-excited and other kinds of low-amplitude tests. Natural frequencies during the San Fernando earthquake, for example, are reduced by factors of around 30% and tentative explanations have been given by various researchers. An attempt is made in Chapter 6 to determine the stiffness distribution during the strong motion. Some of the estimates may not be reliable since not enough information is available to identify a *unique* distribution.

The reliability of the estimates is a topic not frequently treated but it must be addressed before attempting to use them for damage detection. A general discussion of this topic is provided in the first part of Chapter 7 which is based on the results presented in the previous chapters. This study closes with several conclusions in the second part of the chapter.

References for Chapter 1

- [1.1] O'Brien, T.K., "Stiffness Change as a Non-Destructive Damage Measurement", in *Mechanics of Non-Destructive Testing*, W.W. Stinchcomb, editor, Plenum Press, New York, N.Y., 1980, p. 101.
- [1.2] Gudmunson, P., "Eigenfrequency Changes of Structures Due to Cracks, Notches or Other Geometrical Changes", *Journal of the Mechanics and Physics of Solids*, Vol. 30, 1983, p. 339.
- [1.3] Foster, C.D., Mottershead, J.E., "Parameter Estimation Techniques for Monitoring Machines and Structures" in *Stress and Vibration Analysis*, Mottershead, J.E., editor, Pergamon Press, Oxford, 1989, p. 109.
- [1.4] Mottershead, J.E., Foster, C.D., "An Instrumental Variable Method for the Estimation of Mass, Stiffness and Damping Parameters from Measured Frequency Response Functions", *Mechanical Systems and Signal Processing*, Vol. 2, No. 4, 1988, p. 379.
- [1.5] Kaya, I., McNiven, H.D., "Investigation of the Elastic Characteristics of a Three Story Steel Frame Using System Identification", Report UCB/EERC-78/24, University of California, Berkeley, November 1978.
- [1.6] Dimsdale, J.S., "System Identification of Structures with Joint Rotation", Report UCB/EERC-83/16, University of California, Berkeley, July 1983.
- [1.7] Udawadia, F.E, Shah, P.C., "Identification of Structures Through Records Obtained During Strong Earthquake Ground Motion", *Journal of Engineering for Industry*, ASME, Vol. 98, No. 4., 1975, p. 1347.
- [1.8] Agbabian, M.S., Masri, S.F., Miller, R.K., Caughey, T.K., "A System Identification Approach to the Detection of Changes in Structural Parameters", *Proceedings of the Workshop on Structural Safety Evaluation Based on System Identification Approaches*, Lambrecht/Pfalz, Germany, June 29-July 1, 1987, p. 341.
- [1.9] Agbabian, M.S., Masri, S.F., Miller, R.K., Caughey, T.K., "A System Identification Approach to the Detection of Structural Changes", *Journal of Engineering Mechanics*, ASCE, Vol.
- [1.10] Matzen, V.C., "Time Domain Identification of Linear Structures", *Proceedings of the Workshop on Structural Safety Evaluation Based on System Identification Approaches*, Lambrecht/Pfalz, Germany, June 29-July 1, 1987, p. 357.
- [1.11] Banks, H.T., Gates, S.S., Rosen, I.G., Wang, Y., "The Identification of a Distributed Parameter Model for a Flexible Structure", *SIAM Journal of Control and Optimization*, Vol. 26, No. 4, July 1988, p. 743.
- [1.12] Beck, R.T., Beck, J.L., "Evaluation of a Methodology for Model Identification in the Time Domain", *Proceedings of the USAF/NASA Workshop on Model Determination for Large Space Systems*, California Institute of Technology, Pasadena, California, March 22-24, 1988, p. 665.
- [1.13] Cottin, N., Felgenhauer, H.-P., Natke, H.G., "On the Parameter Identification of Elastomechanical Systems Using Input and Output Residuals", *Ingenieur-Archiv*, Vol. 54, pp. 378-387, 1984.
- [1.14] Cottin, N., Natke, H.G., "Updating Mathematical Models on the Basis of Vibration and Modal Test Results - A Review of Experience", *Proceedings of the International Symposium on Aeroelasticity*, Aachen, 1985.
- [1.15] Cottin, N., Felgenhauer, H.-P., Natke, H.G., "On the Parameter Identification of Elastomechanical Systems Using Weighted Input and Modal Residuals", *Ing.-Archiv*, Vol. 56, 1986, p. 106.
- [1.16] Fritzen, C.P., "Identification of Mass, Damping and Stiffness Matrices of Mechanical Systems", *Journal Vibrations, Acoustics, Stress Reliability, Design*, Vol. 108, ASME, 1986, p. 9.
- [1.17] Hoff, C., "The Use of Reduced Finite Element Models in System Identification", *Earthquake Engineering and Structural Dynamics*, Vol. 18, 1989, p. 875.

- [1.18] Hoff, C., Natke, H.G., "Correction of a Finite Element Model by Input-Output Measurements with Application to a Radar Tower", *Proceedings of the 6th International Modal Analysis Conference (IMAC)*, Orlando, Florida, 1988.
- [1.19] Mottershead, J.E., "A Unified Theory of Recursive, Frequency Domain Filters with Application to System Identification in Structural Dynamics", *Journal of Vibrations, Acoustics, Stress Reliability, Design*, Vol. 110, No. 3, ASME, 1988, p. 360.
- [1.20] Kanai, K., "A Method of Determining the Stiffness of Each Story of a N-storied Building", Earthquake Research Institute (ERI), Japan, 1950, p. 161.
- [1.21] Berg, G.V., "Finding System Properties from Experimentally Observed Modes of Vibration", *Jornadas Argentinas de Ingenieria Antisismica*, April, 1962.
- [1.22] Nielsen, N.N., *Dynamic Response of Multistory Buildings*, Report, EERL, California Institute of Technology, Pasadena, California, June, 1964.
- [1.23] Rodden, W.P., "A Method for Deriving Structural Coefficients from Ground Vibration Tests" *AIAA Journal*, Vol. 5, May 1967, p. 991.
- [1.24] Hall, B., Calkin, E.D., Scholar, M.S., "Linear Estimation of Structural Parameters from Dynamic Test Data", *Proceedings of the AIAA/ASME 11th Structural Dynamics and Materials Conference*, Denver, Colorado, April 1970.
- [1.25] Berman, A., Flannelly, W.G., "Theory of Incomplete Models of Dynamic Structures", *AIAA Journal*, Vol. 9, August 1971, p. 1482.
- [1.26] Berman, A., "Mass Matrix Correction Using an Incomplete Set of Measured Modes", *AIAA Journal*, Vol. 17, October 1979, p. 1147.
- [1.27] Berman, A., Wei, F.S., "Automated Dynamic Analytical Model Improvement", NASA Report CR-3452, July 1981.
- [1.28] Berman, A., "System Identification of Structural Dynamic Models - Theoretical and Practical Bounds", AIAA Paper 84-0929, 1984.
- [1.29] Fuh, J.-S., Berman, A., "Comment on Stiffness Matrix Adjustment Using Mode Data", *AIAA Journal*, Readers Forum, Vol. 24, August 1986, p. 1405.
- [1.30] Caesar, B., "Update and Identification of Dynamic Mathematical Models", *Proceedings of the 7th International Modal Analysis Conference (IMAC)*, Las Vegas, NV, p. 394, February, 1989.
- [1.31] Wei, F.S., "Structural Dynamic Model Modification Using Vibration Test Data", *Proceedings of the 7th International Modal Analysis Conference (IMAC)*, Las Vegas, NV, February, 1989, p. 562.
- [1.32] Wei, F.S., "Stiffness Matrix Correction from Incomplete Test Data", *AIAA Journal*, Vol. 18, October 1980, p. 1274.
- [1.33] Ross, R.G., "Synthesis of Stiffness and Mass Matrices from Experimental Vibration Modes", *Proceedings of the SAE Shock and Vibration Conference*, Paper 710787, Los Angeles, California, 1971.
- [1.34] Collins, J.D., Hart, G.C., Haselman, T.K., Kennedy, B., "Statistical Identification of Structures", *AIAA Journal*, Vol. 12, February 1974, p. 185.
- [1.35] Thoren, A.R., "Derivation of Mass and Stiffness Matrices from Dynamic Test Data", *Proceedings of the AIAA/ASME/SAI 13th Structures, Structural Dynamics and Materials Conference*, AIAA Paper 72-346, San Antonio, Texas, April 10, 1972.
- [1.36] Schiff, A.J., "Identification of Large Structures Using Data from Ambient and Low Level Excitation", in *System Identification of Vibrating Structures - Mathematical Models from Test Data*, W. Pilkey, R. Cohen, editors, ASME, New York, N.Y., 1972.
- [1.37] Udawadia, F.E., Sharma, D.K., Shah, P.C., "Uniqueness of Damping and Stiffness Distributions in the Identification of Soil and Structural Systems", *Journal of Applied Mechanics*, ASME, Vol. 45, March 1978, p. 181.
- [1.38] Vandiver, J.K., "Detection of Structural Failure on Fixed Platforms by Measurement of Dynamic Response", *Proceedings of the 1975 Offshore Technology Conference*, Houston, Texas, May 5-8, 1975, Paper OTC 2267, p. 243.
- [1.39] Wojnarowski, M.E., Stiansen, S.G., Reddy, N.E., "Structural Integrity Evaluation of a Fixed Platform Using Vibration Criteria", *Proceedings of the Offshore Technology Conference (OTC)*,

- Vol. 3, Paper OTC 2909, May, 1977, p. 247.
- [1.40] Caravani, P., Thomson, W.T., "Identification of Damping Coefficients in Multidimensional Linear Systems", *Journal of Applied Mechanics*, Vol. 41, ASME, June 1986, p. 379.
- [1.41] Garba, J.A., Wada, B.K., "Applications of Perturbation Method to Improve Analytical Model Correlation with Test Data", *Proceedings of the SAE Aerospace Meeting*, Los Angeles, California, SAE Paper 770959, November, 1977.
- [1.42] Baruch, M., Bar-Itzhack, I.Y., "Optimal Weighted Orthogonalization of Measured Modes", *AIAA Journal*, Vol. 16, April 1978, p. 346.
- [1.43] Baruch, M., "Optimization Procedure to Correct Stiffness and Flexibility Matrices Using Vibration Tests", *AIAA Journal*, Vol. 16, November 1978, p. 1208.
- [1.44] Baruch, M., "Optimal Correction of Mass and Stiffness Matrices Using Measured Modes", *AIAA Journal*, Vol. 20, November 1982, p. 1623.
- [1.45] Baruch, M., "Methods of Reference Basis for Identification of Linear Dynamic Structures", *AIAA Journal*, Vol. 22, April 1984, p. 561.
- [1.46] Chen, J.-Ch., Garba, J.A., "Matrix Perturbation for Analytical Model Improvement", *Proceedings of AIAA/ASME/ASCE/AHS 20th SDM Meeting*, April, 1979.
- [1.47] Chen, J.-Ch., Garba, J.A., "Analytical Model Improvement Using Modal Test Results", *AIAA Journal*, Vol. 18, No. 6, June 1980, p. 684.
- [1.48] Chen, J.-Ch., Garba, J.A., "Structural Damage Assessment Using a System Identification Technique", *Proceedings of the Workshop on Structural Safety Evaluation Based on System Identification Approaches*, Lambrecht/Pfalz, Germany, June 29-July 1, 1987, p. 474.
- [1.49] Chen, J.-Ch., Peretti, L.F., Garba, J.A., "Spacecraft Structural System Identification by Modal Test" *Journal of Spacecraft Rockets*, Vol. 21, No. 4, July-August, 1964, p. 366.
- [1.50] Coppolino, R.N., Rubin, S., "Detectability of Structural Failures in Offshore Platforms by Ambient Vibration Monitoring", *Proceedings of the 1980 Offshore Technology Conference*, Houston, Texas, May 1980, Paper 3865, p. 101.
- [1.51] Rubin, S. "Damage Detection in Offshore Structures by Vibration Measurements", (unknown reference).
- [1.52] Heylen, W., "Model Optimization with Measured Modal Data by Mass and Stiffness Changes", *Proceedings of the 4th International Modal Analysis Conference (IMAC)*, Los Angeles, California, February, 1986, p. 94.
- [1.53] Natke, H.G., Schulze, H., "Parameter Adjustment of a Model of an Offshore Platform from Estimated Eigenfrequencies Data", *Journal of Sound and Vibration*, Vol. 77, No. 2, 1981, p. 271.
- [1.54] Natke, H.G., "Application of System Identification in Engineering", CISM Course, Udine, 1986.
- [1.55] Natke, H.G., "Updating Computational Models in the Frequency Domain Based on Measured Data", *Journal of Probabilistic Engineering Mechanics*, Vol. 3, No. 1, 1988, p. 28.
- [1.56] Zhang, Q., Lallement, G., Fillod, R., Piranda, J. "A Complete Procedure for the Adjustment of a Mathematical Model from the Identified Complex Modes", *Proceedings of the 5th International Modal Analysis Conference (IMAC)*, London, 1987, p. 1183.
- [1.57] Zhang, Q., Lallement, G., "Dominant Error Localisation in a Finite Element Model of a Mechanical Structure", *Mechanical Systems and Signal Processing*, Vol. 1, No. 2, 1987, p. 141.
- [1.58] Lallement, G., "Localization Techniques", *Proceedings of the Workshop on Structural Safety Evaluation Based on System Identification Approaches*, Lambrecht/Pfalz, Germany, June 29-July 1, 1987, p. 212.
- [1.59] Zhang, Q., Lallement, G., "Selective Structural Modifications: Applications to the Problems of Eigensolutions Sensitivity and Model Adjustment", *Mechanical Systems and Signal Processing*, Vol. 3, No. 1, 1989, p. 55.
- [1.60] Zak, M. "Discrete Model Improvement by Eigenvector Updating", *Journal of Engineering Mechanics*, ASCE, Vol. 109, No. 6, December 1983, p. 1437.
- [1.61] Kabe, A.M., "Stiffness Matrix Adjustment Using Mode Data", *AIAA Journal*, Vol. 23, No. 9, September 1985, p. 1431.

- [1.62] Stubbs, N., "A General Theory of Non-Destructive Damage Detection in Structures", *Proceedings of the Second International Symposium on Structural Control*, University of Waterloo, Ontario, Canada, July 15-17, 1985, p. 694.
- [1.63] Stubbs, N., "Global Non-Destructive Damage Evaluation in Solids", *International Journal of Analytical and Experimental Modal Analysis*, Vol. 5, No. 2, April 1990, p. 67.
- [1.64] Stubbs, N., Osegueda, R., "Global Damage/Detection in Solids - Experimental Verification", *International Journal of Analytical and Experimental Modal Analysis*, Vol. 5, No. 2, April 1990, p. 81.
- [1.65] Hanagud, S., Meyyappa, M., Cheng, Y.P., Craig, J.I. "Identification of Structural Dynamic Systems with Nonproportional Damping", *AIAA Journal*, Vol. 24, No. 11, November 1986, p. 1880.
- [1.66] Thomas, M., Massoud, M., Beliveau, J., "Identification of System Physical Parameters from Force Appropriation Technique", *Proceedings of the 4th International Modal Analysis Conference (IMAC)*, Orlando, Florida, 1986, p. 1098.
- [1.67] Beliveau, J.-G., "System Identification of Civil Engineering Structures", *Canadian Journal of Civil Engineering*, Vol. 14, No. 1, 1987, p. 7.
- [1.68] Flanigan, C.C., "Test/Analysis Correlation Using Design Sensitivity and Optimization", *Proceedings of the Aerospace Technological Conference*, Long Beach, California, October 5-8th, 1987, SAE Paper 871443, Society of Automotive Engineers.
- [1.69] Flanigan, C.C., "Test/Analysis Correlation of the STS Centaur Using Design Sensitivity and Optimization Methods", *Proceedings of the 5th International Modal Analysis Conference (IMAC)*, London, 1987.
- [1.70] Gray, S.D., Starke, J.M., "Dynamic Substructure Separation Using Physical and Modal Models" *Proceedings of the 6th International Modal Analysis Conference (IMAC)*, Kissimmee, Florida, January 1988, p. 1119.
- [1.71] Gray, S.D., Starke, J.M., "Mount Property Identification - An Optimization Approach to Dynamic Substructuring", *Proceedings of the 7th International Modal Analysis Conference (IMAC)*, Las Vegas, NV, February, 1989, p. 38.
- [1.72] Kammer, D.C., "Optimal Approximation for Residual Stiffness in Linear System Identification", *AIAA Journal*, Vol. 7, April 1969, p. 774.
- [1.73] Eiber, A., "Determination of Physical System Parameters", *Proceedings of the 7th International Modal Analysis Conference (IMAC)*, Las Vegas, NV, February, 1989, p. 172.
- [1.74] Inman, D.J., "Updating Analytical Models with Experimental Modal Data", *Proceedings of the 2nd USAF/NASA Workshop on System Identification and Health Monitoring of Precision Space Structures*, California Institute of Technology, Pasadena, California, March 27-29, 1990.
- [1.75] Waller and Schmidt, "Application of State Observers", *Mechanical Systems and Signal Processing*, Vol. 4, No. 3, 1990, p. 195.
- [1.76] Waqfi, O.M., "Vibrational Analysis Technique for Nondestructive Evaluation of Bridges", Ph. D. Thesis, University of Southern California, February 1990.
- [1.77] Mitchell, L.D., Wicks, A.L., "Scanning Laser Imaging and its Use in Experimental Modal Analysis", *Proceedings of the 2nd USAF/NASA Workshop System Identification and Health Monitoring of Precision Space Structures*, California Institute of Technology, Pasadena, California, March 27-29, 1990.
- [1.78] Friswell, M.I. "The Adjustment of Structural Parameters Using a Minimum Variance Estimator", *Mechanical Systems and Signal Processing*, Vol. 3, No. 2, 1989, p. 143.
- [1.79] Beck, J.L., "Statistical System Identification of Structures", in *Structural Safety and Reliability*, ASCE, Vol. 2, 1990, p. 1395.
- [1.80] Ojalvo, I.U., Ting, T., Pilon, D., Twomey, W., "Practical Suggestions for Modifying Math Models to Correlate with Actual Modal Test Results", *Proceedings of the 7th International Modal Analysis Conference (IMAC)*, Las Vegas, NV, February, 1989, p. 347.
- [1.81] Ojalvo, I.U., Ting, T., Pilon, D., "PAREDYM - a Parameter Refinement Computer Code for Structural Dynamic Models", *International Journal of Analytical and Experimental Modal Analysis*, Vol. 5, No. 1, January 1989, p. 33.

- [1.82] Beck, J.L., "Determining Models of Structures from Earthquakes Records", Report EERL 78-01, California Institute of Technology, Pasadena, California, 1978.

Chapter 2 : Models

Section 2.1 - Classification of Models

Models in structural identification can be classified as being parametric or non-parametric. Mass density, modulus of elasticity, and frequency of vibration are examples of mechanical parameters. Parameter values, which are constant in time, are usually assigned by an engineer prior to calculating the predicted behavior of the mechanical system. Non-parametric models, on the other hand, are characterized by being represented by just a function of time or frequency. Examples are the use of an impulse response function or transfer function to characterize a linear system. They also provide a characterization of the system which is constant in time. In general, these models are not so informative and they serve simply to relate the input and output in a mathematical form without gaining much insight into the mechanics.

The structural identification field has shifted emphasis from non-parametric to more complex mechanical parametric models since better understanding of the mechanics of systems is available and because of the availability of faster computing devices. With the added model structure comes the ability to understand the interaction between the different response quantities as well as the influence of the different mechanical parameters on the response. Interpretation of the mechanical parameters along with the values of the different response quantities provide an understanding of the *state of the structure*. The new complexity in the models induces more difficult parameter estimation and structural identification: models are not identifiable, parameter values should remain in mechanically-meaningful ranges, parameter values should be unique, etc. These problems are unavoidable and must be dealt with before anyone can assert that the *correct* parameter set accompanying the model and, thus the state of the structure, has been determined.

Section 2.1.1 - Modal Models

The mechanical parametric identification field concentrates on identifying mainly two types

of parameters: (1) modal parameters and (2) physical or structural parameters. The modal identification field has been an active area of research for the last decade or two and may be the most appropriate technique to be used in structural control. The physical parameter identification field has been developed more recently. This field is more complex than the modal field since the number of parameters considered is generally much larger and their extraction from vibratory systems is not as straightforward, particularly because of problems with non-uniqueness and numerical ill-conditioning.

Section 2.1.2 - Physical Parametric Models

Physical parametric models encompass a large set of models. The majority of the models considered in the past are linear but, more recently, much more emphasis has been put on non-linear models. Even though linear models give mathematical relations which are linear with respect to the state variables, they give highly non-linear functions for the determination of the physical parameters from the kinematic quantities or from the modal parameters. This non-linearity increases the complexities in the parameter estimation process.

Ultimate strength is perhaps the most appropriate parameter to be able to assess the health of a structure. As mentioned earlier, ultimate strength identification is very difficult and in practice it is replaced by elastic stiffness identification. Side benefits of elastic stiffness identification include the straightforward calculation of the modal quantities associated with the physical model (these are an approximation, too, and so they are most probably different from those estimated directly from response data with a modal identification algorithm). Internal forces arising during motion can also be easily estimated using the updated model.

Linear physical models are often derived from Finite Element ("FE") modeling. As is well known, FE modeling is based on simple formulas which describe the kinematics of a structure with infinite number of degrees of freedom by local interpolation. Under FE modeling, a finite-dimensional subspace of the infinite-dimensional degree-of-freedom space is used. Coarse discretization of the structure is associated with a small dimensional subspace while fine discretization is associated with a large subset of degrees of freedom. The members of this subset are the so-called generalized degrees of freedom and correspond to certain types of motions at specified points in the structure. The function of the interpolation is to enslave, by some mathematical relation, the motion of what used to be a degree of freedom of the structure to the motion of the generalized degrees of freedom. It is also well known that, in general, the fewer degrees of freedom in the discrete model, the cruder the interpolation and thus the worse the kinematic description. Standard FE texts provide detailed descriptions of the many other aspects of FE modeling which affect the kinematic response prediction.

Assuming linear materials and small strains and deformations and neglecting damping, the FE method leads to the equations of motion

$$M\ddot{u}(t) + Ku(t) = f(t) \quad (2.1.1)$$

where M and K are the mass and stiffness matrices, $u(t)$ are the generalized displacements, dots denote time derivatives, and $f(t)$ is the corresponding forcing vector. Certain features are apparent from the foregoing. One feature, which is a cause of some controversy in structural identification, is the fact that because of the local nature of the interpolation, the nominal symmetric mass matrix M and stiffness matrix K are guaranteed to have zero components outside a certain bandwidth. Depending on the type of interpolation used, there might even be zero matrix components within the band. The structure imposed by FE modeling in the description of the stiffness and mass matrices defines what is commonly called the “topology of the member connectivities”. Some authors try to match observed system behavior by employing identification algorithms which vary the out-of-band components. They also constrain the matrices to remain symmetric. By allowing these components to be non-zero, an interaction or coupling is created between two generalized degrees of freedom disregarding the fact that these two degrees of freedom may be geometrically far apart in the structure. This coupling contradicts directly the local nature of the interpolation intrinsic to FE modeling and thus the FE topology is thereby violated.

Non-FE models are also often considered in structural identification, especially in earthquake and offshore engineering. These models yield dynamical systems with the same structure as in Eq. (2.1.1). Very often the model used is able to capture the essential mechanical behavior of the structure that is analyzed. An example of this is the use of the shear building model (chain model) in earthquake engineering to study the dynamical behavior of medium size buildings under seismic excitation. This model corresponds to masses that are sequentially linked by springs and dash pots with one of the end masses rigidly attached to a stationary base. The arrangement of the masses leads to a tri-diagonal stiffness matrix. A numerically equivalent model may be formally derived from FE modeling but perhaps at the cost of analysis time and increased number of degrees of freedom. Shear-wall models are other examples of engineering-based elements. No matter what model is used, there are nearly always zero matrix components outside a certain bandwidth. The non-FE formulation, because of its ad-hoc nature, does not formally state that the zero components of the stiffness matrix should remain zero throughout the identification process. Thus, no preservation of the original matrix topology is necessary, in contrast to FE models. The flexibility of being able to modify any component of the stiffness and/or mass matrix has computational advantages exploited by some researchers; yet, it has drawbacks that should not be overlooked. One of the drawbacks has to do with the interpretation of the changes in the modified matrices: in general it may not be obvious why two previously unrelated degrees of freedom are now linked and what this means in

terms of damage. These new links can easily obscure the localization and quantification of damage.

Good modeling also implies paying careful attention when defining the boundary conditions, damping mechanisms, numerical algorithms, etc. Loss of accuracy in the parameter estimates can occur since the parameter estimation process relies so strongly on the calculated modal parameters or kinematic response.

Section 2.2 - A Class of Mechanical Models

The damage detection methodology developed herein depends intrinsically on the structure of the parametrized mechanical model. In this section, the class of models is described.

It is assumed that the structures that are studied are excited by low-amplitude forces so that the behavior is well modeled as linear elastic. In this case, the governing equations derived for a linear visco-elastic model are:

$$M\ddot{u}(t) + C\dot{u}(t) + Ku(t) = f(t) \quad (2.2.1)$$

where C is the damping matrix (classical normal modes are assumed). The number of degrees of freedom ("DOF") is N_d .

Damage occurring in a particular member of a structure with a large amount of redundancy is likely to have little effect on the response at any of the monitored degrees of freedom. If vibrational response is used to detect damage through identification of changes in the stiffness parameters of the members themselves, the approach will be rendered ineffective by the ill-conditioned nature of the inverse problem due to the lack of sensitivity and large number of parameters. If the structure can be adequately partitioned into sub-structures (or modules, super-elements, etc.), as proposed here, then damage can be detected and located only to within a sub-structure, but this should reduce the ill-conditioning. With fewer parameters than one for each member in the structure, the problem of trade-off between the different stiffnesses, which accentuates the lack of sensitivity, is reduced.

Section 2.2.1 - Structural Model

Damage is modeled as producing a reduction in the module stiffness. Thus, if the initial stiffness matrix corresponding to an undamaged sub-structure i is K_i , then the matrix corresponding to the damaged module, K_i^d , is given by

$$K_i^d = \theta_i K_i \quad (2.2.2)$$

where $0 \leq \theta_i \leq 1$. The parameter θ_i is called the “stiffness factor” for sub-structure i . The global stiffness matrix K is then written as

$$K = \sum_{i=1}^{N_p} \theta_i K_i, \quad (2.2.3)$$

where K_i now denotes the contribution of sub-structure i to the global stiffness matrix, and N_p , the number of parameters θ_i , equals the number of sub-structures chosen for the structure. If the K_i are correct or calibrated through system identification, then the parameter θ_i is unity. When damage occurs in module i , θ_i decreases. The choice of N_p involves a compromise between the desire for high spatial resolution in localizing any damage and the need to avoid ill-conditioning or non-uniqueness in the identification of the parameters θ_i . In general, a more dense distribution of sensors on the structure allows a larger value of N_p . Stiffness factors, because of the linear character shown in Eq. (2.2.3), can only roughly estimate structural changes associated with parameters which enter with various orders of non-linearity in the expressions for the stiffness matrices. An example of this would be the determination of the length of a beam given information about its response to some excitation. Since the dependence of the matrix coefficients on the length is either inverse, inverse quadratic, or inverse cubic, there is no possible way to substitute these by introducing linear parameters θ_i and maintain the proper ratios. Had the matrix coefficients depended on the length in a inverse cubic manner, only, say, then it would be possible to choose one parameter θ_i to represent such dependency. There are, currently, versions of some of the programs mentioned in later sections which allow for the determination of these kinds of parameters but no thorough examination has been done to date. It should be emphasized that the introduction of the factors θ_i into the linear elastic model (Eq. (2.2.3)) does not change the structural “topology” or connectivity specified by the model, i.e., if there is initially no stiffness linking two degrees of freedom, the corresponding stiffness is zero and the factor θ_i preserves this condition.

The structure of the matrices K_i is generally defined by a finite element model although any other model, empirical or analytic, can be employed. Models such as the chain (or “shear building”) model may be appropriate for specific engineering applications. It should also be mentioned that the K_i need not correspond to relatively large modules. For example, if it is deemed necessary, K_i may be associated with the axial stiffness of only one column in a large structure.

To improve the nominal model of the structure, an extension of the idea of a stiffness factor can be applied to the other dynamic matrices, i.e.,

$$M = \sum_{i=1}^{N_p} \gamma_i M_i \quad (2.2.4)$$

and

$$C = \sum_{i=1}^{N_p} \mu_i C_i \quad (2.2.5)$$

where M, γ_i and M_i are the global mass matrix, the mass factor and the sub-structure mass matrix, respectively. Similarly, C, μ_i and C_i are the global damping matrix, the damping factor (different from the damping ratio), and the module damping matrix, respectively. The matrices M_i can be estimated with an appropriate choice of inertial model and from data obtained from structural drawings. In most cases, the M_i are fairly well determined. In the case of the sub-structure damping matrices C_i , the mathematical structure can be based on Rayleigh damping at the module level, i.e.,

$$C_i = \alpha_i M_i + \beta_i K_i \quad (2.2.6)$$

and so

$$C = \sum_{i=1}^{N_p} \mu_i (\alpha_i M_i + \beta_i K_i) \quad (2.2.7)$$

although this formulation does not, in general, yield classical modes. With an appropriate choice of α_i, β_i and μ_i , namely,

$$\begin{aligned} \alpha_i &= \tilde{\alpha} \gamma_i \\ \beta_i &= \tilde{\beta} \theta_i \\ \mu_i &= 1 \end{aligned} \quad (2.2.8)$$

the global damping matrix takes the global Rayleigh damping form:

$$C = \tilde{\alpha} M + \tilde{\beta} K \quad (2.2.9)$$

where $\tilde{\alpha}$ and $\tilde{\beta}$ are the global Rayleigh damping factors to be determined. In this case, classical modes are ensured. The “general” damping matrix given by Eq. (2.2.7) can be used when non-classical modes are desired in the class of models employed.

Damping models other than generalized Rayleigh damping are also used. Modal damping, introduced via damping ratios in the modal equations to independently control the damping in each of the modes, is employed in most cases presented in later sections. Modal damping is appropriate to use since the structural response is computed via the modal equations rather than by direct integration of the equations of motion Eq. (2.2.1). It is also noted that the sub-structuring for the inertia and stiffness terms need not be the same, i.e., the M_i need not be associated with the same sub-structure to which K_i belongs, unless Rayleigh-like damping is employed. With modal damping, the sub-structuring of the mass matrix is independent from the sub-structuring of the stiffness matrix.

Section 2.2.2 - Reduced Models

Models where the number of degrees of freedom has been reduced would normally present better conditioned identification. From this point of view, it is therefore convenient to use Guyan reduction or some other reduction method. Any convenience is lost, however, whenever the linearity of the equations in the parameters θ_i is lost. In order not to lose this linearity, it is imperative to eliminate degrees of freedom internal to only one sub-structure. Whenever degrees of freedom are “tied” to two or more modules, it is not possible, in general, to end with a system of stiffnesses linear in θ_i . The chain model, often employed in structural engineering, is a good example of a reduced model which can preserve the translational inter-story stiffness distribution of a more complex structural model. Fewer number of degrees of freedom, however, does not always improve parameter identification since it usually worsens the model.

Section 2.2.3 - Numerical Algorithms

The modal parameters employed by the estimation algorithms described in later sections are calculated by standard methods [2.1]. The solution of the eigenvalue problem associated with the equations of motion (2.2.1) is carried out by EISPACK routines BANDR, BISECT and BANDV [2.2]. Since these routines are designed to be used with banded, symmetric matrices and the inverse of the mass matrix is involved in the calculation, it is preferable to use the lumped mass matrices associated with the problem since use of the consistent mass matrix yields, in general, full inverse matrices.

The time histories of displacement, velocity and acceleration are obtained by integrating the matrix equations of motion. The integration of Eq. (2.2.1), because of their linear character, is performed in either of two ways: (1) direct integration of the full set of equations, or (2) conversion of the full set of equations to the modal domain.

Direct integration is employed when the frequency content is expected to be relatively high such as in wave propagation problems. The Trapezoidal method, equivalent to Newmark’s method with $\gamma = \frac{1}{2}$ and $\beta = \frac{1}{4}$, is unconditionally stable. The Central Differences method (Newmark’s with $\gamma = \frac{1}{2}$ and $\beta = 0$) is conditionally stable [2.3] and, thus, care must be taken to avoid the growth of instabilities. For example, because of the unconstrained nature of the iterative parameter-determination algorithms (these may require the evaluation of responses at large values of θ), a very conservative time-step value must be used with central differences. Another reason why the direct approach may be used is to formulate the damping matrix in the general non-classical form.

The alternative approach, more often used in this study, is to convert the matrix equations of motion to modal equations and then to integrate each of the resulting single degree of freedom

(“SDOF”) equations. For structural vibrations, modal superposition is often more useful since the dominant modes are usually the first 10-to-20. The burden of calculating the modal parameter values is offset by the few simple integrations of the modal SDOF equations. If non-classical modes are desired, they can also be integrated in the modal domain but in this case the integration must be carried out in the first order form. Non-classical modes are not treated in this study.

The solution of the modal equations is calculated using the Nigam-Jennings algorithm [2.4]. This algorithm is very efficient for determining all three quantities (displacements, velocities and accelerations) for each time step, requiring only 8 operations per step. The algorithm, furthermore, is unconditionally stable. This algorithm is based on the analytic Duhamel’s integral solution applied to the case where the excitation is linearly interpolated between two consecutive time steps. Beck and Dowling’s approach [2.5] can also be implemented since, for the most part, only one of the three kinematic quantities is needed; this algorithm requires only 3 operations per time step to give the same acceleration values as the Nigam-Jennings algorithm.

If multiple inputs are present, they are handled with the aid of the pseudo-static displacement concept [2.6]. This concept divides the kinematic quantity vectors into two components:

$$u(t) = s(t) + d(t) \quad (2.2.10)$$

where $s(t)$ is the “pseudo-static” component and $d(t)$ is the dynamic component. The idea is that the pseudo-static part is the “response” of the structure ignoring all inertial effects and damping. The dynamic part $d(t)$ is simply the difference between the total response and the pseudo-static response and incorporates the dynamics of the motion, i.e., it can be decomposed into a modal superposition taking into consideration inertial and damping effects.

Substituting the vector $u(t)$ into the matrix equations of motion and also considering the partition of the vector $u(t)$ into prescribed $u^p(t)$ and free $u^f(t)$ motions,

$$u(t) = \begin{Bmatrix} u^p(t) \\ u^f(t) \end{Bmatrix}, \quad (2.2.11)$$

leads to the partitioned matrix equation

$$\begin{aligned} M^{Jf} \left(\ddot{s}^f(t) + \ddot{d}^f(t) \right) + C^{Jf} \left(\dot{s}^f(t) + \dot{d}^f(t) \right) + K^{Jf} \left(s^f(t) + d^f(t) \right) \\ = f^f(t) - M^{Jp} \ddot{u}^p(t) - C^{Jp} \dot{u}^p(t) - K^{Jp} u^p(t). \end{aligned} \quad (2.2.12)$$

The mathematical equality

$$K^{Jf} s^f(t) = -K^{Jp} u^p(t) \quad (2.2.13)$$

is the basis of the pseudo-static technique which leads, in turn, to the following equalities:

$$\begin{aligned} s^J(t) &= -K^{JJ^{-1}} K^{Jp} u^p(t) \\ \dot{s}^J(t) &= -K^{JJ^{-1}} K^{Jp} \dot{u}^p(t) \\ \ddot{s}^J(t) &= -K^{JJ^{-1}} K^{Jp} \ddot{u}^p(t). \end{aligned} \quad (2.2.14)$$

Rearranging Eq. (2.2.12) and making use of the above relations gives

$$\begin{aligned} &M^{JJ} \ddot{d}^J(t) + C^{JJ} \dot{d}^J(t) + K^{JJ} d^J(t) \\ &= f^J(t) + (M^{JJ} K^{JJ^{-1}} K^{Jp} - M^{Jp}) \ddot{u}^p(t) \\ &\quad + (C^{JJ} K^{JJ^{-1}} K^{Jp} - C^{Jp}) \dot{u}^p(t) \\ &\quad + (K^{JJ} K^{JJ^{-1}} K^{Jp} - K^{Jp}) u^p(t). \end{aligned} \quad (2.2.15)$$

Since

$$(K^{JJ} K^{JJ^{-1}} K^{Jp} - K^{Jp}) = 0, \quad (2.2.16)$$

the last term in Eq. (2.2.15), drops out. Furthermore, making the assumption that

$$(C^{JJ} K^{JJ^{-1}} K^{Jp} - C^{Jp}) \approx 0 \quad (2.2.17)$$

then

$$M^{JJ} \ddot{d}^J(t) + C^{JJ} \dot{d}^J(t) + K^{JJ} d^J(t) = f^J(t) + (M^{JJ} K^{JJ^{-1}} K^{Jp} - M^{Jp}) \ddot{u}^p(t). \quad (2.2.18)$$

or

$$M^{JJ} \ddot{d}^J(t) + C^{JJ} \dot{d}^J(t) + K^{JJ} d^J(t) = f^*(t) \quad (2.2.19)$$

where

$$f^*(t) = f^J(t) + (M^{JJ} K^{JJ^{-1}} K^{Jp} - M^{Jp}) \ddot{u}^p(t). \quad (2.2.20)$$

The dynamic motion $d^J(t)$ is then calculated using the methods described at the beginning of this section. Both quantities $s^J(t)$ and $d^J(t)$ are functions of the stiffness matrix and thus of the parameters θ_i . What the pseudo-static approximation implies is that the forces arising from the pseudo-static damping are much smaller than the forces arising from the pseudo-static inertia effects of the pseudo-static contribution. For most problems treated here, this has been the case.

References for Chapter 2

- [2.1] Bathe, K.J., "Solution Methods for Large Generalized Eigenvalue Problems in Structural Engineering", SESM Report 71-20, University of California, Berkeley, California, 1971.
- [2.2] Dongarra, J.J., Bunch, J.R., Moler, C.B., Stewart, G.W., *Linpac Users' Guide*, SIAM, Philadelphia, Pennsylvania, 1979.
- [2.3] Belytschko, T., Mullen, R., "On Dispersive Properties of Finite Element Solutions", *Modern Problems in Wave Propagation*, J. Miklowitz, J.D. Achenback, editors, Wiley, 1978.
- [2.4] Nigam, N.C., Jennings, P.C., "Calculation of Response Spectra from Strong-Motion Earthquake Records", *Bulletin of the Seismological Society of America*, Vol. 59, No. 2, April 1969, p. 909.
- [2.5] Beck, J.L., Dowling, M.J., "Quick Algorithms for Computing Either Displacement, Velocity or Acceleration of an Oscillator", *International Journal of Earthquake Engineering and Structural Dynamics*, Vol. 16, 1988, p. 245.
- [2.6] Clough, R.W., Penzien, J., *Dynamics of Structures*, McGraw-Hill, N.Y., 1975.

Chapter 3 : Parameter Estimation

Section 3.1 - Formulation

The Sub-structure-Identification (“SUB-ID”) problem consists of determining all unknown mechanical parameters in the model of the structure. In most damage detection cases, it reduces to the following simplified problem: Given some knowledge of the response of a structure, determine the set of stiffness factors θ_i belonging to the model

$$K = \sum_{i=1}^{N_p} \theta_i K_i \quad (3.1.1)$$

which provide the “best” fit to the observed data. In the last equation, recall that K is the global stiffness matrix of the mechanical system, K_i are the *module* or *sub-structure* stiffness matrices; and N_p indicates the number of substructures present in the system. The motion of the system and the stiffness matrix are related via the equations of motion, Eq. (2.2.1), where the motion is represented by the displacement vector $u(t)$. The number of degrees of freedom in this discrete model, N_d , is generally larger than the number of substructures present, N_p .

The eigenvalue problem associated with Eq. (3.1.2) provides for an alternate approach when trying to determine the coefficients θ_i . The modal equations are given by

$$\left(\sum_{i=1}^{N_p} \theta_i K_i \right) \phi^r = \omega_r^2 M \phi^r \quad (3.1.2)$$

where ω_r^2 and ϕ^r are an eigenvalue-eigenvector pair of the system; r takes values in $\{1, \dots, N_m\}$ where N_m is the number of modes associated with the discrete mechanical system ($N_m \equiv N_d$).

To determine the values of the θ_i , observations of the motion of the system are made. The location, duration, frequency-content and many other characteristics of the observed signals determine the quality of the identified modal parameters. The practical aspects are discussed elsewhere in this study. In this section, attention is focused on the analytical aspects of the parameter

determination problem.

Four important approaches are considered here. The first approach, the Method of Successive Substitutions, corresponds to a new application of the Contraction Mapping Principle to the non-linear θ estimation problem. The goal of this method is to create a mathematical operator which, when applied iteratively to each of the new estimates, eventually yields the unique “fixed-point” solution. The second approach is an application of the well known generalized non-linear least-squares method. The aim in this approach is to minimize the “output error” between the observations of the system and the values predicted by the model. The problem reduces to a minimization problem. The value of the parameters which minimizes the error quantity is called the “optimal” solution. Well known minimization algorithms are available for this purpose. A third approach is a probabilistic approach based on Bayes Theorem. The Bayesian approach associates a probability with each parameter value that the model can take. The probability value is related to an error or difference between the observed data and the data predicted by the model. The “most probable” solution is that associated with the smallest error subject to constraints placed by the system model. This solution is often very close to the “optimal” solution derived using the generalized least-squares approach. The Bayesian approach is more informative, however, since it emphasizes the whole probability distribution rather than just the most probable value. The fourth method is a new application of the homotopy method. This method “propagates” an easily-determined θ solution to the characteristic equation associated with a simple mechanical model to a solution of the same equation associated with the mechanical system model to be identified. The method stipulates the use of $N_d!$ different initial conditions thus yielding $N_d!$ different θ solutions to the characteristic equation of the mechanical system of interest. Since only the natural frequencies are guaranteed to be satisfied, further selection is needed to reduce the number of acceptable solutions.

All of these methods, when applied to the same real data, may yield different results. The reason for this is that real structural behavior is complex and is not always modeled exactly and also because each method emphasizes different parts of the real data in different ways. Uniqueness of parameters is also an important consideration which is addressed differently by each method and which is of considerable importance when trying to find a set of parameters by which the state of the structure is inferred.

Section 3.2 - Method of Successive Substitutions

This approach is based on the well-documented contraction theorem for (non-linear) operators [3.1]. The vector space \mathfrak{R}^{N_p} to which the vector θ belongs is a Banach space and Θ^c is defined as the closed subset of \mathfrak{R}^{N_p} of interest. The operator F is a contraction operator in Θ^c if $\exists \delta \in [0, 1) : \|F(u) - F(v)\| \leq \delta \|u - v\| \quad \forall u, v \in \Theta^c$. The contraction theorem states that for

the closed subset Θ^c and a contraction $F : \Theta^c \rightarrow \Theta^c$, F has a unique fixed point $\theta^* = F(\theta^*)$. Moreover, if $\theta^0 \in \Theta^c$ and $\theta^{n+1} = F(\theta^n)$ for $n \geq 0$, then

$$\|\theta^n - \theta^*\| \leq \delta^n (1 - \delta)^{-1} \|\theta^1 - \theta^0\|. \quad (3.2.1)$$

The theorem also states that

$$\theta^* = \lim_{n \rightarrow \infty} F^n(\theta^0) \quad (3.2.2)$$

where $F^n(\theta) \equiv F(F^{n-1}(\theta))$, $n \geq 0$ with $F^0(\theta) = \theta^0$.

The idea underlying the method consists of using an operator $F(\theta)$ to map an estimate of the solution vector θ^* , for example, θ^n , to another value θ^{n+1} which is closer to θ^* . The θ^{n+1} is substituted back and F operates on it to produce yet another iterate. θ^* is the expected converging value of the sequence starting at the initial point θ^0 .

Various contraction-like mappings can be constructed from the equations of motion. The following sections describe one of the more natural ones. Whether the subset Θ^c is large enough so that it comprises the physically acceptable domain $0 \leq \theta_i \leq 1$ is not known and is a function of the structure of the operator F . If, indeed, it happens that Θ^c is large enough, then uniqueness of the parameter estimates θ^* is guaranteed by the contraction theorem. If the subset Θ^c is smaller, then uniqueness is guaranteed only locally in $0 \leq \theta_i \leq 1$. The "design" of the best possible operator will thus have significant repercussions.

In the following, it is assumed that the number of observed partial eigenpairs $(\omega_r^2, \check{\phi}_S^r)$ is N_{mo} . The eigenpairs are identified by some external modal-extraction procedure. Although the procedure employed here [3.3] also provides estimates for the participation factors for each input, this information has not been integrated into the formulation of the operator F . This information sometimes is non-redundant and can be used to distinguish between two possible models for which all other modal data is identical.

To approach the new formulation, consider Eq. (3.1.3). For the r^{th} eigenquantity, a compound eigenvector $\phi_c^r(\theta)$ is formed by

$$\phi_c^r(\theta) = \left\{ \begin{array}{l} \check{\phi}_S^r \\ \hat{\phi}_\Theta^r(\theta) \end{array} \right\} \quad (3.2.3)$$

where $\check{\phi}_S^r$ is a subvector of the full system eigenvector ϕ_S^r with N_{od} components determined from observations to within a constant k_ϕ , and $\hat{\phi}_\Theta^r(\theta)$ corresponds to the subvector of the analytically found eigenvector $\phi_\Theta^r(\theta)$ determined from the current estimate for θ . The full eigenvector derived from the model $\phi_\Theta^r(\theta)$ satisfies orthonormality with respect to the mass matrix but the new compound vector $\phi_c^r(\theta)$ does not, in general, satisfy orthogonality. The constant k_ϕ is chosen so that the vector's magnitude (with respect to the mass matrix norm) is unity:

$$\|\phi_c^r(\theta)\|_M = 1 \quad \forall r \in \{1, \dots, N_{mo}\} \quad (3.2.4)$$

where $\|x\|_M \equiv x^T M x$.

The equations of motion Eq. (3.1.3) for the r^{th} mode can be re-written in the following way:

$$\tilde{K}^r(\theta) \theta = \tilde{M}^r(\theta) \quad (3.2.5)$$

where

$$\tilde{K}^r(\theta) \equiv [K_1 \phi_c^r(\theta), K_2 \phi_c^r(\theta), \dots, K_{N_p} \phi_c^r(\theta)] \quad (3.2.6)$$

and

$$\tilde{M}^r(\theta) \equiv \omega_r^2 M \phi_c^r(\theta). \quad (3.2.7)$$

When N_{mo} modes are observed, the set of equations to be satisfied by the vector θ is

$$\tilde{K}^*(\theta) \theta = \tilde{M}^*(\theta) \quad (3.2.8)$$

where

$$\tilde{K}^*(\theta) \equiv \begin{bmatrix} \tilde{K}^1(\theta) \\ \tilde{K}^2(\theta) \\ \vdots \\ \tilde{K}^{N_{mo}}(\theta) \end{bmatrix} \quad (3.2.9)$$

and, likewise,

$$\tilde{M}^*(\theta) \equiv \begin{bmatrix} \tilde{M}^1(\theta) \\ \tilde{M}^2(\theta) \\ \vdots \\ \tilde{M}^{N_{mo}}(\theta) \end{bmatrix}. \quad (3.2.10)$$

To solve for the vector θ , and since in general $N_d N_{mo} > N_p$, a square system of equations can be constructed:

$$S(\theta) \theta = \tilde{K}^*(\theta)^T \tilde{M}^*(\theta) \quad (3.2.11)$$

where $S(\theta)$ is a square $N_p \times N_p$ matrix

$$S(\theta) \equiv \tilde{K}^*(\theta)^T \tilde{K}^*(\theta) . \quad (3.2.12)$$

If $S(\theta)^{-1}$ exists, then an operator $F^J(\theta)$ can be constructed by

$$F^J(\theta) = S(\theta)^{-1} \tilde{K}^*(\theta)^T \tilde{M}^*(\theta) \quad (3.2.13)$$

which satisfies

$$\theta = F^J(\theta) . \quad (3.2.14)$$

For this, the matrix $S(\theta)$ must be non-singular. A check on the singularity of the matrix S can be done by calculating the associated ‘condition number’ [3.4]. A number of different condition numbers can be defined for a given matrix. The one used here is the one calculated by LINPACK’s DGECCO [3.5] routine. Here, the condition number κ represents the ratio between the minimum and the maximum eigenvalue of the matrix (the eigenvalues are guaranteed to be real since S is symmetric). A condition number $\kappa = 0$ indicates that there are one or more zero eigenvalues and thus the matrix is singular. Furthermore, if the condition number κ is such that computationally

$$1 + \kappa \equiv 1,$$

because of round-off error, then the solvability of the system of equations Eq. (3.2.11) is not guaranteed. The system is then termed “ill-conditioned.”

In the exceptional yet important case where all the components of the modeshape vectors are known the equations simplify considerably to

$$S = \tilde{K}^{*T} \tilde{K}^* \quad (3.2.15)$$

where the square matrix \tilde{K}^* is no longer a function of θ , and so neither is the square matrix S . The θ vector is readily solved if the matrix S is non-singular. From a practical point of view, and restricted to simple frame structures, the number of observed modes N_{mo} and observed degrees of freedom N_{od} equal to 2 or 3 are enough for good conditioning of the matrix S , when N_p is in the range 3 to 6.

Section 3.3 - Generalized Least-Squares Approach

Least-squares errors are described in this section, and the procedures employed to find the minimum error configuration are also briefly mentioned.

In general, an error functional $J(f, u_S, \theta) \geq 0$ can be defined in terms of the various quantities, the observed system input $f(t)$, the observed kinematic response $u_S(t)$ of the system S , and the class of linear mechanical models involving parameters θ (including mass, damping, stiffness components, etc.). The functional J is known in the literature in various ways [3.2,3.3,3.6]: “cost function”, “error index”, “loss functional”, “measure-of-fit”, “mean-square error”, “performance index”, “objective function”, and other. Here it will be referred to as “error index J .”

Section 3.3.1 - Output Error

A definition of the magnitude J of the output error is given by

$$J_T = \int_0^T \|\tilde{u}_S(t) - \tilde{u}_\theta(t)\|_W^2 dt, \quad (3.3.1)$$

involving the difference between the observed $\tilde{u}_S(t)$ and associated model $\tilde{u}_\theta(t)$ responses. Displacements, velocities or accelerations, or combinations thereof, can be employed for this purpose. When the error functional $J_T(f, u_S, \theta)$ is minimized, the model’s response time histories will come closest to those observed, *in a least-squares sense*. The values of the parameters θ which minimize J_T are used as the best estimates and the corresponding model is referred to as the optimal model. It is conceivable that there can be models which yield the same error index with real data and yet do not provide a good physical representation of the system. In order to determine the accuracy of the model, it should be tested with more extensive test data. A correct model must perform well with all data sets and also produce a consistent set of parameter estimates. In earthquake engineering, however, the data available are often scarce. This problem cannot be remedied unless an adequate model is employed: this model is calibrated at the outset and damaged-state data will modify the values of the parameters indicating the appropriate amount of stiffness loss at the correct locations. Had an incorrect model been utilized, both the prior and posterior stiffness distributions would bear little relation to the actual stiffness distributions.

The output error approach with diagonal weight matrices W inherently emphasizes the matching of natural frequencies since, if these were incorrectly determined in the mathematical model, then the response quantities $u_\theta(t)$ would be out of phase with respect to the observed response $u_S(t)$. When out of phase, the functional J_T increases in amplitude significantly. When the frequencies are correct and the responses are in phase then the error is greatly reduced. Errors in the modeshapes also increase the error functional but it is less sensitive, generally speaking, than to the natural frequencies. An obvious exception is the situation when a modeshape component derived from the model is negative in value compared to the value it takes in reality. This is equivalent to a constant π phase offset, producing the largest error increase possible for changes in phase. It must be noted that, in general, modeshape vectors are not as sensitive to variations in the parameters θ_i

in the sense described above, as frequencies are.

The actual numerical calculations weighed all degrees of freedom equally. The repercussions of weighing one degree-of-freedom response more than another are that it will produce better estimates for the associated modeshape component and for the modal frequencies participating most actively at that degree of freedom. If, for example, a particular mode k has a node at degree of freedom j and only this degree of freedom has a non-zero weight, then the parameter estimates will retain the node at that degree of freedom but the associated natural frequency can take an arbitrary value. If, on the other hand, only one mode participates at this degree of freedom, then the associated modal frequency will be the most accurately estimated frequency of all modes excited by the forcing function.

Section 3.3.2 - Modal Output Error

In this study, an *ad hoc* extension of the previous definition of output error is formulated in order to incorporate modal data directly into the error minimization process. System modal data may be obtained from existing *modal* identification algorithms [3.11,3.19].

The modal error functional is defined here as

$$J_M = \sum_{r=1}^{N_{mo}} \left[W_r^f \left(\frac{\omega_{S,r} - \omega_{\Theta,r}}{\omega_{S,r} + \omega_{\Theta,r}} \right)^2 + W_r^v \frac{\|\check{\phi}_S^r - \check{\phi}_{\Theta}^r\|^2}{\|\check{\phi}_S^r + \check{\phi}_{\Theta}^r\|^2} \right] \quad (3.3.2)$$

where ω_r is the r^{th} modal natural frequency, $\check{\phi}^r$ is a Euclidean-normalized sub-vector of the r^{th} eigenvector ϕ^r whose indices correspond to the observed degrees of freedom, the weighting coefficients W_r^f and W_r^v are non-negative, and N_{mo} is the number of observed (or measured) modes. In this way, $J_M = 0$ only when the model agrees exactly with the observed system data, and $J_M \geq 0$ for all other cases.

The forcing function does not directly participate in the error as defined by Eq. (3.3.2). Many modal extraction algorithms, including the one employed here, MODE-ID [3.3,3.19], make use of the knowledge of the function $f(t)$ to extract the natural frequencies and (partial) modeshapes associated with the system. Another modal property not often calculated by modal extraction algorithms (although MODE-ID does) is the effective participation factor. In this study, the participation factors have not been included. It was felt, at the outset, that their inclusion was not warranted since the participation factors tend to vary very slowly as functions of the θ_i , thereby not providing much extra information. After encountering non-uniqueness and ill-conditioning problems, however, it is now felt that they may provide the extra information needed to resolve some of the above-mentioned problems.

Different weights are established for each mode. In most test cases, a weight value W^f is assigned to all frequencies and another weight W^v to all eigenvectors. Although a clear path does

not exist between the natural weighting of the *output error* time approach and the weights for the *modal* approach, there are several possibilities that can be considered. The first one makes use of the relative sensitivity of each of the modal parameters on the output error functional as determined in some recent modal identification algorithms [3.12]. This approach emphasizes the trustworthiness of the modal data in terms of its presence in the response signals from which the modal properties are estimated. Another possibility is to use the relative heights of the transfer function as weights. The latter approach is easily used in single-input, multiple-output systems since only one transfer function exists for each output degree of freedom. Different weight possibilities influence not only the convergence rates of the minimization process, but also the optimal. For these reasons, weights should be employed consistently in pre- and post-damage tests.

Section 3.3.3 - Minimization Problem

Three techniques are frequently used for the determination of the parameter estimates corresponding to the state of least error as given by the minimum of J . All of the techniques are gradient based, i.e., they only make use of the gradient of the error functional. No techniques employed here make use of the Hessian matrix which corresponds to second derivatives of the functional J with respect to the independent variables θ_i . Masri and Werner [3.7] have studied various other techniques with applications to structural dynamic problems.

The first and second techniques (Polak-Ribiere and Fletcher-Reeves) belong to the conjugate family of minimization techniques. Their aim is to construct an approximation to the Hessian matrix by making use of gradient vectors only. It has been shown [3.8] that in the case of quadratic functions, conjugate techniques need only N_s iterations to converge to the exact minimum, where N_s is the dimension of the space. For most tests, the first iteration corresponds to a minimization along the direction of steepest descents, just previously mentioned. In this study, the Polak-Ribiere has been employed most frequently since the convergence rate is usually better than the corresponding one for the Fletcher-Reeves technique. These two techniques are more efficient than the better known steepest descent technique since they make use of the curvature of the topology by way of the estimate of the Hessian matrix.

The third technique, Variable Metric, also tries to approximate the Hessian matrix from gradient evaluations. This technique is perhaps the fastest technique of all the ones tested (although it actually depends on the type of function that is used for the minimization) but the algorithm employed here is unstable and can fail when the gradient evaluations yield the same gradient vector in multiple consecutive iterations. This technique also performs better than the steepest descent method because of the use of Hessian matrix estimates.

The convergence criterion used in the minimization procedure is met when relative changes in

the error index J across sequential iterations is less than a prescribed ratio ϵ , i.e., when

$$\frac{J_i - J_{i+1}}{\frac{1}{2}(J_i + J_{i+1})} \leq \epsilon. \quad (3.3.3)$$

Typically, $\epsilon = 10^{-4}$ in the calculations performed in this study. No relative change in the parameter estimates is used as part of the convergence criterion although the latter is often employed by other optimization algorithms.

Gaussian methods based on evaluations of the Hessian matrix and variations of it have not been used in this work. It was felt at the outset of this research that these methods are not the most efficient for large numbers of independent variables θ_i . In the course of this study, it has been learned that the number of independent variables cannot, in general, be so large. Implementations of Gaussian techniques may therefore prove to be useful in further studies.

The gradients needed for the minimization method are calculated in either of two ways: (1) by means of a finite difference technique or (2) by means of an analytical expression. The finite difference scheme used, although not as precise as the analytical scheme, has shown to be robust in the presence of noise. It must be noted that noise may alter the local topology of the J functional hyper-surface and so local minima may be induced. Finite difference, because of their coarser nature, sample the hyper-surface at farther points and so they are less sensitive to local variations of the surface. The finite difference scheme employed here approximates the gradient by fitting a quadratic function over three points, the center one corresponding to the point where the gradient is evaluated. In this case, for each coordinate i ,

$$J = \alpha_1 + \Delta\theta_i\alpha_2 + (\Delta\theta_i)^2\alpha_3 \quad (3.3.4)$$

and so the gradient $\frac{\partial J}{\partial \theta_i}$ is approximated by

$$\frac{\partial J}{\partial \theta_i} \approx \alpha_2 + 2\Delta\theta_i\alpha_3 \quad (3.3.5)$$

where the coefficients α_2 , and α_3 are found by solving the three simultaneous equations

$$\begin{aligned} J(\theta_i + \Delta\theta_i) &= \alpha_1 + \Delta\theta_i\alpha_2 + (\Delta\theta_i)^2\alpha_3 \\ J(\theta_i) &= \alpha_1 \\ J(\theta_i - \Delta\theta_i) &= \alpha_1 - \Delta\theta_i\alpha_2 + (\Delta\theta_i)^2\alpha_3. \end{aligned} \quad (3.3.6)$$

The gradient is given by

$$\frac{\partial J}{\partial \theta_i} \approx \frac{1}{2\Delta\theta_i} (J(\theta_i + \Delta\theta_i) - J(\theta_i - \Delta\theta_i)). \quad (3.3.7)$$

The analytically evaluated gradient as derived by Beck [3.13], and tailored here to the pseudo-static displacement method, can be formulated for the full-matrix or modal-superposition integration approaches. Other algorithms have been developed, like those surveyed by Baldwin and Hutton [3.14]. One of these, the first one discussed by Fox and Kapoor [3.15], has the same basis as the one presented here.

The gradient of the functional J , where J is given by Eq. (3.3.1), can be written as

$$\frac{\partial J}{\partial \theta_i} = 2 \int_0^T \left[\frac{\partial \tilde{e}}{\partial \theta_i}{}^T W \tilde{e} \right] dt \quad (3.3.8)$$

where

$$\begin{aligned} \frac{\partial \tilde{e}}{\partial \theta_i} &= \Upsilon \frac{\partial e}{\partial \theta_i} \\ &= \Upsilon \frac{\partial u}{\partial \theta_i} \end{aligned} \quad (3.3.9)$$

where Υ is a simple transformation matrix that extracts the observed degree-of-freedom components from the full vector. The motions $u = u(\theta)$ are partitioned according to the boundary conditions as in Eq. (2.2.11). Since there are prescribed motions $u^p(t)$ at boundaries of the structure, these do not vary with respect to any parametrization of the stiffness matrix and so

$$\frac{\partial u}{\partial \theta_i} = \left\{ \begin{array}{c} \frac{\partial u^f}{\partial \theta_i} \\ 0 \end{array} \right\}. \quad (3.3.10)$$

Introducing the pseudo-static decomposition leads to

$$\frac{\partial u^f}{\partial \theta_i} = \frac{\partial s^f}{\partial \theta_i} + \frac{\partial d^f}{\partial \theta_i} \quad (3.3.11)$$

where

$$\begin{aligned} \frac{\partial s^f}{\partial \theta_i} &= \frac{\partial (-K^{ff-1} K^{fp})}{\partial \theta_i} u^p \\ &= - \left[\frac{\partial K^{ff-1}}{\partial \theta_i} K^{fp} + K^{ff-1} \frac{\partial K^{fp}}{\partial \theta_i} \right] u^p \\ &= - \left[K^{ff-1} \frac{\partial K^{ff}}{\partial \theta_i} K^{ff-1} K^{fp} + K^{ff-1} \frac{\partial K^{fp}}{\partial \theta_i} \right] u^p \\ &= - \left[K^{ff-1} K_i^{ff} K^{ff-1} K^{fp} + K^{ff-1} K_i^{fp} \right] u^p. \end{aligned} \quad (3.3.12)$$

Also, for modal decomposition $d^f(t) = \sum_{r=1}^{N_m} \varphi_r(t; \theta) \phi^r(\theta)$ where $\varphi_r = \varphi_r(t; \theta)$ are the modal coordinates and $\phi^r(\theta)$ the corresponding modeshape, then

$$\frac{\partial d^f}{\partial \theta_i} = \sum_{r=1}^{N_m} \left[\frac{\partial \varphi_r}{\partial \theta_i} \phi^r(\theta) + \varphi_r \frac{\partial \phi^r(\theta)}{\partial \theta_i} \right]. \quad (3.3.13)$$

The $\frac{\partial \phi^r(\theta)}{\partial \theta_i}$ are calculated using the modal matrix equations of motion

$$-\omega_r^2 M^{ff} \phi^r + K^{ff} \phi^r = 0 \quad (3.3.14)$$

by taking derivatives with respect to θ_i :

$$-\frac{\partial \omega_r^2}{\partial \theta_i} M^{ff} \phi^r - \omega_r^2 M^{ff} \frac{\partial \phi^r}{\partial \theta_i} + \frac{\partial K^{ff}}{\partial \theta_i} \phi^r + K^{ff} \frac{\partial \phi^r}{\partial \theta_i} = 0. \quad (3.3.15)$$

Rearranging,

$$\left(-\frac{\partial \omega_r^2}{\partial \theta_i} M^{ff} + \frac{\partial K^{ff}}{\partial \theta_i} \right) \phi^r + (-\omega_r^2 M^{ff} + K^{ff}) \frac{\partial \phi^r}{\partial \theta_i} = 0. \quad (3.3.16)$$

Pre-multiplying the previous relation by $\phi^s(\theta)^T$ and taking advantage of the orthogonality of the eigenvectors with respect to the mass and stiffness matrices leads to

$$\left(-\frac{\partial \omega_r^2}{\partial \theta_i} \delta_{sr} + \phi^s(\theta)^T K_i^{ff} \phi^r(\theta) \right) + (\omega_s^2 - \omega_r^2) \phi^s(\theta)^T M^{ff} \frac{\partial \phi^r(\theta)}{\partial \theta_i} = 0 \quad (3.3.17)$$

where δ_{sr} is the Kronecker delta function. There are two distinct possibilities: $s = r$ and $s \neq r$. For $s = r$ the term $\omega_s - \omega_r$ vanishes and so

$$\frac{\partial \omega_r^2}{\partial \theta_i} = \phi^r(\theta)^T K_i^{ff} \phi^r(\theta). \quad (3.3.18)$$

For $s \neq r$

$$\left(\phi^s(\theta)^T K_i^{ff} \phi^r(\theta) \right) + (\omega_s^2 - \omega_r^2) \phi^s(\theta)^T M^{ff} \frac{\partial \phi^r(\theta)}{\partial \theta_i} = 0. \quad (3.3.19)$$

Allowing $\frac{\partial \phi^r(\theta)}{\partial \theta_i}$ to be expanded in a series whose terms are the orthonormal vectors $\phi^i(\theta)$,

$$\frac{\partial \phi^r(\theta)}{\partial \theta_i} = \sum_{j=1}^{N_m} c_{ri,j} \phi^j(\theta) \quad (3.3.20)$$

and introducing this into Eq. (3.3.19) leads to

$$\phi^s(\theta)^T K_i^{Jf} \phi^r(\theta) + (\omega_s^2 - \omega_r^2) c_{ri,s} = 0 \quad (3.3.21)$$

and if $\omega_s^2 \neq \omega_r^2$ (valid for most civil engineering structures with or without foundation compliance)

$$c_{ri,s} = \left(\frac{1}{\omega_r^2 - \omega_s^2} \right) \phi^s(\theta)^T K_i^{Jf} \phi^r(\theta). \quad (3.3.22)$$

Then

$$\frac{\partial \phi^r(\theta)}{\partial \theta_i} = \sum_{j=1}^{N_m} \left(\frac{1}{\omega_r^2 - \omega_j^2} \right) \left(\phi^j(\theta)^T K_i^{Jf} \phi^r(\theta) \right) \phi^j(\theta). \quad (3.3.23)$$

To calculate $\frac{\partial \varphi_r}{\partial \theta_i}$ the SDOF equation associated with the mode is integrated:

$$\ddot{\varphi}_r + (2\omega_r \xi_r) \dot{\varphi}_r + \omega_r^2 \varphi_r = \phi^r(\theta)^T f^*, \quad (3.3.24)$$

where $f^*(t)$ is given by Eq. (2.2.20), i.e.,

$$f^*(t) = f^J(t) + \left(M^{Jf} K^{Jf-1} K^{Jp} - M^{Jp} \right) \ddot{u}^p(t).$$

Taking derivatives with respect to θ_i gives

$$\frac{\partial \ddot{\varphi}_r}{\partial \theta_i} + 2\xi_r \left(\frac{\partial \omega_r}{\partial \theta_i} \dot{\varphi}_r + \omega_r \frac{\partial \dot{\varphi}_r}{\partial \theta_i} \right) + \left(\frac{\partial \omega_r^2}{\partial \theta_i} \varphi_r + \omega_r^2 \frac{\partial \varphi_r}{\partial \theta_i} \right) = \frac{\partial \phi^r(\theta)^T}{\partial \theta_i} f^* + \phi^r(\theta)^T \frac{\partial f^*}{\partial \theta_i} \quad (3.3.25)$$

or, rearranging,

$$\frac{\partial \ddot{\varphi}_r}{\partial \theta_i} + \left(2\xi_r \omega_r \frac{\partial \dot{\varphi}_r}{\partial \theta_i} \right) + \omega_r^2 \frac{\partial \varphi_r}{\partial \theta_i} = \frac{\partial \phi^r(\theta)^T}{\partial \theta_i} f^* + \phi^r(\theta)^T \frac{\partial f^*}{\partial \theta_i} - 2\xi_r \frac{\partial \omega_r}{\partial \theta_i} \dot{\varphi}_r - \frac{\partial \omega_r^2}{\partial \theta_i} \varphi_r. \quad (3.3.26)$$

The last equation is integrated using the same methods as the usual modal equations (in this case with the Nigam-Jennings algorithm) to give the time history for $\frac{\partial \varphi_r}{\partial \theta_i}$.

Using the quantities $\frac{\partial \varphi_r}{\partial \theta_i}$ and $\frac{\partial \phi^r(\theta)}{\partial \theta_i}$, the quantity $\frac{\partial d^f}{\partial \theta_i}$ in Eq. (3.3.13) can be constructed. Substituting back into equations Eq. (3.3.11), Eq. (3.3.9) and Eq. (3.3.8) provides a means to evaluate the gradient of the output error functional J .

Eq. (3.3.20) expresses the derivative of a modeshape as a series with the same modeshapes as the basis. The number of terms N_m can be truncated in order to avoid the calculation of large number of eigenvalue quantities. The variation of the modeshapes is slow with respect to the variables θ_i and thus the contributions of higher modes should not be necessary to obtain a good approximation to the derivative. Number of terms of the order of 5 to 10 are adequate for typical civil engineering structures where the modes are well separated. For space structures, the modes are frequently closer together and so larger numbers of terms may be needed.

Section 3.3.4 - Uniqueness via Minimization

The minimization of the functional J will produce some “optimal” parameter vector θ . However, in this study it is imperative to know whether this optimal value corresponds to the overall global best fit. It is possible that the minimization algorithm has converged to a local minimum and not the global minimum implying that some damage pattern is identified but it is not the most likely one. What could be done with the generalized least squares method is to set the initial value θ^0 to significantly different values and run the minimization code repeatedly [3.9]. Unfortunately, reaching the same solution in all runs does not guarantee uniqueness of the parameter vector since not all the θ space has been sampled. Equally misleading is the fact that solutions obtained by reaching a local minimum do not indicate a lack of uniqueness, *no matter how close the value at the local minimum is to that at a known global minimum* unless exactly the same value for J is obtained for more than one value of the parameter vector. The problem is compounded since it can never be asserted that the global minimum is known.

If the function taken for the minimization process was convex then it is guaranteed within the region of interest that a local minimum is the global minimum [3.10]. The output error method yields a function in θ which is not convex; so, for any finite domain of interest, it is generally true that there are both local and global minima. The global minima may occur either within the domain or at the boundaries of it. It is because of these facts that the generalized least squares approach is not considered to be a reliable method to test uniqueness of parameters.

Section 3.4 - Bayesian Model Identification

In this study, the approach formulated by Beck [3.16] based on Bayes Theorem [3.17] is described as applied to the θ parameter model. This is done in order to find the probability for each θ_i parameter value based on the available data and the chosen class of models. Probability is used here in the Bayesian sense that $p(a|b)$ is a measure of the *plausibility* of proposition a given the information in proposition b . Evaluating the probability of all models within a class of models yields a probability density function from which it is possible to extract important statistical information. The class of models allowed here is restricted to a particular mathematical form of the class of models given by Eq. (3.1.1) and Eq. (3.1.2), leaving the parameter values undetermined. The particular mathematical form can be based on FE modeling as described in Section 2.1.2; the probability density function is then evaluated for all possible values of the parameters θ_i .

From the probability axioms:

$$p(\theta|S_{N_t}) = \frac{p(S_{N_t}|\theta)p(\theta)}{p(S_{N_t})} \quad (3.4.1)$$

where

$$S_{N_t} = \{\tilde{u}_S^{(n)} \in \mathfrak{R}^{N_{od}} : n = 1, 2, \dots, N_t\} \quad (3.4.2)$$

is a set of measurements, e.g., N_t samples of the response or output of a system. The prior distribution $p(\theta)$ is based on the engineer's intuition regarding the relative plausibilities of the different models in the class, that is, of different values of θ . This allows engineering judgment to be introduced naturally into the formulation. Moreover, it is possible to allow the data to "speak for itself" by assuming that $p(\theta)$ is a locally non-informative prior distribution, i.e., it is assumed that $p(\theta) = \hat{k}$ is constant over Θ^c , the finite subset of \mathfrak{R}^{N_p} of interest, then

$$p(\theta|S_{N_t}) = \frac{\hat{k} p(S_{N_t}|\theta)}{p(S_{N_t})}. \quad (3.4.3)$$

Because the probability of the data $p(S_{N_t})$ is also independent of θ ,

$$p(\theta|S_{N_t}) = k p(S_{N_t}|\theta) \quad (3.4.4)$$

where $k = \frac{\hat{k}}{p(S_{N_t})}$. In order to calculate $p(\theta|S_{N_t})$, the probability function $p(S_{N_t}|\theta)$ must be defined and evaluated.

The model-predicted values $\tilde{u}_\theta^{(n)} \equiv \tilde{u}(t_n; f, \theta) \in \mathfrak{R}^{N_{od}} (n = 1, 2, \dots, N_t)$ are given by a deterministic model with parameter vector $\theta \in \mathfrak{R}^{N_p}$ and correspond to the observed values $\{\tilde{u}_S^{(n)}\}$. For a given θ , the prediction error (or output error) $\tilde{e}^{(n)}(\theta)$ is the difference between the system and model response:

$$\tilde{e}^{(n)}(\theta) = \tilde{u}_S^{(n)} - \tilde{u}_\theta^{(n)}. \quad (3.4.5)$$

An important step in this Bayesian approach is to define a probability model for the prediction errors. Here the prediction errors $\tilde{e}^{(n)}(\theta)$ are modeled as Gaussian discrete white noise with covariance matrix Σ . The prediction errors represent both model and measurement errors. The mean value is assumed to be zero but the covariance is unknown and is determined from the data. Because of this, Σ is here included as part of the unknown model parameters.

Letting $g(\tilde{e}, \Sigma)$ be a Gaussian probability model for the prediction error e where the most probable value of e is zero, then the probability of getting the system response $\tilde{u}_S^{(n)}$ given the deterministic model $\tilde{u}_\theta^{(n)}$ and the prediction error model $g(\tilde{e}, \Sigma)$ is:

$$p(\tilde{u}_S^{(n)}|\theta, \Sigma) = g(\tilde{e}^{(n)}(\theta), \Sigma) \quad (3.4.6)$$

Given θ and any Σ , the most probable value of $\tilde{u}_S^{(n)}$ is clearly $\tilde{u}_\theta^{(n)}$.

As implied by Eq. (3.4.2), the probability of obtaining the set S_{N_t} given the probability model is

$$p(S_{N_t}|\theta, \Sigma) = p(\check{u}_S^{(1)}, \check{u}_S^{(2)}, \dots, \check{u}_S^{(N_t)}|\theta, \Sigma) \quad (3.4.7)$$

or

$$p(S_{N_t}|\theta, \Sigma) = \prod_{n=1}^{N_t} p(\check{u}_S^{(n)}|\theta, \Sigma) \quad (3.4.8)$$

since it is assumed that the $\check{e}^{(n)}$ are temporally independent. It is also assumed that the components $\check{e}_m^{(n)}(\theta), \{m = 1, 2, \dots, N_{od}\}$ corresponding to different observed degrees of freedom are spatially independent, so the covariance matrix Σ is diagonal, $\Sigma = \text{diag}(\sigma_1, \sigma_2, \dots, \sigma_{N_{od}})$.

Letting σ denote the vector of diagonal elements of Σ , then the probability model takes the form

$$g(\check{e}, \sigma) = g(\check{e}_1, \check{e}_2, \dots, \check{e}_{N_{od}}, \sigma_1, \sigma_2, \dots, \sigma_{N_{od}}) \quad (3.4.9)$$

$$= \frac{1}{(2\pi)^{\frac{N_{od}}{2}} \sigma_1 \sigma_2 \dots \sigma_{N_{od}}} \exp\left(-\frac{1}{2} \sum_{m=1}^{N_{od}} \left(\frac{\check{e}_m}{\sigma_m}\right)^2\right) \quad (3.4.10)$$

and so

$$p(S_{N_t}|\theta, \sigma) = \prod_{n=1}^{N_t} p(\check{u}_S^{(n)}|\theta, \sigma) \quad (3.4.11)$$

$$= \prod_{n=1}^{N_t} g(\check{e}^{(n)}, \sigma) \quad (3.4.12)$$

$$= \left[\frac{1}{(2\pi)^{\frac{N_{od}}{2}} \sigma_1 \sigma_2 \dots \sigma_{N_{od}}} \right]^{N_t} \exp\left[-\frac{1}{2} \sum_{n=1}^{N_t} \sum_{m=1}^{N_{od}} \left(\frac{\check{e}_m^{(n)}}{\sigma_m}\right)^2\right]. \quad (3.4.13)$$

From Eq. (3.4.4), the "plausibility of (θ, σ) " given the data S_{N_t} is given by

$$p(\theta, \sigma|S_{N_t}) = \left[\frac{k}{(2\pi)^{\frac{N_{od}}{2}} \prod_{m=1}^{N_{od}} \sigma_m} \right]^{N_t} \exp\left[-\frac{1}{2} \sum_{n=1}^{N_t} \sum_{m=1}^{N_{od}} \left(\frac{\check{e}_m^{(n)}}{\sigma_m}\right)^2\right] \quad (3.4.14)$$

where $(\theta, \sigma) \in (\Theta^c \times \Sigma^c)$, Σ^c representing the set of permissible values for the parameter vector σ .

For identification purposes, the single most important piece of information to be determined is the most probable model given the data. The most probable value corresponds to the model which

maximizes the probability density function in Eq. (3.4.14), i.e., the most probable model is the one which gives the model response closest to the observed data given the prior probabilistic information.

Let $(\hat{\theta}, \hat{\sigma})$ be the most probable values of the parameters based on the data S_{N_t} , i.e.,

$$p(\hat{\theta}, \hat{\sigma}|S_{N_t}) = \underset{(\theta, \sigma) \in (\Theta^c \times \Sigma^c)}{\text{Max}} p(\theta, \sigma|S_{N_t}). \quad (3.4.15)$$

These values can be found by maximizing the function $p(\theta, \sigma|S_{N_t})$, or equivalently, maximizing the function

$$\ln p(\theta, \sigma|S_{N_t}) = N_t \ln \frac{k}{(2\pi)^{\frac{N_{od}}{2}}} - N_t \sum_{m=1}^{N_{od}} \ln \sigma_m - \frac{1}{2} \sum_{n=1}^{N_t} \sum_{m=1}^{N_{od}} \left(\frac{\tilde{\epsilon}_m^{(n)}}{\sigma_m} \right)^2. \quad (3.4.16)$$

For fixed θ , maximizing $\ln p(\theta, \sigma|S_{N_t})$ with respect to σ requires

$$\begin{aligned} 0 &= \frac{\partial}{\partial \sigma_m} \ln p(\theta, \sigma|S_{N_t}) \\ &= -\frac{N_t}{\sigma_m} - \frac{1}{2} \sum_{n=1}^{N_t} -\frac{2}{\sigma_m^3} \left[\tilde{\epsilon}_m^{(n)}(\theta) \right]^2 \end{aligned} \quad (3.4.17)$$

thus

$$\begin{aligned} \hat{\sigma}_m^2(\theta) &= \frac{1}{N_t} \sum_{n=1}^{N_t} \left[\tilde{\epsilon}_m^{(n)}(\theta) \right]^2 \\ &= \frac{1}{N_t} \sum_{n=1}^{N_t} \left[\tilde{u}_{S,m}^{(n)} - \tilde{u}_{\theta,m}^{(n)} \right]^2 \end{aligned} \quad (3.4.18)$$

$\forall m = 1, 2, \dots, N_{od}$. This shows how the most probable variances, for a given θ , depend on the choice of model parameters θ_i . The solution $\hat{\sigma}_m(\theta) = \infty$ to Eq. (3.4.17) can be ruled out since it gives all models zero probability on the data.

Introducing the optimal variance into Eq. (3.4.14) yields

$$\ln p(\theta, \hat{\sigma}(\theta)|S_{N_t}) = N_t \ln \frac{k}{(2\pi)^{N_{od}/2}} - N_t \sum_{m=1}^{N_{od}} \ln \hat{\sigma}_m(\theta) - \frac{N_{od}N_t}{2}. \quad (3.4.19)$$

Thus, the most probable θ , $\hat{\theta}$, is obtained by minimizing the functional J_p , given by

$$\begin{aligned} J_p(\theta) &\equiv 2 \sum_{m=1}^{N_{od}} \ln \hat{\sigma}_m(\theta) \\ &= \sum_{m=1}^{N_{od}} \ln \hat{\sigma}_m^2(\theta) \end{aligned}$$

$$= \sum_{m=1}^{N_{od}} \ln \left[\frac{1}{N_t} \sum_{n=1}^{N_t} \left(\tilde{u}_{S,m}^{(n)} - \tilde{u}_{\theta,m}^{(n)} \right)^2 \right]. \quad (3.4.20)$$

The minimization of the function $J_p(\theta)$ can be performed by any of the standard optimization procedures discussed in the Least-Squares section. As a matter of fact, if the variances σ_m^2 are all assumed to be equal and the optimal value for it is found following a similar procedure to the one shown above, then the resulting functional $J_p(\theta)$ takes the same mathematical form as the least-squares “output error functional”. The “most probable” model would then correspond to the “optimal model” in the least-squares sense. If the variances are allowed to be different for each response location, then the results of the two methods are, in general, different.

For damage detection, on the other hand, what is important is to know if there is considerable probability of the existence of failed members within a structure. The probability distribution $p(\theta, \hat{\sigma}(\theta) | S_{N_t})$ can be reduced to marginal probability distributions for each θ_i . By updating the marginal distributions in time using new test data, it may be possible to detect stiffness degradation in each sub-structure.

A characteristic of the joint probability density, however, is the presence of large “spikes” which correspond to the points in Θ^c where the probability is (locally) highest. In reference to Eq (3.4.19), any smooth surface

$$\frac{1}{\prod_{m=1}^{N_{od}} \hat{\sigma}_m(\theta)} \quad (3.4.21)$$

with local maxima will be largely distorted since the N_t exponent in Eq. (3.4.14) is usually very large. To be able to obtain a good estimate of the marginal probability distribution it is necessary to know exactly where the local and global maxima are located. The width of the spikes can be so small that no practical discretization of the Θ^c domain can guarantee high accuracy numerical integration over the maxima to obtain a good estimate of the marginal probability distribution. From the above discussion, it is then clear that the marginal probability distribution should not be used for this purpose. Instead, however, use is made of the pseudo-marginal distribution, defined as the marginal probability projection of the “pseudo-probability” represented by Eq. (3.4.21) :

$$\tilde{p}(\theta_i, S_{N_t}) \equiv \tilde{k}_i \int_0^{c_j} \int_0^{c_k} \dots \int_0^{c_m} \frac{1}{\prod_{m=1}^{N_{od}} \hat{\sigma}_m(\theta)} d\theta_j d\theta_k \dots d\theta_m \quad (3.4.22)$$

with $i \neq j, k, \dots, m$. The constant \tilde{k}_i is a normalizing factor such that the integral of the pseudo-marginal probability in $[0, c_i]$ is 1. This new quantity is much smoother than the true marginal distribution and may allow for a better monitoring of stiffness degradation through numerical integration.

Bayesian methods, as proposed here, require evaluation of J_p usually at a large number of θ values. Consequently, their practical use might be limited to problems where the number of θ

parameters is not large. An application of this method to the 2 DOF chain model will be discussed in Chapter 4.

Section 3.5 - Homotopy-based Parameter Estimation

Chu [3.18] has presented an approach which determines the values of the components of a diagonal matrix which, when added to a Jacobi matrix, yields a system whose eigenvalues match exactly a predetermined set. The approach is based on the homotopy technique which is extended here to the problem of determining the θ_i values which define a structural model so as to match a set of observed natural frequencies.

The extension of Chu's homotopy method also assumes that a solution for the values of the θ_i is propagated from an initial time $\tau_0 = 0$ to the final time $\tau_f = 1$. This new parameter, "time τ ", is not associated with the time history of the physical process; it is merely a dimensionless history parameter describing the homotopy process as in the following. The present formulation assumes that the number of unknown parameters θ_i is equal to the number of predetermined natural frequencies. Extensions of this case to more general cases will be a topic for future research.

At "homotopy time" τ_0 the values θ_i^s satisfy the characteristic equations $q_k^s(\theta, \omega_k) = 0$ associated with a simplified mechanical structure and with the observed natural frequencies. In vector form, the equations to be satisfied are

$$Q^s(\theta^s, \omega) \equiv \left\{ \begin{array}{c} q_1^s(\theta^s, \omega_1) \\ q_2^s(\theta^s, \omega_2) \\ \vdots \\ q_{N_{m_o}}^s(\theta^s, \omega_{N_{m_o}}) \end{array} \right\} = \left\{ \begin{array}{c} 0 \\ 0 \\ \vdots \\ 0 \end{array} \right\}. \quad (3.5.1)$$

Proper construction of the simplified structure provides ready determination of the roots θ_i^s .

At "time" τ_f , the values of the θ_i^* must satisfy the characteristic polynomials Q^* associated with the structural model to be identified and with the observed natural frequencies, as described in the previous equations. The determination of the coefficients θ_i^* is no longer a trivial problem since the underlying predetermined mathematical model is much more complex, in general, than the simplified model used for time τ_0 . A homotopy function $h(\theta, \omega; t)$ can then be constructed such that at time τ_0 it takes the form of $Q^s(\theta, \omega)$ and at time τ_f it takes the form of $Q^*(\theta, \omega)$:

$$h(\theta, \omega; \tau) \equiv (1 - \tau)Q^s(\theta, \omega) + \tau Q^*(\theta, \omega). \quad (3.5.2)$$

In Chu's work, the functions Q^s and Q^* are not exactly the characteristic polynomials but polynomials associated with the characteristic equations such that, when they are set to zero, the characteristic equations are satisfied identically. The specific form of Q^s taken by Chu was tailored

to the efficient computational solution of the components of a diagonal matrix which was then added to a Jacobi matrix. The formulation presented here, although perhaps not as computationally efficient as Chu's, is directed to deal with stiffness matrices of arbitrary "topology". The homotopy function employed here, h^τ , is different from the one presented by Chu in that it represents the characteristic polynomials of a *time τ -varying* mechanical system:

$$h^\tau(\theta, \omega; \tau) \equiv \left\{ \begin{array}{c} q_1^\tau(\theta, \omega_1; \tau) \\ q_2^\tau(\theta, \omega_2; \tau) \\ \vdots \\ q_{N_{m0}}^\tau(\theta, \omega_{N_{m0}}; \tau) \end{array} \right\} \quad (3.5.3)$$

where

$$q_k^\tau(\theta, \omega_k; \tau) \equiv \det[K^s(\theta) + \tau K^a(\theta) - \omega_k^2 M] \quad (3.5.4)$$

and, assuming M is diagonal,

$$K^s(\theta) = \text{diag}(k_{11}^1 \theta_1, k_{22}^1 \theta_1, \dots, k_{nn}^{N_m} \theta_{N_m}) \quad (3.5.5)$$

and

$$K^a(\theta) = K(\theta) - K^s(\theta). \quad (3.5.6)$$

Representative examples of these will be given in later sections. In this way, the characteristic polynomial at τ_0 is readily determined (since the diagonal matrix K^s has only one θ_i in each of its components) and the characteristic polynomial at τ_f corresponds to Q^* .

The homotopy function $h(\theta, \omega; \tau)$ is nevertheless required to be zero for all times τ . Those paths which connect each of the initial roots θ_i^s of the initial characteristic equation with the roots θ_i^* of the target structure characteristic equation Q^* are called homotopy paths and are defined by the following equations:

$$h(\theta, \omega; \tau) = 0 \quad \forall \tau \in [\tau_0, \tau_f] \quad (3.5.7)$$

which imply

$$\frac{dh}{d\tau} = 0 \quad (3.5.8)$$

where

$$\frac{dh}{d\tau} = \frac{\partial h}{\partial \tau} + \frac{\partial h}{\partial \theta_i} \frac{d\theta_i}{d\tau}. \quad (3.5.9)$$

The latter equality can then be used to formulate an initial value problem for the trajectories for the θ_i :

$$\frac{d\theta_i}{d\tau} = -\frac{\partial h}{\partial \theta_i}^{-1} \frac{\partial h}{\partial \tau} \quad (3.5.10)$$

with initial values $\theta_{i,0} = \theta_i^s$ which are the roots of the characteristic polynomial associated with the simplified structure. After integrating $\frac{d\theta}{dt}$ in the interval $[\tau_0, \tau_f]$, the values of the θ_i approach the values θ_i^* . Integration must be carried in the complex domain since as time τ progresses, the roots of the transient characteristic polynomials are not necessarily real. Neither are the final values θ_i^* required by this method to be real, since the only requirement is that they satisfy the characteristic equations at time τ_f . Complex quantities are then possible solutions (and they may or may not be associated with structural damping) but only the real solutions are of interest here.

No theorems have been developed which guarantee the good behavior of the integration (of equations Eq. (3.5.10)) as there are for Chu's case. In all integrations carried out up to the present moment, however, no signs of ill-conditioned problems arise; these are not expected because of the physical nature of Eq. (3.5.4).

In the numerical procedures, both Euler's and Runge-Kutta's schemes have been employed to solve Eq. (3.5.10) numerically. Some care must be taken, especially for those homotopy paths where the variables θ_i change their character, from purely real to complex. Because of the inaccuracy of both Euler's method and the finite precision of the computer, the solutions turn out to be inexact; but, if the time step $\Delta\tau$ is small, these paths should be close to the true homotopy paths. To track the homotopy paths accurately, especially near these real-to-complex transition points, it is necessary to take the homotopy estimates at τ and then to optimize locally similar to the SUB-ID-Modal approach. No problems arise since the initial estimates for the optimization algorithms are bound to predict accurately the natural frequency values.

Extensions to cases where the number of degrees of freedom exceed the number of parameters (as long as the latter equal the number of observed natural frequencies) is a future topic to be studied. Although not as prohibitive as the probabilistic approach with numerical integration, this method seems to require the evaluation of an excessive ($N_d!$) number of homotopy paths in order to find all possible solutions. Experience with the implementation presented here indicates that for paths that start at real θ values, if these enter the complex domain along the homotopy path, then they remain complex. Complex solutions also come in complex conjugate pairs. So, on some related basis, it may be possible to discard some homotopy paths assuming that only the real solutions for θ are required. There are cases, however, where some of the parameters θ_i have multiple roots at τ_0 . Then, the values for $\theta_i(\tau_0)$ are complex but during the trajectory may eventually become purely real. Also, there is the issue of whether parameters $\theta(\tau_f)$ being slightly imaginary (relative to the real component) qualify since, presumably, small perturbations to the mass or stiffness matrices may then bring the slightly imaginary roots θ_i to the real line. Matrix perturbations should be considered since often the model may not allow for the exact mass or stiffness distributions. These and other related questions are deferred to a later study.

References for Chapter 3

- [3.1] Rall, L.B., *Computational Solution of Nonlinear Operator Equations*, Krieger, Huntington, N.Y., 1979.
- [3.2] Franklin, G.F., Powell, J.D., Workman, M.L., *Digital Control of Dynamic Systems*, Addison Wesley, Reading, Massachusetts, 1990; Chapter 8.
- [3.3] Beck, J.L., "Determining Models of Structures from Earthquake Records", Report EERL 78-01, California Institute of Technology, Pasadena, California, 1978.
- [3.4] Franklin, J.N., *Matrix Theory*, Prentice-Hall, Englewood Cliffs, N.J., 1968.
- [3.5] Dongarra, J.J., Moler, C.B., Bunch, J.R., Stewart, G.W., *EISPACK Users' Guide*, SIAM, Philadelphia, PA, 1979.
- [3.6] Astrom, K.J., Eykhoff, P., "System Identification - A Survey", *Automatica*, Vol. 7, 1971, p. 123.
- [3.7] Masri, S.F., Werner, S.D., "An Evaluation of a Class of Practical Optimization Techniques for Structural Dynamics Applications", Report R-8222-5817, Agbabian Associates, El Segundo, California, 1985.
- [3.8] Polak, E., *Computational Methods in Optimization*, Academic Press, N.Y., 1971.
- [3.9] Jayakumar, P., "Modeling and Identification in Structural Dynamics", Report EERL 87-01, California Institute of Technology, Pasadena, California, May 1987.
- [3.10] Zeidler, E., *Nonlinear Functional Analysis and its Applications, Vol. III: Variational Methods and Optimization*, Springer-Verlag, N.Y., 1984.
- [3.11] Snyder, V.W., "Structural Modification and Modal Analysis - A Survey", *International Journal of Modal Analysis*, January 1986.
- [3.12] McVerry, G.H., "Frequency Domain Identification of Structural Models from Earthquake Records", Report EERL 79-02, California Institute of Technology, Pasadena, California, October 1979.
- [3.13] Beck, J.L., Personal Communication, 1987.
- [3.14] Baldwin, J.F., Hutton S.G., "Natural Modes of Modified Structures", *AIAA Journal*, Vol. 23, No. 11, 1985, p. 1737.
- [3.15] Fox, R.L., Kapoor, M.P., "Rates of Change of Eigenvalues and Eigenvectors", *AIAA Journal*, Vol. 6, 1968, p. 2426.
- [3.16] Beck, J.L., "Statistical System Identification of Structures", *Proceedings of the 5th International Conference on Structural Safety and Reliability*, August 1989.
- [3.17] Box, D.E.P., Tiao, G.C., *Bayesian Inference in Statistical Analysis*, Addison-Wesley, Reading, Massachusetts, 1973.
- [3.18] Chu, M.T., "Solving Additive Inverse Eigenvalue Problems for Symmetric Matrices by the Homotopy Method", *IMA Journal of Numerical Analysis*, Vol. 9, 1990, p. 331.
- [3.19] Werner, S., Beck, J.L., Levine, M.B., "Seismic Response Evaluation of Meloland Road Overpass Using 1979 Imperial Valley Earthquake Records", *International Journal of Earthquake Engineering and Structural Analysis*, Vol. 15, 1987, p. 249.

Chapter 4 : Simulated Data

The results of a large number of numerical experiments are presented in this chapter. These tests with simulated data were chosen as a testing procedure for various reasons: (1) all independent variables can be controlled and thus varied independently; (2) there is such a concept of “correct model” to judge the accuracy of the procedures, since a model is employed to generate the “observed” response of the structure, i.e., model error can be eliminated; (3) numerical tests are economical to perform. It is understood, on the other hand, that numerical tests cannot conclusively validate any method which is meant to be used ultimately with real data; but they can serve as a useful first check on proposed methods.

The aim of these experiments is to test the properties of the different parameter estimation algorithms under different conditions and to foresee any potential problems that may be encountered when treating real data. Among the properties of interest are: (1) robustness: this property deals with the stability of the parameter estimates when the conditions are not optimum, e.g., in the presence of noise; (2) uniqueness: the parameter estimates may not be unique and this fact may not show up in the results of each algorithm; (3) detection of stiffness loss: although the stiffness parameter estimates may not be “readily intuitive”, the algorithm should be able to detect localized changes in the stiffness. For damage detection purposes, this is the most important feature; (4) determination of interplay between the properties of the mechanical system and ill-conditioning in the numerics leading to erroneous parameter estimation.

Because of the large volume of numerical tests and results, data is presented in the following way:

1. All parameter estimation algorithms are employed to generate estimates for the structural identification problem of a 2 degree-of-freedom chain system. Analytical expressions are available that characterize this model exactly. This system is particularly attractive since it presents many “difficult” features present in much larger problems. This system is also attractive since it is not computationally demanding and thus all algorithms can be employed.
2. A reduced number of algorithms is used for larger problems since only those which are more computationally efficient are examined. The types of structures which are used as systems

are: 10 degree-of-freedom chain models, and 20 degree-of-freedom beams. These systems are considered to present representative problems associated with real engineering systems. Testing these structures under all conditions is an enormous task especially since the larger systems require very large computation times. The tests performed on the structures are enough to convey an idea of what the problem areas are in the identification of structural parameters. One section is devoted to each of the major problem areas and illustrative examples are provided.

In the following set of simulations, the mass matrix is assumed to be known and thus is kept constant throughout the identification process. The assumption that the mass is known is made in order to improve the uniqueness and convergence rate for the solutions. In practice, good knowledge of the mass distribution is available for most structures from the structural drawings. For offshore structures, however, the estimation of mass factors may be necessary since these structures present time-varying mass distribution histories through fluid-structure interaction. Other conditions under which the simulations are performed are described at the beginning of each of the sections below.

Characteristic of this study is that for each simulation, only one sample set of excitation-response signals is employed to determine the values of the different parameters. A reason for doing this is, in part, because of the orientation of this research to earthquake engineering applications. In the earthquake problem, researchers are often restricted to excitation-response signals from only one earthquake. Data for other structures, e.g., offshore and space structures, is more abundant since, in general, there are more available resources. For the methodologies presented in this study, additional data can always be easily incorporated into the parameter estimation procedure.

Section 4.1 - Chain Model Simulations

The chain model (or “shear building”) is a useful tool in earthquake engineering since framed and other structures present natural frequencies which vary in similar proportions to the natural frequencies associated with a uniform chain model. Fig. (4.1ab) shows two typical structures which are modeled with the chain system in Fig. (4.1c).

The degrees of freedom of the prototype model of Fig. (4.1c) are numbered starting from next to the base to the topmost degree of freedom, or “roof.” The stiffness matrix associated with the mechanical model is tri-diagonal while the mass matrix is diagonal. The dynamic response of the structure to both base “earthquake-like” loading or roof “shaker-like” loading is calculated using the modal approach mentioned in Section 2.2.3. All characteristics describing the tests are presented at the beginning of each section below.

A property of the chain model is that it is able to match arbitrary response histories generated by many other linear models. Although the match is fairly good for a specific excitation, it may

not be true that the identified model will produce good matches for other excitations. Likewise, the stiffness values obtained from a specific *dynamic* structure identification run may be significantly different from another one using *static* test results, the latter being the easiest to interpret. In order for the chain system to be a good overall and reliable structural building model, the building structure should have columns of high axial stiffness *and* beams of high bending stiffness. Under these circumstances, a frame structure's interstory stiffness is reasonably approximated by a chain model's, both statically and dynamically.

Section 4.1.1 - Simulation with a 2-DOF Chain System

The two-degree-of-freedom chain system is used here to determine the characteristics of each of the methods mentioned in the previous chapter. The chain system has many properties which are also present in large systems and which make the identification of the system difficult.

The goal of each of the methods is to determine the stiffness distribution over the "height" of the structure. The data falls in two categories: modal parameters and response time histories. Modal data consists of the modal frequencies, modeshapes and participation factors. Response data consists of the type of quantities measured and the locations where these are measured. There are six data sets from which stiffness estimates are determined in this section:

- (A) Fundamental mode, 1st degree of freedom measured.
- (B) Fundamental mode, 2nd degree of freedom measured.
- (C) Fundamental mode, both degrees of freedom measured.
- (D) Two modes, 1st degree of freedom measured.
- (E) Two modes, 2nd degree of freedom measured.
- (F) Two modes, both degrees of freedom measured.

The success of each method depends mainly on the data available. Uniqueness also depends on the data employed. Results from Udwadia et al. [4.1] predict that when all modes are excited and measurements have been performed at the first floor (as in sets D and F), then uniqueness can be guaranteed. Udwadia et al. have also shown that for set E, non-unique parameter estimates are to be expected.

Section 4.1.1.1 - Characteristics of the Two-Degree-of-Freedom Chain System

The modal equations of motion for the linear system shown in Fig. (4.2) are

$$\begin{bmatrix} (\theta_1 k_1 + \theta_2 k_2) & -\theta_2 k_2 \\ -\theta_2 k_2 & \theta_2 k_2 \end{bmatrix} \phi^r = \omega_r^2 \begin{bmatrix} m_1 & 0 \\ 0 & m_2 \end{bmatrix} \phi^r \quad (4.1.1)$$

for the r^{th} mode of vibration, $r = 1, 2$. k_1 is the nominal stiffness between the ground and the first mass (or first story stiffness) and k_2 is the nominal stiffness between the first and second masses (second story). The θ_1 and θ_2 are the stiffness factors which modify the nominal values to adjust to system observations. The $\omega_r^2 = constant$ curves in the θ plane can be easily found by expanding the expression for the determinant and rearranging:

$$[\theta_1 k_1 - \omega_r^2 (m_1 + m_2)] [\theta_2 k_2 - \omega_r^2 m_2] = \omega_r^4 m_2^2, \quad r = 1, 2. \quad (4.1.2)$$

Solving these equations for the eigenvalue ω_r^2 yields the following relations:

$$\begin{aligned} 2\omega_1^2 &= \frac{\theta_1 k_1}{m_1} + \frac{\theta_2 k_2}{m_1} + \frac{\theta_2 k_2}{m_2} - \left[-\frac{4\theta_1 \theta_2 k_1 k_2}{m_1 m_2} + \left(\frac{\theta_1 k_1}{m_1} + \frac{\theta_2 k_2}{m_1} + \frac{\theta_2 k_2}{m_2} \right)^2 \right]^{\frac{1}{2}} \\ 2\omega_2^2 &= \frac{\theta_1 k_1}{m_1} + \frac{\theta_2 k_2}{m_1} + \frac{\theta_2 k_2}{m_2} + \left[-\frac{4\theta_1 \theta_2 k_1 k_2}{m_1 m_2} + \left(\frac{\theta_1 k_1}{m_1} + \frac{\theta_2 k_2}{m_1} + \frac{\theta_2 k_2}{m_2} \right)^2 \right]^{\frac{1}{2}}. \end{aligned} \quad (4.1.3)$$

Assuming that an initial “undamaged” system at $\theta = (1, 1)$ has been weakened and now has stiffness parameters $\theta = (0.5, 0.5)$, it is possible to calculate readily the two frequencies associated with this weakened state. In the example treated here, $m_1 = m_2 = k_1 = k_2 = 1$. The dynamic characteristics of the 2 degree-of-freedom chain system are given by

$$\begin{aligned} \omega_1^{*2} &= \frac{3-\sqrt{5}}{2} \approx 0.191 \\ \omega_2^{*2} &= \frac{3+\sqrt{5}}{2} \approx 1.309 \end{aligned} \quad (4.1.4)$$

The type of problems that this study addresses are those whose goal is to find the values θ_i given the time histories of the excitations and responses, or the modal data. Using Eq. (4.1.2) above and matching the data in Eq. (4.1.4) produces two sets of curves shown in Fig. (4.3). The two sets of curves are described by

$$\begin{aligned} (\theta_1 - 2\omega_1^{*2}) (\theta_2 - \omega_1^{*2}) &= \omega_1^{4*} \\ (\theta_1 - 2\omega_2^{*2}) (\theta_2 - \omega_2^{*2}) &= \omega_2^{4*}. \end{aligned} \quad (4.1.5)$$

The first of Eq. (4.1.5) corresponds to loci of θ values denoted “Curve 1” while the second expression corresponds to “Curve 2.” The particular geometries exhibited by these curves demonstrate that certain problems related to uniqueness can easily arise even from simple low-degree-of-freedom systems. In the last figure, it can be clearly seen that there are two vector points $\theta^1 = (0.5, 0.5)$ and $\theta^2 = (1.0, 0.25)$ such that both conditions $\omega_1^2 = 0.191$ and $\omega_2^2 = 1.309$ are simultaneously satisfied. The interpretation of the Curve 1a in the same figure is that all

the corresponding θ_i values have a fundamental mode whose frequency equals ω_1^* . Curve 1b corresponds to the values of θ whose *second* modal frequency equals ω_1^* . Curves 2a and 2b have similar interpretation, i.e., curve 2a corresponds to values of θ_i such that the fundamental mode has an associated frequency ω_2^* . Curve 2b corresponds to the second mode. It is noticed that Curves 1a and 1b do not overlap; these curves actually asymptotically approach $\theta_1 = 2\omega_1^{*2}$ and $\theta_2 = \omega_1^{*2}$ as $\theta_2 \rightarrow \pm \infty$ and $\theta_1 \rightarrow \pm \infty$, respectively. Likewise, there is an asymptote at $\theta_1 = 2\omega_2^{*2}$ and $\theta_2 = \omega_2^{*2}$ for Curves 2a and 2b as $\theta_2 \rightarrow \pm \infty$ and $\theta_1 \rightarrow \pm \infty$. The only two curves that can intersect are Curves 1a and 2b. Choosing the natural frequencies in an arbitrary fashion allows the number of possible solution vectors θ to be two, one or zero. The number of solutions depends on whether the curves associated with each of these frequencies can intersect or at least make contact with each other.

The two points θ^1 and θ^2 are both at the intersection of Curves 1a and 2b, i.e., points where $\omega_1^2 = 0.191$ and $\omega_2^2 = 1.309$, respectively. Whether the two models given by these θ values actually predict the same acceleration time histories or not depends on which degrees of freedom are observed. Besides having the same frequencies, these two models have the same top degree-of-freedom effective participation factors, which implies that the two time histories at this degree of freedom are equal [4.2]. If the response is recorded at the top degree of freedom only, there is no possible way to distinguish which of the two θ^i solutions is the correct one. In this case, additional information coming from the first degree of freedom clears all ambiguity since the effective participation factors there are distinct for the two models. Thus, for any base excitation, the response at the first degree of freedom is different for the two models. Comparison of acceleration signals is shown in Fig. (4.4) for a broad band excitation, showing that the response for the two θ_i solutions is indistinguishable at the top degree of freedom (Fig. (4.4a)).

Local uniqueness can be enforced whenever the gradients to the $\omega = \text{constant}$ curves do not both lie in parallel. This is the case for the solution points θ^1 and θ^2 . Numerically, it may be difficult to reach the true minimum with an optimization algorithm since the two nearly tangent curves induce a very flat local topology.

Section 4.1.1.2 - Method of Successive Substitutions

The "SUB-ID-SS" algorithm of successive substitutions is applied to the 2-DOF Chain problem. The chain system is undamaged originally at $\theta^0 = (1, 1)$ and then is weakened to $\theta^* = (0.5, 0.5)$. The method uses only natural frequencies and modeshapes. When the number of observed degrees of freedom is one, the method uses, essentially, only frequency data. In this case, the only component of the observed modeshape vector does not contribute any information since this vector is normalized prior to any comparison.

The operator $F(\theta)$ for this model will map a point in the (θ_1, θ_2) space to another point in the same space. The particular form of the operator depends on what information is available. For the chain system of Fig. 4.2, assuming that the mass distribution is known and that the two modal frequencies correspond to the system $\theta = (0.5, 0.5)$, the contraction-like operator F about the point θ^0 is given by very large expressions (not shown here) obtained with WRI's *Mathematica* [4.3] computer program. Even for the simplest model, the analytical aspects of the operator F are not easily derivable, namely, to prove that $F(\theta)$ is a contraction in Θ^c if for $\delta \in [0, 1)$,

$$\|F(\theta^u) - F(\theta^v)\| \leq \delta \|\theta^u - \theta^v\|, \quad \forall \theta^u, \theta^v \in \Theta^c;$$

so the convergence aspects of the sequence are studied a posteriori. The region of interest Θ^c in this case would be $0 \leq \theta_i \leq 1$, nominally, or perhaps $0 \leq \theta_i \leq 1.5$ to accommodate for large model errors.

Table (4.1) presents the solutions for various combinations of modal information versus degree-of-freedom information. The estimates should converge to the correct value of $\theta^* = (0.5, 0.5)$ since this is the "damaged" configuration.

Since the form of the operator $F(\theta)$ is the same when only modal frequency is used, Sets A and B in Table (4.1) yield the same results: convergence is achieved in one iteration to θ values which yield a fundamental frequency equal to the one at $\theta^* = (0.5, 0.5)$. There is no uniqueness as can be seen since all three converged values are different and yet the convergence criteria is strictly enforced. In fact, any point on curve 1a of Fig. (4.3) would be equally useful. Had the effective participation factors been incorporated into the formulation of the operator $F(\theta)$, a distinction between sets A and B would be evident (since these factors are different at each of the two degrees of freedom).

Set C presents the case where both components of the fundamental modeshape vector are known. This case, as well as case F, below, corresponds to full knowledge of the eigenvector and thus a linear system of equations is constructed. From this, the resulting $\theta^* = (0.5, 0.5)$ is obtained along with a condition number for matrix S indicating that the first eigenvector contains enough information to guarantee uniqueness.

Sets D and E show that if two modes are measured at only one of the two degrees of freedom, either of two possible solutions is obtained. These two solutions, $\theta^1 = (0.5, 0.5)$ and $\theta^2 = (1, 0.25)$ correspond to θ values for which both frequencies are the same. Disregarding Fig. (4.3) (which clearly indicates that there are only two solutions) or any other theoretical information, it is impossible to guarantee that there are only two solutions. There seems to be local uniqueness around the converged values since the condition numbers corresponding to the sets are non-zero.

Set F presents the same results as Set C: the point $\theta^* = (0.5, 0.5)$ is uniquely determined since matrix for the set of linear equations is independent of θ . With more than one complete modeshape

vector, the rank of the new matrix can only increase and thus if set C yields the correct result, set F also yields the same result. In the presence of noise, parameter estimates may not be exact, so with less ill-conditioning it is expected that set F would provide better results than set C.

Section 4.1.1.3 - Generalized Least-Squares, Output Error, Modal Domain

The "SUB-ID-Modal" code only uses frequency and modeshape modal data. Table (4.2) presents the comparison among the various test sets. The modal data comprising the natural frequencies and modeshape vectors (and disregarding the damping and participation factors) are obtained from the modal superposition program. The Fletcher-Reeves minimization technique with finite difference gradient evaluations was employed for the modal domain. The error index referred to in this section corresponds to J_M defined in Eq. (3.3.2.)

As in the method of successive substitutions, sets A and B share the same results since the known modeshape vector can only be known up to a constant. Since sets A and B assume knowledge of only one modeshape component, its absolute magnitude is meaningless. This same circumstance is also present in sets D and E. Thus, only modal frequency data is available in these four cases. The full modeshape does provide additional information in sets C and F.

Matching only one frequency can be easily done in practice. Sets A and B show that convergence is achieved to θ values for which the fundamental frequency equals that for $\theta = (0.5, 0.5)$. The resulting parameter estimates, however, are incorrect. There are no unique values of θ as solutions to this dataset. As before, any point on Curve 1a in Fig. (4.3) is consistent with assumed modal data.

Set C which contains knowledge of all modeshape components shows convergence to the exact θ^* although the number of iterates needed is large. Sets D and E contain more modal frequency information but converge to two θ values: $\theta^* = (0.5, 0.5)$ and $\theta^* = (1.0, 0.25)$. As mentioned in other sections, these two values θ share the same frequencies.

Finally, set F makes use of all frequency and modeshape information to converge to the exact $\theta^* = (0.5, 0.5)$ in about the same number of iterations as for the other sets, a number which is large.

Section 4.1.1.4 - Generalized Least-Squares, Output Error, Time Domain

The 2-DOF chain system is considered again but here it is excited by a broad band excitation at the base. Fig. (4.4c) and Fig. (4.4d) show the Fourier amplitude of the response at the top degree of freedom and the Fourier amplitude of the excitation. The responses decay to small amplitudes towards the end of the signals. The empirical (i.e., numerically calculated) transfer function between the base motion and that at the top degree of freedom is shown in Fig. (4.2b).

Table (4.3) shows the results for the time-domain output error approach implemented in the “SUB-ID-Time” algorithm. The Polak-Ribiere minimization technique with analytical gradient evaluations was employed to arrive at the results. The error index referred to here corresponds to J_T defined in Eq. (3.3.1.)

Set A values converge to the exact results for all initial values of θ tested. Set B does not converge to the exact results although it converges to values which match the fundamental mode up to four significant figures. It must be recalled that Curve 1a in Fig. (4.3) is a locus of θ values which have the same fundamental frequency. If in addition to this, the participation factor is a slowly varying function of θ along this curve then it is conceivable that there is accentuated ill-conditioning along this locus. Ill-conditioning almost always causes spurious premature convergence of the optimization procedure. The objective function $J_T(\theta_1, \theta_2)$ is contour plotted in Fig. (4.5.) The ill-conditioning in the plot is the so-called “banana-shaped” valley which follows curve 1a in Fig. (4.3) and whose valley floor is nearly flat. All other sets contain information in excess of the information present in Set A. This allows SUB-ID-Time to reach the correct, unique solution without any further complications.

Section 4.1.1.5 - Bayesian Approach

The application of the Bayesian approach to the SUB-ID problem is very convenient because it assigns a probability value to each value of θ . This probability distribution function is far more informative than just the most probable value, which is effectively what SUB-ID-Time and SUB-ID-Modal produce.

Fig. (4.6) shows six plots (Sets A-F) derived from the “SUB-ID-Prob” algorithm in which different amount of modal and response information are considered. Each plot is a plot of the probability of θ as a function of θ itself and on an actual set of data. These data are the same as those used for the study of other identification methodologies, namely, a 1024 point (204.8 sec), broad-band, earthquake-like amplitude acceleration at the base. In the absence of noise and model error, the prediction error variances of Eq. (3.4.18) would be zero, causing an unrealistic spiked function to appear. Since this is not typical of real processes, 10% r.m.s. noise in the form of Gaussian-white noise is added to the system signals.

Sets A-C correspond to knowledge of the fundamental frequency while sets D-F correspond to knowledge of the two modal frequencies. Set A makes use of the response at the first degree of freedom of the 2-DOF chain system. It identifies the most probable value of $\hat{\theta} = (0.5, 0.5)$ and gives little or no probability of occurrence to most other values. Set B makes use of the response signal at the top degree of freedom. It is seen in Fig. (4.6b) that the pseudo-probability is non-zero for values of θ where $\omega_1^2 = \hat{\omega}_1^{2*} = 0.191$ and it reaches two peaks: one at $\theta = (0.5, 0.5)$ and the

other at $\theta = (1, 0.25)$ (the other peaks being caused by the discretization of the plot surface but actually form a continuous ridge from one peak to the other). The locus of points lying at the crest of the $\omega_1^2 = \hat{\omega}_1^{2*}$ ridge form the inverse of a “banana” valley.

Sets C (first mode, both responses), D (two modes, first DOF response), and F (both modes, both responses), present no identification problems. Set C, however, still shows traces of the locus of constant fundamental frequency due to the dominant contribution of the fundamental mode in the top-degree-of-freedom response. Set E (two modes, response at the top degree of freedom), again presents similar behavior as in set B, although the peaks at $\theta = (0.5, 0.5)$ and $\theta = (1, 0.25)$ are more pronounced. The addition of the second mode in set E eliminates the intermediate points. The probability value at the two peaks are equal, meaning that based on the given data alone (two modes and the top response) the two models are equally probable. This is expected since the model response is the same at the two values of θ .

Set F, although it emphasizes the correct $\theta^* = (0.5, 0.5)$ solution, presents a small local maximum at the other critical θ , i.e., $\theta^* = (1, 0.25)$. Optimization algorithms may, if started very close to $\theta = (1, 0.25)$, converge “inadequately” to this second possibility. In the latter case, choosing a different starting condition would, most probably, converge to the global maximum.

For damage detection purposes, the pseudo-marginal distributions would definitely be dominated by the peak at $\theta = (0.5, 0.5)$ and, if existent, at $\theta = (1, 0.25)$. Fig. (4.7gh) shows marginal distributions for θ_1 and θ_2 for Set B corresponding to the complete set. The “complete” case employs probability values evaluated at the grid $\theta_i = (n - 1)\Delta\theta_i$ for $n = 1, 2, \dots, 20$ with $\Delta\theta_i = 0.05$. The marginal distributions are constructed by integrating out the other θ_i . This process is a special projection of the higher-dimensional plot to one dimension. θ_1 peaks at around 0.45 and then it decays slowly away from this value. This indicates that it is very plausible that the structure has weakened. Looking at the marginal distribution for θ_2 it is clear that it has also “failed” since the most probable value occurs at $\theta_2 \approx 0.25$. In either case, stiffness loss is conclusive.

If the distributions are highly dominated by the values at the true peaks $\theta = (0.5, 0.5)$ and $\theta = (1, 0.35)$, it may be more convenient to search for the most probable values and not have to exhaustively search through all the Θ space. Procedures to do this have been implemented as in the least-squares method but it is known that not all peaks are guaranteed to be found. If the most probable values are found, however, then local distributions can be calculated for each peak. The pseudo-marginal distributions corresponding to the two peaks of the 2-DOF chain model are shown in Fig. (4.7abcd.) In the last figures, “P1” denotes marginals derived from probability data in the neighborhood of $\theta = (0.5, 0.5)$ and “P2”, likewise, from the neighborhood of $\theta = (1, 0.25)$. The “P1+P2” case employs both neighborhoods. These distributions are referred to as “partial” since they ignore θ values not close to the peaks. The addition of all partial marginal distributions is

also shown in Fig. (4.7e) and Fig. (4.7f) . Comparison between partial and actual distributions shows that the most probable values of θ_1 and θ_2 are well represented in the partial marginals and somewhat more blurred in the actual marginals, as is expected. From the P1+P2 marginals it can be inferred that the plausibility of damage is high, although the marginal for θ_1 shows slight probability that it is not damaged.

Section 4.1.1.6 - Homotopy Method

The homotopy algorithm (“SUB-ID-H”) is applied to the previously described 2-DOF chain system. The weakened $\theta^* = (0.5, 0.5)$ configuration is considered. The method uses only the natural frequencies but any predictions can then be ratified by comparing the model’s response with any other available information.

The particular form of the system of ordinary differential equations depends on the choice of the characteristic polynomial associated with the “simplified structure.” In this case, the stiffness matrix K^s takes the form:

$$K^s(\theta) = \begin{bmatrix} \theta_1 k_1 & 0 \\ 0 & \theta_2 k_2 \end{bmatrix} \quad (4.1.6)$$

while the stiffness matrix at τ_f , K^a , is just the difference between $K(\theta)$ and $K^s(\theta)$. The resulting transient stiffness matrix corresponding to homotopy time τ is then

$$K^\tau(\theta, \tau) = \begin{bmatrix} \theta_1 k_1 + \tau \theta_2 k_2 & -\tau \theta_2 k_2 \\ -\tau \theta_2 k_2 & \theta_2 k_2 \end{bmatrix}. \quad (4.1.7)$$

From this expression it can be verified that at $\tau_0 = 0$ the stiffness matrix corresponds to $K^s(\theta)$, a simple structure with each mass attached to a base by a single spring, and at $\tau_f = 1$ the stiffness matrix corresponds to the two degree-of-freedom chain system under study. Assuming, as before, that $m_1 = m_2 = k_1 = k_2 = 1$, the transient characteristic polynomial for mode i is

$$q^\tau(\theta_1, \theta_2, \omega_i; \tau) = (\theta_1 + \tau \theta_2 - \omega_i^2)(\theta_2 - \omega_i^2) - \tau^2 \theta_2^2. \quad (4.1.8)$$

The construction of the homotopy function $h(\theta, \omega; \tau)$ is now straight forward:

$$h(\theta, \omega; \tau) = \begin{Bmatrix} (\theta_1 + \tau \theta_2 - \omega_1^2)(\theta_2 - \omega_1^2) - \tau^2 \theta_2^2 \\ (\theta_1 + \tau \theta_2 - \omega_2^2)(\theta_2 - \omega_2^2) - \tau^2 \theta_2^2 \end{Bmatrix}. \quad (4.1.9)$$

It is clearly seen from the last equation that the homotopy function’s dependence on the parameter τ is quadratic, significantly different from Chu’s formulation [4.6]. The set of ordinary differential equations for the vector $\frac{d\theta}{d\tau}$ associated with the 2 DOF chain model (see Eq. (3.5.9),) as determined by *Mathematica* [4.3], takes the form

$$\frac{d\theta_1}{d\tau} = \left\{ -\frac{(-\omega_2^2 - \omega_2^2 \tau \theta_1 + 2\tau \theta_2 - 2\tau^2 \theta_2)(-\omega_1^2 \theta_2) + \theta_2^2 - 2t \theta_2^2}{-(\omega_1^2 \theta_1) + \omega_2^2 \theta_1 + \omega_1^2 \theta_2 \omega_2^2 \theta_2 - \omega_1^2 \tau \theta_2 + \omega_2^2 \tau \theta_2 + 2\omega_1^2 \tau^2 \theta_2 - 2\omega_2^2 \tau^2 \theta_2} \right\}$$

$$\frac{d\theta_2}{d\tau} = \left\{ \frac{(\omega_1^2 + \omega_1^2\tau - \theta_1 - 2\tau\theta_2 + 2\tau^2\theta_2) (- (\omega_2^2\theta_2) + \theta_2^2 - 2\tau\theta_2^2)}{-(\omega_1^2\theta_1) + \omega_2^2\theta_1 + \omega_1^2\theta_2 - \omega_2^2\theta_2 - \omega_1^2\tau\theta_2 + \omega_2^2\tau\theta_2 + 2\omega_1^2\tau^2\theta_2 - 2\omega_2^2\tau^2\theta_2} \right\} \\ - \left\{ \frac{(\omega_2^2 - \theta_2) (- (\omega_1^2\theta_2) + \theta_2^2 - 2\tau\theta_2^2)}{-(\omega_1^2\theta_1) + \omega_2^2\theta_1 + \omega_1^2\theta_2 - \omega_2^2\theta_2 - \omega_1^2\tau\theta_2 + \omega_2^2\tau\theta_2 + 2\omega_1^2\tau^2\theta_2 - 2\omega_2^2\tau^2\theta_2} \right. \\ \left. - \frac{(-\omega_1^2 + \theta_2) (- (\omega_2^2\theta_2) + \theta_2^2 - 2\tau\theta_2^2)}{-(\omega_1^2\theta_1) + \omega_2^2\theta_1 + \omega_1^2\theta_2 - \omega_2^2\theta_2 - \omega_1^2\tau\theta_2 + \omega_2^2\tau\theta_2 + 2\omega_1^2\tau^2\theta_2 - 2\omega_2^2\tau^2\theta_2} \right\}. \quad (4.1.10)$$

The integration of the above equations with two starting initial conditions (associated with the roots θ_i^s of the simplified structure) yield two homotopy paths in the $(\theta_1, \theta_2, \tau)$ space. Such paths are shown in Fig. (4.8) where it can be seen that the initial roots are connected to the roots of the characteristic polynomial of the chain system, $\theta^1 = (0.5, 0.5)$ and $\theta^2 = (1, 0.25)$. Whether the two roots satisfy the observed mode-shapes and/or participation factors can be verified by direct substitution into the model and calculation of these quantities.

As has already been discussed, θ^1 is a solution for all sets (A-F) while the other (non-unique) solution, θ^2 , is only a solution for sets B and E even if the participation factors are taken into account.

Section 4.1.1.7 - Summary for the 2-DOF Chain System

The method of successive substitutions and the modal output error method rely on the data in similar ways and their predictions are similar. Neither makes use of the participation factor information so they do not perform well when only one degree of freedom is monitored, converging to any value θ which shares the same natural frequency. The time output error approach makes use of the participation factor in an implicit manner (since the latter is needed to calculate the response of the model) and so it is not as sensitive to ill-conditioning as the previous two methods, but neither of the three address the non-uniqueness issue, formally. The Bayesian approach gives the most information. The joint probability distribution has been projected onto a two-dimensional plot of θ_i versus pseudo-probability, for all sub-structures present. From this plot, it is easy to determine the state of the system. Non-uniqueness can also be identified as long as a relatively fine grid is used. The finer the grid, the more computing time needed; the fine grid used here made the Bayes method the most computationally demanding method. The homotopy method is restrictive in that there should be as many observed natural frequencies as there are parameters θ_i . The method does, however, identify exactly all non-unique solutions.

Section 4.1.2 - Simulation with a 10-DOF Chain Model

The time output-error approach is the primary tool used in the following identification runs. The modal output error does not take full advantage of the data (i.e., no use of effective participation

factors) nor does the method of successive substitutions; the latter has also proven to be non-convergent in certain situations. The probabilistic approach is the most informative but requires excessive computational times when the number of structural parameters becomes larger. The homotopy method appears to have considerable potential but further study is needed to examine potential shortcomings of the technique (such as the considerable amount of computational effort required). Although uniqueness is still an area which is not fully resolved by the output-error approaches, they do provide a compromise between computational efficiency and reliability. Program SUB-ID-Time has been employed to calculate the stiffness parameter estimates for the 10-DOF chain system under different circumstances. The Polak-Ribiere minimization technique with analytical gradient evaluation was employed in all SUB-ID-Time tests, except in those where noise was added. In these, the gradient evaluations were performed using the finite differences scheme previously mentioned.

The conditions for most tests are nearly constant with only one or two variables changing in each test. The “standard conditions” are the following: the excitation is placed either at the base as a prescribed base acceleration (“base excitation”) or at the top degree of freedom of the structure as a force (“roof excitation”). Accelerations are monitored at all ten degrees of freedom of the system. Possible errors in real signals such as noise, lack of synchronization or miscalibration are present in the “standard” simulated signals. The excitation signal shown in Fig. (4.9) is applied in most numerical tests both at the base and at the top degree of freedom. The signals consist of 1024 time points with $\Delta t = 0.02$ sec. yielding a 20.48 second duration signal, approximately 10 times the fundamental period. The signal is Gaussian distributed in time multiplied by a time envelope decaying to zero amplitude at 10.24 sec. The excitation is broad-band in the frequency domain with a Nyquist frequency of 25 Hz, nearly twice the largest natural frequency of the system ($f_{10} \approx 10Hz$). Damage is represented by a stiffness degradation of approximately 27% in the second and third interstory levels, and 11% in the fourth level. This pattern is chosen to model the complete flexural stiffness degradation of four columns in level 2, four columns in level 3 and one column in level 4 in a typical ten-story, ten-bay building structure. In this way, the stiffness at the damaged stories reduces to approximately 7/11, 7/11 and 10/11 of the nominal interstory stiffness, respectively. The structural characteristics typical of the 10 degree-of-freedom chain system under consideration are shown in Table (4.4). The effects of the “damage” (or weakening of some members) on the *structural* and *modal* parameters are also shown in the same table. The effects of the weakening on the *response* signals are shown in Fig. (4.10) which shows the response of the undamaged and damaged system to the excitation. The qualitative nature of the responses does not clearly indicate the considerable loss of stiffness in the second, third, and fourth inter-story levels.

Section 4.1.2.1 - Frequency Content of the Excitation

The effects of bandwidth of the excitation are shown by examining both frequency content and excitation location.

Procedure and Results: Two frequency bands are chosen in order to observe the influence of frequency content on the parameter estimates. The “low” frequency signal contains frequencies in the range 0 to 2 Hz. From the transfer function plots presented in Fig. (4.11), it can be seen that only the first mode can be significantly excited. The “high” frequency signal contains frequencies in the range 0 to 25 Hz as shown previously in Fig. (4.9). The identification results for both the roof and the base-excitation cases are shown in Table (4.5). The manner in which each excitation case participates in the response can be clearly seen in the transfer function plots in Fig. (4.11). These plots show that roof excitation excites practically all modes of vibration while base excitation excites primarily the first three or four modes (for the case of a uniform chain model). If the structure was moderately damped and was to be excited with a sinusoidal signal with a constant frequency equal to that of a natural mode of the system, then that frequency will be dominant in the response. For reasons similar to those discussed in the two-degree-of-freedom case, generally there are large number of θ vectors which have this same natural frequency in common. All of these models having the same natural frequency are referred to as “similar models.” Since the participation factor does not vary rapidly with variations in θ_i (for moderate ranges of the latter), then the response of any similar model can be similar to the original model. The output error approach can rapidly find a similar model. To try to find the point of lowest output error corresponds to moving tangentially along a flat banana valley. This flat banana valley now corresponds to the locus of points in ten-dimensional θ space, all points sharing this same natural frequency. In the base excitation case, the system “filters” the excitation signal and produces a nearly monochromatic response with the dominant frequency equal to the fundamental frequency of the structure, then, as argued above, a large number of other models can produce nearly the same response. The optimization algorithm then tends to prematurely converge to one of these models which give a small output error. In the roof case, however, there are more modes participating in the response and convergence is better behaved. For each modal frequency alone there is a flat banana valley, but for the joint problem with multiple frequencies in the output, there is a “superposition” of flat banana valleys. Most of these banana valleys have the same characteristics in that they concave out from the origin, although not all of these higher dimensional banana valleys coincide exactly. Also, higher modes may also present convex curves such as Curve 2b in Fig. (4.3.) The end result of this superposition is that the joint banana valley is now defined along a locus different from the individual banana valleys corresponding to the individual modes. The level of flatness decreases with the amount of separation among the different individual banana valleys. If the flatness of the joint banana valley has been removed, then the optimization algorithm converges at a much faster rate than before and without premature convergence. There may be situations where if there are four modes participating simultaneously in the response, the optimization algorithm may converge matching three frequencies correctly but

not the fourth, hence, yielding significant parameter errors and output error. These cases have not occurred in the actual tests, even in those cases where large departures are common.

The parameter matches in Table (4.5) are very good in all cases. The low values of the error index indicate almost perfect fit to the target signals. The worst parameter identification case corresponds to the low-frequency base-excitation signal (within 1.2% from the exact) while the other cases are nearly exact. As expected, the smaller the high frequency content in the output signal, the lower the resolution and, thus, the slower the rate of convergence with possible premature convergence.

Section 4.1.2.2 - Duration of the Excitation

The effect of duration of the excitation on the accuracy of the stiffness estimates is examined in the absence of noise.

Procedure and Results: Standard test conditions apply. The duration of the excitation seems not to corrupt the results for all recording times greater than 0.7 of the fundamental period. In the absence of noise, the stiffness estimates agreed with the exact values to within 0.001 for durations as small as a quarter of a fundamental period.

Section 4.1.2.3 - Selection of Monitored Degrees of Freedom

The effects of monitoring different degrees of freedom on the parameter estimates are studied here.

Procedure and Results: Standard test conditions apply. Three sets of signals are considered. In set 1, all degrees of freedom are monitored; in set 2, only the top degree of freedom is monitored; and in set 3, only the first degree of freedom is monitored.

Table (4.6) shows the results for the roof and base-excitation cases. Here, the results for sets 1 and 3 are accurate while for set 2 the results are poor. The results for set 1 are almost exact, the results for set 2 deviate considerable from the exact while, for set 3, the results are completely different from the exact. The poor results are expected in both situations because of non-uniqueness conditions. Udwardia and Sharma [4.1] have presented a discussion on output configurations for a chain system from which unique stiffness parameter values can be obtained in the base-excitation case. Udwardia et al. have also extended the study to the roof-excitation case [4.4] where he finds similar conditions. The output configurations that produced the poor results are the input-output configurations that lead to non-unique stiffness determinations. In the other situations, however, uniqueness is only guaranteed as long as "clean" information from all modes is present in the output signals as in this noise-free case. In the presence of noise, uniqueness is no longer guaranteed, but

the more higher-mode information there is, the better accuracy that can be expected.

Deviations from the exact distribution, however, do not necessarily imply a bad match in the response signals. For the roof-excited, set 3 case, for example, the match at the first degree of freedom is nearly perfect as can be seen in Fig. (4.12). In this case the algorithm has converged to another solution equivalent to the exact one as far as the observed input and output are concerned. This case seems to be analogous to that already discussed in Section 4.1.1.3 and in Fig. (4.3b) for the 2-DOF chain model.

Section 4.1.2.4 - Response Quantity to Monitor

The effects of using either measured response displacements or accelerations are examined.

Procedure and Results: Standard test conditions apply except that both accelerations and displacements are employed in the identification.

Table (4.7) shows the identified stiffness distribution for the base and roof-excitation cases. It is seen that the values corresponding to displacement signals differ only slightly from the exact distribution, with a maximum of 4%. The estimates corresponding to the acceleration signals, in comparison, are essentially perfect.

The frequency content of the displacement signals involves only the lower frequencies. The higher-frequency content inherent in the acceleration signals leads to faster convergence rates in the parameter estimates while integration of the displacement signals reduces the high frequency content, thereby losing valuable system information. As previously discussed, the lack of higher mode information in the displacement signals leads to the creation of the shallow “banana valleys” for the functional $J_T(\theta)$, which greatly retards convergence to the minimum of J_T . The increase in the slope of the valley floor resulting from higher mode information allows the minimization techniques to reach the minimum with less difficulty.

Displacements might prove to be useful in cases where the acceleration signals contain very low amplitudes in the low frequency domain. In these cases, both displacement and acceleration signals could be used simultaneously. However, as a practical matter, it is usually easier to measure structural accelerations in the field using inertial devices than to measure displacements relative to some reference system.

Section 4.1.2.5 - Noise in the Excitation and Response Signals

Unrealistically high levels of noise are added to the system signals to produce “noisy signals” to test the robustness of the method.

Procedure and Results: Standard test conditions apply. Noise in the form of a Gaussian white-noise signal is added to both the input and the output of the system. The noise signals added to the input have an r.m.s. (root-mean-square) value equal to a specified fraction of the r.m.s. value of the input signal. Similarly, the noise signals added to the output have an r.m.s. value equal to a specified fraction of the r.m.s. value of the response signal corresponding to the topmost degree of freedom. An illustration of the construction of one of these noisy signals is presented in Fig. (4.13). The first level of noise considered corresponds to the case where the r.m.s. noise ratio is 50%. The second level of noise corresponds an *extreme* case of adding 100% noise. It is important to note that since the r.m.s. for the signal at the topmost degree of freedom is normally the largest, the ratios between the r.m.s. of the noise and the r.m.s. of the signals from the lower levels of the system are larger than the prescribed ratio.

Table (4.8) shows the results for the noise-free case and for the 50% and 100% noise-added cases. For the 50% noise case, the results remain considerably close to the exact distribution, within 13% for base excitation and within 5% for roof excitation. For the 100% noise case, even though the stiffness values vary considerably, they remain within 46% of the exact values for the base-excitation case and within 9% for roof excitation.

Section 4.1.2.6 - Type of Damage Present in the Structure

The sensitivity of the algorithm to different stiffness degradation distributions is examined.

Procedure and Results: Standard test conditions apply. The sensitivity of the results to the “damage” pattern in the structure is considered. The first pattern consists of a reduction of interstory stiffness at the 2nd, 3rd, and 4th interstory levels. The second pattern consists of a similar stiffness reduction at the 9th, 8th, and 7th levels. The third pattern is a combination of the two former patterns. The fourth pattern is characterized by an extreme reduction in the stiffness factor in the 4th and 7th interstory stiffnesses. Table (4.9) shows that the estimates in all four cases are in excellent agreement with the exact values, suggesting that the algorithm works well regardless of the “damage” distribution in this noise-free case.

Section 4.1.2.7 - Signal Synchronization

The aim in this section is to determine whether time shifts from lack of synchronization among the signals induces significant errors in the parameter estimates, since such time shifts are known to produce substantial errors in the identification of the higher modes [4.5].

Procedure and Results: The standard test conditions are assumed. With 11 available signals, it is possible to construct a large number of time shift combination among the signals. It is expected that the largest errors occur when the shift takes place between the excitation signal and all the

response signals. Two time shifts between the input and the output of $2\Delta t = 0.04$ and $4\Delta t = 0.08$ sec. were considered. Table (4.10) shows the estimates from program SUB-ID-Time. Results show excessively high sensitivity to these shifts, both in the roof and in the base excitation cases. This sensitivity is expected to be due to the active participation of the higher modes since their periods are of the same order as the shifts.

Section 4.1.2.8 - Miscalibration of the Signals

The effects of accelerometer miscalibration in the parameter estimates are studied in this section.

Procedure and Results: Standard test conditions are given. It is assumed here, a priori, that the excitation signals are not calibrated adequately. Three "miscalibration levels" are considered: 0%, 5%, and 10% increases in the excitation signal. Since the excitation is larger than the one used for the reference system, the predicted response calculated by any dynamic algorithm is larger than expected. It is then expected that the damping ratios increase in order to decrease the response amplitudes to levels comparable with those corresponding to the "system" signals. It is not clear, however, whether the θ value estimates are influenced significantly. Any change in the θ parameters should always be consistent with the natural frequencies since discrepancies in the latter cause the largest contributions to the error. Table (4.11) shows the estimates derived from program SUB-ID-Time. It is seen in this table that the values are quite accurate. As a rule of thumb, the θ estimates incur percentage error levels lower than those in the calibration. Based on these results, it is expected that miscalibration does not generate much more error even when only a few of the degrees of freedom are measured.

Section 4.1.2.9 - Summary for the 10-DOF Chain System

Ignoring any shortcomings in terms of lack of uniqueness, the time-based output error method presents good characteristics. The method was sensitive to ill-conditioning when very few modes participated in the response. Low frequency breadth in the input, location of the excitation, monitoring of displacements rather than accelerations, sampling and duration of the signals, choice of degrees of freedom to monitor, and noise, are some of the effects studied here which have an effect in the participation of more than a few modes. The first two effects mentioned above affect the results the strongest.

For normal experimental setups, special attention should be placed on signal synchronization. This seemed to have a very strong effect on the results since lack of synchronization can cause the model higher modes to be out of phase with respect to observed data, thereby corrupting the estimates of their modal parameters.

Section 4.2 - Beam-Column Model Simulations

The chain model studied in the previous sections is a discrete version of the shear beam. In this section, a bending beam is modeled to examine whether any significant differences appear in the parameter estimation process for this type of element.

Bending beams present very different mechanical characteristics from the chain system studied in the last sections, which appear to make the beam identification problem far more difficult to solve. The difficulty stems from the excessive ill-conditioning present when relatively few modes contribute to the response used to determine the structural stiffness parameter values. Results suggest that in the bending beam case, a small neighborhood around a set of modal parameters is “mapped” to a much larger range of stiffness parameter values. In the chain system case, larger variations in the modal properties are needed to differentiate one set of stiffness parameters from another. The results that follow, although not conclusive, give the impression that there may be identifiability problems where one set of modal parameters may be mapped to two or more stiffness parameter vectors.

The comparisons presented in this section are restricted to four areas: (1) location of the excitation, (2) frequency content of the excitation, (3) selection of the monitored degrees of freedom, and (4) the effect of noise in the determination of the values of the structural parameters. In most simulation tests below, only the *translational* degrees of freedom are used since the *rotational* degrees of freedom are difficult to measure in real-life situations.

All beam models treated here have one end fixed so as to simulate the cantilever condition; the degrees of freedom at each node consist of a transverse displacement and of a rotation. The cantilever beam is divided into 10 elements giving a total of 20 degrees of freedom. Fig. (4.14) shows a schematic of this beam indicating how the “sub-structures” or modules are associated with the degrees of freedom. The “standard test conditions” are similar to those for the chain system: accelerations are monitored at all 10 transverse degree of freedom of the system. No noise, lack of synchronization or miscalibration is present in the signals. The excitation signal shown in Fig. (4.9) is applied in numerical tests both at the base and at the top degree of freedom except that in the present tests the time step has been reduced. The signals consist of 1024 time points with $\Delta t = 0.002$ sec. giving a 2.048 second duration, of the same order of the fundamental period. The signal is Gaussian distributed in time with an envelope decaying to zero amplitude at 1.024 sec. The excitation is broad-band in the frequency domain with a Nyquist frequency of 250 Hz, nearly twice the largest natural frequency of the system ($f_{10} \approx 130\text{Hz}$). Damage is represented by a stiffness degradation of approximately 27% in the second and third inter-story levels, and 11% in the fourth level as in the chain case. The effects of the “damage” (or weakening of some members) on the *modal* parameters are also shown in Table (4.12). The effects of the weakening on the *response* signals are

shown in Fig. (4.15) which shows the response of the undamaged and damaged system to the excitation. Table (4.4) and Table (4.12) illustrate that the ratio of the higher mode frequencies with respect to the fundamental mode frequency is very different between the chain and beam model cases. The natural frequency band in the beam case is significantly wider than in the chain model case. The wider the band is, in practice, the more difficult it is to excite the higher modes.

The code SUB-ID-Time is used in all of the tests to determine the stiffness distributions and damping ratios from the simulated signals. It is found, in general, that the results associated with roof excitation are closer to the exact values than those associated with base excitation. In the same way as for the chain model, the roof loading excites more strongly the higher modes, thereby giving more information about the dynamics than base motion, which excites mainly the first modes of vibration. This is illustrated by the corresponding transfer functions given in Fig. (4.16).

Section 4.2.1 - Frequency Content of the Excitation

Observations are made to determine whether the parameters are estimated accurately with few modes present in the response signals.

Procedure and Results: The standard test conditions are assumed except that the excitation frequency bandwidth is between 0 Hz and 7 Hz in one test and between 0 Hz and 250 Hz in another test. The number of modes excited is 2 in the 0 - 7 Hz case and approximately 15 in the 0 - 250 Hz case. Table (4.13) shows the results for the two cases for the two locations.

The results indicate that the estimates are highly unreliable when only few modes are excited. The measures of fit, however, are quite good, which seems to imply that the match of the properties of the first few modes was good. Table (4.13b) shows that, indeed, the modal properties match quite well (within 1.7%). It is believed that numerical ill-conditioning or a local minimum was the reason why the optimization algorithm converged (prematurely) to inaccurate results. Non-uniqueness in this case would have given an optimal error index of zero, since there is no noise in the signals. There is also the possibility that the algorithm may have stopped prematurely before getting to the non-unique solution.

Section 4.2.2 - Selection of Monitored Degrees of Freedom

The aim of this section is to determine whether the parameter estimates are affected if different degrees of freedom are monitored.

Procedure and Results: Standard test conditions apply although different degrees of freedom are monitored in each of the four tests. Set 1 consisted of measuring all 20 degrees of freedom in

the model, Set 2 consisted of all 10 *transverse* degrees of freedom, Set 3 consisted of only the first transverse degree of freedom, and Set 4 consisted of only the tenth transverse degree of freedom.

Table (4.14) shows that the output error index is almost zero in all cases, indicating excellent matching of the system time histories by the models. The fact, however, that there are various stiffness distributions which render almost identical time histories shows that either numerical ill-conditioning or non-uniqueness is definitely present. For non-uniqueness, the optimal error index must be zero and Tab 4.14 suggests that this does not occur. However, there is still the possibility that the algorithm converged prematurely, or that it converged to a local minimum, so it is not possible to rule out the existence of a non-unique solution. Non-unique parameter estimates were found in the *chain* model case when certain degrees of freedom were monitored. The same pattern of tests is assumed here as in the chain system, although no theoretical study like that of Udwadia and Sharma has been done for the beam model which would tell when non-uniqueness is to be expected. Numerical ill-conditioning, where different stiffness distributions yield *almost but not exactly* identical modal parameters (producing almost the same response), may also be the reason why the algorithm converged to the wrong set of values. Table (4.14b) shows how close the modal parameters are for the different stiffness distributions. The active participation of only a few of the 15 modes, as shown in Fig. (4.16), may be the reason why differences between the system and model only arise in the higher modes. The error in the fundamental frequency is most likely due to the short duration of the signals compared to the fundamental period.

Section 4.2.3 - Noise in the Excitation and Response Signals

An idea of the extent of deterioration in the parameter estimates introduced by measurement noise is determined here.

Procedure and Results: Standard test conditions apply except that noise in the form of a Gaussian white-noise signal is added to both the input and the output of the system. The noise signals added to the input have r.m.s. (root-mean-square) values equal to a specified fraction, e.g., 5 %, of the r.m.s. value of the input, and likewise for the response signals. Table (4.15) shows results corresponding to 0 and 10% r.m.s. ratios. From the table it is evident that the introduction of the noisy signals deteriorates the parameter estimates to greater extent than in the chain system results. Part of the reason for this is that in the chain case all degrees of freedom are measured while in the beam case only the translational degrees of freedom are considered.

The roof excitation case presents worse estimates than the base excitation, a fact that contradicts the expectation that the roof case excites more higher modes thus making more information available for the stiffness parameter estimation. The chain case was consistent with this expectation. A possible explanation is that more modes are active in the roof excitation case and thus more

conditions must be satisfied. If these conditions are incorrect, as here where noise is added to the signals, then the SUB-ID-Time algorithm is more likely to have to change the parameter values to be able to accommodate to the incorrect modal conditions. In the beam case, not all degrees of freedom are monitored, while in the chain case all degrees of freedom are measured. The incorrect conditions are more likely to be satisfied in the beam case since there is more flexibility in the stiffness parameter estimation because of the fact that not all degrees of freedom are constrained to take prescribed motions.

Section 4.2.4 - Summary of the 20-DOF Beam-Column System

The results shown in this section are analogous to those presented for the 10-DOF chain system although in the 20-DOF beam-column case, however, the modal frequencies are very separated. This separation induces much more ill-conditioning in the results since it is very difficult to retrieve the smaller higher-mode participation from the measured signals. It is expected that in real situations, however, modes are much closer together thus providing much more information from which to extract more modal data.

References for Chapter 4

- [4.1] Udwadia, F.E., Sharma, D.K., "Some Uniqueness Results Related to Building Structural Identification", *SIAM Journal of Applied Mathematics*, Vol. 24, 1978, p. 104.
- [4.2] Beck, J.L., "Determining Models of Structures from Earthquake Records", Report EERL 78-01, California Institute of Technology, Pasadena, California, June 1978.
- [4.3] Wolfram, S. *Mathematica*, Addison Wesley, Redwood City, California, 1988.
- [4.4] Udwadia, F.E., Sharma, D.K., Shah, P.C., "Uniqueness of Damping and Stiffness Distributions in the Identification of Soil and Structural Systems", *Journal of Applied Mechanics*, ASME, Vol. 45, March 1978, p. 187.
- [4.5] McVerry, G.H., Beck, J.L., "Structural Identification of JPL Building 180 Using Optimally Synchronized Earthquake Records", Report EERL 83-01, California Institute of Technology, Pasadena, California, August 1983.

Data Set	Stiffness Parameters				Modes	DOFs	Error Index	Eval.
	Starting Value		Converged Value					
	θ_1	θ_2	θ_1	θ_2				
A & B								
	1	1	0.531	0.435	1	-	$6.4 \cdot 10^{-17}$	2
	2	1	0.783	0.282	1	-	$1.0 \cdot 10^{-16}$	2
	2	0.5	1.183	0.237	1	-	$1.4 \cdot 10^{-16}$	2
C								
	1	1	0.5	0.5	1	1, 2	$1.4 \cdot 10^{-17}$	2
D & E								
	1	1	0.5	0.5	1,2	-	$9.4 \cdot 10^{-9}$	190
	2.5	1	1	0.25	1,2	-	$9.4 \cdot 10^{-9}$	229
	2.5	0.5	1	0.25	1,2	-	$9.9 \cdot 10^{-9}$	185
F								
	1	1	0.5	0.5	1,2	1, 2	$4.0 \cdot 10^{-17}$	2

Table 4.1: SUB-ID-SS results for the 2-DOF chain model, using only modal frequencies and modeshape components at the measured degree(s) of freedom.

Data Set	Stiffness Parameters				Modes	DOFs	Error Index	Eval.
	Starting Value		Converged Value					
	θ_1	θ_2	θ_1	θ_2				
A & B								
	1	1	0.491	0.526	1	-	$6.2 \cdot 10^{-24}$	132
	2.5	1	2.343	0.210	1	-	$4.0 \cdot 10^{-30}$	175
	2.5	0.5	2.483	0.208	1	-	$4.0 \cdot 10^{-30}$	174
C								
	1	1	0.5	0.5	1	1, 2	$1.1 \cdot 10^{-11}$	209
D & E								
	1	1						
	2.5	1	0.5	0.5	1,2	-	$1.6 \cdot 10^{-11}$	186
	2.5	0.5	1	0.25	1,2	-	$6.7 \cdot 10^{-12}$	141
F								
	1	1	0.5	0.5	1,2	1, 2	$5.1 \cdot 10^{-11}$	136

Table 4.2: SUB-ID-Modal results for the 2-DOF chain model, using only modal frequencies and modeshape components at the measured degree(s) of freedom.

Data Set	Stiffness Parameters				Modes	DOFs	Error Index	Eval.
	Starting Value		Converged Value					
	θ_1	θ_2	θ_1	θ_2				
A	1	1	0.5	0.5	1	1	$1.9 \cdot 10^{-7}$	274
	2	1	0.5	0.5	1	1	$1.1 \cdot 10^{-8}$	665
	2	0.5	0.5	0.5	1	1	$2.5 \cdot 10^{-7}$	482
	1	0.25	0.5	0.5	1	1	$6.0 \cdot 10^{-11}$	537
B	1	1	0.498	0.506	1	2	$7.5 \cdot 10^{-6}$	612
	2	1	1.014	0.249	1	2	$9.5 \cdot 10^{-6}$	393
	2	0.5	1.054	0.245	1	2	$1.3 \cdot 10^{-4}$	56
	1	0.25	1	0.25	1	2	$1.6 \cdot 10^{-16}$	53
C	1	1	0.5	0.5	1	1, 2	$2.0 \cdot 10^{-8}$	316
	2	1	0.5	0.5	1	1, 2	$3.4 \cdot 10^{-8}$	606
	2	0.5	0.5	0.5	1	1, 2	$1.6 \cdot 10^{-7}$	647
	1	0.25	0.5	0.5	1	1, 2	$1.4 \cdot 10^{-7}$	532
D	1	1	0.5	0.5	1, 2	1	$2.1 \cdot 10^{-16}$	703
	2	1	0.5	0.5	1, 2	1	$2.1 \cdot 10^{-16}$	677
	2	0.5	0.5	0.5	1, 2	1	$1.5 \cdot 10^{-16}$	608
E	1	1	0.5	0.5	1, 2	2	$2.7 \cdot 10^{-12}$	390
	2	0.5	1	0.25	1, 2	2	$1.5 \cdot 10^{-16}$	833
F	1	1	0.5	0.5	1, 2	1, 2	$1.7 \cdot 10^{-16}$	596
	2	1	0.5	0.5	1, 2	1, 2	$1.7 \cdot 10^{-16}$	653
	2	0.5	0.5	0.5	1, 2	1, 2	$1.7 \cdot 10^{-16}$	595
	1	0.25	0.5	0.5	1, 2	1, 2	$1.7 \cdot 10^{-16}$	760

Table 4.3: SUB-ID-Time results for the 2-DOF chain model subjected to broad band excitation.

		Stiffness Parameters										
		θ_1	θ_2	θ_3	θ_4	θ_5	θ_6	θ_7	θ_8	θ_9	θ_{10}	Max_{Dif}
Undam		1.000	1.000	1.000	1.000	1.000	1.000	1.000	1.000	1.000	1.000	-
Dam		1.000	0.727	0.727	0.909	1.000	1.000	1.000	1.000	1.000	1.000	27.3%

		Modal Natural Frequencies (Hz)										
		f_1	f_2	f_3	f_4	f_5	f_6	f_7	f_8	f_9	f_{10}	Max_{Dif}
Undam		1.005	2.991	4.911	6.721	8.381	9.854	11.11	12.11	12.85	13.29	-
Dam		0.939	2.917	4.824	6.503	8.092	9.509	10.54	11.41	12.44	13.18	6.6%

Table 4.4: Modal frequency comparison between the damaged and the undamaged Chain System configurations. The damping used to create the response signals for the damaged structure is 5% of critical.

		Stiffness Parameters										Max_{Error}^{θ}	$Error_{Index} J_T$
		θ_1	θ_2	θ_3	θ_4	θ_5	θ_6	θ_7	θ_8	θ_9	θ_{10}		
Exact		1.000	0.727	0.727	0.909	1.000	1.000	1.000	1.000	1.000	1.000	-	-
Roof													
2Hz		1.000	0.727	0.727	0.909	1.000	1.000	1.000	1.000	1.000	1.000	0%	$1.0 \cdot 10^{-10}$
25Hz		1.000	0.727	0.727	0.909	1.000	1.000	1.000	1.000	1.000	1.000	0%	$2.7 \cdot 10^{-5}$
Base													
2Hz		1.002	0.724	0.733	0.898	1.003	1.009	0.996	0.996	1.000	1.000	1.2%	$5.7 \cdot 10^{-6}$
25Hz		1.000	0.727	0.727	0.909	1.000	1.000	1.000	1.000	1.000	1.000	0%	$4.0 \cdot 10^{-6}$

Table 4.5: SUB-ID-Time results for different frequency content in the excitation signals. Ill-conditioning is introduced when only few modes are excited and induces the numerical scheme to converge prematurely.

	Stiffness Parameters										<i>Max θ Error</i>	<i>Error Index J_T</i>
	θ_1	θ_2	θ_3	θ_4	θ_5	θ_6	θ_7	θ_8	θ_9	θ_{10}		
Exact	1.000	0.727	0.727	0.909	1.000	1.000	1.000	1.000	1.000	1.000	-	-
Roof												
All	1.000	0.727	0.727	0.909	1.000	1.000	1.000	1.000	1.000	1.000	0%	$2.7 \cdot 10^{-5}$
1st	0.098	0.738	0.740	0.885	0.918	1.049	1.066	0.984	1.000	1.000	90.2%	n/a
Roof	1.000	0.727	0.727	0.909	1.000	1.000	1.000	1.000	1.000	1.000	0%	$2.0 \cdot 10^{-9}$
Base												
All	1.000	0.727	0.727	0.909	1.000	1.000	1.000	1.000	1.000	1.000	0%	$4.0 \cdot 10^{-6}$
1st	1.000	0.727	0.727	0.909	1.000	1.000	1.000	1.000	1.000	1.000	0%	$9.4 \cdot 10^{-9}$
Roof	0.900	0.864	0.764	0.863	0.888	0.888	0.941	1.03	1.21	1.10	21%	n/a

Table 4.6: The placement of the sensors in a structure is important since there are sensor distributions which prevent the unique determination of the stiffness parameter estimates. The basement excited-roof monitored case, above, shows stiffness parameters with large deviation from the “exact” stiffness distribution yet produces identically the same response.

	Stiffness Parameters										<i>Max θ Error</i>	<i>Error Index J_T</i>
	θ_1	θ_2	θ_3	θ_4	θ_5	θ_6	θ_7	θ_8	θ_9	θ_{10}		
Exact	1.000	0.727	0.727	0.909	1.000	1.000	1.000	1.000	1.000	1.000	-	-
Roof												
Displ	0.961	0.731	0.751	0.927	0.977	0.971	1.00	1.04	1.03	0.970	4%	n/a
Accel	1.000	0.727	0.727	0.909	1.000	1.000	1.000	1.000	1.000	1.000	0%	$2.7 \cdot 10^{-5}$
Base												
Displ	0.974	0.738	0.732	0.916	0.978	1.01	0.997	0.988	1.04	0.990	4%	n/a
Accel	1.000	0.727	0.727	0.909	1.000	1.000	1.000	1.000	1.000	1.000	0%	$4.0 \cdot 10^{-6}$

Table 4.7: SUB-ID-Time results when monitoring displacements and accelerations. The acceleration signals contain higher frequency information that prevent the premature convergence of the minimization algorithm thus arriving at the correct results.

	Stiffness Parameters										$Max \theta$ Error	$Error$ Index J_T
	θ_1	θ_2	θ_3	θ_4	θ_5	θ_6	θ_7	θ_8	θ_9	θ_{10}		
Exact	1.000	0.727	0.727	0.909	1.000	1.000	1.000	1.000	1.000	1.000	-	-
Roof												
0%	1.000	0.727	0.727	0.909	1.000	1.000	1.000	1.000	1.000	1.000	0%	$2.7 \cdot 10^{-5}$
50%	0.985	0.722	0.747	0.922	0.982	0.961	1.02	1.05	1.03	0.972	5%	n/a
100%	0.959	0.747	0.727	0.960	1.01	0.945	1.01	1.08	1.05	0.918	8.2%	n/a
Base												
0%	1.000	0.727	0.727	0.909	1.000	1.000	1.000	1.000	1.000	1.000	0%	$4.0 \cdot 10^{-6}$
50%	0.874	0.669	0.771	0.970	1.02	0.977	1.03	1.05	1.06	1.01	12.6%	n/a
100%	0.643	0.738	0.938	0.889	1.07	0.975	0.991	1.23	1.15	1.06	45.7%	n/a

Table 4.8: SUB-ID-Time results for different noise-to-signal levels. The stiffness parameter estimates distort slowly as the noise levels are increased.

	Stiffness Parameters										$Max \theta$ Error	$Error$ Index J_T
	θ_1	θ_2	θ_3	θ_4	θ_5	θ_6	θ_7	θ_8	θ_9	θ_{10}		
Exact												
Pat 1	1.000	0.727	0.727	0.909	1.000	1.000	1.000	1.000	1.000	1.000	-	-
Pat 2	1.000	1.000	1.000	1.000	1.000	1.000	0.909	0.727	0.727	1.000	-	-
Pat 3	1.000	0.727	0.727	0.909	1.000	1.000	0.909	0.727	0.727	1.000	-	-
Pat 4	1.000	1.000	1.000	0.200	1.000	1.000	0.200	1.000	1.000	1.000	-	-
Roof												
Pat 1	1.000	0.727	0.727	0.909	1.000	1.000	1.000	1.000	1.000	1.000	0%	$2.7 \cdot 10^{-5}$
Pat 2	0.999	1.001	1.000	0.999	0.999	1.001	0.908	0.727	0.727	1.000	0.1%	$7.7 \cdot 10^{-7}$
Pat 3	0.999	0.727	0.727	0.909	1.000	1.000	0.910	0.727	0.727	1.000	0.1%	$2.0 \cdot 10^{-7}$
Pat 4	1.000	1.000	1.000	0.200	1.000	1.000	0.200	1.000	1.000	1.000	0%	$1.5 \cdot 10^{-7}$

Table 4.9: SUB-ID-Time results show essentially no errors in the stiffness parameter estimates for different damage patterns. Approximately 5 of the 10 fundamental modes participate in the response monitored at the 10 degrees of freedom.

	Stiffness Parameters										$\text{Max } \theta$ Error	Error Index J_T
	θ_1	θ_2	θ_3	θ_4	θ_5	θ_6	θ_7	θ_8	θ_9	θ_{10}		
Exact	1.000	0.727	0.727	0.909	1.000	1.000	1.000	1.000	1.000	1.000	-	-
Roof												
0.0	1.000	0.727	0.727	0.909	1.000	1.000	1.000	1.000	1.000	1.000	0%	$2.7 \cdot 10^{-5}$
0.04	1.126	0.693	0.758	0.933	1.003	1.022	0.958	0.924	0.868	0.580	42%	0.84
0.08	1.125	0.819	0.683	0.758	1.014	1.033	0.915	0.828	0.644	0.341	66%	1.02
Base												
0.0	1.000	0.727	0.727	0.909	1.000	1.000	1.000	1.000	1.000	1.000	0%	$4.0 \cdot 10^{-6}$
0.04	0.694	0.641	0.787	1.049	1.043	1.095	1.132	1.082	0.980	0.762	31%	0.146
0.08	0.476	2.375	0.561	1.418	1.026	1.095	1.287	0.838	0.942	1.087	227%	0.339

Table 4.10: Results from SUB-ID-Time for the 10-DOF chain system corresponding to lack of synchronization. Time shifts between the excitation and response signals produce very large deviations in the stiffness parameter estimates.

	Stiffness Parameters										$\text{Max } \theta$ Error	Error Index J_T
	θ_1	θ_2	θ_3	θ_4	θ_5	θ_6	θ_7	θ_8	θ_9	θ_{10}		
Exact	1.000	0.727	0.727	0.909	1.000	1.000	1.000	1.000	1.000	1.000	-	-
Roof												
0 %	1.000	0.727	0.727	0.909	1.000	1.000	1.000	1.000	1.000	1.000	0%	$2.7 \cdot 10^{-5}$
5 %	0.999	0.729	0.731	0.912	0.998	0.987	0.993	1.010	1.007	1.003	1.3%	$1.1 \cdot 10^{-2}$
10 %	1.004	0.726	0.735	0.899	1.008	0.974	0.993	1.001	1.030	0.990	3.0%	$4.8 \cdot 10^{-2}$
Base												
0 %	1.000	0.727	0.727	0.909	1.000	1.000	1.000	1.000	1.000	1.000	0%	$4.0 \cdot 10^{-6}$
5 %	0.971	0.717	0.737	0.923	1.027	1.008	1.012	1.004	1.006	0.977	2.9%	$9.7 \cdot 10^{-3}$
10 %	0.944	0.711	0.747	0.935	1.046	1.016	1.013	1.017	1.007	0.968	5.6%	$3.8 \cdot 10^{-2}$

Table 4.11: SUB-ID-Time results show relatively low sensitivity of the stiffness parameters to different miscalibration levels.

	Stiffness Parameters									
	θ_1	θ_2	θ_3	θ_4	θ_5	θ_6	θ_7	θ_8	θ_9	θ_{10}
Undam	1.000	1.000	1.000	1.000	1.000	1.000	1.000	1.000	1.000	1.000
Dam	1.000	0.727	0.727	0.909	1.000	1.000	1.000	1.000	1.000	1.000
	First 10 Modal Natural Frequencies (Hz)									
	f_1	f_2	f_3	f_4	f_5	f_6	f_7	f_8	f_9	f_{10}
Undam	0.964	5.96	16.5	31.8	51.6	75.6	103	133	161	183
Dam	0.891	5.88	16.0	30.7	49.9	72.9	99.4	128	153	177

Table 4.12: Modal frequency comparison for the Bending Beam undamaged and damaged configurations (the comparison is limited to only the first 10 modes). The damping ratio used to create the damaged structure response signals is 5% of critical in the first 10 modes (only 10 modes are included in the computed response).

Stiffness Parameters												
	θ_1	θ_2	θ_3	θ_4	θ_5	θ_6	θ_7	θ_8	θ_9	θ_{10}	Max θ Error	Error Index J_T
Exact	1.000	0.727	0.727	0.909	1.000	1.000	1.000	1.000	1.000	1.000	-	-
Roof												
7Hz	0.858	0.777	0.820	0.932	1.033	1.075	1.055	1.004	0.964	0.950	14.2%	$1.3 \cdot 10^{-2}$
250Hz	1.000	0.727	0.727	0.909	1.000	1.000	1.000	1.000	1.000	1.000	0%	$3.1 \cdot 10^{-9}$
Base												
7Hz	0.946	0.763	0.756	0.865	0.981	1.045	1.052	1.029	1.008	1.001	5.4%	$9.4 \cdot 10^{-4}$
250Hz	1.000	0.727	0.726	0.910	1.000	1.000	0.999	1.000	1.000	1.000	0.1%	$7.7 \cdot 10^{-11}$

Table 4.13a: SUB-ID-Time results for the 20-DOF beam with different frequency bandwidths. The 7-Hz excitation can, at best, excite two modes while the 250-Hz case can excite 15 modes of the possible 20 modes.

First 10 Modal Natural Frequencies (Hz)											
	f_1	f_2	f_3	f_4	f_5	f_6	f_7	f_8	f_9	f_{10}	Max f Error
Exact	0.891	5.88	16.0	30.7	49.9	72.9	99.4	128	153	177	
Roof											
7Hz	0.891	5.88	16.0	30.8	50.1	73.3	99.9	128	155	180	1.7%
250Hz	0.891	5.88	16.0	30.7	49.9	72.9	99.4	128	153	177	0.0%
Base											
7Hz	0.891	5.88	16.0	30.8	50.1	73.2	99.8	128	154	178	0.4%
250Hz	0.891	5.88	16.0	30.7	49.9	72.9	99.4	128	153	174	1.7%

Table 4.13b: SUB-ID-Time natural frequency results for the beam problem with different frequency bandwidth excitations.

	Stiffness Parameters										<i>Max θ Error</i>	<i>Error Index J_T</i>
	θ_1	θ_2	θ_3	θ_4	θ_5	θ_6	θ_7	θ_8	θ_9	θ_{10}		
Exact	1.000	0.727	0.727	0.909	1.000	1.000	1.000	1.000	1.000	1.000	-	-
Roof												
Set 1	1.000	0.727	0.727	0.909	1.000	1.000	1.000	1.000	1.000	1.000	0%	$5.6 \cdot 10^{-12}$
Set 2	1.000	0.727	0.727	0.909	1.000	1.000	1.000	1.000	1.000	1.000	0%	$3.1 \cdot 10^{-9}$
Set 3	1.033	0.690	0.788	0.993	1.033	1.013	0.943	0.917	0.979	0.985	8.4%	$1.6 \cdot 10^{-5}$
Set 4	0.973	0.708	0.754	0.949	1.025	1.004	0.986	0.984	0.994	0.994	4.4%	$1.6 \cdot 10^{-5}$
Base												
Set 1	1.000	0.727	0.727	0.909	1.000	1.000	1.000	1.000	1.000	1.000	0%	$6.0 \cdot 10^{-10}$
Set 2	1.000	0.727	0.726	0.910	1.000	1.000	0.999	1.000	1.000	1.000	0.1%	$7.7 \cdot 10^{-11}$
Set 3	0.984	0.743	0.723	0.897	1.015	1.039	1.036	1.000	0.973	0.964	3.9%	$3.3 \cdot 10^{-4}$
Set 4	0.904	0.753	0.797	0.901	1.037	1.031	1.077	0.975	0.967	0.932	9.9%	$7.9 \cdot 10^{-4}$

Table 4.14a: SUB-ID-Time θ results for the 20-DOF beam model for various monitoring patterns. Excitation monitored at fewer than all 20 degrees of freedom may be nearly matched by more than one stiffness parameter set.

	First 10 Modal Natural Frequencies (Hz)										<i>Max f Error</i>
	f_1	f_2	f_3	f_4	f_5	f_6	f_7	f_8	f_9	f_{10}	
Exact	0.891	5.88	16.0	30.7	49.9	72.9	99.4	128	153	177	
Roof											
Set 1	0.891	5.88	16.0	30.7	49.9	72.9	99.4	128	153	177	0.0%
Set 2	0.891	5.88	16.0	30.7	49.9	72.9	99.4	128	153	177	0.0%
Set 3	0.899	5.89	16.0	30.7	49.9	72.9	99.4	128	153	177	0.9%
Set 4	0.891	5.88	16.0	30.7	49.9	72.9	99.4	128	153	177	0.0%
Base											
Set 1	0.891	5.88	16.0	30.7	49.9	72.9	99.4	128	153	177	0.0%
Set 2	0.891	5.88	16.0	30.7	49.9	72.9	99.4	128	153	174	1.7%
Set 3	0.891	5.88	16.0	30.7	49.9	72.9	99.4	128	153	174	0.0%
Set 4	0.891	5.88	16.0	30.7	49.9	72.9	99.4	128	153	179	1.1%

Table 4.14b: Natural frequencies associated with the θ distributions shown in Table (4.14a.)

	Stiffness Parameters										<i>Max</i> <i>Error</i>	<i>Error</i> <i>Index J_T</i>
	θ_1	θ_2	θ_3	θ_4	θ_5	θ_6	θ_7	θ_8	θ_9	θ_{10}		
Exact	1.000	0.727	0.727	0.909	1.000	1.000	1.000	1.000	1.000	1.000	-	-
Roof												
0%	1.000	0.727	0.727	0.909	1.000	1.000	1.000	1.000	1.000	1.000	0%	$3.1 \cdot 10^{-9}$
10%	1.001	0.715	0.759	0.890	0.913	1.118	1.021	0.961	1.006	0.995	11.8%	$4.4 \cdot 10^{-3}$
Base												
0%	1.000	0.727	0.726	0.910	1.000	1.000	0.999	1.000	1.000	1.000	0.1%	$7.7 \cdot 10^{-11}$
10%	0.985	0.762	0.685	0.914	1.082	0.939	0.992	1.077	0.969	0.983	8.2%	$9.9 \cdot 10^{-3}$

Table 4.15: Noise added to the input and output signals of the bending beam system produce relatively large deviations in the estimated stiffness parameters from the exact. These deviations are caused by the loss of information from the higher frequency modes since their contribution to the response is small compared to the amplitude of the added noise.

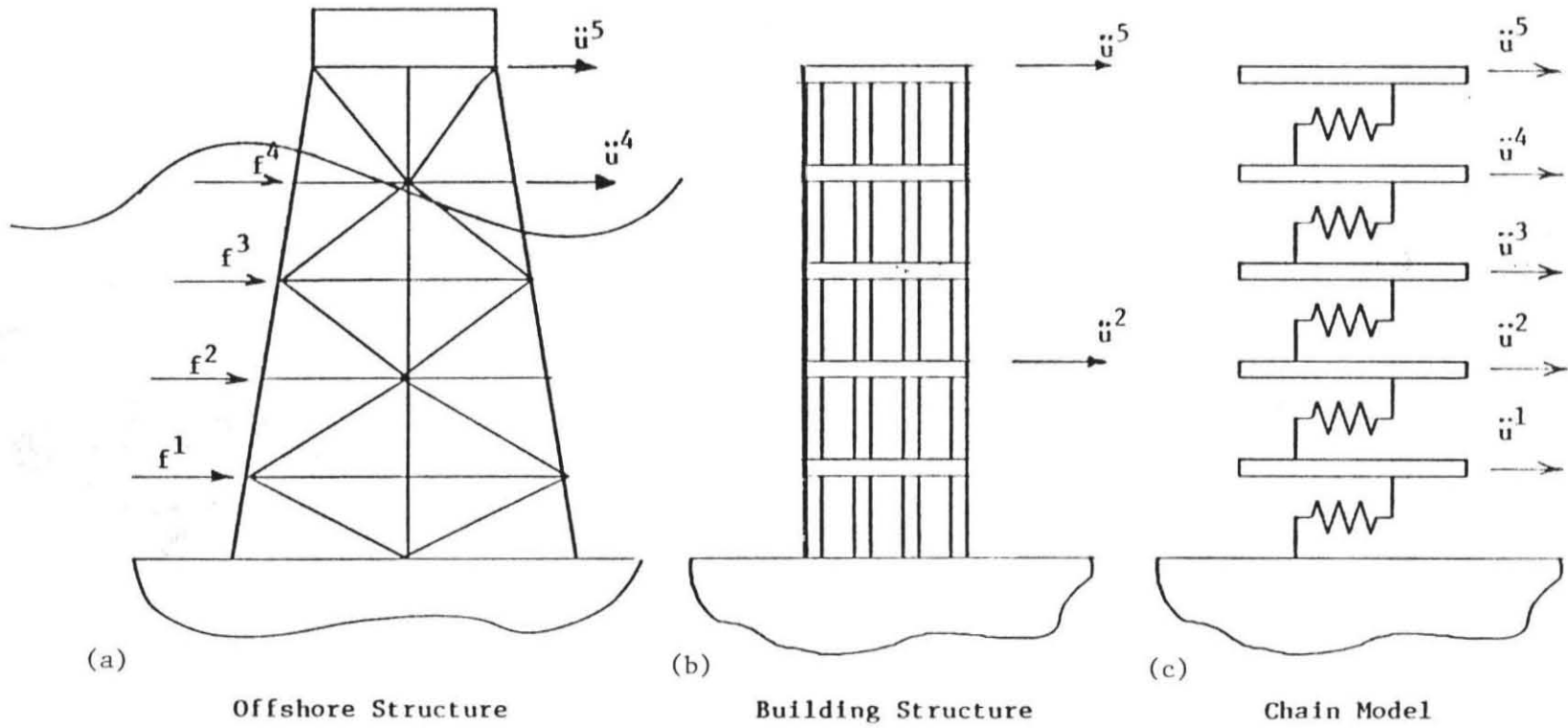


Figure 4.1: (a) Offshore structures and (b) civil buildings can be adequately modeled by the chain model (c) with the appropriate mass and stiffness distributions.

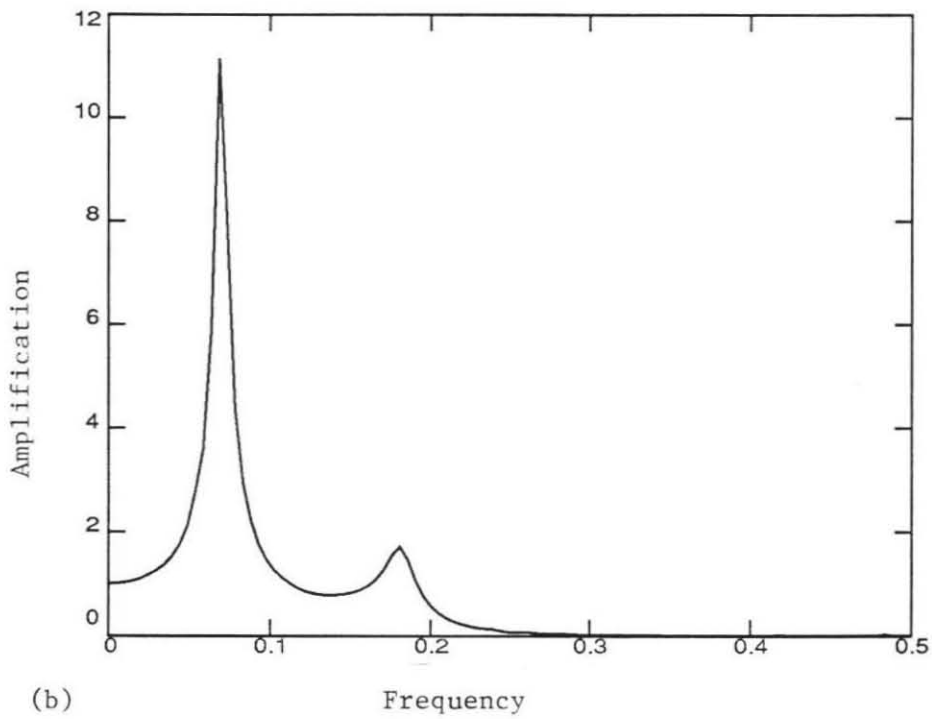
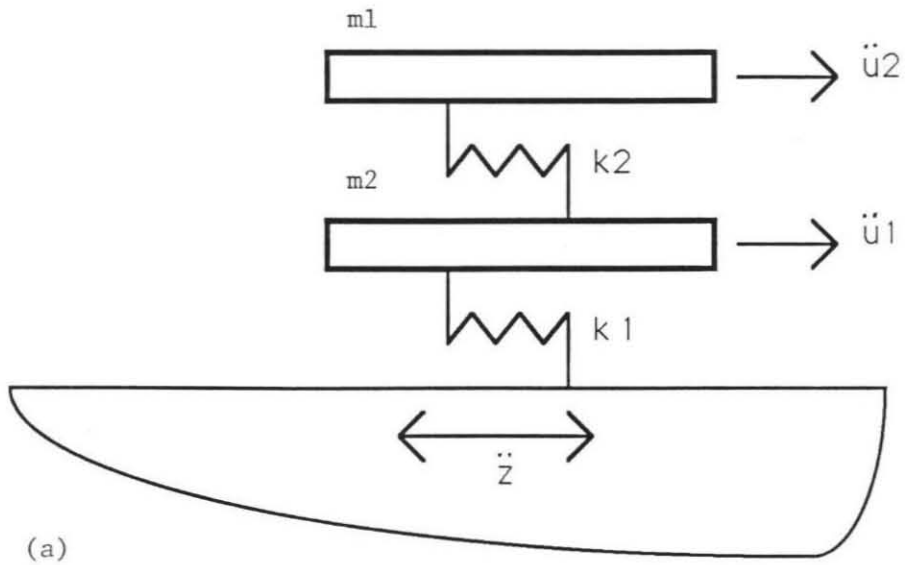


Figure 4.2: A simple 2-DOF chain model (a) and the corresponding transfer function (b) between its base and top-degree-of-freedom responses with $\theta = (0.5, 0.5)$.

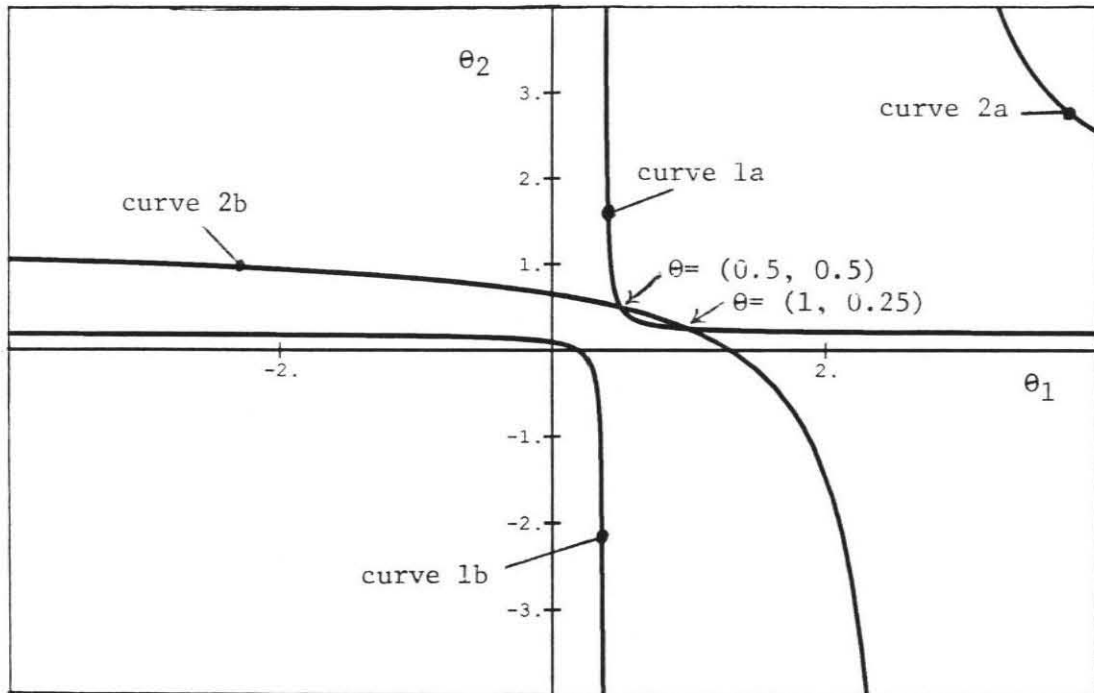


Figure 4.3: Curves 1a and 1b correspond to the θ values for which $\omega^2 = \omega_1^2 \approx 0.191$. Curves 2a and 2b correspond to $\omega^2 = \omega_2^2 \approx 1.309$. There are two models, $\theta^1 = (0.5, 0.5)$ and $\theta^2 = (1.0, 0.25)$ which share both frequencies. (Only first quadrant is relevant for “physical” models.)

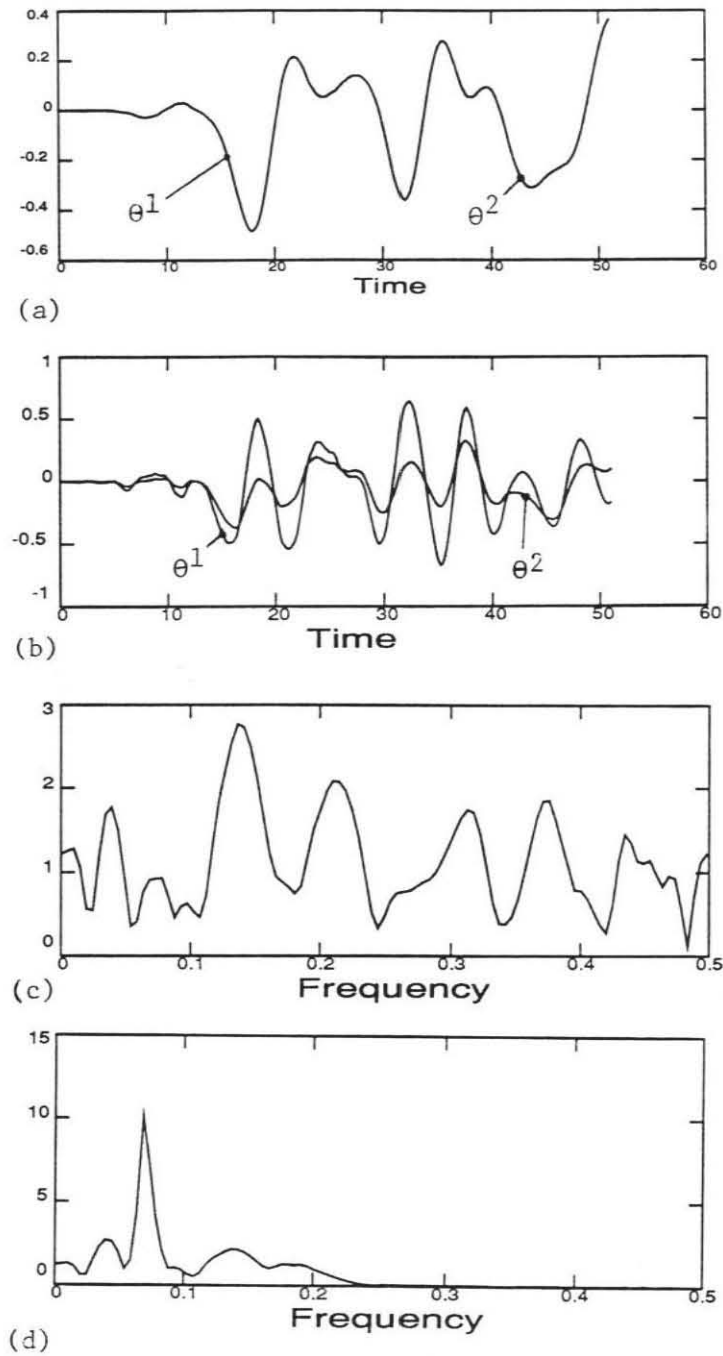


Figure 4.4: (a) Second DOF and (b) first DOF acceleration responses of the “damaged” 2-DOF chain model. The two responses in each diagram correspond to the two possible stiffness distributions sharing the same frequencies. The spectra of the excitation at the base is shown in (c) while the spectra of the response at the second DOF is shown in (d).

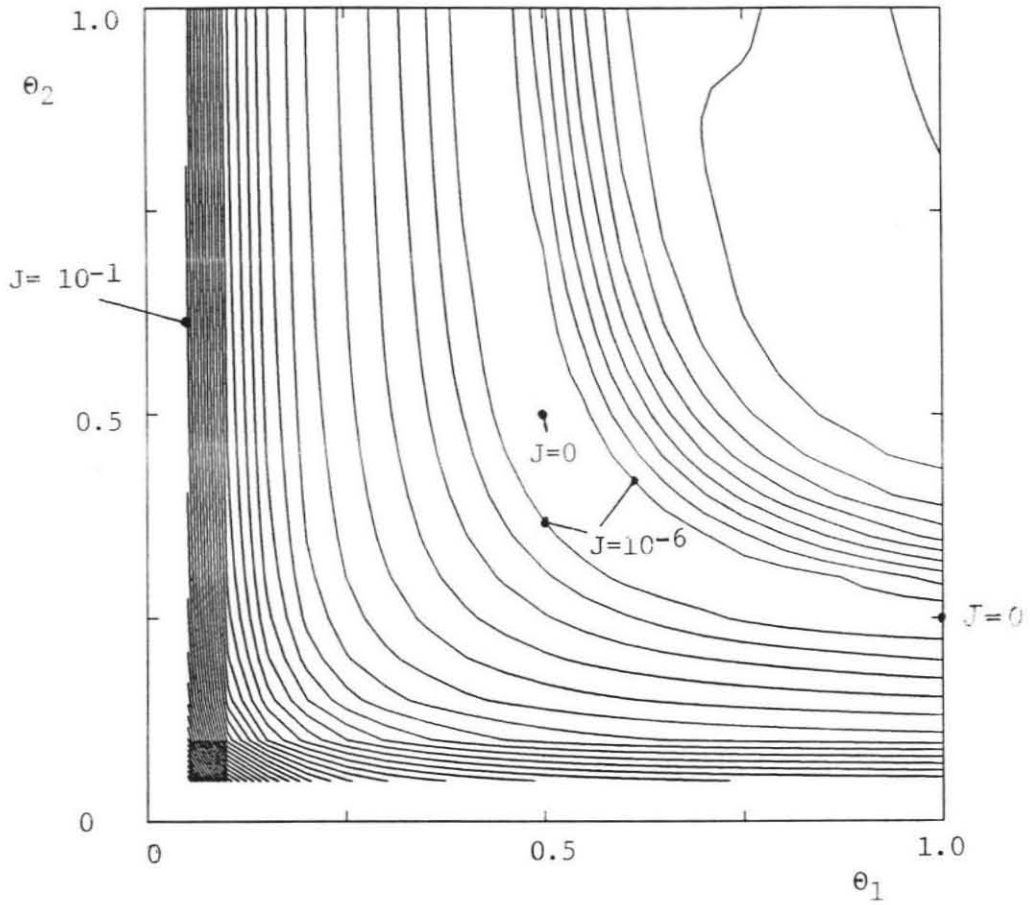


Figure 4.5: Contours for J_T corresponding to base excitation and monitoring of the top-DOF response. The contours indicate the so-called "banana valley" which very often, because of its relative flatness, induces spurious premature convergence of the minimization algorithm.

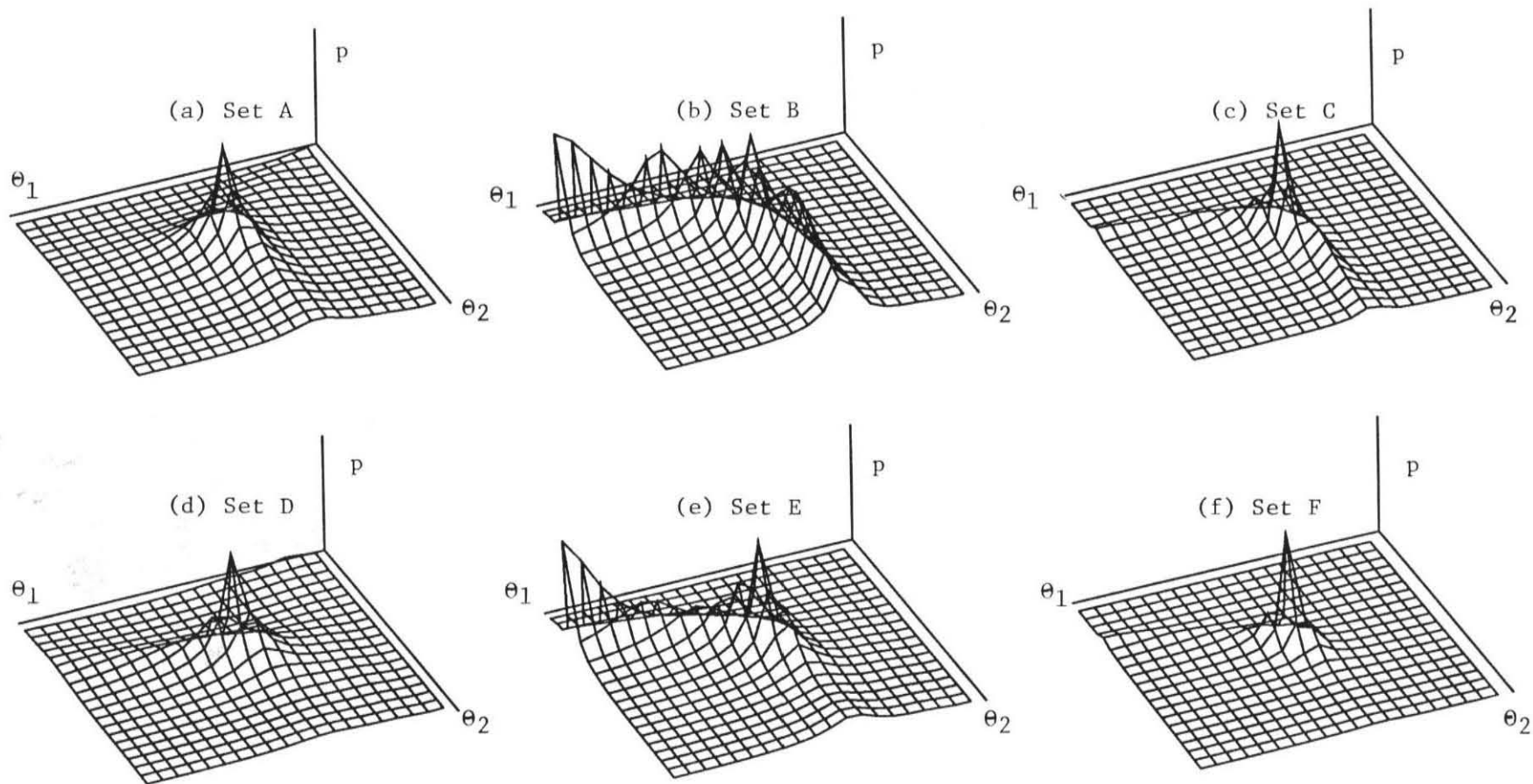


Figure 4.6: Joint pseudo-probability plots derived from SUB-ID-Prob for six different sets of information. Each set comprises different modal and/or degree-of-freedom information (see text). (Because of the plotting algorithm, (b) and (e) visually appear to have multiple peaks when in reality there are only two peaks at $\theta^1 = (0.5, 0.5)$ and $\theta^2 = (1.0, 0.25)$ joined by a smooth crest.)

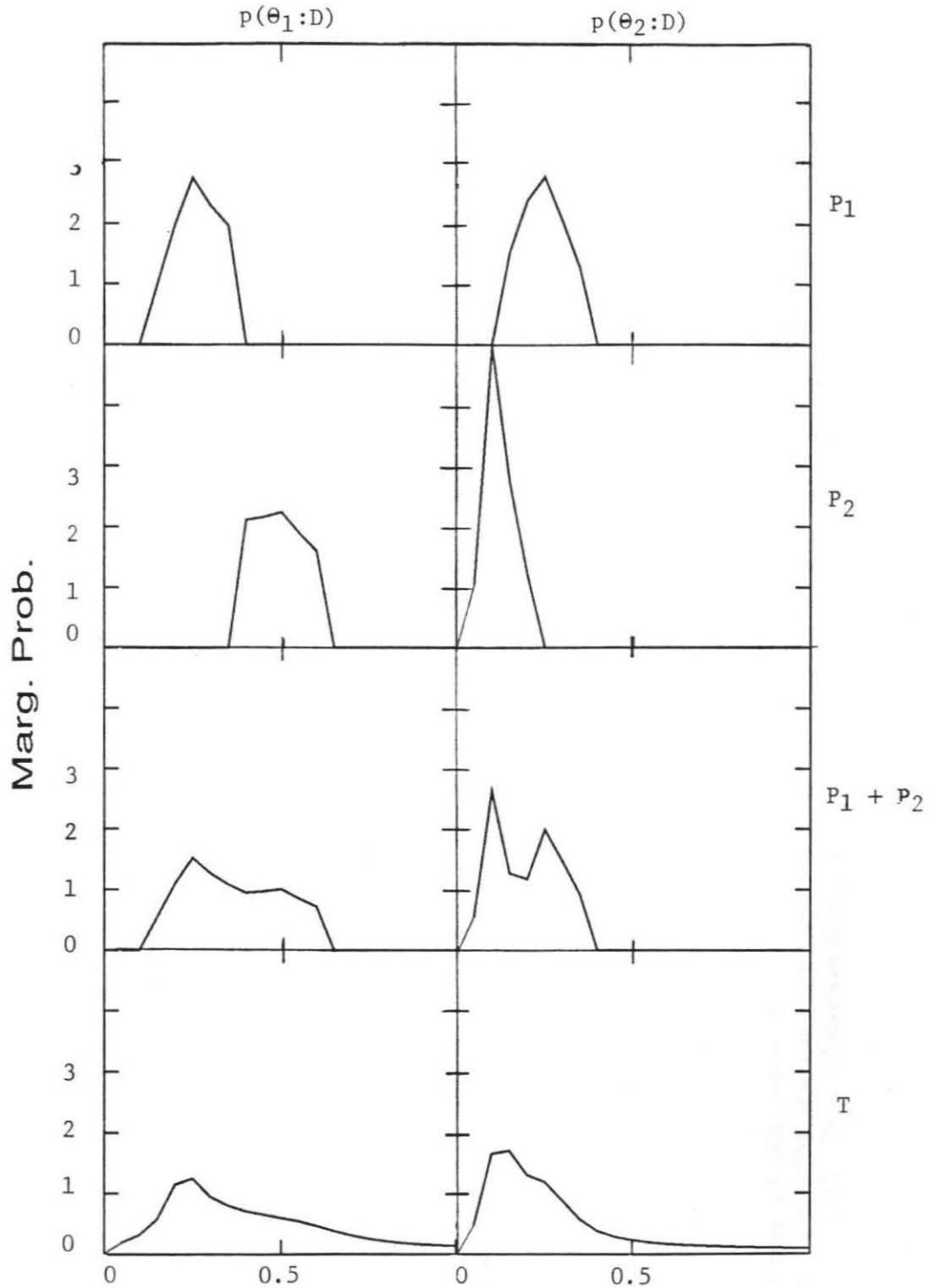


Figure 4.7: Marginal pseudo-probability distributions obtained from set B (Fig. (4.6.b)). Marginal distributions (g) and (h) correspond to the discrete version of Eq. 3.4.1. Distributions (c) and (d) are analogous versions but are constructed from pseudo-probability distributions local to the peaks $\theta^1 = (0.5, 0.5)$ and $\theta^2 = (1.0, 0.25)$ as shown in Fig. 4.6. In this case, the marginal pseudo-probability distributions in (e) and (f) are the addition of the contributions from around θ^1 , referred to as P1, Figs. (a) and (b), and from the neighborhood of θ^2 , P2, in Figs. (c) and (d).

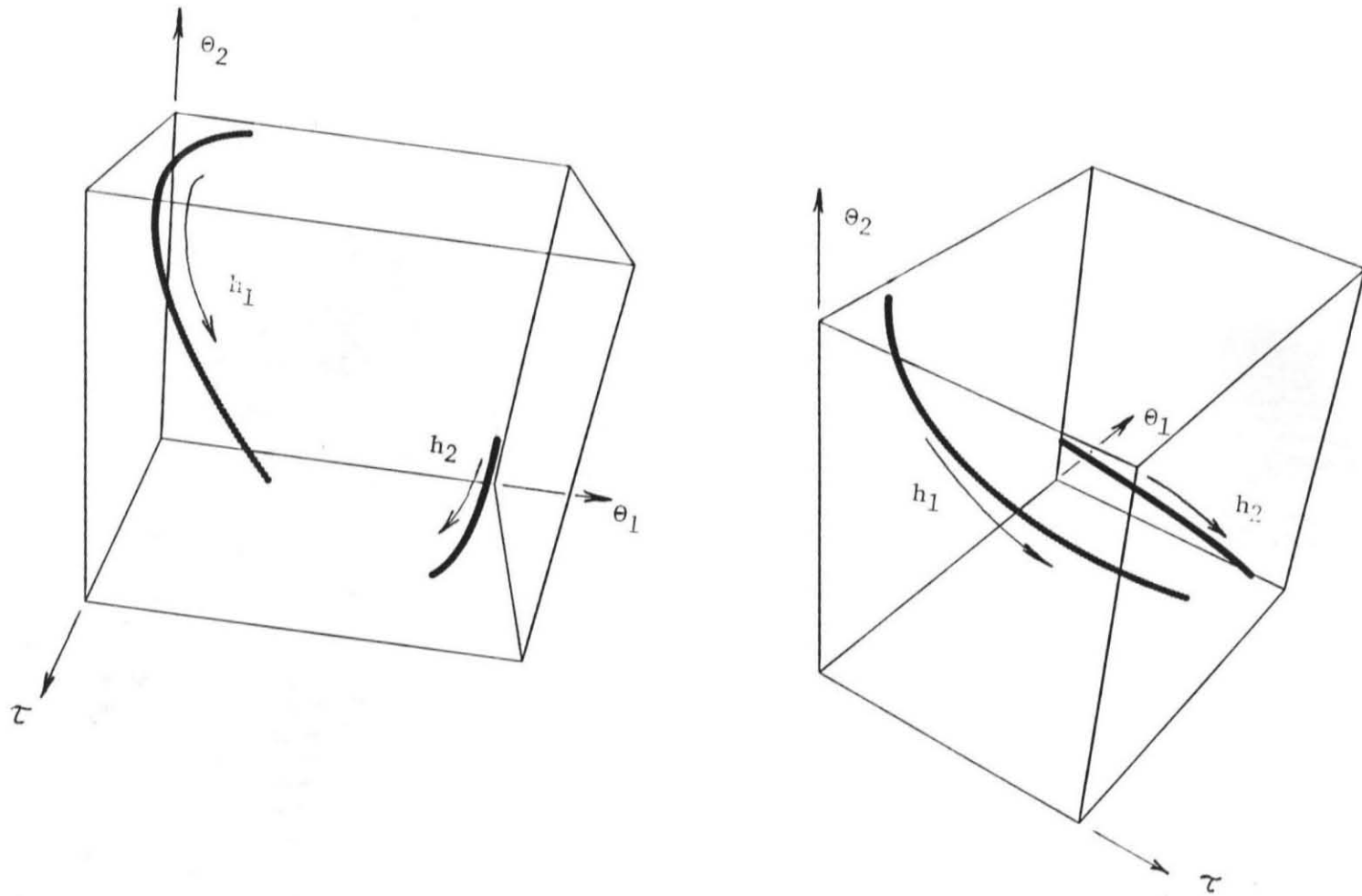


Figure 4.8: Illustration of the homotopy paths associated with the damaged 2-DOF chain system. Homotopy path 'h1' starts at a solution of the simple structure problem $\theta_0^1 \approx (0.191, 1.309)$ and converges to $\theta^1 = (0.5, 0.5)$. Path 'h2' starts at $\theta_0^2 \approx (1.309, 0.191)$ and converges to $\theta^2 = (1.0, 0.25)$.

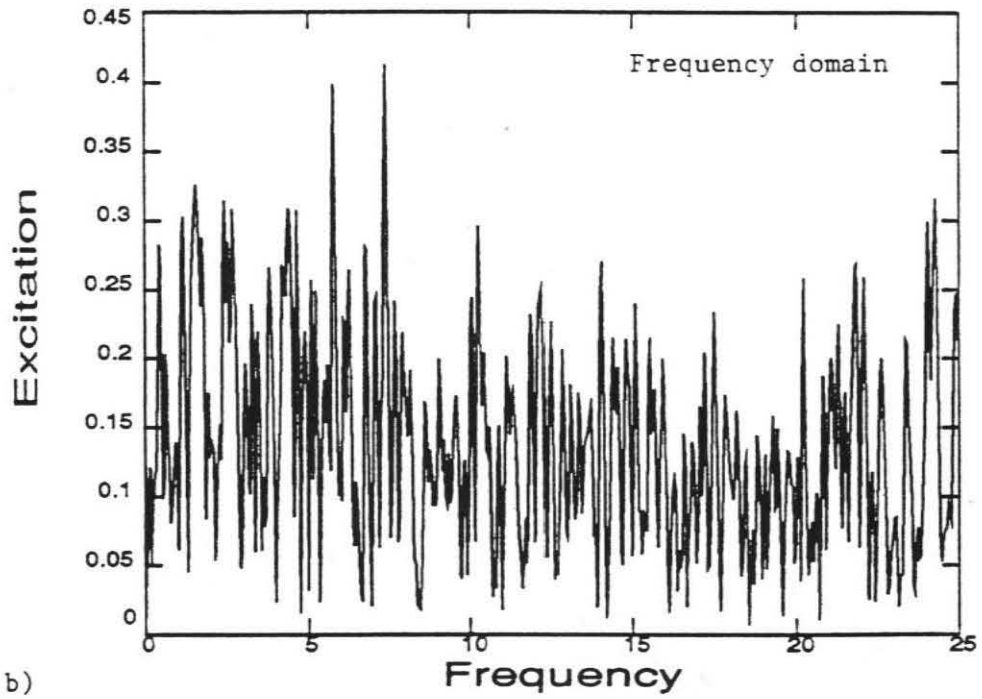
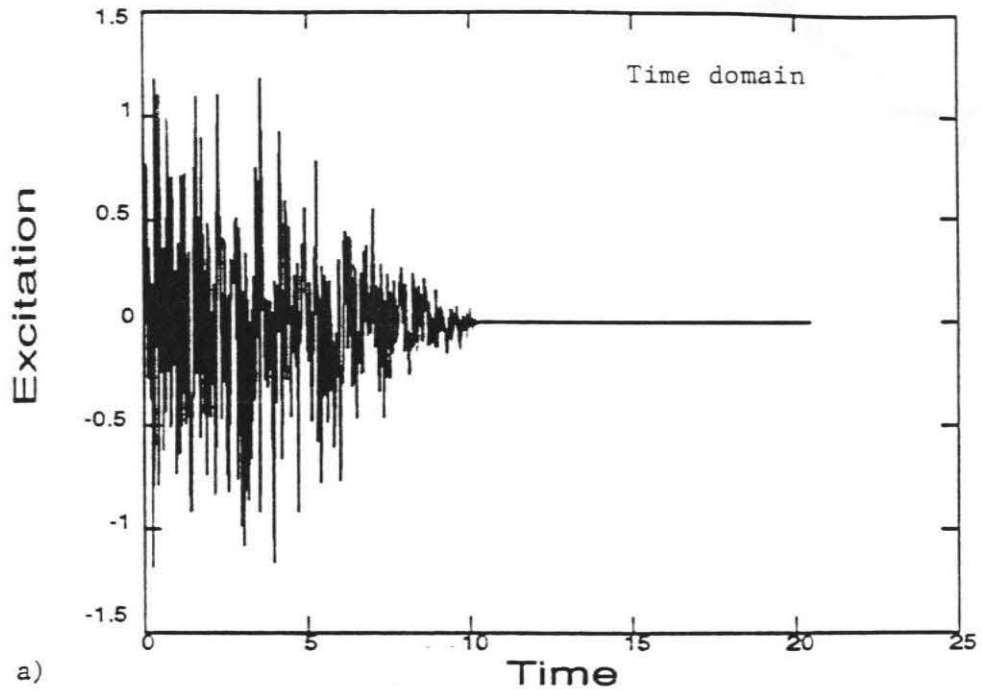


Figure 4.9: Excitation signal used in the numerical tests. When used at the base, it is interpreted as acceleration. When used at any story, it is interpreted as a force. (a) Time history, (b) Frequency spectrum.

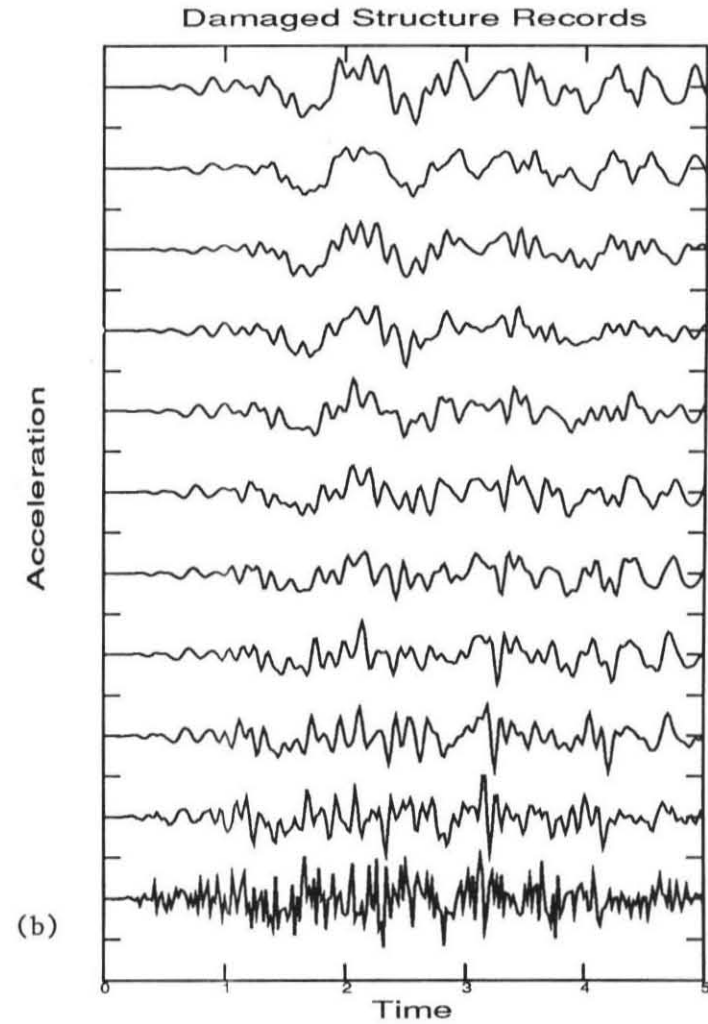
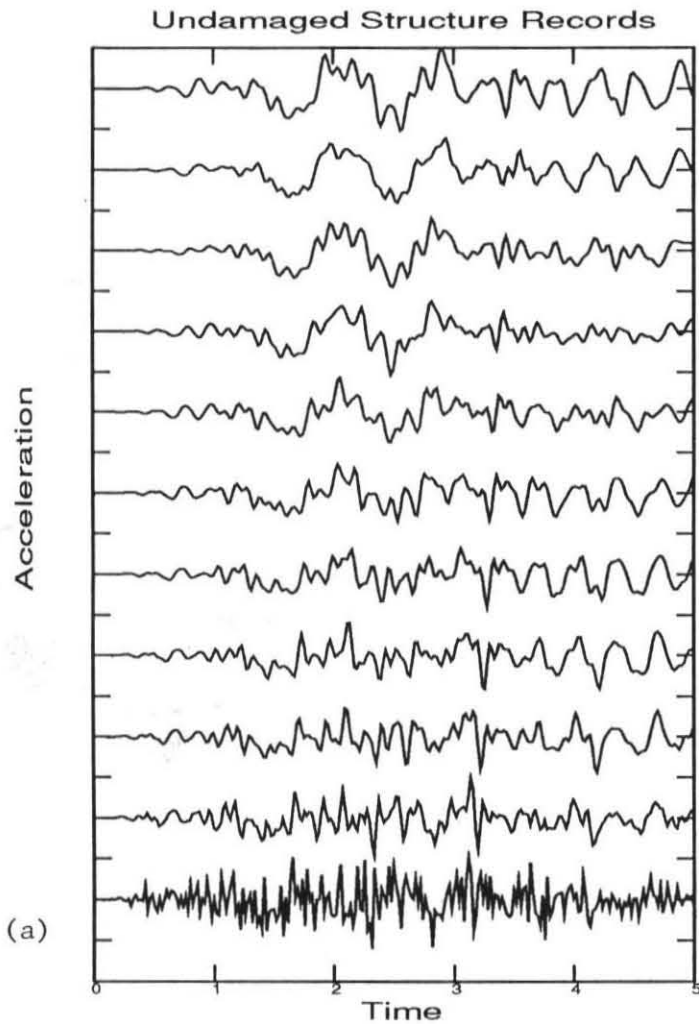


Figure 4.10: Acceleration time histories corresponding to a chain model of a ten-story, ten-bay building subject to base excitation. Set (a) corresponds to an undamaged structure, and (b) to the damage pattern presented in Table 4.4. Signals range from the lowest signal, corresponding to the base acceleration, to the top-most signal, corresponding to the roof acceleration.

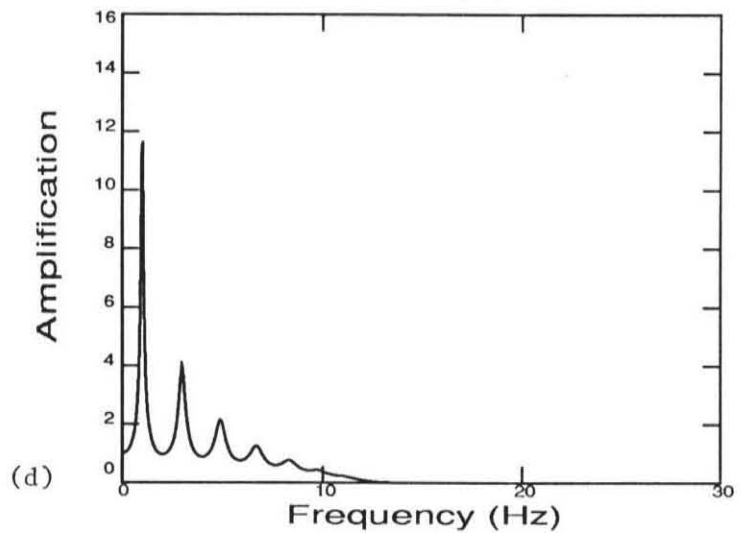
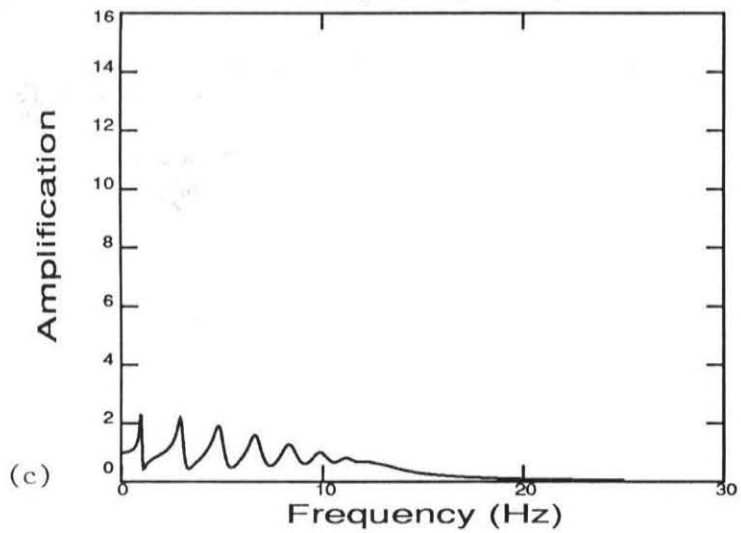
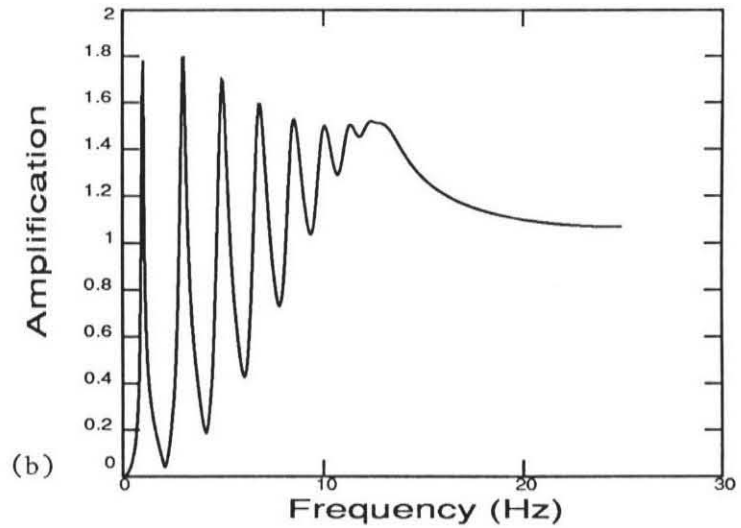
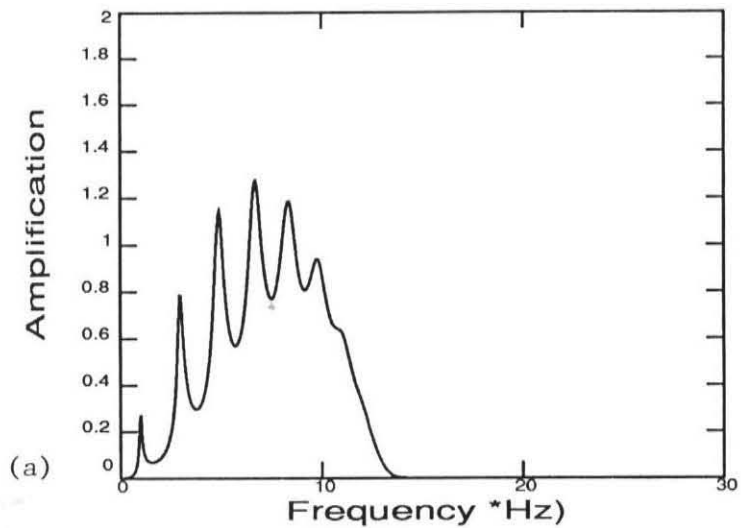


Figure 4.11: Transfer function for chain model with roof and base excitation. Spectra (a) corresponds to roof excitation, monitoring the first DOF; (b) roof excitation, roof monitoring; (c) base excitation, first DOF monitoring; (d) base excitation, roof monitoring.

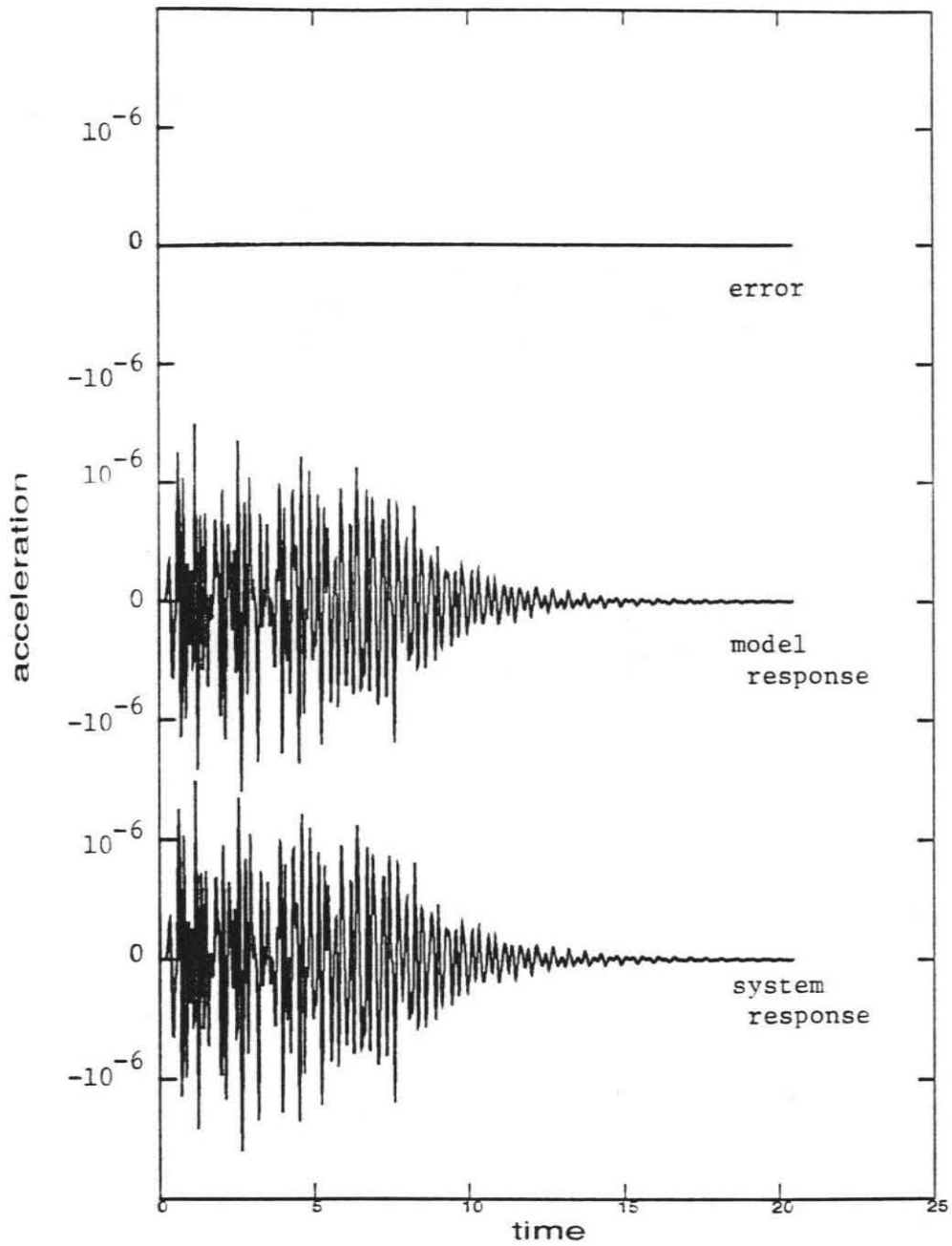


Figure 4.12: Matching of the system response by a model response can be quite accurate as seen in the error signal above. The situation corresponds to the roof excited, first DOF-monitored case of Fig. 4.11. This accuracy, however, does not always imply a correct stiffness distribution, as Table 4.6 demonstrates.

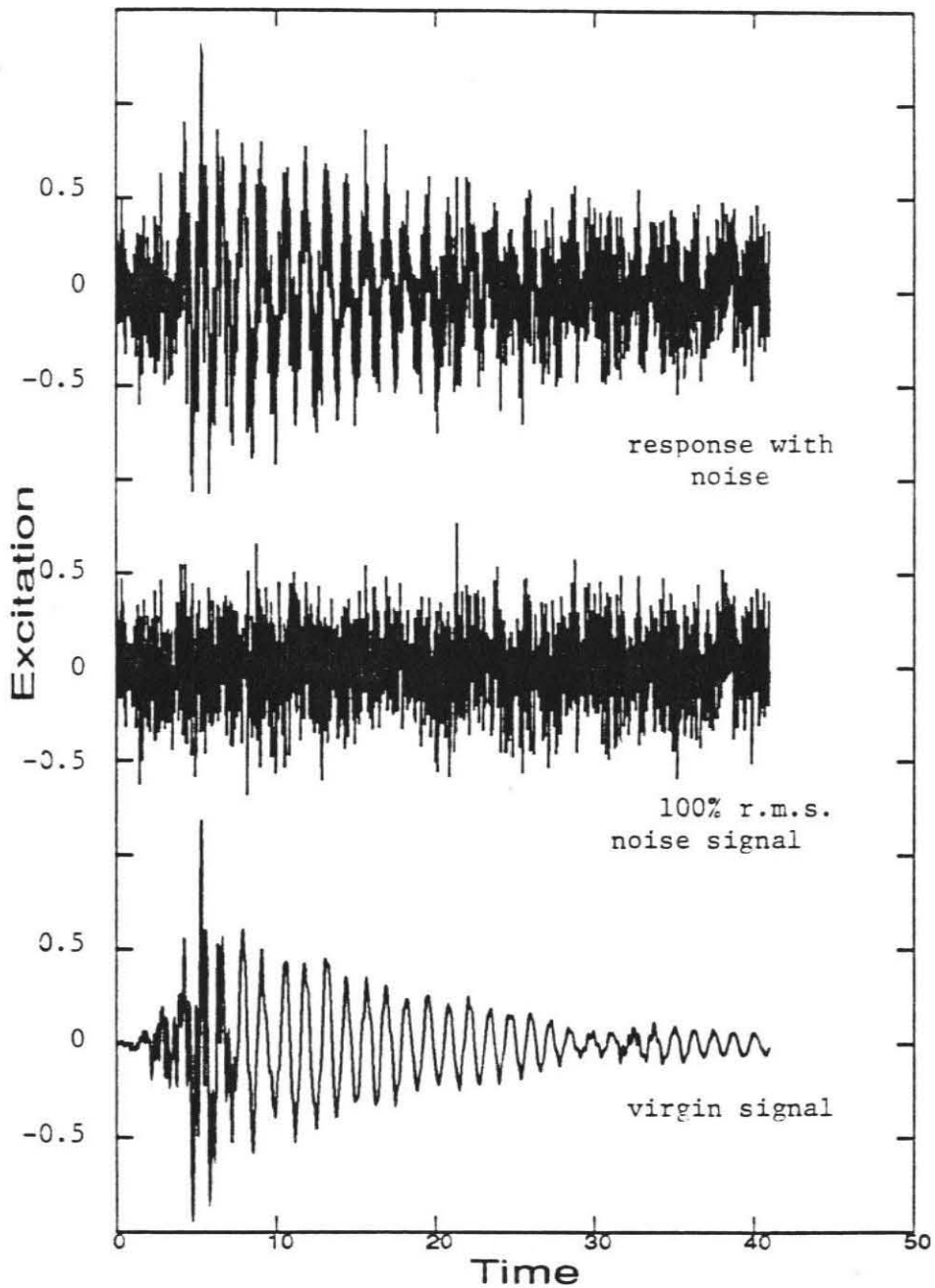


Figure 4.13: This diagram shows the method employed to construct the “noisy” signals. Noise in the form of a Gaussian white-noise signal was added to all input and output signals. The size of a noise signal was characterized by its r.m.s. value. This r.m.s. value was predefined as a fraction of the r.m.s. value of the base acceleration (for input signals) or of the r.m.s. value of the roof acceleration (for output signals).

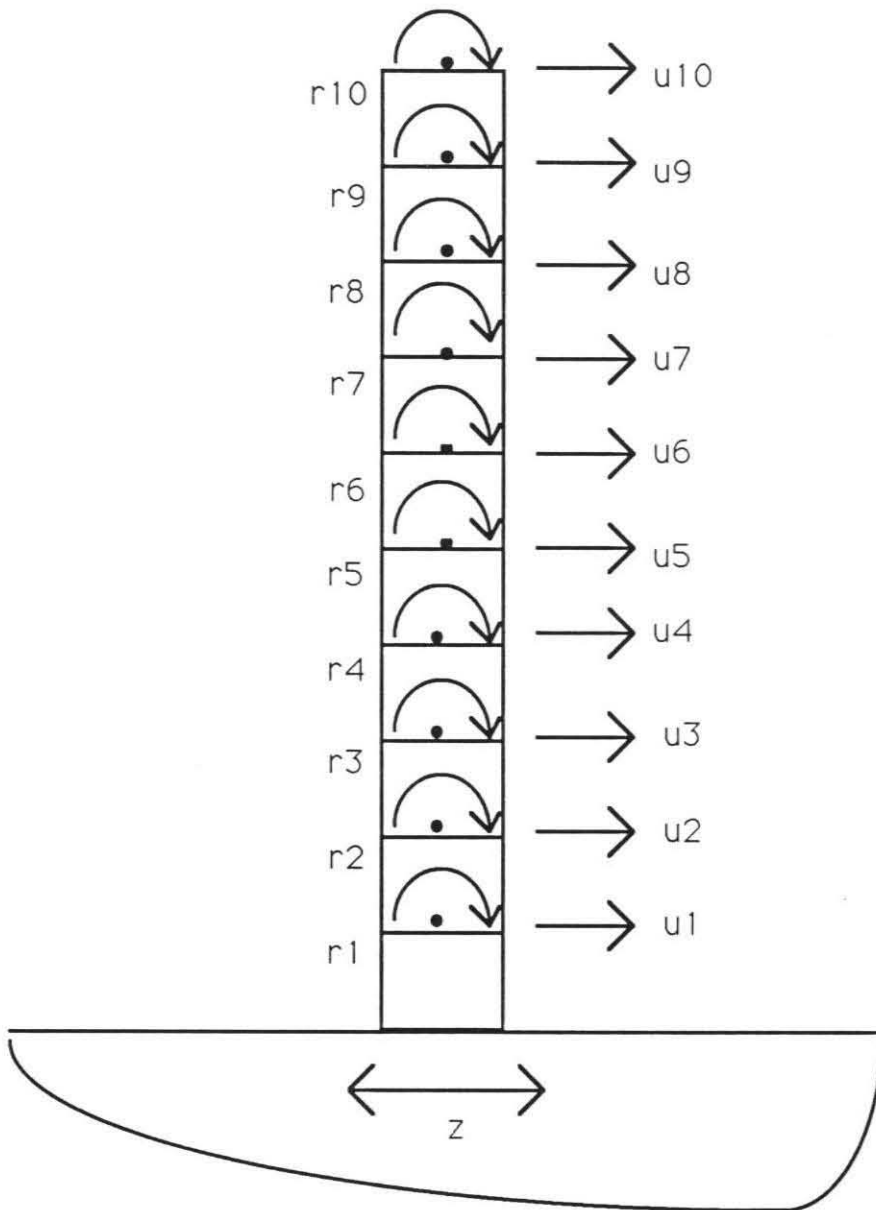


Figure 4.14: 20-DOF beam model employed in the simulations.

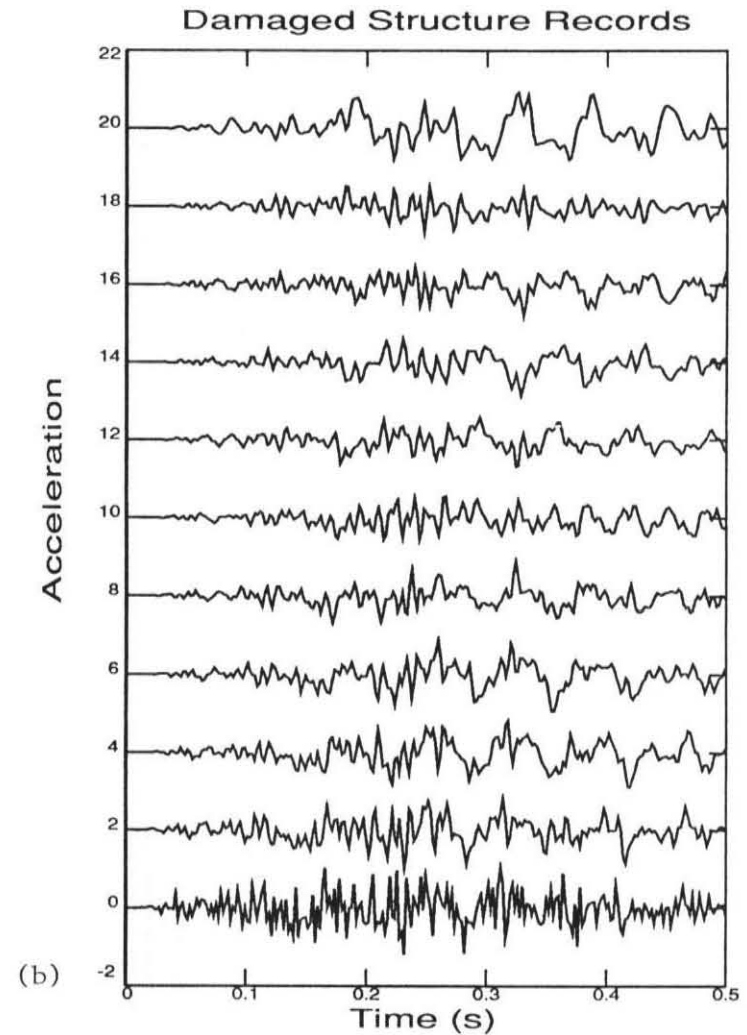
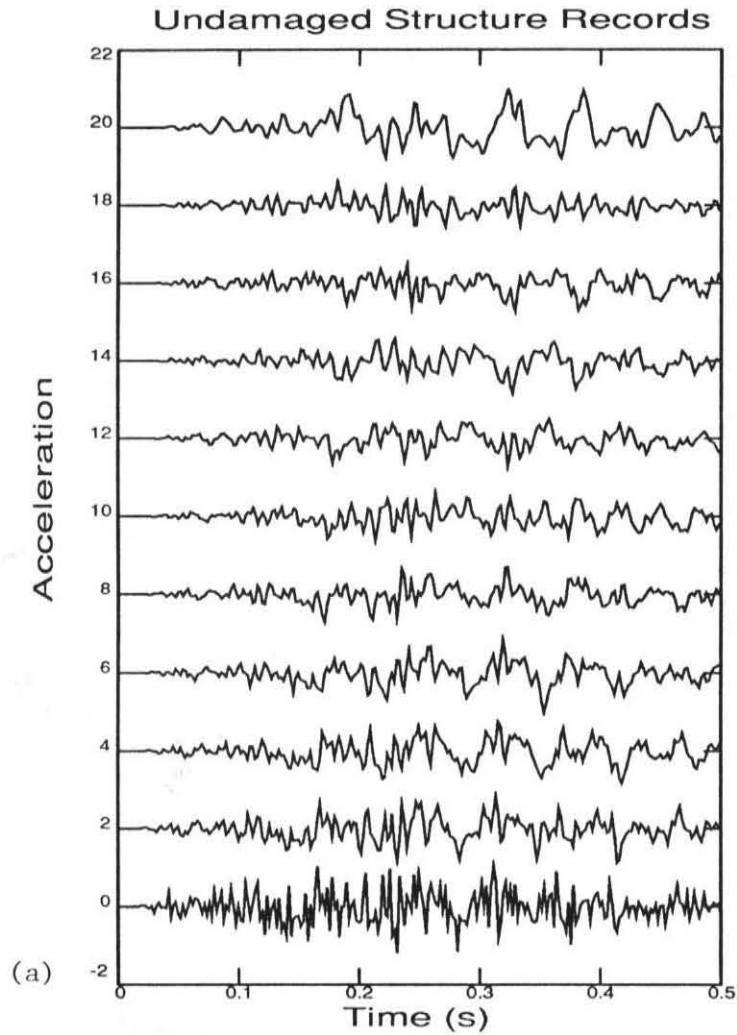


Figure 4.15: Acceleration time histories corresponding to a beam model of a ten-story building subject to base excitation. Set (a) corresponds to an undamaged structure, and (b) to the damage pattern presented in Table 4.4. Signals range from the lowest signal, corresponding to the base acceleration, to the top-most signal, corresponding to the roof acceleration.

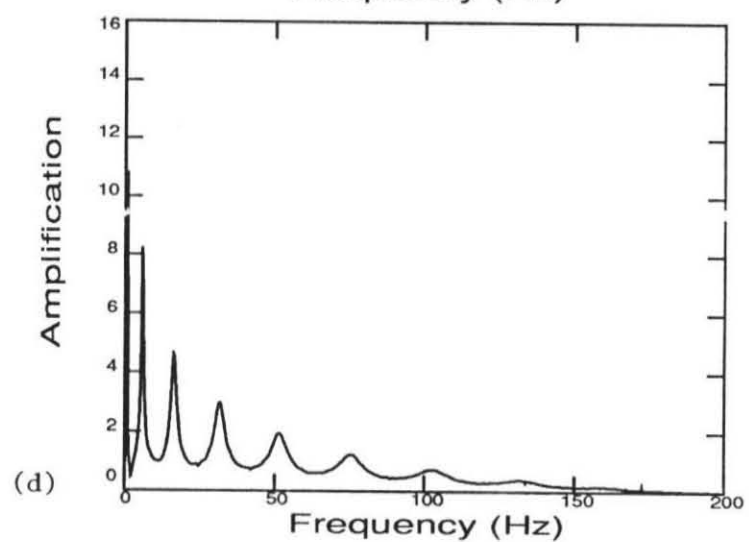
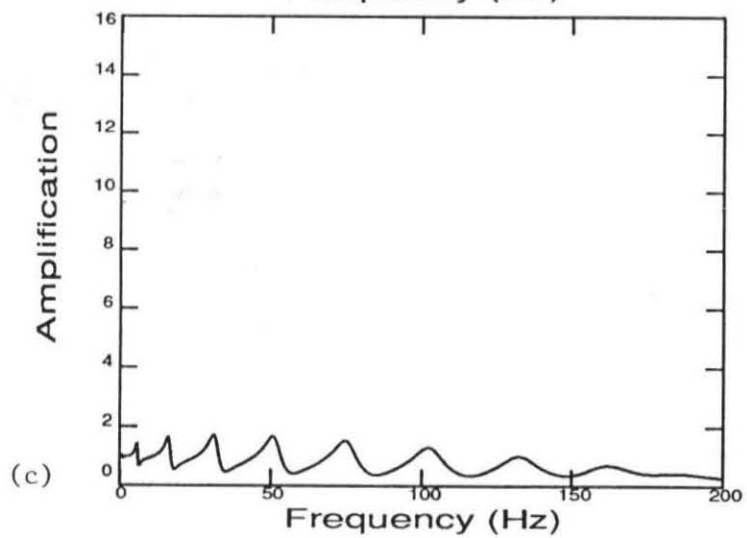
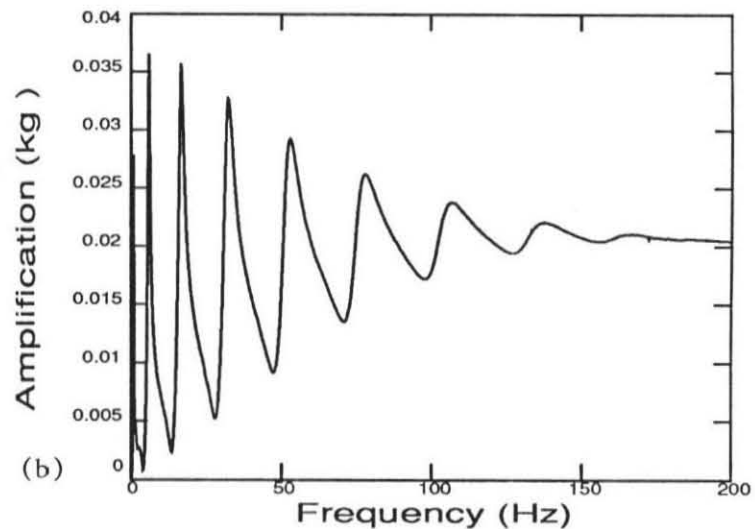
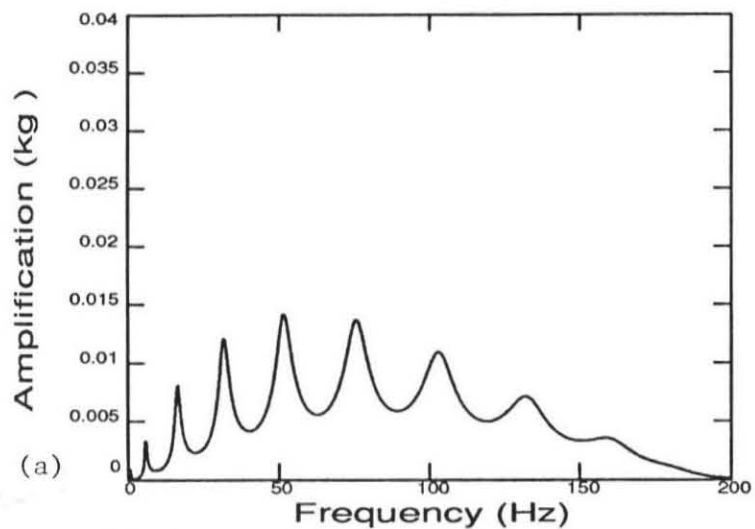


Figure 4.16: Transfer function for a beam model with roof and base excitation. Spectra (a) corresponds to roof excitation, monitoring the first DOF; (b) roof excitation, roof monitoring; (c) base excitation, first DOF monitoring; (d) base excitation, roof monitoring.

Chapter 5 : Data from a Model Structure

In this section, the structural identification algorithms are applied to experimental data in order to examine their damage detection capabilities. Experimental data from a model structure are useful since model error is involved, which is always present in all applications to real structural data, and yet damage can still be easily introduced.

The “3-story” frame structure depicted in Fig. (5.1a) is shaken in its undamaged state and responses are recorded at each of the “floors” (the “undamaged” state refers to the structure just after assemblage). From these, it is possible to calibrate the θ models so that these fit the observed data. The frame is then shaken in its damaged state, where a specified structural member is replaced by a weaker member. Based on the analytical model and on this new data, the aim is to detect any changes in the parameters representing stiffness degradation.

Section 5.1 - Experimental Setup and Procedures

A 6061-T6 aluminum skeleton is assembled as shown in Fig. (5.1a). The beam-column elements are connected by aluminum elbows. Each elbow end and each beam-column element end is drilled four times. Each hole is placed at the vertex of a square fitting inside the ends. The spacing between the holes allowed the screws and nuts to be fastened very securely without interference. The thickness of all aluminum parts is 3.175 mm (1/8 in) and the width is 25.4 mm (1 in). The length of the beam-column elements is 254.0 mm (10 in). Damage is simulated by replacing member M3 by a vinyl member (of unknown viscous properties) thereby changing the elastic modulus by several orders of magnitude. The skeleton lower elbows are bolted to a 25.4 mm (1 in) thick aluminum plate which is itself securely clamped to a laboratory table. The width and length of the plate is 200.0 mm by 400.0 mm, respectively. The elbows on the top corners are used to attach accelerometers.

A hammer with a transducer at the tip is used in the experiments to excite the frame structure. These experiments are referred to as Hammer-Impulse Experiments (“HIE”). The output from the hammer is connected to an amplifier which itself is connected to the data acquisition system.

Endevco Model 2226C piezoelectric accelerometers are placed on different parts of the frame. A dual-surface adhesive tape is used to attach these accelerometers to the structure. The output cables of the accelerometers are connected to Endevco 2713B amplifiers. The output of the amplifiers is connected to an RC Electronics analog-to-digital data acquisition card inside a Compaq 8086 portable computer. The triggering and scope capabilities were provided by the accompanying Computerscope ISC-16 program. The computer files are transferred to a VAX/VMS computer and the signal processing and reduction are performed using the *SIG* [5.2] computer program.

In the experiments, an impulse is imparted to the frame at approximately 1.5 inches above the second "floor" level by means of a hammer pulse. The pulse is captured by the hammer transducer and transmitted to the RC Electronics input box and then stored in the Compaq computer. One hammer pulse and two acceleration response signals are recorded on each run. The sampling is performed every $2.0 \cdot 10^{-4}$ seconds. The two accelerometers measure the horizontal motion and are attached to the structure in the following way:

Run	Channel 1	Channel 2
1	Above "2nd Floor"	Below "1st Floor"
2	Above "2nd Floor"	Above "1st Floor"
3	Above "2nd Floor"	Below "2nd Floor"
4	Above "2nd Floor"	Above "2nd Floor"
5	Above "2nd Floor"	"3rd Floor"

Program *SIG* is used to reduce the data in the following way: Channel 1 remains fixed as the "reference" channel to verify that all excitations are consistent. Fig. (5.4a) and Fig. (5.4b) show the hammer pulses and the accelerations for Channel 1, respectively, corresponding to runs 1-5 as monitored in the "undamaged" test. The transfer function between the hammer pulse and the motion at Channel 1 is calculated to determine whether the structure suffers any changes between the impact tests. The transfer function between the hammer pulse and the Channel 2 output is also calculated for each of runs 1-5 and, in this way, the impulse response functions are obtained. All transfer functions are then convolved by a "typical" hammer pulse (with the same characteristics as those shown in Fig. (5.2a)) to obtain the response at each level due to the specified Run-2 pulse. In this way, the transfer functions address the fact that no two hammer pulses between different runs are identically equal. This procedure is necessary because only 2 accelerometer channels are available or trustworthy. The response signals for runs 1 and 2 are averaged to provide a signal corresponding to the model node at the "1st Floor" level. The same is done for signals 3 and 4 for the node at the "2nd Floor" level. All signals are then filtered with a low-pass bell filter with cosine decay between 90 and 100 Hz thereby removing all noise as well as any very high mode information. The resulting signals are then decimated eight-fold so that the time step increases to $1.6 \cdot 10^{-3}$

seconds. The associated Nyquist frequency is now close to 310 Hz. The whole procedure is done twice: once for the “undamaged” setup and a second time for the “damaged” situation.

Section 5.2 - SUB-ID Results

Section 5.2.1 - Preliminary Simulation Results

To investigate the effects of model error and possible non-uniqueness in the parameter estimation for the actual experimental set-up, a set of numerical experiments was first carried out. These experiments were chosen to mimic the actual set-up so they would give insight into what results should be expected from the experimentally acquired data.

The procedure using the simulated data is the same as that used with the actual data:

- (1) Create a computationally-efficient model.
- (2) Determine the level of accuracy of the model. If the accuracy is poor, create another model.
- (3) For the level of accuracy in the computational model, determine the maximum number of parameters θ_i allowed.
- (4) “Calibrate” the parameter values for the undamaged configuration.
- (5) Run the identification codes employing the damaged data and localize the damage.
- (6) In the damage areas, discretize the model further in such a way that more parameters θ_i can be assigned to previous members of the damaged module. Repeat steps 4-6 until all stiffness factors in the damaged estimates are lower or equal to the undamaged estimates, since the damage corresponds to a loss of stiffness.

A frame model with 148 degrees of freedom is used to mimic the true structure for the numerical experiments and is referred to as the “complex system model” within this section. The elbows, the change of moments of inertia along the length of the beam-column elements, and the boundary conditions are taken into account. As is necessarily done in practical situations, two simpler, more computationally-efficient models are employed for identification purposes: a 3-DOF chain model and an 18-DOF frame model. Fig. (5.1) and Fig. (5.3) show details in the development of the complex and simple models. The simpler models have different dynamic characteristics than the more complex model yet it is believed that the essential interstory stiffness properties are similar. Thus, just as in the actual experiment, the models are only an approximation to the true system. The complex model is used to generate “undamaged” and “damaged” state data in the same way

as discussed in the Chapter 4. Table (5.1) shows the modal parameter values obtained from the 148-DOF system model in the various states.

The 148-DOF model was constructed based on the nominal geometric and material properties of the real structure. The damage, however, is simulated by arbitrarily reducing the stiffness values of specific members within the complex structure. Damage pattern D1 corresponds to a 50% reduction of stiffness in member M1 and damage pattern D2 corresponds to a 80% reduction in member M3. Both of these members are indicated in Fig. (5.1).

The “system” or reference signals for the 1st and 2nd floors are constructed in the same manner as in the experimental procedure: the transverse acceleration at the *3-DOF chain and 18-DOF model node* location is taken to be the average of the acceleration signals of the complex model measured immediately below and above this node. The signals are constructed in this way since the physical structure cannot be monitored exactly at the nodes of the simpler models. The accelerations, though, can be monitored slightly below and slightly above the joints where no bolts and nuts interfere with the placement of the transducers. The accelerations at the 3rd floor of the real structure are measured directly since there is, in practice, no interference and so, in the simulations these correspond exactly to the model node.

The complex 148-DOF and the simpler 18-DOF frame and 3-DOF chain models produce different responses at the monitored degrees of freedom. Fig. (5.4) shows the transfer functions of both the complex system and the nominal simple models for the undamaged configuration. (The nominal models corresponded to uniform stiffness distributions whose first modal frequency matched the observed value.) Damping 5% of critical is used in the actual simulations to reduce the duration of the latter but low damping (2% of critical) was used in Fig. (5.4) in order to illustrate how the higher modes participate in the response. The similarities between the two transfer functions appear in only the first three modes; the higher mode information is significantly different. It is well known, however, that once a “coarse” model is used, inaccurate solutions at all frequency ranges are expected, especially in the higher modes. Since it is conjectured that the simpler model still possesses the essential interstory properties of the complex system model, the simpler model is accepted as a viable model for the system as long as no attempt is done to predict modal properties of modes beyond the first three, which correspond to the important horizontal translational modes. This problem of choosing a reasonable model to approximate the actual system is a particularly delicate one in real situations. The model should be able to capture the essential features of the dynamics of the system, and its parameters should be physically interpretable.

Only ill-conditioning and non-uniqueness are considered in the simulations, so given that only three modes are trustworthy, what distribution of stiffness factors θ_i is optimum? From a geometric point of view, since each modal quantity is constant on a hypersurface in the parameter space, to pin down one such θ vector requires, at least, as many intersecting surfaces as the dimension of

the space. With N_p linearly independent normal vectors to the hypersurfaces, it is theoretically possible to guarantee local uniqueness of an N_p -dimensional vector θ . If some of these normal vectors are nearly parallel, however, then there is a direction perpendicular to these normal vectors along which the modal properties vary very slowly, i.e., ill-conditioning is present. The number of modal quantities for the problem at hand is 12 (3 modes and 4 modal quantities per mode). With this information, it is expected that a vector with 12 different θ_i values can be resolved. But since the modeshapes change very slightly with changing values of θ_i , it is probably more realistic to assume that there are no more than 3 independent modal quantities (3 modes and only one frequency for each mode). Thus, a model with 3 parameters θ_i ought to be identified without incurring ill-conditioning problems. The above uniqueness condition refers to a local property and not necessarily a global one. The SUB-ID-H homotopy algorithm can resolve global uniqueness results but it is only applied to the 3-DOF chain model where the number of possible stiffness combinations ($3!$) is small. For the 18-DOF simple frame model, the maximum number of possible stiffness combinations is $18!$, which is excessive for the computing facilities available. SUB-ID-SS is also used with the 3-DOF model since the number of measured eigenvector components equals the number of degrees of freedom ensuring, most likely, a convergent solution. For the 18-DOF model, reliance is placed solely on the SUB-ID-Modal and SUB-ID-Time algorithms.

In the tests described below, SUB-ID-Modal weighted errors in the modal frequencies by $2/3$ and errors in the modeshapes by $1/3$ as given by Eq. (3.3.2) in Chapter 3. This scheme emphasizes the modeshape vectors significantly more than the natural weighting implied in the output error approach of program SUB-ID-Time. The minimization technique employed in SUB-ID-Modal is Fletcher-Reeves with finite difference gradient evaluation. SUB-ID-Time employed even weight on all monitored degrees of freedom. Stiffness parameters as well as damping ratios are estimated for 3 modes. The number of points in the time histories is 1024 and the time step is $2 \cdot 10^{-3}$ sec. producing signals 2.048 sec. in duration. The minimization technique used is also Fletcher-Reeves with analytical gradient evaluation in SUB-ID-Time. Convergence for both algorithms corresponds to relative error index changes of less than $\epsilon = 10^{-4}$ across major conjugate gradient iterations.

Section 5.2.1.1 - 3-DOF Chain Model of System

The 3-DOF chain model depicted in Fig. (5.3) provides a relatively simple representation of the frame structure, but to find all possible stiffness combinations which match the observed properties may be a difficult task. Fig. (5.6abc) show surfaces in θ space for constant natural frequency values associated with a uniform 3-DOF chain system. From these figures, it can be appreciated that to find all the points θ which have the three natural frequencies in common is a non-trivial problem. Table (5.3) shows the results provided by the SUB-ID-H algorithm applied to the 3-DOF chain model. As described earlier, the homotopy method is able to determine all non-unique

solutions to this problem. In the results, all stiffness distributions (real and complex) match the modal frequencies, exactly. Whether the modeshapes associated with each stiffness distribution also matches the modeshapes of the 148-DOF frame model or not can be succinctly evaluated by applying an error norm similar to the one used by SUB-ID-Time. The error index for such norm is presented in the last columns of Table (5.3). This norm resolves which of the distributions is the most likely one. There is some indication that there is damage in the lower module in the D1 case and there is damage in the middle module in the D2 when looking at all results. But when attention is focused on the most likely values, #5 distribution in the undamaged case, #3 in D1, and #6 in the D2 case, then the numbers do not make much sense since some of the stiffnesses increase dramatically, in going from the undamaged to the damaged state.

SUB-ID-H also predicts θ estimates with imaginary components, but in this study only the real solutions give valid chain models. Complex distributions are understood to be purely mathematical in nature (a solution to a polynomial system) but may, nevertheless, imply some physical state. For example, the class of models may not be able to match the prescribed modal frequencies with real scalars in the expected region of the θ space even though these frequencies correspond to the modes of the actual system. A reason for this is that the model might not be accurate enough, as is the case when the mass distribution is not well known, for example. In these cases it is expected, nevertheless, that each complex θ_i is dominated by the real component. Distributions #3 and #5 for the D2 damage case in Table (5.3) are dominated by such component, which is close to the solution identified by SUB-ID-Time in Table (5.4), but the latter solution gives a second mode frequency of 28.33 Hz, 4% less than the actual frequency of 29.47 Hz in Table (5.1). This suggests that the 3-DOF chain model is not capable, indeed, of matching the damaged system frequencies with a real solution in the neighborhood of the undamaged stiffness distribution. Incidentally, the #3 distributions predicted by SUB-ID-H in all three cases - undamaged, D1, and D2 - come closest to those predicted by SUB-ID-Time even though these do not minimize the functional J_M associated with SUB-ID-Modal, as seen in Table (5.3).

SUB-ID-Time results are shown in Table (5.4) where it is clear that the solutions match closely just one of the many solutions given by SUB-ID-H. That SUB-ID-Time's result match one set of the SUB-ID-H results is reasonable since SUB-ID-Time is very sensitive to the natural frequencies and so it is very likely to arrive at some stiffness distribution which shares the three observed natural frequencies. Table (5.2) presents the results from SUB-ID-Modal for the same model. In general, the stiffness distributions are more consistent than those predicted by the homotopy method and are useful to determine the location of the error. This indicates that the chain model, after all, is viable candidate for the detection of damage in the more complex 148-DOF system. The frequencies are, in general, not matched well in the SUB-ID-Modal results. The reason for this is that SUB-ID-Modal places more weighting on minimizing the Euclidean error between the observed and model partial modeshape vectors.

Lastly, the results from SUB-ID-SS shown in Table (5.5) indicate clearly the location of damage for both the D1 and the D2 patterns. The values come close to those previously estimated by SUB-ID-Modal, even though the method of successive substitutions has a different implied weighting of the frequencies and modeshape vectors.

Section 5.2.1.2 - 18-DOF Frame Model of System

Although the SUB-ID algorithms using the 3-DOF chain model of the 148-DOF system do suggest the correct location of the damage, the model error created by this highly simplified model of the system prevents correct estimation of the degree of damage. For example, both SUB-ID-Time and SUB-ID-Modal show a stiffness loss in the first story of 10% for damage case D1, but the 50% decrease in stiffness in “damaged” member M1 should produce closer to a 25% decrease in the overall stiffness of module S1.

To reduce the model error, a better model of the 148-DOF system is studied using the 18-DOF frame model. Because of its detail, it might be possible to both (1) localize the damage more closely, and (2) predict the degree of damage better. In this model, there are many more ways to define the sub-structures associated with the θ_i than in the 3-DOF chain model. Fig. (5.5) depicts the different sub-structuring schemes used by the programs SUB-ID-Modal and SUB-ID-Time with this 18-DOF frame model. Sub-structure SS_3 is the initial, most obvious discretization choice from which any damage pattern should become evident. SS_4^7 corresponds to a sub-structuring with 4 independent θ_i , one of them corresponding to member M7; SS_4^8 , likewise, has 4 independent parameters with one corresponding to member M8. SS_6 corresponds to the case where there are six independent parameters, three for each of the beams and the other three for each pair of columns, both at each of the three interstory levels.

Table (5.6) shows the results obtained from the SUB-ID-Modal program while the results in Table (5.7) correspond to SUB-ID-Time. In each table, the first three θ_i correspond to the column parameter stiffnesses while the second three θ_i correspond to the beam stiffnesses. The estimated values as shown in the tables indicate discrepancies in the identifications. For the undamaged cases, values larger than unity were found for some of the θ_i . These values were not expected at first since the 18-DOF model response ought to be a very good approximation to the 148-DOF system. This characteristic, plus the fact that the error indices are not close to zero, indicate that there is still significant model error, especially since no other type of corruption of the data exists. A closer look at the reference 148-DOF system indicates that the the “joints” are fairly stiff and that indeed one must expect values for the θ_i larger than unity. That the stiffnesses are not evenly distributed in the undamaged case in the absence of noise is a result that is not well understood, since both the 148-DOF system and the nominal 18-DOF model (with all θ_i ’s unity) are mathematically constructed with the same stiffness distribution in each sub-structure. The best answer to the

question of non-uniformity in the stiffness may lie in considering the boundary conditions on the lowest sub-structure. The complex model has been created without rigid rotational attachments. Only the horizontal and vertical displacements have been constrained in an effort to simulate the bolt connections present in the experimental case. Some of the modal properties of the 148-DOF system (not shown here) indicate that indeed the rotational degrees of freedom are not fixed and that they rotate very slightly. The rigidity present in the simple system model prevents the rotations of the joints and thus it is expected that the identified stiffness of the sub-structure immediately above decreases to accommodate this effect. The larger-than-one value for θ_1 is attributed to the large stiffness introduced by the beam. This will be seen more clearly in the following discussion.

The coarse discretization of the structure into only three modules (sub-structuring SS_3), as shown in Fig. (5.5), can be seen as one in which two modules (vertical members and horizontal members) had their corresponding θ_i "slaves" to each other. The prediction of damage for damage cases D1 and D2 based on this sub-structuring is relatively accurate since the damage patterns are well identified in the results from Table (5.6) and Table (5.7). Damage pattern D1 shows as a reduction of approximately 25% in the overall stiffness of module S1, which is roughly what is expected since member M1's stiffness is reduced by 50%. This is seen in both the SUB-ID-Modal and SUB-ID-Time results, although the values themselves are different. This reduction also incorrectly reduces the stiffness of member M7 since it is part of module S1. Unless member M7 remains relatively stiff, axially and in bending, it is expected that the other modules take the loads that member M7 sheds because of the reduced stiffness. Thus, it would normally be the case that the adjacent modules slightly increase their overall stiffness factors θ_i . Less than 2% deviation from the undamaged case is shown for either quantity (θ_2 or θ_3) for the SUB-ID-Modal results and 5% for SUB-ID-Time in damage pattern D1.

Pattern D2, however, shows a reduction of 50% for the SUB-ID-Modal case as opposed to the expected overall 40% reduction from the 80% reduction in member M3. Because of this reduced stiffness, it is expected that an increase should appear in the stiffness of the adjacent sub-structures (S1 or S3). The increase of almost 30% in θ_3 shows how much sub-structure S3 had to be altered to compensate for the 50% decrease in sub-structure S2's overall stiffness. Sub-structure S1, on the other hand, decreased slightly. SUB-ID-Time results for damage D2 are similar to those of SUB-ID-Modal although the decrease of stiffness in sub-structure S2 is larger, close to 55%. Parameter θ_3 also increased by about 40% and θ_1 also decreased slightly. The larger decrease in the θ_2 stiffness than the actual amount can only be attributable to incorrect modeling. In this case, modeling not only includes the details about the joints and the changing values of the moments of inertia throughout the system which are not present in the simpler model, but also the fact that the sub-structuring of the system into only three modules is constraining both column and beam members in each module to be scaled with only one θ_i parameter. The modal properties are not well matched, which is a strong sign of incorrect modeling, although keeping Table (5.1) in mind, the results seem

to be much better in Table (5.7) than in Table (5.6). The increase in the stiffness parameter θ_3 is also another sign which calls for better modeling and in this case, with the results available, it almost implies that sub-structure S2 should be further discretized into smaller sub-structures. The number of θ parameters would increase in this case and so there may not be enough independent modal quantities to prevent ill-conditioning and/or non-uniqueness.

It is possible to discretize the structure using a finer discretization around the areas where damage is suspected. For example, for damage pattern D1, which is associated with the weakening of member M1, sub-structure S1 can be split into two sub-modules, a new S1 and S4. This new arrangement of sub-structures corresponds to sub-structuring SS_4^7 in Fig. (5.5). The region to which the old θ_1 was associated has now two θ_i 's, namely, the new θ_1 and θ_4 . The stiffness distributions for four-parameter sub-structuring present good convergent characteristics and interesting results. Table (5.6) shows the results corresponding to the four-parameter discretization derived from SUB-ID-Modal using sub-structuring SS_4^7 . Slight damage in module S1 can be seen from these results but not enough to agree intuitively with the 25% reduction expected from the 50% reduction in member M1's stiffness. The same table shows that the adjacent modules to the "damaged" module also undergo slight changes in their parameter values when the damage is added.

Sub-structuring the system in the form SS_4^8 , as depicted in Fig. (5.5), allows the determination of four parameters with a model emphasizing potential damage in module S2. The old S2 is now split into a new S2 and the new S4. Table (5.6) also shows the results for this case. A 46% stiffness reduction can be seen in sub-structure S2 but increase is seen in S1 (3%) and in S4 (15%). Also, the stiffness increase in S4 may account for the slight decrease in stiffness in module S3.

Refining the model further results in one with six θ_i : the first three correspond to each of the three pairs of vertical members and the second three θ_i correspond to each of the horizontal members (increasing order of the θ_i with increasing height). This refined model corresponds to sub-structuring SS_6 in Fig. (5.5). Unfortunately, numerical tests have shown that six parameters are too many for the amount of modal information that is used (first three modes) in program SUB-ID-Modal. Minimizations performed on this basis have yielded non-unique sets of parameters (not shown here). This may come as a surprise since there are 12 pieces of information (4 modal parameters per mode and 3 modes). In the SUB-ID-Time case, the implicit introduction of the participation factors has added one more modal parameter per mode yielding a total of 15 modal quantities. In Table (5.7), it can be seen that the estimates for the columns agree closely with the estimates in the four-parameter case given by SUB-ID-Modal in Table (5.6). The beam stiffness parameter estimates take on values much larger than those for the columns, but this happens to be reasonable. By looking at the structure more carefully, it can be seen that the beams are indeed stiffer: one elbow element is connected to the end of each column while two elbows are connected at the end of each beam. The error indices are of lower order in the six theta case compared to the

three theta case indicating that the additional freedom in the sub-structuring allows better matching of the responses. The match can be seen in Fig. (5.7).

Using sub-structuring SS_6 , the damage has also been adequately identified in both cases, with damage (stiffness loss) in member M1 of the order of 27% and damage in member M3 of the order of 48%. These results make more sense than those from using SUB-ID-Modal. The modal frequencies, as expected, are better approximated with SUB-ID-Time since this algorithm is highly sensitive to them. From these results, however, it seems that member M8 has too low of a value in the undamaged state and member M9 has too large of a value. Once damage has been inflicted, their values change considerably. To understand this, it is noted that the accuracy of the parameter values depend on the sensitivity of the results on the particular parameter of interest. For this frame structure, the dynamics are not sensitive to changes in the bending stiffness as long as the beam bending stiffnesses are high. Conversely, slight changes in the dynamics may induce large changes in these “insensitive” parameters. If the model is incorrect, the dynamics will be different and thus the “insensitive” parameter values will have to incur large changes in order to match the observed data appropriately. An overall evaluation of the results suggests that the model with 6 parameters is the most reliable and the one with least error. Incidentally, the discrepancies between the Modal and Time versions of SUB-ID tend to decrease as SUB-ID-Modal places more emphasis on the natural frequencies and less on the modeshapes. Table (5.8) shows various results for the SS_3 sub-structuring, D1-damage case from where it can be seen that, indeed, the SUB-ID-Modal results approach those estimated by SUB-ID-Time.

Section 5.2.2 - Experimental Results

In this section, results are presented for the identification runs with various sub-structuring based on the actual test data from the three-story experimental model. Much similarity is present between experimental results and simulation results. The undamaged structure results are similar for both types of tests. The damaged structure is similar to case D2 in the simulated data tests.

Table (5.9) shows the modal parameter estimates associated with the real structure obtained with program MODE-ID [5.1], which can be viewed as the best estimates of the test structure modal properties since, apart from the assumption of linearity and classical normal modes, no structural model is assumed.

Section 5.2.2.1 - 3-DOF Chain Model of Test Structure

Results from the 3-DOF chain model resemble those from the simulations. Indeed, the results shown in Table (5.10), Table (5.11), and Table (5.12), and Table (5.13) for the homotopy, modal, time, and successive substitution approaches, respectively, demonstrate the disadvantages of using

such simplistic 3-DOF model. Some idea of damage can be inferred from the results but the results are not all consistent. This is attributed to the 3-DOF chain not being a good model for the real structure, reflecting the same type of problems that showed up in the simulated data tests.

Section 5.2.2.2 - 18-DOF Frame Model of Test Structure

The next model to be considered is the 18-DOF frame model with SS_3 sub-structuring. The damaged-structure results clearly indicate the point of failure in the frame structure, namely, somewhere in sub-structure S2. These results are shown in Table (5.14) and Table (5.15) for SUB-ID-Modal and SUB-ID-Time, respectively. The damage location agrees entirely with the location where the aluminum member was substituted with the vinyl-plastic member, i.e., member M3. The stiffness for sub-structures S1 and S3 (Fig. (5.5)) have increased and it is believed that this is due to modeling error. By decreasing the stiffness for sub-structure S2 by such a large amount (more than 75% decrease), the stiffness of the horizontal member belonging to sub-structure S2 is also reduced by the same amount. In reality this member did not suffer any damage so its stiffness reduction affects the behavior of the sub-structure above it, module S3. The latter must therefore increase its stiffness to account for the overall reduction of the former. A similar argument can perhaps be applied to sub-structure S1.

A finer sub-structuring, as done in the previous section, leads to the other results shown in Table (5.14) and Table (5.15). These results are based on sub-structuring models SS_4^8 and SS_6 , respectively. By breaking up the middle module as shown in Fig. (5.5) into two other modules, the number of coefficients θ_i has increased to 4 but this amount of modal information was not enough to uniquely estimate the stiffness distribution. Table (5.14) indicates that, indeed, the middle horizontal member is stiffer as shown in previous sections. The results are very satisfactory since it is now seen that the introduction of the weak member has only affected substantially the estimate corresponding to that specific sub-structure. All other sub-structures have remained close to their previous estimated values which is consistent with the actual damage induced. The stiffness parameters associated with sub-structures S1 and S3 of Table (5.14) are average stiffnesses for the sub-structures. The fact that they are closer to the stiffnesses of the vertical members than to the stiffnesses of the horizontal member is attributed to the higher sensitivity of the translation motion to the interstory stiffness provided by these vertical members. The horizontal members can have an effect on the horizontal motion but only if their stiffness decreases to the point where the two sets of vertical columns become nearly independent. The motion then changes from shear-type to bending-type. For the stiffness distribution in the test structure, the vertical elements affect the horizontal motion more and, so, the shear-type behavior is dominant.

The large stiffness reduction for sub-structure S2 is unexpected. One would normally expect that if one of the two vertical members lost all horizontal stiffness then the overall reduction would

correspond to 50% and not to 75%. Something similar is seen in the previous section where the simulated damage in module S2 is a reduction of 80% in one of the two vertical members. A reduction of 80% in one member should correspond roughly to a 40% reduction for the module, but reductions of nearly 55% are present in that simulated case.

An attempt to calculate six parameters with SUB-ID-Modal, one for each pair of vertical members and one for each horizontal member, leads to non-unique parameter distributions. These results for sub-structuring SS₆ in Fig. (5.5) are not shown here because of their unreliability. The time domain program SUB-ID-Time, on the other hand, did determine the set of six parameters reliably and these are presented in Table (5.15). From this table and from Fig. (5.8), it is seen that the match this model allows is relatively better than the matches of the models with less parameter freedom. The parameter estimates are the common result of two different numerical minimizations starting with different initial estimates. Uniqueness, as explained later in this study, cannot be asserted but this solution seems physically reasonable. The stiffness distribution is quite uniform except for the fact that it is somewhat lower in sub-structure S1. It is argued here, as it was done in the previous section, that this may be caused by the rigidity imposed by the 18-DOF model on the joints at the base.

Section 5.3 - Summary

Model error is studied in a structure where damage can be easily introduced. Preliminary simulated results agreed fairly well with the actual experiment results. Both indicated that the better the model, the more accurate the predictions of damage. From the results it became clear that modeling involved two aspects: (1) modeling in the traditional sense: the analytical model should contain enough degrees of freedom and the correct geometric and material properties to enable a good representation of the system. In the case of the 3-DOF chain model, the results were very difficult to assess since they were inconsistent according to the parameter estimation procedure used. The 18-DOF frame model enabled the SUB-ID-Time procedure to define the location and seriousness of damage within the frame structure. (2) The second aspect of modeling is related to the fact that the choice of sub-structuring can hinder the estimation procedures from reaching reliable results. It is clear that the choice of sub-structuring should be such that the damaged member(s) should eventually be represented by at least one sub-structure. For the 18-DOF frame model, this was done by first performing a crude identification. Sub-structures that incurred loss of stiffness were discretized further and sub-structures that incurred gains of stiffness were kept constant. The latter gains are generally considered to be due to the mismodeling of the damaged sub-structures.

Results also show that even very crude models, such as the 3-DOF chain model for the

experimental frame, can give some idea about the location of damage. The extent of damage, however, cannot be clearly determined in these cases.

References for Chapter 5

- [5.1] Werner, S., Beck, J.L., Levine, M.B., "Seismic Response Evaluation of Meloland Road Overpass Using 1979 Imperial Valley Earthquake Records", *International Journal of Earthquake Engineering and Structural Analysis*, Vol. 15, 1987, p. 249.
- [5.2] Beck, R.T., "SIG", in *CADRE Reference Manual*, Melvin, J.D., editor, California Institute of Technology, Pasadena, California.

	Natural Frequencies			Eigenvectors		
	Damping Ratios			$\check{\phi}_1$	$\check{\phi}_2$	$\check{\phi}_3$
	f_1	f_2	f_3			
ξ_1	ξ_2	ξ_3				
Undamaged:	9.873	30.37	48.62	0.359	-0.949	1.421
	5.0	5.0	5.0	0.776	-0.452	-1.523
				1.000	1.000	1.000
Damaged D1:	9.468	29.20	47.67	0.399	-0.978	1.229
	5.0	5.0	5.0	0.793	-0.379	-1.470
				1.000	1.000	1.000
Damaged D2:	9.181	29.47	42.76	0.328	-1.143	0.842
	5.0	5.0	5.0	0.815	-0.346	-1.094
				1.000	1.000	1.000

Table 5.1: Exact parameters for the first three modes corresponding to the complex 148-DOF frame model. (Frequencies in Hz, damping ratios in % of critical.)

Stiffness Parameters			Natural Frequencies			Eigenvectors			$Error\ Index\ J_M$
θ_1	θ_2	θ_3	f_1	f_2	f_3	$\check{\phi}_1$	$\check{\phi}_2$	$\check{\phi}_3$	
Undamaged:									
1.669	2.078	1.695	11.88	32.22	46.83	0.508	-0.937	1.44	$1.4 \cdot 10^{-3}$
						0.819	-0.332	-1.82	
						1.00	1.00	1.00	
Damage D1:									
1.501	2.007	1.618	11.41	31.25	45.78	0.529	-0.930	1.42	$1.4 \cdot 10^{-3}$
						0.825	-0.313	-1.82	
						1.00	1.00	1.00	
Damage D2:									
1.709	1.327	1.579	11.03	30.63	41.41	0.418	-1.23	0.932	$1.1 \cdot 10^{-3}$
						0.832	-0.292	-1.36	
						1.00	1.00	1.00	

Table 5.2: SUB-ID-Modal Results for the 3-DOF chain model associated with the modal properties of the complex 148-DOF system model. (Frequencies in Hz.)

	Stiffness Parameters			Natural Frequencies			Error	Error
	θ_1	θ_2	θ_3	f_1	f_2	f_3	Index J_M	Index J_T
Undamaged:								
1	4.78+i3.38	2.24-i1.70	0.236+i0.01					
2	4.78-i3.38	2.24+i1.70	0.236-i0.01					
3	0.946	2.56	1.60	9.873	30.37	48.62	5.9 · 10 ⁻²	1.9
4	6.18	0.605	1.04	9.873	30.37	48.62	8.8 · 10 ⁻²	2.6
5	1.10	1.40	2.54	9.873	30.37	48.62	3.0 · 10 ⁻²	2.2
6	1.85	0.761	2.76	9.873	30.37	48.62	5.1 · 10 ⁻²	2.3
Damage D1:								
1	4.54+i3.14	2.14-i1.57	0.216+i0.01					
2	4.54-i3.14	2.14+i1.57	0.216-i0.01					
3	0.860	2.52	1.46	9.468	29.20	47.67	3.0 · 10 ⁻³	1.9
4	5.97	0.553	0.961	9.468	29.20	47.67	4.6 · 10 ⁻²	2.6
5	1.01	1.27	2.47	9.468	29.20	47.67	1.5 · 10 ⁻²	2.2
6	1.72	0.695	2.66	9.468	29.20	47.67	2.5 · 10 ⁻²	2.4
Damage D2:								
1	3.92+i3.11	1.84-i1.56	0.203+i0.01					
2	3.92-i3.11	1.84+i1.56	0.203-i0.01					
3	0.851-i0.041	1.63+i0.367	1.70-i0.297					
4	4.70	0.525	0.994	9.181	29.47	42.76	5.1 · 10 ⁻³	2.4
5	0.851-i0.041	1.63+i0.367	1.70-i0.297					
6	1.89	0.610	2.12	9.181	29.47	42.76	1.5 · 10 ⁻³	2.1

Table 5.3: SUB-ID-H Results for the 3-DOF chain model based on the modal properties of the complex 148-DOF system model. (Frequencies in Hz.)

Stiffness Parameters			Natural Frequencies			Eigenvectors			<i>Error Index_{J_T}</i>
θ_1	θ_2	θ_3	Damping Ratios			$\check{\phi}_1$	$\check{\phi}_2$	$\check{\phi}_3$	
			f_1	f_2	f_3				
			ξ_1	ξ_2	ξ_3				
Undamaged :									
0.952	2.552	1.608	9.89	30.40	48.58	0.688	-0.775	1.67	$7.4 \cdot 10^{-2}$
			4.29	3.08	5.40	0.868	-0.250	-2.19	
						1.00	1.00	1.00	
Damage D1 :									
0.863	2.478	1.517	9.474	29.52	47.60	0.701	-0.760	1.72	$7.2 \cdot 10^{-2}$
			4.33	3.91	5.09	0.871	-0.249	-2.25	
						1.00	1.00	1.00	
Damage D2 :									
0.866	1.732	1.519	9.216	28.33	42.76	0.647	-0.957	1.04	$1.4 \cdot 10^{-1}$
			3.76	10.3	4.82	0.878	-0.149	-1.62	
						1.00	1.00	1.00	

Table 5.4: SUB-ID-Time results for the 3-DOF chain model employing the acceleration responses of the 148-DOF system. (Frequencies in Hz, damping ratios in % of critical.)

Stiffness Parameters			Natural Frequencies			Eigenvectors		
θ_1	θ_2	θ_3	Damping Ratios			$\check{\phi}_1$	$\check{\phi}_2$	$\check{\phi}_3$
			f_1	f_2	f_3			
Undamaged:								
1.880	2.123	1.737	12.38	33.06	47.58	0.482	-0.938	1.52
						0.808	-0.368	-1.84
						1.00	1.00	1.00
Damage D1:								
1.590	2.096	1.669	11.70	31.88	46.72	0.523	-0.923	1.46
						0.821	-0.325	-1.85
						1.00	1.00	1.00
Damage D2:								
1.793	1.345	1.622	11.21	31.14	41.90	0.403	-1.24	0.933
						0.832	-0.300	-1.35
						1.00	1.00	1.00

Table 5.5: SUB-ID-SS Results for the 3-DOF chain model associated with the modal properties of the complex 148-DOF system model. (Frequencies in Hz.)

Stiffness Parameters			Natural Frequencies			Eigenvectors			<i>Error Index J_M</i>
θ_1	θ_2	θ_3	f_1	f_2	f_3	$\check{\phi}_1$	$\check{\phi}_2$	$\check{\phi}_3$	
θ_4	θ_5	θ_6							
a) Sub-structuring SS ₃									
Undamaged:									
1.239	1.235	1.484	9.222	29.62	49.19	0.349	-1.05	1.52	$6.3 \cdot 10^{-4}$
						0.774	-0.500	-1.65	
						1.00	1.00	1.00	
Damage D1:									
0.980	1.256	1.498	8.608	28.53	48.22	0.391	-1.07	1.33	$6.5 \cdot 10^{-4}$
						0.786	-0.416	-1.58	
						1.00	1.00	1.00	
Damage D2:									
1.221	0.603	1.919	8.098	27.82	44.01	0.270	-1.42	0.988	$3.7 \cdot 10^{-3}$
						0.787	-0.472	-1.30	
						1.00	1.00	1.00	
b) Sub-structuring SS ₄ ⁷									
Undamaged:									
1.101	1.279	1.574	8.745	29.42	47.38	0.379	-1.06	1.37	$5.3 \cdot 10^{-4}$
0.931						0.800	-0.436	-1.58	
						1.00	1.00	1.00	
Damage D1:									
0.965	1.267	1.486	8.717	28.47	48.23	0.393	-1.07	1.33	$2.2 \cdot 10^{-4}$
1.077						0.797	-0.416	-1.59	
						1.00	1.00	1.00	
c) Sub-structuring SS ₄ ⁸									
Undamaged:									
1.096	1.197	1.530	9.247	30.71	48.52	0.409	-1.03	1.37	$3.1 \cdot 10^{-4}$
	2.272					0.825	-0.402	-1.58	
						1.00	1.00	1.00	
Damage D2:									
1.124	0.651	1.462	8.709	29.76	42.66	0.355	-1.28	0.953	$3.3 \cdot 10^{-4}$
	2.604					0.850	-0.347	-1.281	
						1.00	1.00	1.00	

Table 5.6: SUB-ID-Modal Results for the simple 18-DOF frame model associated with the modal properties of the complex 148-DOF system. (Frequencies in Hz).

Stiffness Parameters			Natural Frequencies			Eigenvectors			<i>Error Index J_T</i>	
θ_1	θ_2	θ_3	f_1	f_2	f_3	$\check{\phi}_1$	$\check{\phi}_2$	$\check{\phi}_3$		
θ_4	θ_5	θ_6	ξ_1	ξ_2	ξ_3					
a) Sub-structuring SS ₃										
Undamaged :										
1.690	1.055	1.402	9.711	30.48	48.74	0.273	-1.02	1.84	$3.5 \cdot 10^{-2}$	
			4.32	5.79	4.31	0.734	-0.647	-1.70		
						1.00	1.00	1.00		
Damage D1 :										
1.414	1.101	1.329	9.334	29.28	47.78	0.306	-1.02	1.75	$4.2 \cdot 10^{-2}$	
			4.32	6.80	4.25	0.748	-0.591	-1.72		
						1.00	1.00	1.00		
Damage D2 :										
1.618	0.477	2.029	8.142	29.31	42.88	0.199	-1.42	1.11	$1.2 \cdot 10^{-1}$	
			14.9	6.08	4.07	0.771	-0.615	-1.27		
						1.00	1.00	1.00		
b) Sub-structuring SS ₆										
Undamaged :										
1.268	1.101	1.383	9.883	30.40	48.62	0.333	-1.13	1.36	$9.7 \cdot 10^{-3}$	
2.070	1.326	2.181	4.05	4.25	4.64	0.768	-0.493	-1.56		
						1.00	1.00	1.00		
Damage D1 :										
0.937	1.150	1.409	9.478	29.25	47.67	0.407	-1.11	1.20	$9.9 \cdot 10^{-3}$	
1.880	1.725	1.839	4.05	4.15	4.61	0.802	-0.373	-1.55		
						1.00	1.00	1.00		
Damage D2 :										
1.147	0.631	1.496	9.210	29.50	42.77	0.310	-1.37	0.942	$1.6 \cdot 10^{-2}$	
2.144	1.741	1.595	3.95	4.11	4.29	0.814	-0.402	-1.28		
						1.00	1.00	1.00		

Table 5.7: SUB-ID-Time results for the 18-DOF frame model given the averaged joint accelerations of the 148-DOF system. (Frequencies in Hz, damping ratios in % of critical.)

W^f	W^m	Stiffness Parameters			Natural Frequencies		
		θ_1	θ_2	θ_3	f_1	f_2	f_3
SUB-ID-Modal:							
2/3	1/3	0.980	1.256	1.498	8.608	28.53	48.22
9/10	1/10	1.130	1.110	1.540	8.830	28.91	47.96
99/100	1/100	1.309	1.062	1.453	9.113	29.23	47.72
SUB-ID-Time:							
		1.414	1.101	1.329	9.334	29.28	47.77

Table 5.8: SUB-ID-Modal results with different weights come close to those obtained from SUB-ID-Time if the error norm emphasizes the natural frequencies (with W^f) much more than the modeshape vectors (with W^m). (Frequencies in Hz.)

	Natural Frequencies			Eigenvectors			$\text{Error Index } J_T$
	Damping Ratios			$\check{\phi}_1$	$\check{\phi}_2$	$\check{\phi}_3$	
	f_1	f_2	f_3				
	ξ_1	ξ_2	ξ_3				
Undamaged:							
	8.986	28.63	48.00	0.308	-0.719	1.30	$5.2 \cdot 10^{-2}$
	0.83	0.46	0.45	0.610	-0.291	-1.21	
				1.00	1.00	1.00	
Damaged (D2-type):							
	7.601	27.04	38.06	0.236	-1.358	0.595	$7.4 \cdot 10^{-2}$
	1.49	0.83	1.01	0.769	-0.242	-1.023	
				1.000	1.000	1.000	

Table 5.9: MODE-ID Results obtained from the hammer test impulse-acceleration time histories for the three-story experimental model. (Frequencies in Hz.)

	Stiffness Parameters			Natural Frequencies			Error	Error
	θ_1	θ_2	θ_3	f_1	f_2	f_3	Index J_M	Index J_T
Undamaged:								
1	4.54 + i3.05	2.15 - i1.53	0.193 + i0.01					
2	4.54 - i3.05	2.15 + i1.53	0.193 - i0.01					
3	0.755	2.63	1.40	8.986	28.63	48.00	$1.6 \cdot 10^{-2}$	$2.0 \cdot 10^{-1}$
4	6.147	0.488	0.930	8.986	28.63	48.00	$1.2 \cdot 10^{-1}$	1.4
5	0.865	1.29	2.51	8.986	28.63	48.00	$6.7 \cdot 10^{-2}$	$8.7 \cdot 10^{-1}$
6	1.74	0.585	2.73	8.986	28.63	48.00	$1.1 \cdot 10^{-1}$	$9.7 \cdot 10^{-1}$
Damaged (D2-type):								
1	3.17 + i2.63	1.50 - i1.32	0.136 + i0.004					
2	3.17 - i2.63	1.50 + i1.32	0.136 - i0.004					
3	0.547 + i0.03138	1.38 - i0.436	1.36 + i0.363					
4	3.81	0.345	0.852	7.60	27.04	38.06	$2.0 \cdot 10^{-1}$	1.9
5	0.547 - i0.03	1.38 + i0.436	1.36 - i0.363					
6	1.74	0.375	1.71	7.60	27.04	38.06	$3.3 \cdot 10^{-2}$	$2.8 \cdot 10^{-1}$

Table 5.10: SUB-ID-H (homotopy) results for the 3-DOF chain model given the modal properties of the real structure.

	Stiffness Parameters			Natural Frequencies			Eigenvectors			Error
	θ_1	θ_2	θ_3	f_1	f_2	f_3	$\check{\phi}_1$	$\check{\phi}_2$	$\check{\phi}_3$	Index J_M
Undamaged:										
	1.477	2.148	1.492	11.41	30.57	46.11	0.536	-0.852	1.77	$3.8 \cdot 10^{-3}$
							0.810	-0.362	-2.10	
							1.00	1.00	1.00	
Damaged (D2-type):										
	1.484	0.890	1.375	9.696	27.82	36.92	0.361	-1.55	0.651	$1.2 \cdot 10^{-3}$
							0.851	-0.224	-1.16	
							1.00	1.00	1.00	

Table 5.11: SUB-ID-Modal Results for the 3-DOF chain model associated with the modal results obtained by MODE-ID from the time histories of the real structure. (Frequencies in Hz.)

Stiffness Parameters			Natural Frequencies			Eigenvectors			Error
θ_1	θ_2	θ_3	Damping Ratios			$\check{\phi}_1$	$\check{\phi}_2$	$\check{\phi}_3$	Index J_T
			f_1	f_2	f_3				
			ξ_1	ξ_2	ξ_3				
Undamaged:									
0.754	2.645	1.390	8.979	28.53	48.03	0.730	-0.699	2.10	$1.9 \cdot 10^{-1}$
			3.84	0.00	0.82	0.874	-0.274	-2.61	
						1.00	1.00	1.00	
Damaged (D2-type):									
1.700	0.371	1.702	7.548	29.77	37.92	0.181	-4.59	0.148	$2.3 \cdot 10^{-1}$
			1.55	3.58	5.12	0.927	-0.084	-0.838	
						1.00	1.00	1.00	

Table 5.12: SUB-ID-Time results for the 3-DOF chain model obtained employing the time histories corresponding to the hammer-impulse tests. (Frequencies in Hz, damping ratios in % of critical.)

Stiffness Parameters			Natural Frequencies			Eigenvectors		
θ_1	θ_2	θ_3	Damping Ratios			$\check{\phi}_1$	$\check{\phi}_2$	$\check{\phi}_3$
			f_1	f_2	f_3			
Undamaged:								
1.921	2.144	1.506	12.39	31.74	46.81	0.461	-0.857	2.03
						0.778	-0.456	-2.17
						1.00	1.00	1.00
Damaged (D2-type):								
1.482	0.891	1.376	9.763	27.95	37.48	0.375	-1.55	0.634
						0.854	-0.199	-1.16
						1.00	1.00	1.00

Table 5.13: SUB-ID-SS Results for the 3-DOF chain model associated with the modal results obtained by MODE-ID from the time histories of the real structure. (Frequencies in Hz.)

Stiffness Parameters			Natural Frequencies			Eigenvectors			Error
θ_1	θ_2	θ_3	f_1	f_2	f_3	$\check{\phi}_1$	$\check{\phi}_2$	$\check{\phi}_3$	Index J_M
θ_4	θ_5	θ_6							
a) Sub-structuring SS ₃									
Undamaged:									
0.964	1.451	1.306	8.708	28.27	48.26	0.404	-0.974	1.60	$2.4 \cdot 10^{-4}$
						0.793	-0.452	-1.75	
						1.00	1.00	1.00	
Damaged (D2-type):									
1.139	0.321	2.343	6.969	25.84	38.97	0.213	-1.82	0.729	$1.4 \cdot 10^{-3}$
						0.810	-0.453	-1.13	
						1.00	1.00	1.00	
b) Sub-structuring SS ₄ ⁸									
Undamaged:									
0.995	1.322	1.317	8.945	29.17	47.67	0.417	-0.951	1.61	$2.1 \cdot 10^{-4}$
	2.042					0.811	-0.436	-1.75	
						1.00	1.00	1.00	
Damaged (D2-type):									
0.995	0.406	1.332	7.683	27.03	38.05	0.311	-1.59	0.688	$5.2 \cdot 10^{-4}$
	1.987					0.864	-0.293	-1.119	
						1.00	1.00	1.00	
Table 5.14: SUB-ID-Modal results for the 18-DOF frame model based on the modal parameter values estimated by MODE-ID for the real structure. (Frequencies in Hz.)									

Stiffness Parameters			Natural Frequencies			Eigenvectors			Error
θ_1	θ_2	θ_3	f_1	f_2	f_3	$\check{\phi}_1$	$\check{\phi}_2$	$\check{\phi}_3$	Index J_T
θ_4	θ_5	θ_6	ξ_1	ξ_2	ξ_3				
a) Sub-structuring SS ₃									
Undamaged:									
1.149	1.273	1.308	9.018	28.62	48.00	0.358	-0.995	1.67	$7.8 \cdot 10^{-2}$
			0.83	0.47	0.49	0.772	-0.512	-1.74	
						1.00	1.00	1.00	
Damaged (D2-type):									
1.342	0.252	2.681	6.773	26.95	38.03	0.168	-1.968	0.702	$1.7 \cdot 10^{-1}$
			11.7	0.81	0.46	0.820	-0.519	-1.07	
						1.00	1.00	1.00	
b) Sub-structuring SS ₆									
Undamaged:									
1.194	1.243	1.326	8.983	28.63	47.99	0.349	-0.998	1.68	$7.0 \cdot 10^{-2}$
1.124	1.203	1.283	1.17	0.36	0.43	0.768	-0.525	-1.73	
						1.00	1.00	1.00	
Damaged (D2-type):									
1.085	0.315	1.587	7.561	26.99	38.03	0.231	-1.98	0.579	$1.1 \cdot 10^{-1}$
1.650	1.064	1.740	1.55	0.36	0.51	0.846	-0.348	-1.05	
						1.00	1.00	1.00	
Table 5.15: SUB-ID-Time results for the 18-DOF frame model obtained employing the time histories corresponding to the hammer-impulse tests. (Frequencies in Hz, damping ratios in % of critical.)									

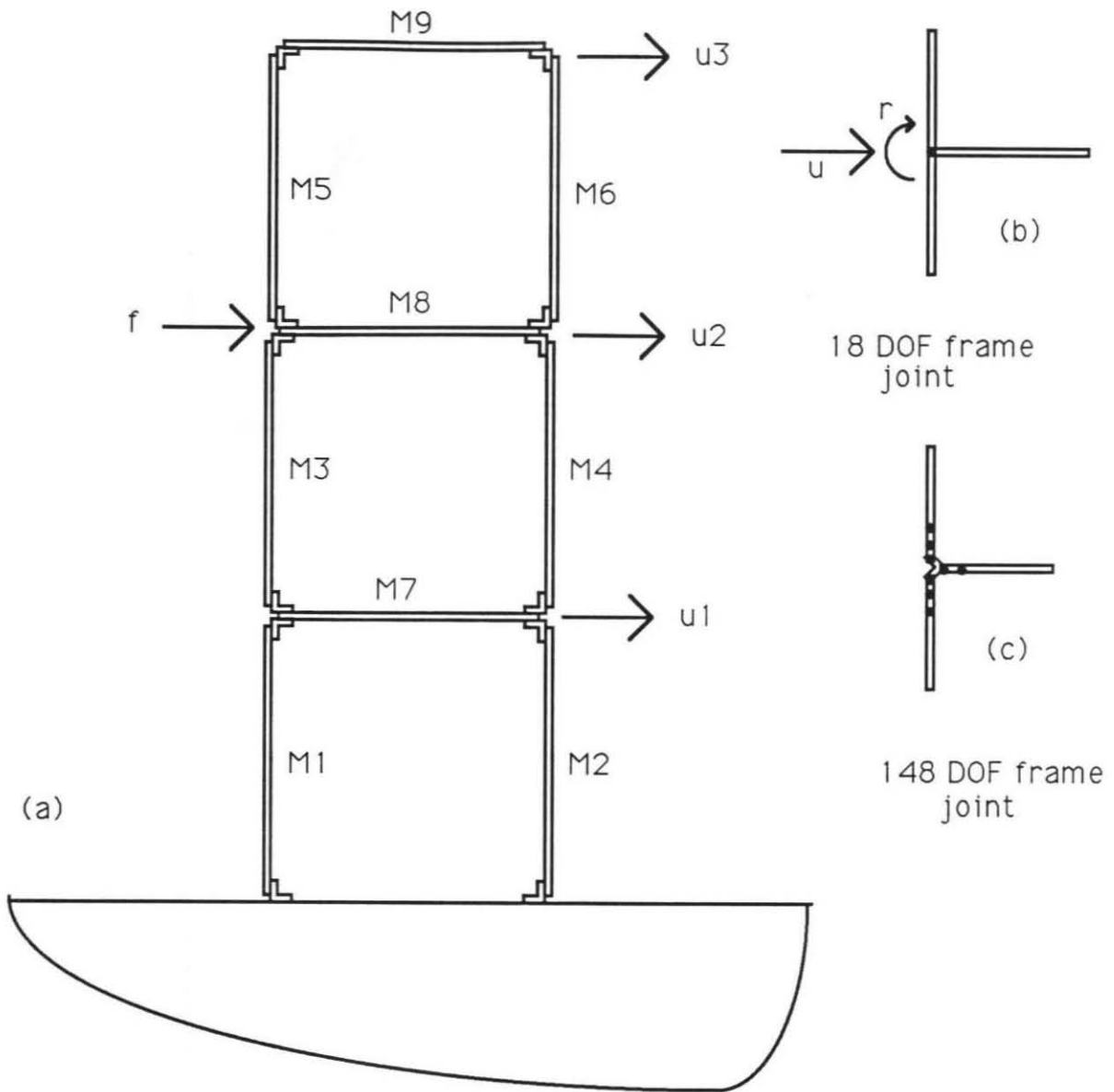


Figure 5.1: Two models of the test structure (a) are shown. Fig. (b) shows the one-node joint used in the simple 18-DOF frame model. Fig. (c) shows the same joint modeled by several elements, each having different properties. "Damage" consists of replacing either member M1 or M3 by another member with much lower stiffness.

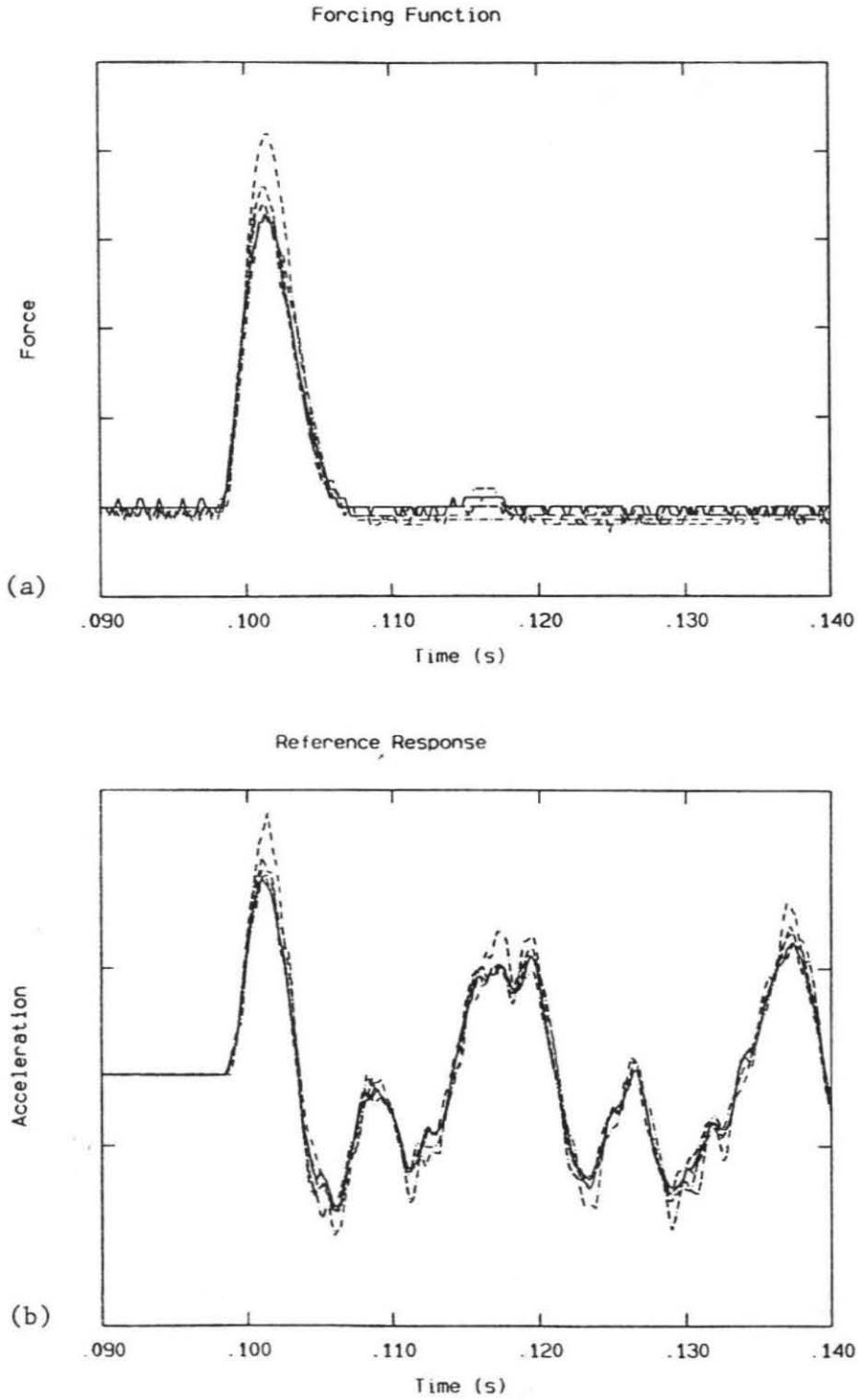


Figure 5.2: (a) Forcing function at the second level as applied in the various test runs. (b) For each excitation signal, the corresponding reference response signal at second floor is shown.

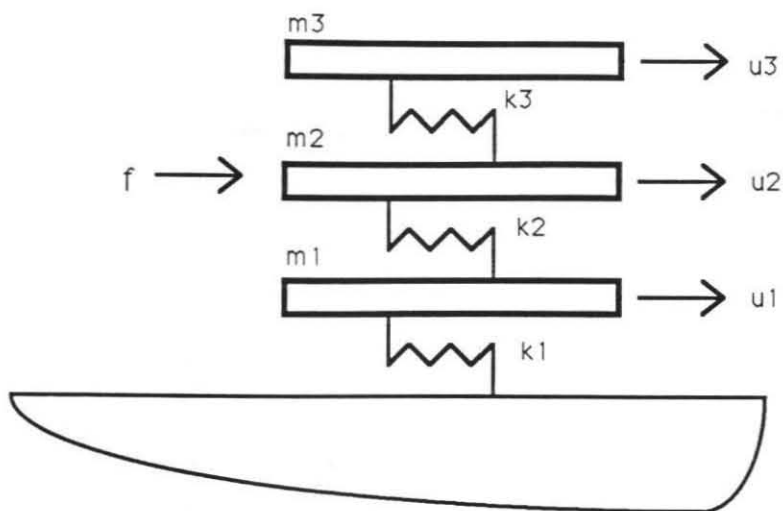


Figure 5.3: 3-DOF chain model corresponding to the test structure of Fig. 5.1a.

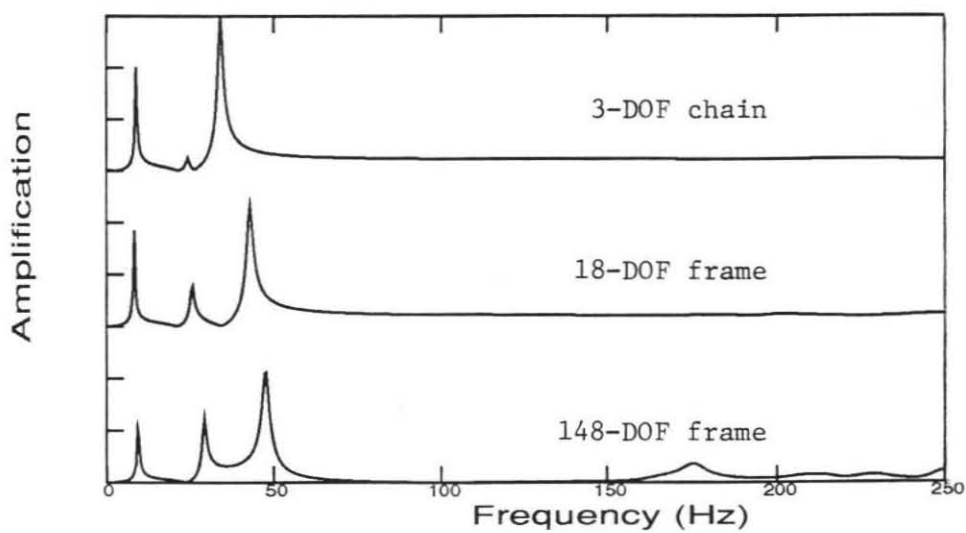


Figure 5.4: Transfer functions between the excitation at the second floor level and the acceleration response at the second floor level for the three different models.

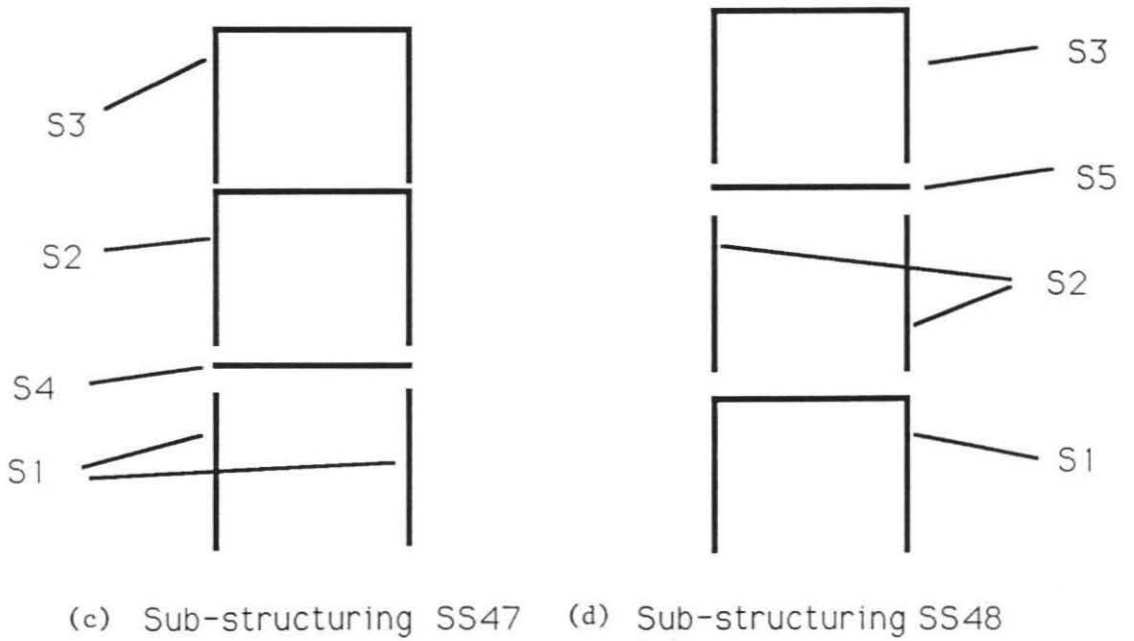
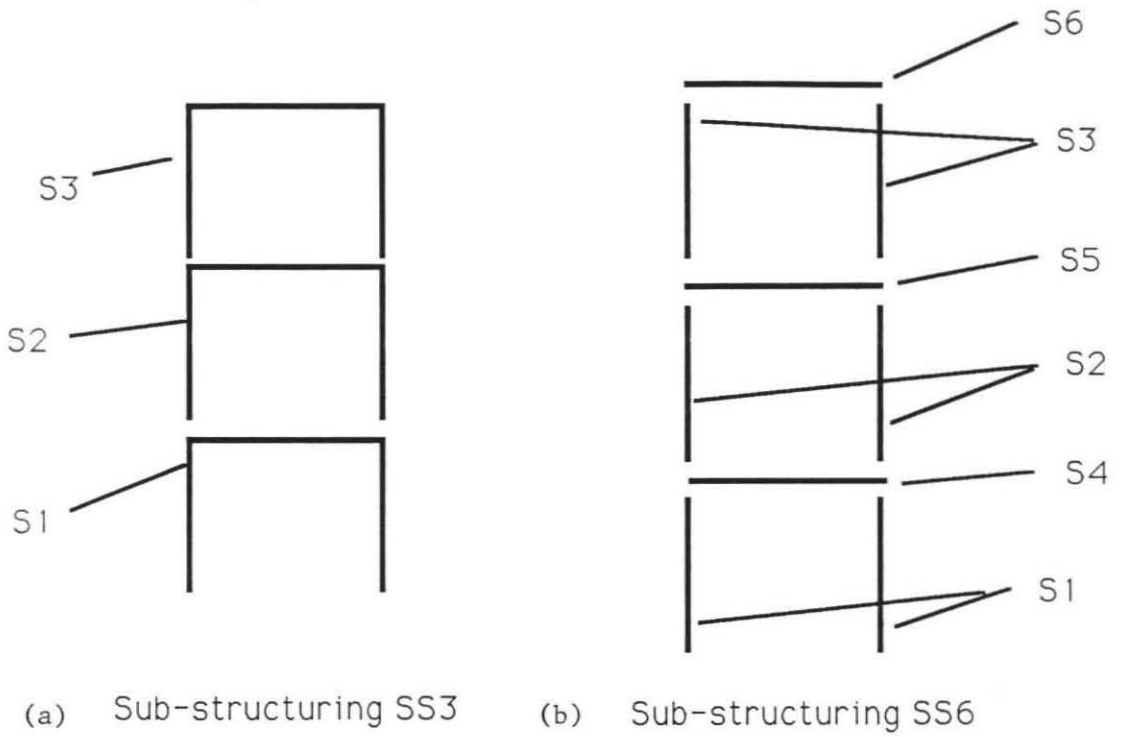


Figure 5.5: Different sub-structuring schemes employed with the 18-DOF frame model.

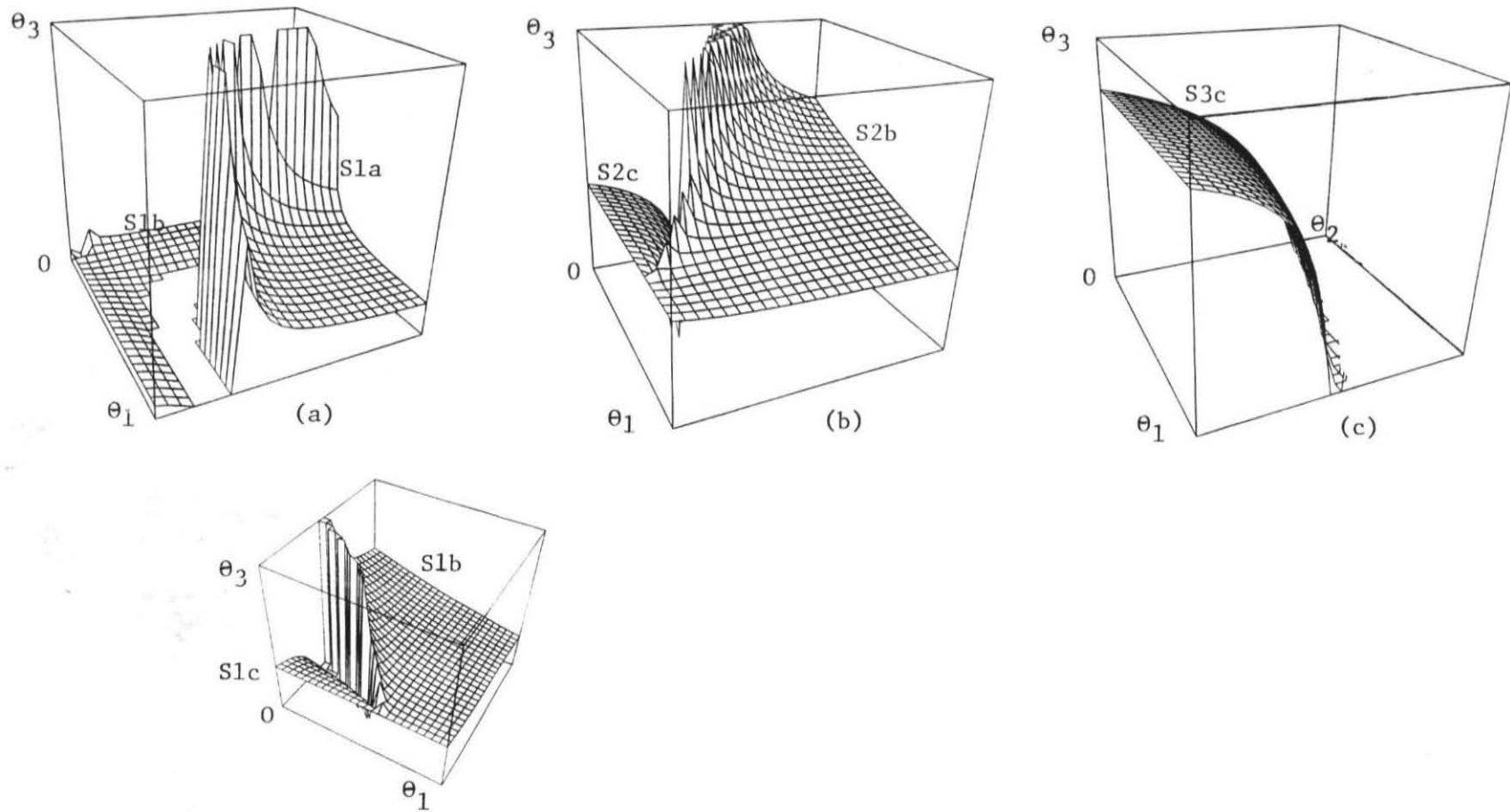


Figure 5.6: Iso-frequency curves in θ space. (a), (b) and (c) show surfaces for which $\omega_1^2 = 0.0990$, $\omega_2^2 = 0.778$, $\omega_3^2 = 1.62$, respectively. (d) shows a detail of (a) close to the origin, which has the same identical structure as (b). Surfaces $S2a$, $S3a$, and $S3b$ do not appear in the chosen ranges.

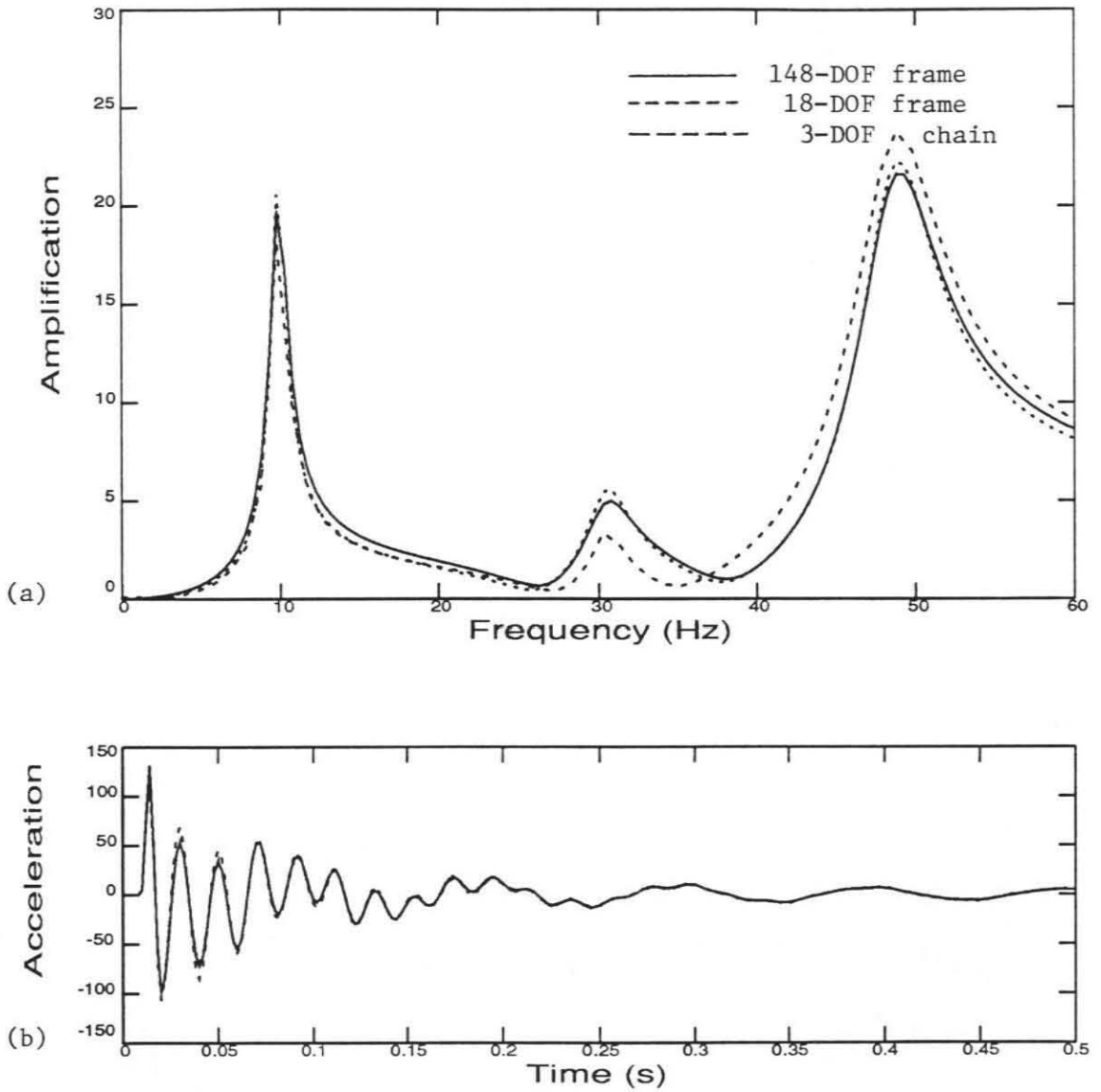


Figure 5.7: (a) Empirical transfer functions for the undamaged 148-DOF system and the two approximating 18-DOF frame and 3-DOF chain models. The θ parameters for each model are given in Table (5.4) for the 3-DOF model and in Table (5.7b) for the 18-DOF model. (b) Match of the same responses of (a) in the time domain.

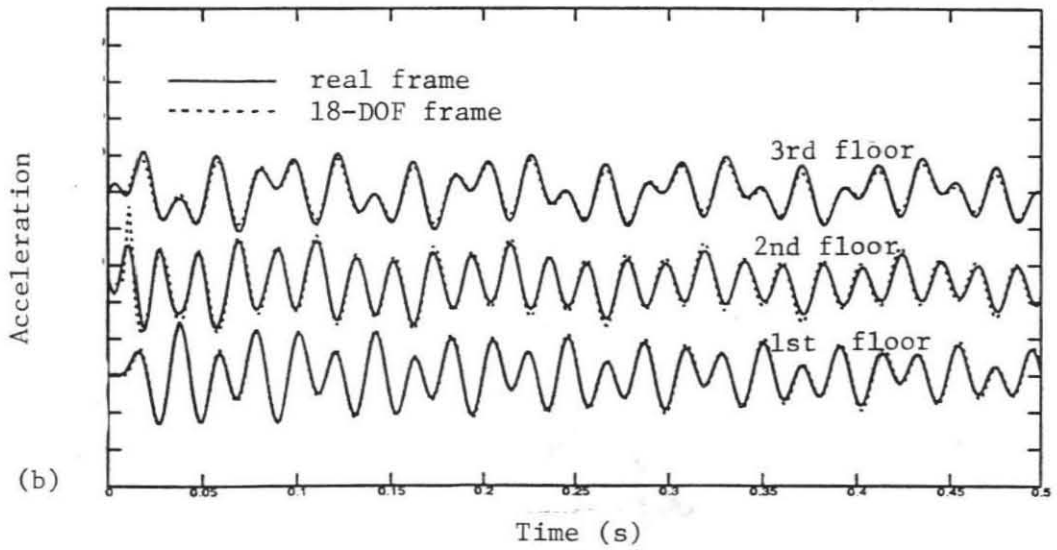
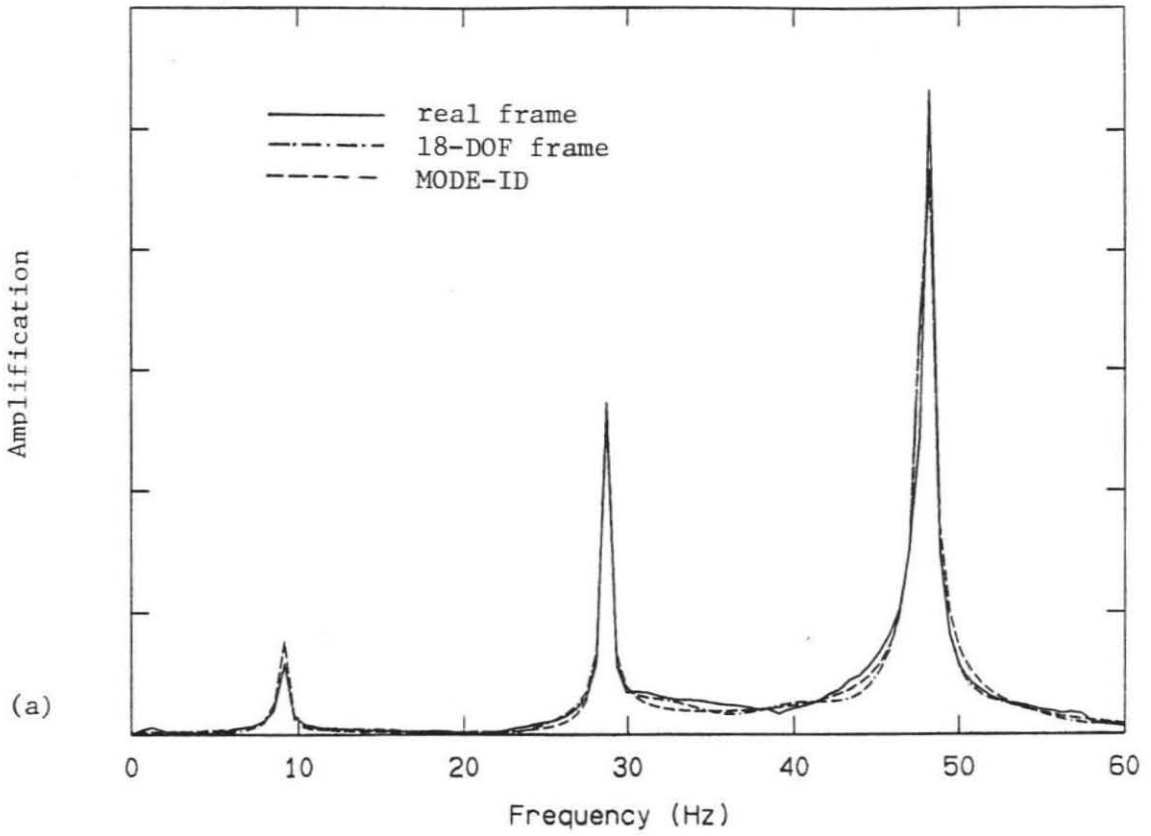


Figure 5.8: Empirical transfer functions for the real experimental frame and calculated from the identified 3-DOF and 18-DOF models. The SUB-ID-Time fit to the measured response is shown in (b).

Chapter 6 : Data from a Real Building

The East-West (“E-W”) motion of Building 180 on the JPL campus is studied with the foregoing methods in order to investigate what changes occurred in the structure during the strong earthquakes it has experienced. Previous studies [6.4,6.6,6.8] have shown that substantial changes in the values of the periods of vibration have occurred, especially during the 1971 San Fernando earthquake. No visual signs of damages were detected in the structure during inspections following this earthquake, except for some minor cracking of non-structural elements. To explain the lengthening of the periods, some researchers [6.5] have proposed that the structure weakened during large amplitude motions of the earthquake because of cracking of the concrete that encases the steel columns. The cracking introduces non-linear behavior, and indeed, some evidence of such behavior is present in the San Fernando earthquake records [6.6,6.8]. The overall behavior, however, seems to be represented quite well by a linear elastic model. In this study, a simple linear chain system is employed to model the structure and the SUB-ID programs are used to determine the corresponding stiffness distributions. Use is made of the San Fernando earthquake records and of other data, including some dynamic tests and the response of the building to other earthquakes. The identified stiffness distributions can offer insight into the location of stiffness loss induced by the earthquakes.

JPL Building 180 is a 10-story, symmetric steel-frame structure, approximately 67.0 meters (220 feet) long, 12.2 meters (40 feet) wide and 44.5 meters (146 feet) high (from the base of the foundation to the roof) located on the grounds of the Jet Propulsion Laboratory in Pasadena, California. Fig. (6.1) shows a schematic of JPL Building 180. The foundation of the structure is a continuous strip footing running longitudinally on both sides of the building. A shear wall was designed for the sub-basement and basement levels thus increasing significantly the stiffness relative to the upper stories. The latter all have an identical design except for the roof. The structure distributes the load in the longitudinal (East-West) direction with a eleven-bay frame consisting of steel trussed girders and steel columns. In the transverse (North-South) direction, the load is distributed by welded steel spandrel trusses and by steel columns. The steel columns are partially encased in concrete. The soil at the basement level consisted of very dense well-graded sandy gravel. From a typical test boring [6.4], the dry density is 1,850-1,990 kg/m³ (115-124 lbs./cf), moisture content is 7.6-8.7%, and the shear strength is 82-221 kPa (1.7-4.6 kips/sf), for the upper 4 meters (12 feet) of soil. With depth,

the density decreases slightly, the moisture varies considerably, and the shear strength doubles, down to a depth of approximately 20 meters (60 feet). The symmetry of the building has justified the use of two-dimensional models in the various analyses, even though the surrounding soil slopes down by about one story in the north-south direction. It has been assumed that the added soil stiffness acting on the north wall produces a rather small torsional component, thereby not affecting the plane motion of the structure.

Section 6.1 - Available Data for Building 180

Section 6.1.1 - Nielsen's Tests of 1963-1964

Nielsen's tests [6.1] consisted of both "man-excited" and steady-state resonance tests using an eccentric-mass harmonic shaker. The tests were carried out during various stages in the construction of JPL Building 180 and thus the effects of the addition of the different structural and non-structural components are visible in both the modal frequency and modeshape data.

Nielsen determined a total of four normal modes in the E-W direction from the steady-state resonance runs of his Test No. 14. The building stage corresponded to that before the final finishing touches prior to occupancy, i.e., no plaster on inner side of columns, no finished floors, no partitions, curtain walls and windows. For the E-W translational modes, the natural frequencies were $f_1 = 1.01$ Hz, $f_2 = 3.00$ Hz, $f_3 = 5.07$ Hz, and $f_4 = 7.50$ Hz. The modeshapes for the first three experimentally determined modes are shown in Fig. (6.2) where the motion at the ground and basement floors is assumed zero. Most of the modes were excited at various force levels but it was found that the modeshapes remained nearly constant at all levels tested. The frequencies, however, did demonstrate slight non-linear effects: as the force increased, the modal frequency decreased slightly as shown in Fig. (6.3ab).

The data from Nielsen's tests No. 14, 16 and 18 are shown in Table (6.1) along with many other tests and analyses results. Test No. 16 corresponds to a similar stage in the construction as No. 14 except that fire-proofing material was sprayed on all girders and trusses. Test No. 18, however, was performed after all windows, partitions, and curtain walls were put in place, and a wire mesh and plaster were used to cover the inner side of all columns.

Section 6.1.2 - 1970 Lytle Creek Earthquake Records

Earthquake records from the $M_L = 5.4$ Lytle Creek earthquake of September 12, 1970, were studied [6.11]. The corrected signals comprised a little more than 20 sec. of motion both at the

base and at the roof of JPL Building 180 (the initial part of the signals seems not to have been recorded). The maximum acceleration in the E-W direction at the base is 14.5 cm/s/s at 2.22 sec. and 25.25 cm/s/s at the roof at 3.24 sec. Fig. (6.4) shows the base acceleration and its spectrum while Fig. (6.5) shows the roof acceleration and the empirical transfer function between the base and roof signals. The Fourier spectrum plotted in Fig. (6.4) shows that the dominant frequencies at the base are in the 0-12 Hz range. The maximum 10.5 cm/sec peak is located at around 2 Hz. The peaks corresponding to the first two modes can be located easily at about 1 Hz and 3 Hz in Fig. (6.5a).

Section 6.1.3 - 1971 San Fernando Earthquake Records

Strong-motion records from the $M_L = 6.4$ 1971 San Fernando earthquake corresponding to accelerations monitored at the base and roof of Building 180 on February 9, 1971, were also studied [6.12]. The processing yielded slightly more than 97-second-duration signals with a time step of 0.02 seconds. The processed records show a maximum acceleration of 207.8 cm/s/s at 5.1 sec. in the E-W (longitudinal) direction at the basement and about 374.8 cm/s/s at 5.34 sec. at the roof in this direction. The Fourier spectrum plotted in Fig. (6.6) shows that the dominant frequencies are also in the 0-12 Hz range. The maximum 130 cm/sec peak is located at around 3 Hz. The transfer function between the roof response record and the base record shows a large amount of jaggedness as shown in Fig. (6.7). The smoother modal peaks, however, are found at 0.8, and 2.5 Hz, implying a substantial drop in the stiffness compared to what was observed for the Lytle Creek earthquake.

Section 6.1.4 - Teledyne's Tests of November, 1971

Measurements using Teledyne's "Ambient Vibration Survey" system [6.2] were made in the E-W direction on every floor at the west end of the building in November 1971 by Teledyne Geotech engineering firm. For the E-W translational modes, the measured natural frequencies were $f_1 = 0.95$ Hz, $f_2 = 3.00$ Hz, $f_3 = 4.98$ Hz, and $f_4 = 7.50$ Hz, all of these differing somewhat from the earlier values of Nielsen, especially those determined after occupancy. Fig. (6.8) presents the modeshapes for the first three modes of vibration. These modeshapes seem to agree well with those of Nielsen (Fig. (6.2)).

Section 6.1.5 - Nielsen's Tests of February, 1972

In February, 1972, man-excitation tests were conducted jointly by Teledyne Geotech and Nielsen [6.2]. The first two modal frequencies were determined at the 6th floor level: $f_1 = 1.0$ Hz and $f_2 = 3.3$ Hz. These frequencies differed from the results obtained by Teledyne Geotech three

months earlier, the frequency now increasing approximately 5% in the first mode and 10% in the second translational mode.

Section 6.2 - Previous Dynamic Analyses of Building 180

Section 6.2.1 - Nielsen's Analysis of 1964

Nielsen [6.1] derived the equations necessary to determine the stiffness and damping matrix components from the experimentally determined modal properties. His method is equivalent to an equation-error method applied to the modal equations of motion similar to that implemented by SUB-ID-SS. In determining the structural parameters, Nielsen considered two scenarios: (1) simply-coupled systems (chain-type system), and (2) close-coupled systems (chain-type with floor-to-base attachments). A least-squares solution to the set of simultaneous equations was employed whenever more modes than necessary were available.

From his measured data, and assuming that the girders in the E-W direction were sufficiently rigid to make the effect of joint rotation negligible, Nielsen determined the stiffness matrix components corresponding to the close-coupled system. The determined components are shown in Table (6.2) where it is evident that they come close to being those of a uniform chain model. The errors found by Nielsen substituting into the modal equations are reasonably small indicating that the close-coupled model is a good model. Nielsen argued that the small differences between the close-coupled stiffness values and the ones corresponding to the simple chain model could stem from inaccuracies in the data. The frequencies and modeshapes derived from the identified model compared closely to the experimental values as shown in Table (6.1) and Fig. (6.2), but they did not compare well for the fourth mode not shown.

Damping values were independently determined by Nielsen from the acceleration response at resonance. Table (6.1) also shows his damping estimates for the first three modes.

Section 6.2.2 - Brandow and Johnston Associates Analysis of 1971

Brandow and Johnston's report [6.3] describes an attempt to visually match the dynamic response of a structural model to the actual behavior incurred by Building 180 during the strong motion part of the San Fernando earthquake. The match, however, was not good in comparison to others such as the one performed by Wood, described in the next section.

Section 6.2.3 - Wood's Analysis of October, 1972

In Wood's studies [6.4,6.5], a structural model was corrected by trying to match its response to the San Fernando earthquake response of Building 180. The model was then employed to estimate the level of the seismic inter-story forces experienced by the building during the strong motion part of the earthquake. The report suggests that some of the structural columns nearly reached their yield level.

Wood employed a "reduced" model for the E-W direction analyses: the two-dimensional, eleven-bay, longitudinal structure elevation was modeled as a one-bay frame structure. Furthermore, he assumed that the stiffness is homogeneous over the height of the building. Modeling of the longitudinal girders was approximated in three different ways: (1) a trussed girder, (2) a rigid girder, and (3) an equivalent girder, but the trussed girder was selected as the best model. Wood further synthesized two different models for the columns, each for a different behavior regime. The "full composite" model corresponded to low-amplitude response of the structure in the linear range. In this range, it was assumed that the motion of the structure would not cause the concrete encasing the columns to open at the cracks. On the other hand, the "partial-composite" strong-motion model assumed no contribution to the stiffness from the column concrete wherever it underwent tensile strain. The models roughly approximated the observed structural response so in order to obtain a better match, Wood resorted to *directly* changing the modal frequencies of the chosen "reduced" model and not the properties of the structural model themselves, so that any implications that the new modal frequencies might have on the structural inter-story stiffness properties were not addressed. Wood's trial-and-error modification of the modal frequencies was done in such a way that better *visual* matching between the recorded responses and those calculated for the models was achieved. The damping ratios were also adjusted by matching the observed Fourier amplitudes of the roof accelerations. Table (6.1) shows how Wood's models compare with other predictions and Fig. (6.8) presents Wood's modeshapes in comparison to Teledyne's experimental data.

Section 6.2.4 - McVerry and Beck's Analysis of 1983

McVerry and Beck's analysis [6.8] is an extension of the modal studies performed individually by both Beck [6.9] and McVerry [6.10] in 1978 and 1979, respectively, in which Building 180's modal parameters were estimated from the response to the San Fernando earthquake. Their methods seem to present better parameter estimates than competing modal identification methods (see, for example, [6.6,6.7]). The results of their more recent study showed a previously undetected time shift of 0.08 seconds between the San Fernando earthquake base and roof signals. Taking this time shift into account, the methods developed by both authors were able to extract more reasonable modal parameters estimates, particularly for the higher modes.

Time-invariant parameter estimates were determined and the corresponding model provided a

good overall fit to the measured roof response, their error index J_T being approximately $4.8 \cdot 10^{-2}$. These estimates, also shown in Table (6.1), correspond mainly to the estimates for the strongest motion part (5-30 sec.), since output-error approaches weigh the absolute error difference and not the relative error. The corresponding response match from their MODE-ID algorithm is shown in Fig. (6.7).

Table (6.10) shows modal estimates which were computed for different time windows by McVerry and Beck, a procedure which provides some idea of the time-varying behavior produced by any non-linear response of the structure. The fact that their two methods yield natural frequencies which started from values close to those measured in previous vibration tests and then decrease by approximately 20% implies that the structure lost substantial stiffness during the strong motion part of the San Fernando earthquake. The good overall match of a linear model with the observed behavior implies that changes in the dynamic properties of the structure occurred primarily during early parts of the earthquake before the long strong-motion segment. Some lack of overall matching may also occur since the methods did not allow for non-classical modes. Non-classical modes may be needed but the authors found that the classical-modes model fitted the response data accurately, particularly for the smaller time-windows studied.

The initial values of the fundamental frequency for the E-W direction corresponded closely to values estimated from previous tests, approximately 0.98 Hz, but then decreased to a minimum of 0.78 Hz during the largest amplitude response segment, implying a decrease of 37% in the modal stiffness. The value towards the end of the response was found to be approximately 0.81 Hz. The second E-W mode frequencies decreased by approximately 26 % from 3.23 Hz (0-10 sec. segment) to 2.38 Hz (10-20 sec. segment) to 2.56 Hz (30-40 sec. segment), the maximum decrease being 46%. The damping ratios were also found to vary in time. The damping estimates were compared with their previous results [6.9,6.10] using the unsynchronized records and were found to be more reliable.

Section 6.2.5 - Teledyne's Analysis of November, 1971

Teledyne's analysis [6.2] of their own ambient vibration E-W translational modal data was restricted to the determination of the damping ratios from the power spectra plots and to cross spectra among different records. Damping was determined using the half-power point method and the results, along with the natural frequencies, are shown in Table (6.1). A limited comparison with Nielsen's 1964 data was also present in their report.

Section 6.3 - SUB-ID Results for Building 180

The programs described in earlier chapters, SUB-ID-Modal, SUB-ID-SS (successive substitutions) and SUB-ID-Time are used here to study the loss of stiffness in Building 180. SUB-ID-Modal and SUB-ID-SS are used with Nielsen's data to estimate the stiffness distribution before the earthquakes. SUB-ID-Time is then used with the Lytle Creek and San Fernando earthquake records to try to estimate the stiffness distribution during various time segments of the response. Finally, SUB-ID-Modal and SUB-ID-SS are used again with Teledyne's data in order to estimate the stiffness distribution shortly after the occurrence of the San Fernando earthquake. In all circumstances, a 10-degree-of-freedom chain model is employed. When the information is abundant, as for Nielsen's and Teledyne's data, a determination of all ten interstory stiffnesses is performed. For the time history strong motion data, however, non-uniqueness considerations restrict the number of parameters to be determined.

Section 6.3.1 - Results from Nielsen's Data

Nielsen's data consists of modal frequencies and modeshapes corresponding to his test No. 14, prior to the occupancy of the building. The model employed here is a 10-story chain system and the data available is the modeshape components for the upper eight of the ten floors. Table (6.5) and Table (6.6) show the results obtained by SUB-ID-Modal weighing the natural frequencies by 9/10 and the modeshapes by 1/10, and by SUB-ID-SS, respectively.

In Table (6.5), two models with their associated stiffness distributions are shown: model N-1 corresponds to Nielsen's original mass distribution (417,680 kg. (920 kips) for each floor and 744,560 kg. (1640 kips) for the roof mass), and model N-Opt. corresponds to an identical mass distribution except with an estimated top mass value of 718,407 kg. This mass estimate is close to Nielsen's value. The results in Table (6.5) and Table (6.6) show stiffness distributions fairly uniform, except for the first two inter-story stiffnesses which are higher than the rest (Table (6.5)). The agreement of the model predictions with the observed modal frequencies and modeshapes is good and the upper story stiffness components match well those estimated by Nielsen, as seen by comparing Table (6.3) with Table (6.2).

Table (6.4) shows the corresponding stiffness matrix for the SUB-ID-SS program. The stiffness distributions are somewhat different from the ones obtained with SUB-ID-Modal even though the modal data employed is the same. The reason for this is perhaps due to the existence of model error and the different implicit weighting of both algorithms. In the SUB-ID-SS case, in order to avoid non-convergence of the method, the first two degrees of freedom had to remain fixed. Since no mass optimizations can be performed by SUB-ID-SS, the roof mass estimated by SUB-ID-Modal was employed, in the model N-Opt.

Section 6.3.2 - Results from the 1970 Lytle Creek Records

Unfortunately, as has been documented in Section 4.1.2.3, the chain model excited at the ground level and monitored at the topmost degree of freedom does not provide a unique stiffness parameter distribution when all inter-story stiffnesses are to be determined. By reducing the number of parameters, however, the uniqueness properties of the problem improve. Three parameters (the first corresponding to the third and fourth inter-story stiffnesses, the second corresponding to the fifth through seventh stiffnesses, and the third corresponding to the last three stiffnesses) were chosen in order to investigate more closely the behavior of the structure. Thus, the analyses described in this and in the next section should be taken to be indicative of possible "stiffness-loss" patterns over large regions. In general, it is seen that the error indices are only slightly larger than the ones achieved with the more general modal methods of Beck and McVerry, which provide the best match whenever linearity and classical modes are valid assumptions since no structural model is employed. The relative proximity of SUB-ID's error indices to the latter gives confidence that an adequate structural model has been employed.

The SUB-ID-Time results from the Lytle Creek records presented in Table (6.1) and Table (6.7) indicate that there is some stiffness loss at various locations in the structure. (The model employs the optimized mass estimates derived from Teledyne's data, described later in this chapter.) The $\theta_3 = \theta_4$ stiffness starts around 9 to $10 \cdot 10^8 Nm^{-1}$ and drops to $7 \cdot 10^8 Nm^{-1}$. Unexpectedly, $\theta_5 = \theta_6 = \theta_7$ has the opposite behavior: it starts low and then increases towards the end of the records. The last set, $\theta_8 = \theta_9 = \theta_{10}$, starts high at $10^9 Nm^{-1}$, dips and then increases to a greater value, $1.2 \cdot 10^9 Nm^{-1}$. These patterns of behavior seem to indicate that the structure is undergoing significant non-linear behavior despite the fact that the earthquake produces only modest shaking (2.5 %g at the roof). From the records (Fig. (6.4) and Fig. (6.5)), however, one can see that the high accelerations are not concentrated in one time segment, unlike some other strong motion records. The frequency values estimated for the time windows shown in Table (6.8), including those estimated by MODE-ID, give little evidence of the slight stiffness degradation predicted by the SUB-ID-Time algorithm. The error index J_T in Table (6.7) is quite large in the initial segment 0-2.56 sec. The error is probably due to the assumption that the initial conditions are always zero displacement and velocity when in fact some information at the beginning of the strong motion records was not recorded. As is expected, the effects of the missing data decays in time and so the error index is shown to improve for the latter time windows even in the light of higher accelerations occurring in the 4-6 sec. time segment. Fig. (6.4) shows how the accelerations start off at relatively large values while Fig. (6.5) shows the acceleration match produced by both SUB-ID-Time and the more flexible MODE-ID program.

The base acceleration spectrum is fairly broad-band, inducing many modes to participate in the response, but the models employed only considered three modes to be trustworthy. The higher

modes and the measurement noise tend to deteriorate the match. The plot in Fig. (6.5a) shows a fairly jagged empirical transfer function along with the two predictions implied by the identified models; it is evident from this match that at least the first two modes have been correctly extracted, the third mode not being easily identified visually.

Section 6.3.3 - Results from the 1971 San Fernando Records

The response match shown in Fig. (6.7) is for an optimal three-parameter model of the type described in the last section. It compares well to the match of McVerry and Beck, also shown in Fig. (6.7). The three-parameter model yields an error index ($J_T = 7.8 \cdot 10^{-2}$) somewhat larger than for the ten-parameter model example case referred to in Table (6.1) ($J_T = 6.4 \cdot 10^{-2}$) when the wide 0-41 sec. segment is employed. The increase in the error index is large enough to create some concern about the adequacy of the three-parameter model although the visual match in the acceleration signals match is still good as can be seen in Fig. (6.7).

In Table (6.9), when employing this three-parameter model for different time windows, this index is seen to remain relatively low. The high error index values, the drop in the natural frequencies (Table (6.10)), and the larger damping values in the first two modes at the beginning of the strong motion records may indicate that the structure underwent some non-linear stiffness-loss behavior. Indeed, in the different time segments, it is possible to see substantial variations in the stories' stiffness values compared to the earlier values derived from Lytle Creek's earthquake data. When comparing the first two windows' results, the estimated stiffness parameters seem to indicate the existence of a mild 10% overall loss of stiffness in the middle stories and a large stiffness loss in the higher floors. Towards the end of the records, it is possible to see nearly 50% stiffness loss in the middle stories and slight recovery in the higher stories. The stiffness loss is probably due to the cracking in the concrete encasing as suggested by Wood although in his model the cracking could not account for more than 3% drop in any of the modal frequency values. McVerry and Beck's results show also the drop in the natural frequency values, although in their case the drop was more accentuated: from 0.98 Hz. to 0.80 Hz. as seen in Table (6.10). The latest version of Beck's MODE-ID algorithm was employed, this time with a slightly different synchronizing time shift ($3 \Delta t$ instead of $4 \Delta t$) and with the uncorrected version of the earthquake records. The modal values predicted differed slightly from those previously calculated by McVerry and Beck, this time corresponding rather closely with those predicted by SUB-ID-Time (Table (6.10)).

The error index decreases considerably in the 10-20 sec. and 20-41 sec. time segments. These time segments are characterized by the large presence of the first mode relative to the second and to the third, and so by matching just this first mode, the error index is reduced greatly. The stiffness and damping values do not vary as much in these segments, implying that the concrete encasings,

if cracked, remained completely cracked throughout the high amplitude first mode response and did not bond again even during the small amplitude motion towards the end of the response.

Section 6.3.4 - Results from Teledyne's Data

When employing Teledyne's data, use is made of the mass distribution predicted by Wood for his own analytical model [6.4] since Nielsen's mass estimates are valid for an unoccupied stage in the construction of the building. Wood's mass model W-1 corresponds to floor masses of 576,580 kg. (1270 kips) and a roof mass of 688,718 kg. (1517 kips), all values obtained by Wood from the structural drawings. As expected, Wood's floor mass values are larger (by approximately 38%) than those predicted by Nielsen for the unoccupied structure, but Wood's roof mass is unexpectedly 8% lower than Nielsen's prediction. Table (6.11) presents the results for the original W-1 model and also, since the lower roof mass value is questionable, for a second W-Opt. roof-mass optimized model. Results show that the latter model estimated a roof mass of 1,176,220 kg., 104% larger than the typical floor mass (576,580 kg.), a value which is significantly different from the one employed by both Nielsen (744,560 kg.) and by Wood (688,718 kg.). The error indices for Teledyne's data and Wood's mass model are remarkably worse than those obtained from Nielsen's data. The optimized model W-Opt., however, improves the match considerably, i.e., it reduces the error index from $9.8 \cdot 10^{-4}$ to $4.9 \cdot 10^{-4}$. The worsening in the match from Nielsen's results to the present results may be attributed to the quality of the data itself. The accuracy of the modeshape from the ambient vibration tests is probably not as good as those estimated by Nielsen during his tests with a building shaker.

SUB-ID-SS results are shown in Table (6.12), the trends being the same as from SUB-ID-Modal. From the data one can see that the θ_8 and θ_9 stiffness ratios decrease considerably, except in the W-Opt. case in Table (6.11), where θ_8 increases significantly. This value is rather questionable. The accuracy of the stiffness distributions is also difficult to assess since the results may be influenced by the mass distribution which is not well known. By comparing the results in Table (6.5) and Table (6.6) with those in Table (6.11) and Table (6.12) it is seen, however, that a pattern exists in all models and that it corresponds to a decreased 9th inter-story stiffness following the San Fernando earthquake.

Section 6.4 - Discussion

The estimation of the mass distribution proposed by Nielsen seems to contradict the one proposed by Wood. Both mass distributions correspond to different stages in the building construction and it is because of this that it is not possible to select one of the two for all the

numerical tests performed by the SUB-ID programs. The typical floor masses were substantially higher in Wood's model, which agrees with the fact that Wood's model corresponds to the occupied building stage. The mass at the roof, however, differs significantly and it seems unlikely that it should decrease in value after occupancy, as predicted by Wood. The optimal values for the roof mass, as estimated by SUB-ID-Modal, agree well with Nielsen's own estimates but disagree greatly from the values estimated by Wood. The large increase in the roof mass for the occupied stage could only be attributed to the mass of non-structural components such as the elevator machinery and perhaps other mass neglected from inclusion in the structural drawings. Although the optimized roof mass values are assumed more correct and thus employed for all final analyses, they do not always provide optimal error measures J , as can be seen in Table (6.7) and Table (6.9).

The natural frequencies estimated by McVerry and Beck and with the SUB-ID programs indicate that the structure softened during the first few seconds in the strong motion part and regained some of its stiffness towards the end of the San Fernando earthquake. McVerry and Beck's results show substantial decreases in the natural frequencies which imply even higher decreases in the modal stiffnesses. In the eventuality that there was damage localized at some interstory level, it is assumed here that it would have to appear ever so slightly when comparing results from Teledyne's data to results from Nielsen's data. "Damage" such as the cracking in the concrete that encases the steel columns, is less likely to be detected from small amplitude steady-state, man-excited, or ambient vibration tests. Table (6.13) and Table (6.14) show the ratio of Teledyne's estimates to Nielsen's estimates as determined by the SUB-ID-Modal and SUB-ID-SS programs, respectively. The ratios suggest that the structure was generally much stiffer in November 1971 than in the construction year 1963-1964. A reason for this might be that Nielsen's data corresponds to a stage in the construction of the building where many non-structural and perhaps some structural components were missing. Nevertheless, since the ratios depend on the stiffness estimates and the latter depend on the mass estimates, all of which are not completely trustworthy, the absolute value of the ratios may not be trustworthy as well, but the *relative* stiffness values along the height of the building are more likely to be so. One can observe from Table (6.13) and Table (6.14), and perhaps more clearly from Fig. (6.9), that the stiffness ratios are relatively low in the lower story and at the ninth story level. If any "damage" did occur during the San Fernando earthquake, it is most likely that it took place in the lower stories. The reduction at the ninth floor level is not intuitive, however, and also in light of the SUB-ID-Time results of Table (6.10) where the largest stiffness loss occurred in the middle floors.

Damage of the type proposed by Wood, i.e., cracking of the concrete encasing, would explain how the stiffness of the columns would decrease in the strong motion segment of the earthquake and immediately recover to the initial stiffness when the motions become small again. This is consistent with the behavior observed by McVerry and Beck and also here, except that it is unlikely that there was nearly 50% loss of stiffness from the cracking in the tensile region of the concrete encasing.

Also, this hypothesis would predict that all the modal frequencies would return to the original values after the motion stopped, but the results obtained by McVerry and Beck and with SUB-ID-Time, shown in Table (6.10), indicate that there is no clear tendency for the structure to stiffen to the same level that it had prior to the beginning of the earthquake. The initial stiffness values are already considerably lower than the results from the Lytle Creek earthquake, which occurred five months prior to the San Fernando earthquake. Observing the excitation and response of Building 180 towards the beginning of the San Fernando records indicates that an acceleration of 62 cm/s/s takes place at 2.28 sec., the latter acceleration being nearly three times larger than any acceleration suffered by the building during the Lytle Creek earthquake. This increase of amplitudes can account for the increased softening suffered by the structure.

Teledyne's results of November, 1971, show that the structure regained much of its stiffness, as evidenced in Table (6.1). Teledyne and Nielsen's data of February, 1972, show recovery to levels slightly lower than those corresponding to Nielsen's Test No. 18. This confirms that the decrease in the stiffness values during the San Fernando earthquake was temporary and that "the structure healed with time."

All of this information leads to several speculations:

(1) There was a reduction in stiffness in the structural members, such as cracking of the concrete encasing during the prior, albeit weaker, Lytle Creek 1970 earthquake.

(2) There may be effects such as a partial loss of stiffness in non-structural components and their connections to the structural system. The non-structural components stiffened the structure initially (as seen in Nielsen's Test No. 18 results) but may have loosened up during the large amplitude excitation of the San Fernando earthquake.

(3) There is a possible reduction in the stiffnesses of the basement and first stories which may be partly due to the loss of contact between the structure and the surrounding soil, particularly at the first story where normally only the north side is in contact with the soil.

Since it is unlikely that the cracking in the concrete encasing can account for nearly 50% stiffness loss, it is probable that all three effects participated together. The large stiffness reductions, however, cause some concern about the adequacy of the original building structure to withstand a similar or larger earthquake without incurring excessive damage. Strengthening of the structure has been done subsequent to the tests enhancing, in this way, the resistance of the structure to future earthquakes.

References for Chapter 6

- [6.1] Nielsen, N.N., "Dynamic Response of Multistory Buildings", Report EERL, California Institute of Technology, June 1964.
- [6.2] Teledyne Geotech, "Ambient Vibration Survey of Building 180, JPL", Report for CIT, Teledyne Geotech West, Long Beach, California, November 1971.
- [6.3] Brandow and Johnston, "Design Analysis of the JPL, Building 180", Report to the California Institute of Technology, 1971.
- [6.4] Wood, J.H., "Analysis of the Earthquake Response of a Nine-Story Steel Frame Building During the San Fernando Earthquake", Report EERL 72-04, California Institute of Technology, Pasadena, California, October 1972.
- [6.5] Wood, J.H., "Earthquake Response of a Steel Frame Building", *International Journal of Earthquake Engineering and Structural Dynamics*, Vol. 4, 1976, p. 349.
- [6.6] Udawadia, F.E., Trifunac, M.D., "Time and Amplitude Dependent Response of Structures", *International Journal of Earthquake Engineering and Structural Dynamics*, Vol. 2, 1974, p. 359.
- [6.7] Beck, R.T., Beck, J.L., "Comparison Between Transfer Function and Modal Minimization Methods for System Identification", Report EERL 85-06, California Institute of Technology, Pasadena, California, 1987.
- [6.8] McVerry, G.M., Beck, J.L., "Structural Identification of JPL Building 180 Using Optimally Synchronized Earthquake Records", Report EERL 83-01, California Institute of Technology, Pasadena, California, August 1983.
- [6.9] Beck, J.L., "Determining Models of Structures from Earthquake Records", Report EERL 78-01, California Institute of Technology, Pasadena, California, June, 1978.
- [6.10] McVerry, G.M., "Frequency Domain Identification of Structural Models from Earthquake Records" Report EERL 79-02, California Institute of Technology, Pasadena, California, October, 1979.
- [6.11] "Strong Motion Earthquake Accelerograms, Index Volume", Report EERL 76-02, California Institute of Technology, Pasadena, California, August, 1976; Records W344-345, p.16.
- [6.12] "Strong Motion Earthquake Accelerograms, Index Volume", Report EERL 76-02, California Institute of Technology, Pasadena, California, August, 1976; Records G110-111, p.16.

		JPL Building 180					
Data Set	Study	Modal Frequency (Hz)			Modal Damping (% critical)		
		f_1	f_2	f_3	ξ_1	ξ_2	ξ_3
Nielsen's 1964 Test No. 14 Data (steady-state)							
	Nielsen (experimental)	1.01	3.00	5.07	0.55	0.85	2.00
	Nielsen (close-coupled)	0.99	3.02	5.12			
	SUB-ID-SS (Opt. mass)	1.04	3.07	5.04			
	SUB-ID-Modal (Opt. mass)	1.01	3.00	5.07			
Nielsen's 1964 Test No. 16 Data (steady-state)							
	Nielsen	1.04	2.95	n/a			
Nielsen's 1964 Test No. 18 Data (man-excited)							
	Nielsen	1.10	3.40	n/a			
Lytle Creek 1970 Eq. E-W comp.							
	SUB-ID-Time (3p: 0-20 sec)	0.993	3.00	5.02	4.0	5.3	7.9
	SUB-ID-Time (10p: 0-20 sec)	0.983	3.04	5.20	4.1	4.7	7.4
	MODE-ID (0-20 sec)	0.979	3.05	5.20	4.4	5.4	6.9
San Fernando 1971 Eq. E-W comp.							
	Brand. & Johnst. (model 1)	0.94	2.63	4.35			
	Brand. & Johnst. (model 2)	0.81	2.22	3.57			
	Wood (partial compos.)	0.83	2.39	3.89	5.0	5.0	5.0
	Wood (modified)	0.78	2.38	3.84	4.0	6.0	6.0
	McVerry-Beck (0-41 sec)	0.784	2.42	3.92	3.6	7.4	12
	SUB-ID-Time (3p: 0-41 sec)	0.783	2.32	3.77	3.9	7.1	10
	SUB-ID-Time (10p: 0-41 sec)	0.781	2.36	3.73	3.9	6.9	11
	MODE-ID (0-41 sec)	0.781	2.37	3.60	3.6	6.9	16
Teledyne's 1971 Data (ambient vibrations)							
	Teledyne (experimental)	0.95	3.00	4.98	1.1	0.1	0.2
	Wood (full compos.)	0.92	2.77	4.70			
	SUB-ID-SS (Opt. mass)	0.86	2.46	4.39			
	SUB-ID-Modal (Opt. mass)	0.97	2.99	4.98			
Teledyne & Nielsen's 1972 Data (man-excited)							
	Teledyne & Nielsen	1.00	3.33	n/a			

Table 6.1: Comparison of modal frequency and damping values for JPL Building 180 in the E-W direction, as estimated by various methods and at different points in time.

JPL Building 180, E-W Direction (Nielsen's 1964 Data)											
Inter-story Stiffness Values											
	θ_1	θ_2	θ_3	θ_4	θ_5	θ_6	θ_7	θ_8	θ_9	θ_{10}	<i>Error Index</i> J_M
Model	(All stiffness values $\times 10^8 Nm^{-1}$)										
N-1	59.39	50.97	9.419	4.953	6.736	6.214	6.416	5.611	5.623	5.044	$4.66 \cdot 10^{-5}$
N-Opt	53.12	45.40	8.006	5.060	6.607	6.177	6.416	5.492	5.529	4.940	$4.26 \cdot 10^{-5}$

Table 6.5: SUB-ID-Modal Parameter estimates corresponding to two models using 9/10 frequency and 1/10 mode-shape weights in J . The data used is Nielsen's Test 14 with mode-shape components for the top eight floors. The optimized model predicts a roof mass 1.72 times larger than the typical floor mass.

JPL Building 180, E-W Direction (Nielsen's 1964 Data)										
Inter-story Stiffness Values										
	θ_1	θ_2	θ_3	θ_4	θ_5	θ_6	θ_7	θ_8	θ_9	θ_{10}
Model	(All stiffness values $\times 10^8 Nm^{-1}$)									
N-1	∞	∞	7.042	6.386	6.602	5.723	6.010	5.940	5.748	5.030
N-Opt.	∞	∞	7.045	6.383	6.586	5.713	5.986	5.832	5.563	4.776

Table 6.6: SUB-ID-SS parameter estimates corresponding to the two models appropriate for Nielsen's data. The first model assumes the original mass distribution while the second uses the SUB-ID-Modal optimized mass estimate. For the method to converge, the basement and ground levels were restrained from moving.

JPL Building 180, E-W Direction (1970 Lytle Creek Earthquake)											
Inter-story Stiffness Values											
	θ_1	θ_2	θ_3	θ_4	θ_5	θ_6	θ_7	θ_8	θ_9	θ_{10}	<i>Error Index</i> J
Model	(All stiffness values $\times 10^8 Nm^{-1}$)										
W-Opt (3p)											
(0-2.6 sec)	61.7	61.7	8.97	8.97	6.68	6.68	6.68	10.4	10.4	10.4	$15 \cdot 10^{-2}$
(2.6-5.1 sec)	61.7	61.7	9.82	9.82	7.14	7.14	7.14	8.86	8.86	8.86	$5.1 \cdot 10^{-2}$
(5.1-10 sec)	61.7	61.7	7.14	7.14	9.92	9.92	9.92	9.63	9.63	9.63	$4.6 \cdot 10^{-2}$
(10-20 sec)	61.7	61.7	6.98	6.98	9.84	9.84	9.84	12.2	12.2	12.2	$3.2 \cdot 10^{-2}$

Table 6.7: SUB-ID-Time three-parameter stiffness estimates obtained from the 1970 Lytle Creek earthquake records. The W-Opt. model corresponds to the mass distribution which optimized Wood's model with Teledyne's post-earthquake data. The basement and first floor stiffnesses were fixed at previously estimated value of $61.7 \cdot 10^8 Nm^{-1}$.

JPL Building 180, E-W Direction (1970 Lytle Creek Earthquake)							
Study	Time Window	Modal Frequency (Hz)			Modal Damping (% critical)		
		f_1	f_2	f_3	ξ_1	ξ_2	ξ_3
SUB-ID-Time (3p, W-Opt.)							
	(0-2.6 sec)	0.951	3.08	4.94	4.1	3.7	6.5
	(2.6-5.1 sec)	0.973	3.03	4.88	6.7	4.3	2.9
	(5.1-10 sec)	0.987	2.97	4.99	2.8	6.7	8.2
	(10-20 sec)	0.983	3.04	5.19	3.1	5.2	4.8
MODE-ID (3 modes)							
	(0-2.6 sec)	0.991	3.08	5.07	4.9	4.1	9.1
	(2.6-5.1 sec)	0.958	3.03	4.89	6.0	5.1	-0.2 (?)
	(5.1-10 sec)	0.965	3.05	5.20	3.1	6.0	6.9
	(10-20 sec)	1.01	3.20	5.47	3.4	9.6	4.9

Table 6.8: Comparison of time-windowed modal frequency and damping values.

JPL Building 180, E-W Direction (1971 San Fernando Earthquake)											
Model	Inter-story Stiffness Values										<i>Error Index J</i>
	θ_1	θ_2	θ_3	θ_4	θ_5	θ_6	θ_7	θ_8	θ_9	θ_{10}	
	(All stiffness values $\times 10^8 Nm^{-1}$)										
W-Opt (3p)											
(0-2.6 sec)	61.7	61.7	6.16	6.16	8.69	8.69	8.69	9.76	9.76	9.76	$8.9 \cdot 10^{-2}$
(2.6-5.1 sec)	61.7	61.7	6.21	6.21	8.06	8.06	8.06	7.20	7.20	7.20	$2.2 \cdot 10^{-2}$
(5.1-10 sec)	61.7	61.7	6.04	6.04	5.05	5.05	5.05	5.95	5.95	5.95	$6.2 \cdot 10^{-2}$
(10-20 sec)	61.7	61.7	5.76	5.76	5.02	5.02	5.02	5.19	5.19	5.19	$4.3 \cdot 10^{-3}$
(20-31 sec)	61.7	61.7	5.71	5.71	4.64	4.64	4.64	6.92	6.92	6.92	$1.0 \cdot 10^{-3}$
(31-41 sec)	61.7	61.7	6.00	6.00	4.72	4.72	4.72	7.19	7.19	7.19	$2.2 \cdot 10^{-3}$

Table 6.9: SUB-ID-Time three-parameter stiffness estimates obtained from the San Fernando earthquake base and roof records. The W-Opt. model corresponds to the mass distribution which optimized Wood's model with Teledyne's post-earthquake data. The basement and first floor stiffnesses were constrained to the previously estimated value of $61.7 \cdot 10^8 Nm^{-1}$.

JPL Building 180 (1971 San Fernando Earthquake)								
Study	Time Window	Modal Frequency (Hz)			Modal Damping (% critical)			
		f_1	f_2	f_3	ξ_1	ξ_2	ξ_3	
McVerry-Beck (2 modes)								
	(0-2.5 sec)	0.98	3.2	n/a	n/a	n/a	n/a	
	(0-5 sec)	0.84	2.6	n/a	3.3	2.9	n/a	
	(5-10 sec)	0.80	2.3	n/a	4.7	7.4	n/a	
	(10-20 sec)	0.78	2.4	n/a	3.4	4.5	n/a	
	(20-30 sec)	0.81	2.6	n/a	4.1	5.2	n/a	
SUB-ID-Time (3p, W-Opt.)								
	(0-2.6 sec)	0.927	2.95	5.00	0.92	4.4	9.9	
	(2.6-5.1 sec)	0.900	2.71	4.65	4.1	5.9	7.3	
	(5.1-10 sec)	0.802	2.48	4.06	4.7	5.9	9.9	
	(10-20 sec)	0.787	2.38	3.94	3.4	6.0	11	
	(20-31 sec)	0.785	2.38	3.97	3.4	6.8	10	
	(31-41 sec)	0.799	2.41	4.03	3.6	11	12	
MODE-ID (3 modes)								
	(0-2.6 sec)	0.935	2.94	4.86	4.5	7.1	26	
	(2.6-5.1 sec)	0.858	2.68	4.58	2.3	9.2	9.4	
	(5.1-10 sec)	0.782	2.43	4.05	3.9	6.8	11	
	(10-20 sec)	0.784	2.38	4.20	3.2	5.0	11	
	(20-31 sec)	0.788	2.48	4.28	3.8	6.3	6.2	
	(31-41 sec)	0.818	2.57	4.39	5.0	6.2	5.5	

Table 6.10: Comparison of time-windowed modal frequency and damping values.

JPL Building 180, E-W Direction (Teledyne's 1971 Data)											
Inter-story Stiffness Values											$\frac{Error}{Index J_M}$
θ_1	θ_2	θ_3	θ_4	θ_5	θ_6	θ_7	θ_8	θ_9	θ_{10}		
Model	(All stiffness values $\times 10^8 Nm^{-1}$)										
W-1(10p)	13.8	12.4	8.94	7.52	8.98	9.55	7.57	6.95	5.50	6.48	$9.8 \cdot 10^{-4}$
W-Opt(10p)	13.8	12.4	8.57	6.95	9.22	9.37	6.80	11.0	7.17	9.18	$4.9 \cdot 10^{-4}$

Table 6.11: SUB-ID-Modal parameter estimates corresponding to different models for 9/10 frequency and 1/10 mode-shape weights. Only the first three modes in Teledyne's data were used with the corresponding natural frequencies and mode-shape components for the top eight floors. The optimized model predicts a roof mass 2.04 times larger than the typical floor mass.

JPL Building 180, E-W Direction (Teledyne's 1971 Data)										
Inter-story Stiffness Values										
	θ_1	θ_2	θ_3	θ_4	θ_5	θ_6	θ_7	θ_8	θ_9	θ_{10}
Model	(All stiffness values $\times 10^8 Nm^{-1}$)									
W-1	22.8	42.4	2.79	3.77	6.12	6.04	6.16	3.89	3.07	4.54
W-Opt	33.9	61.8	3.91	5.24	8.56	8.36	8.49	5.14	5.01	8.66

Table 6.12: SUB-ID-SS parameter estimates corresponding to Teledyne's modal data (only three modes were employed). The first model assumes the original mass distribution while the second uses the SUB-ID-Modal optimized mass estimate.

JPL Building 180, E-W Direction (SUB-ID-Modal)										
Inter-story Stiffness Ratios										
	θ_1	θ_2	θ_3	θ_4	θ_5	θ_6	θ_7	θ_8	θ_9	θ_{10}
Model										
W/N -1	0.232	0.243	0.949	1.52	1.33	1.54	1.18	1.24	0.979	1.28
W/N -Opt	0.259	0.273	1.07	1.37	1.39	1.52	1.06	1.72	1.31	1.86

Table 6.13: Ratios of stiffnesses for each interstory level from results estimated by SUB-ID-Modal. The numerator corresponds to the stiffness level calculated after the San Fernando earthquake from Teledyne's data and the denominator corresponds to the stiffnesses derived from Nielsen's data prior to the earthquake.

JPL Building 180, E-W Direction (SUB-ID-SS)										
Inter-story Stiffness Ratios										
	θ_1	θ_2	θ_3	θ_4	θ_5	θ_6	θ_7	θ_8	θ_9	θ_{10}
Model										
W/N -1	n/a	n/a	0.757	0.893	0.986	1.08	1.04	0.663	0.534	0.903
W/N -Opt	n/a	n/a	1.04	1.23	1.37	1.49	1.44	0.893	0.901	1.813

Table 6.14: Ratios of stiffnesses for each interstory level from results estimated by SUB-ID-SS. The numerator corresponds to the stiffness level calculated after the San Fernando earthquake from Teledyne's data and the denominator corresponds to the stiffnesses derived from Nielsen's data prior to the earthquake. The lowest two stories were fixed when using Nielsen's data in order for the algorithm to converge.

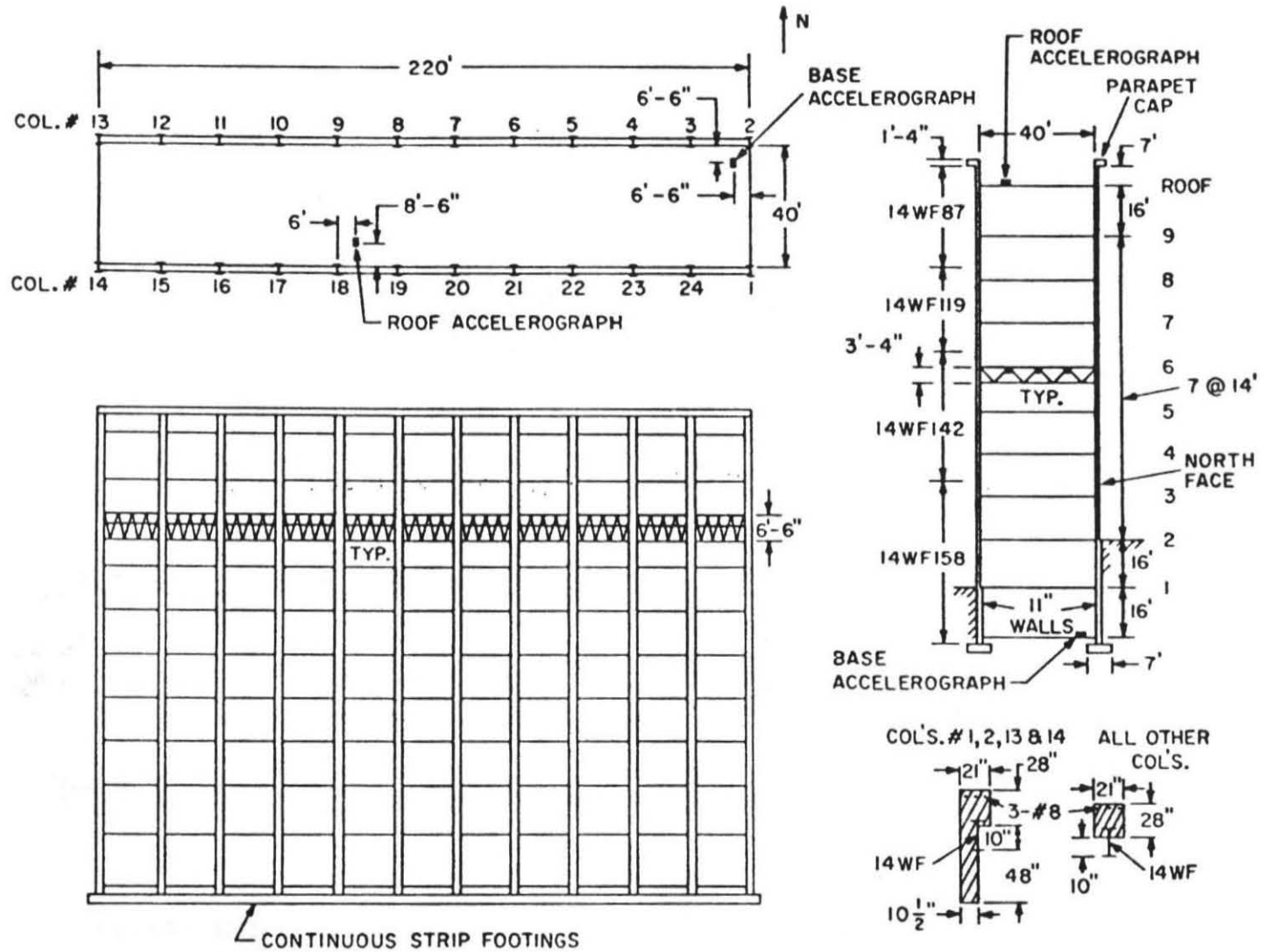


Figure 6.1: Schematic drawings of JPL Building 180 (taken from Nielsen [6.1]).

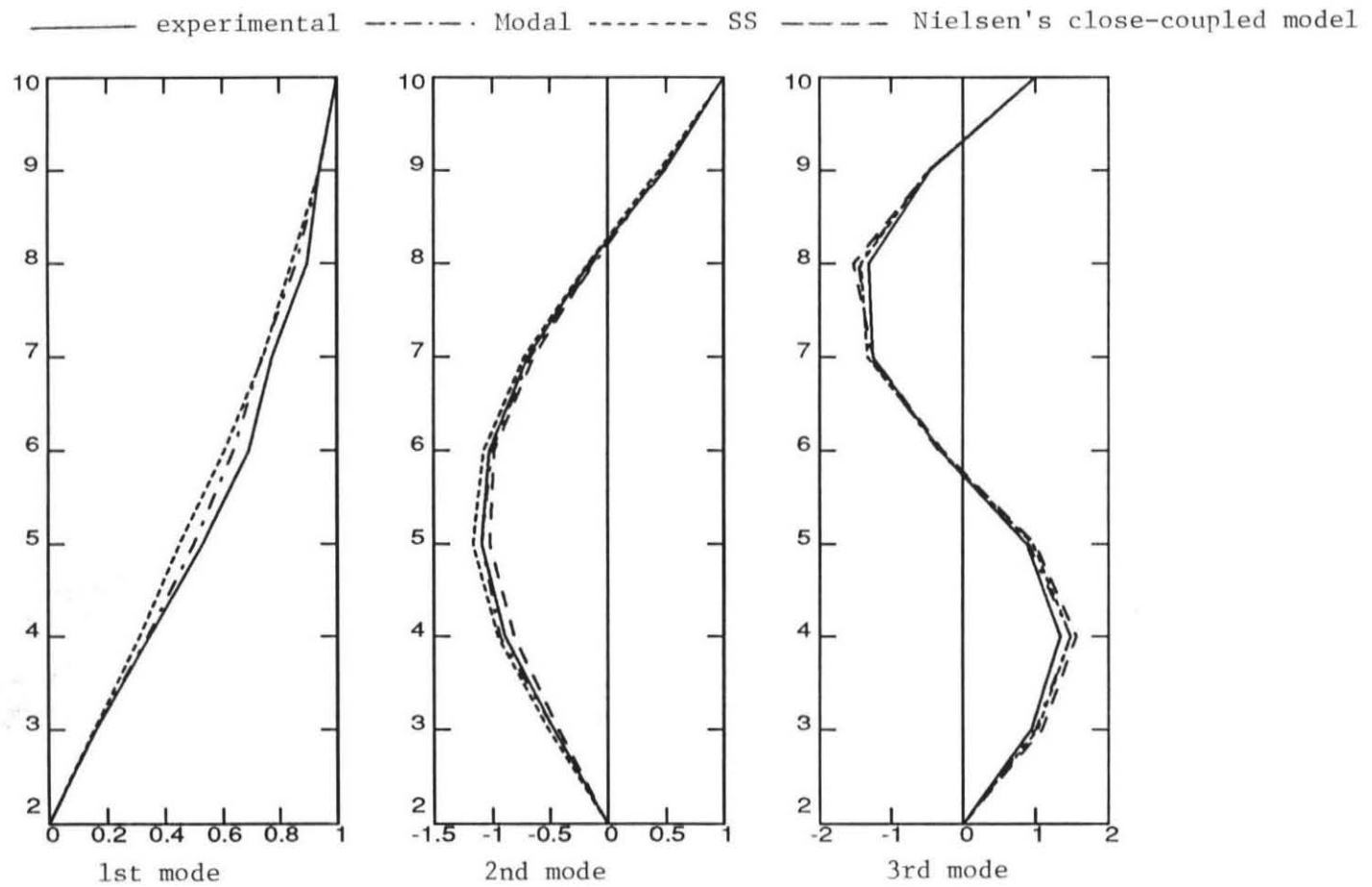
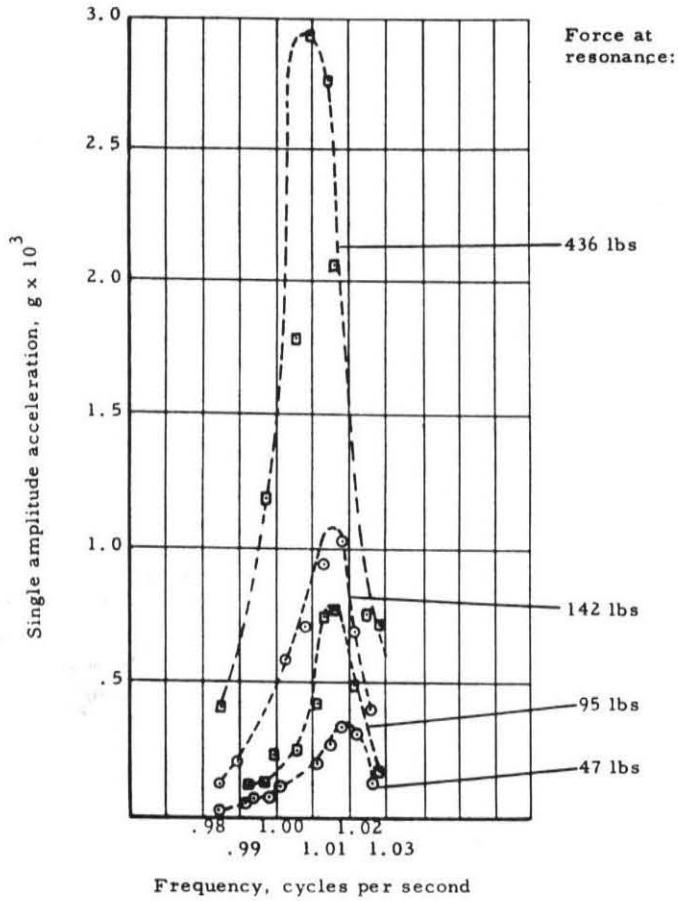
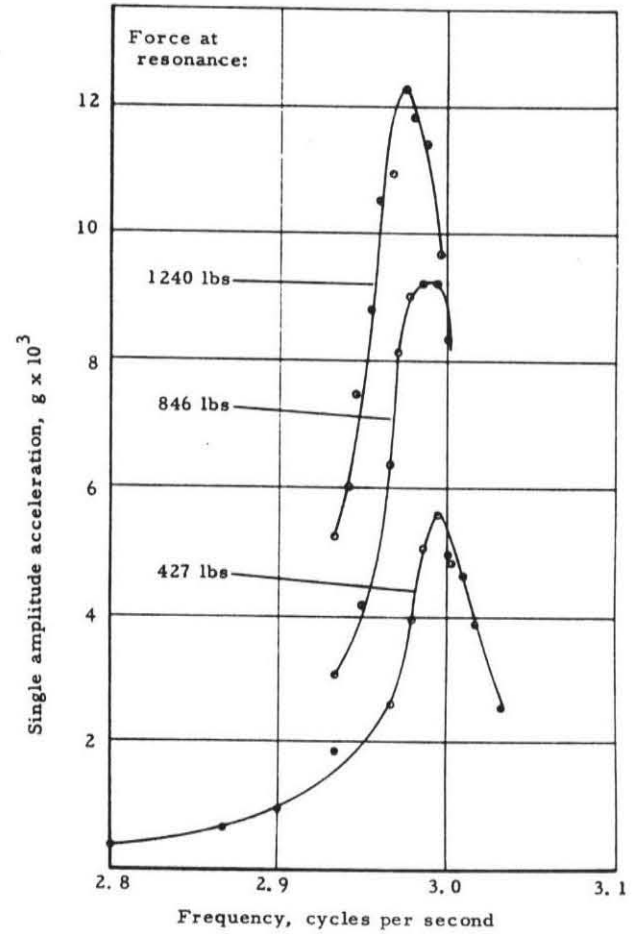


Figure 6.2: Modeshapes corresponding to the first three modes of JPL Building 180 determined from Nielsen's experimental data and various identified models (E-W direction).



(a) 5th FLOOR RESPONSE, LOWEST TRANSLATIONAL MODE (E-W), VIBRATION EXCITER A.



(b) 5th FLOOR RESPONSE, SECOND LOWEST TRANSLATIONAL MODE (E-W), VIBRATION EXCITER A.

Figure 6.3: Resonance curves for JPL Building 180 (from Nielsen[6.1]).

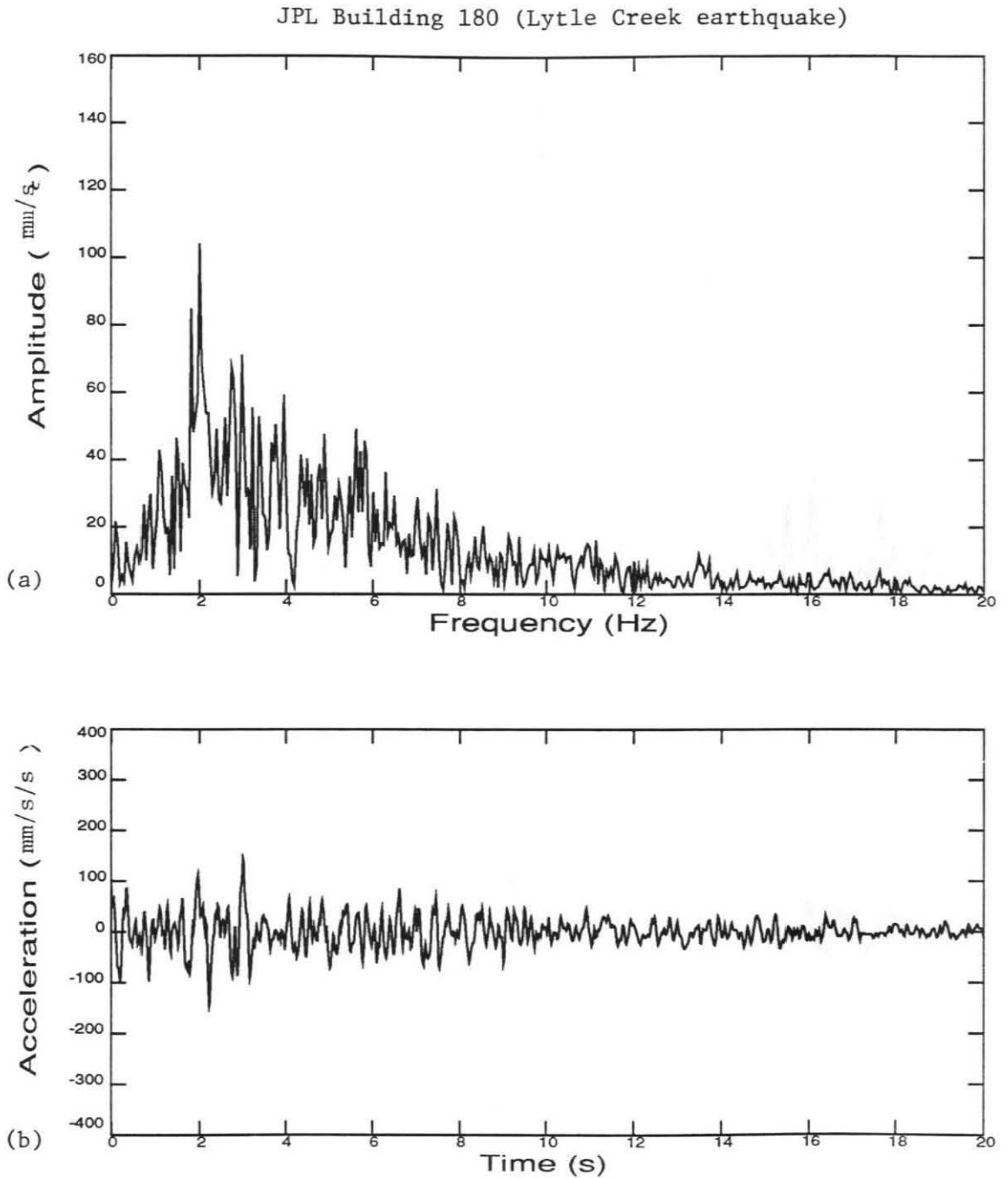


Figure 6.4: (a) Amplitude spectrum and (b) time history of the 1970 Lytle Creek earthquake accelerations at the base of JPL Building 180 (E-W direction).

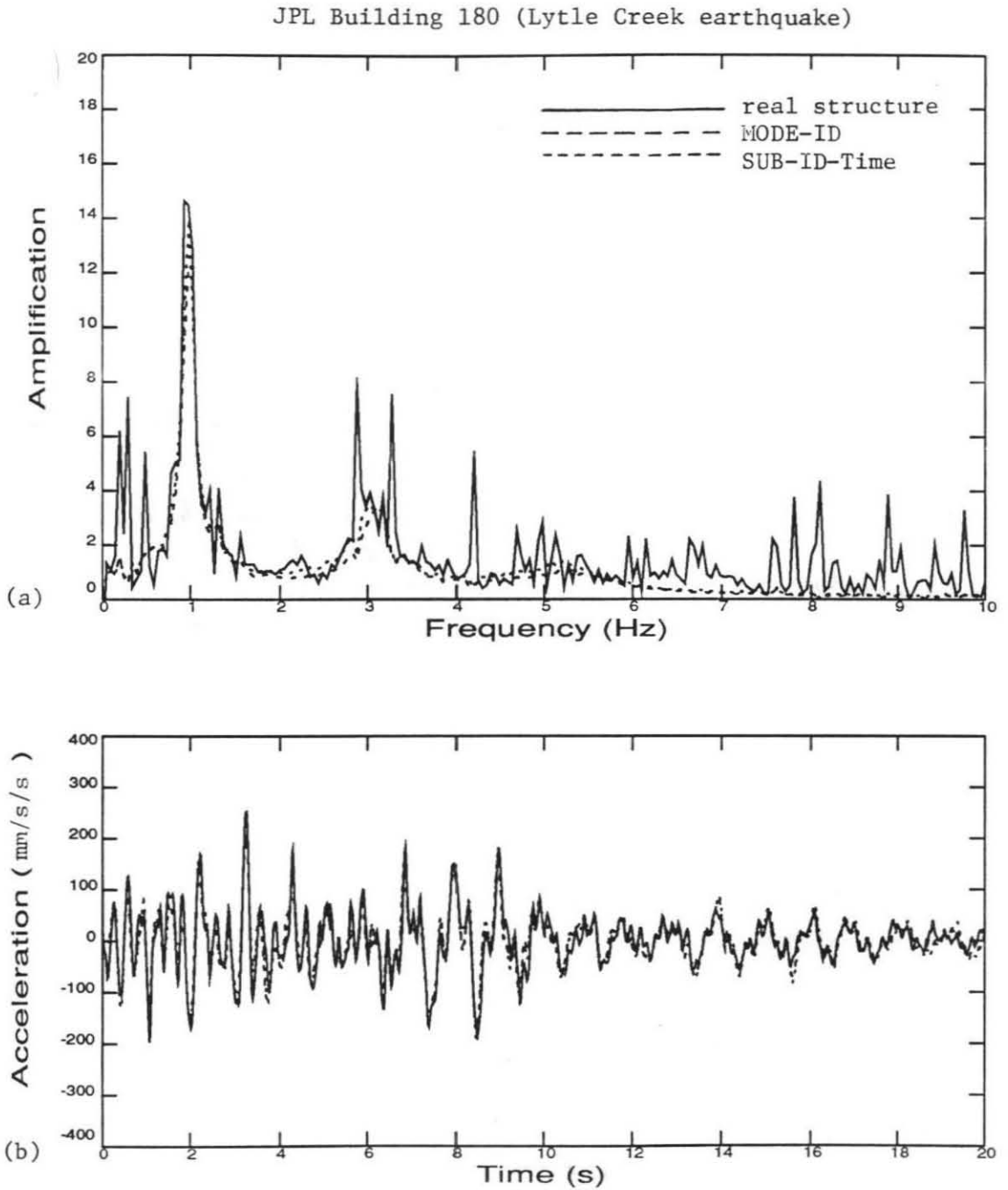


Figure 6.5: (a) Empirical transfer function between the 1970 Lytle Creek earthquake base motion and the roof response for JPL Building 180 (E-W direction), and for the MODE-ID and SUB-ID-Time predicted models; (b) match in the time domain.

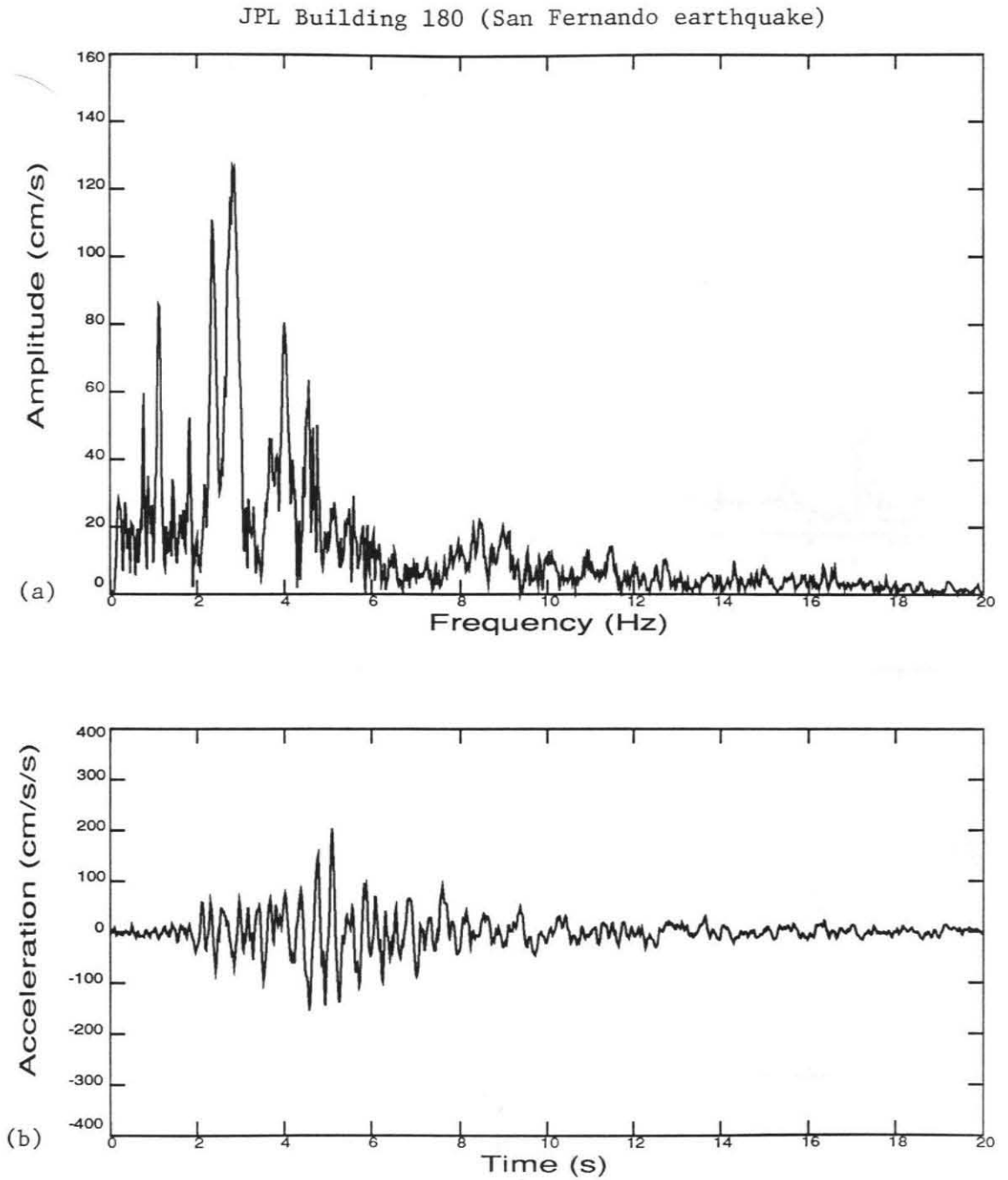


Figure 6.6: (a) Amplitude spectrum and (b) time history of the 1971 San Fernando earthquake accelerations at the base of JPL Building 180 (E-W direction).

JPL Building 180 (San Fernando earthquake)

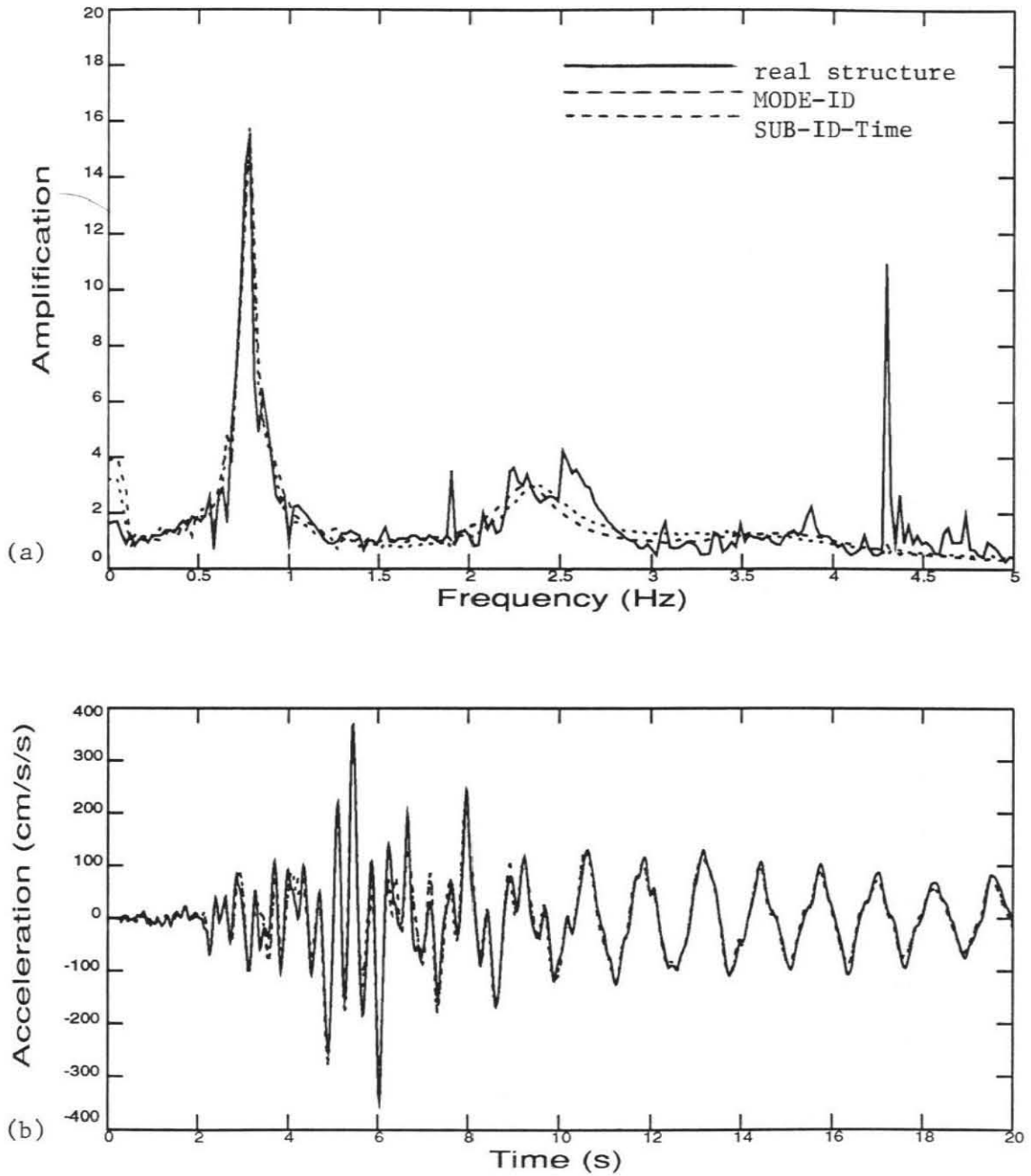


Figure 6.7: (a) Empirical transfer function between the 1971 San Fernando earthquake base motion and the roof response for JPL Building 180 (E-W direction), and for the MODE-ID and SUB-ID-Time predicted models; (b) match in the time domain.

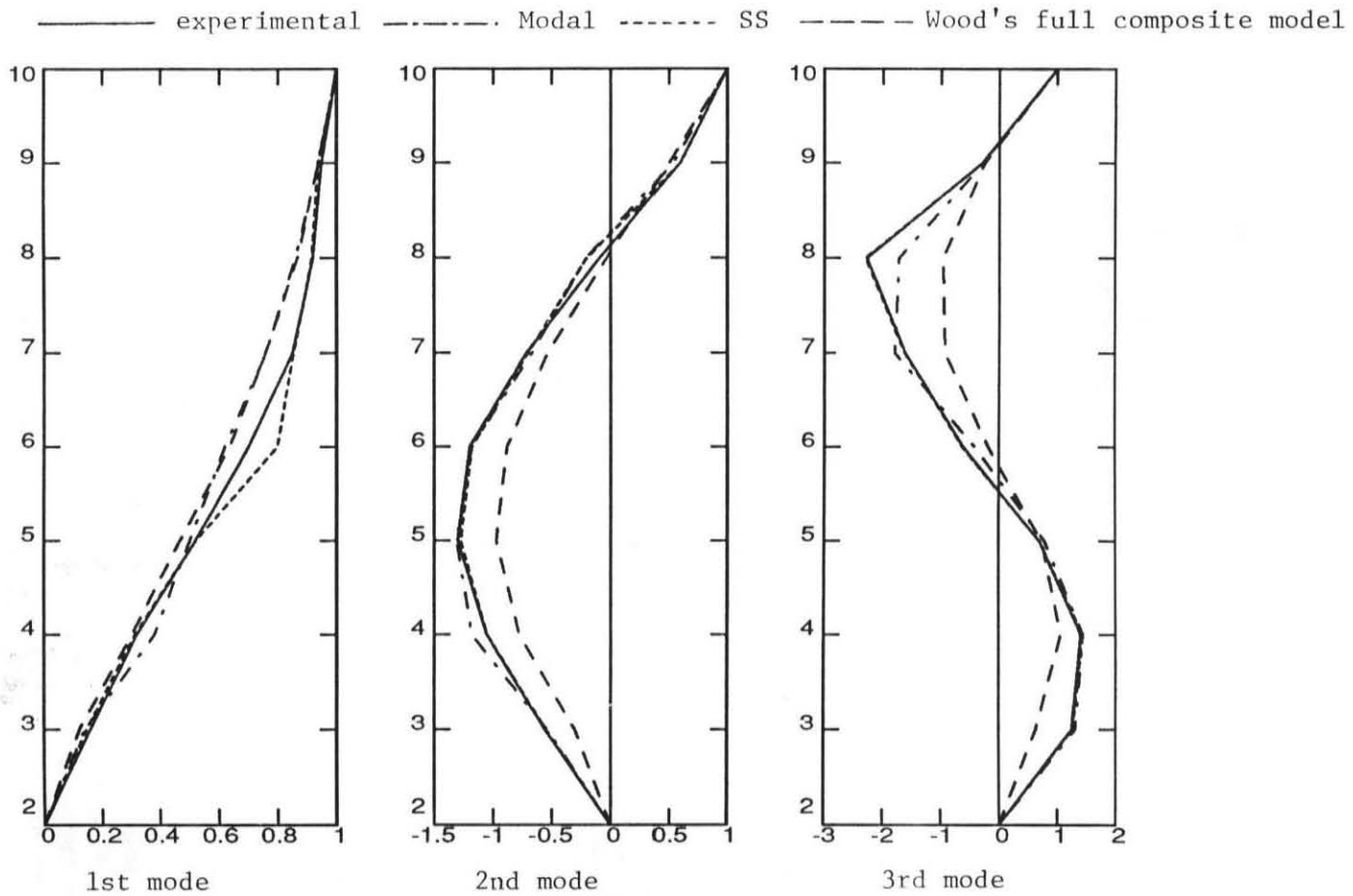


Figure 6.8: Modeshapes corresponding to the first three modes of JPL Building 180 determined from Teledyne's experimental data and various identified models (E-W direction).

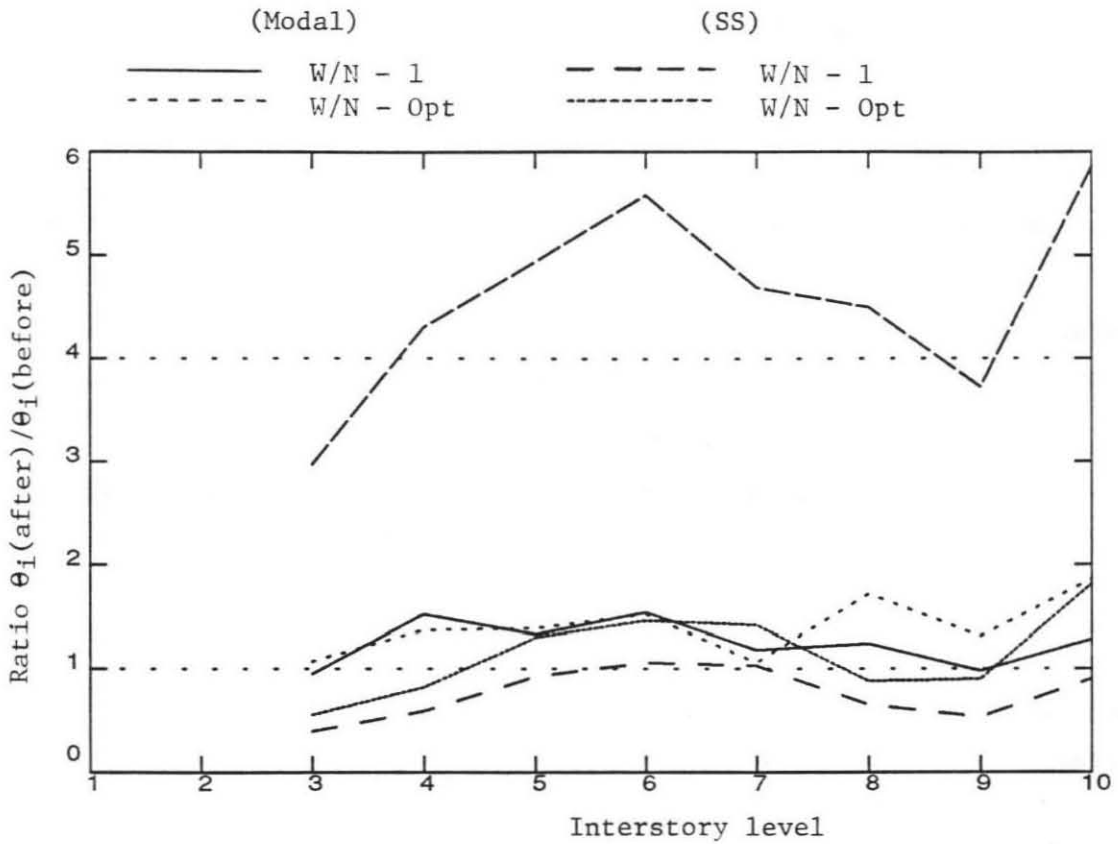


Figure 6.9: Stiffness distribution after calibration with prior-to-earthquake data as determined by the various techniques/models (Tables 6.13 and 6.14). The curve at the '4' ratio level represents the addition of all calibrated curves. This curve conveys an idea of the average stiffness distribution. The stiffness at the ninth floor level dips but it does not go much below the value determined from Nielsen's data, before the addition of the non-structural elements.

Chapter 7 : Discussion and Conclusions

Section 7.1 - Problems in Structural Identification

Both small and large structures present characteristics or “problems” which prevent the precise identification of a structural model. Problems in identification fall primarily into three areas:

(1) Experimentally-based problems: These problems relate to variations in the values of the signals attributable to errors in the measurements. Among these, three stand out as the most important: (1a) measurement noise, (1b) calibration error, and (1c) synchronization error. Measurement noise can induce ill-conditioning since modal information (such as that coming from higher modes) may not be recovered from the response signals, thus reducing the number of independent data significantly. Noise should virtually disappear when modern instrumentation is used. Calibration errors are the worst type of problems since they are almost impossible to detect from the records alone, although the instruments can be periodically re-calibrated. Changes in the amplitudes of the recorded signals influence all modes of vibration and can, in particular, alter the estimated modeshape values. Lack of synchronization among the signals alter the estimates more than any other error but with proper use of correlation procedures, these problems can be avoided almost entirely.

(2) Model-data interaction problems: These are problems in which both the amount of data available and the model chosen determine whether the estimates are reliable. The data is assumed to be clean data, i.e., data effectively free from experimental problems. Model-data interaction problems include two most important problems: (2a) ill-conditioning in the optimization process, and (2b) non-uniqueness in the parameter estimates. Ill-conditioning is present whenever the model response is not sensitive to the individual model parameters. A characteristic of ill-conditioning is the very slow convergence of the optimization procedure to a minimum. Often, the optimization algorithm prematurely converges to parameter estimates which predict modal parameters or time-histories close to those observed. To remedy this, more information should be obtained from the structural response. For most applications, it is also important to know whether there is uniqueness

in the parameter estimation. For example, is there a unique parameter vector producing the global minimum of the error index J in the output-error approach? Uniqueness requires a sufficiently parsimonious model relative to the amount and nature of the data available. The simplified structural model used in this work, involving the addition of sub-structure stiffness matrices scaled with stiffness factors, would benefit from the development of sufficient conditions for uniqueness, but this has proved to be a very challenging task.

(3) Model-based problems: These problems are related to choosing a model which can predict the observed behavior. Modeling from the point of view of this study includes both the discretization of the structure in terms of a finite number of degrees of freedom and also discretization of the structure in terms of sub-structures. The choice of the appropriate model is a difficult problem since there is generally a trade-off between the desired precision in resolving the stiffness distribution and the amount of computation time needed for the estimation algorithms to converge to a solution. Choosing a model with a small number of degrees of freedom which is not able to represent closely the observed response leads inevitably to parameter estimates which do not have direct physical interpretation and may give misleading conclusions. Refining the model usually requires increasing the number of degrees of freedom in the structure or rearranging the sub-structuring of the structure. Increasing the number of degrees of freedom by itself increases the computational time needed to calculate either the modal parameters or the response time histories. There is a remote possibility that overall optimization computational time may be reduced when the number of degrees of freedom is increased. It is possible, in other words, that the improved model and the data allow a faster convergence to a physically-acceptable solution. On the other hand, increasing the number of degrees of freedom in the model may not necessarily improve the model. The choice of sub-structures also affects the modeling since it does not allow the independent identification of the stiffness factors associated with *each* member in the structure. However, if a stiffness factor is assigned to each member, it is most likely that the estimation problem will suffer from excessive ill-conditioning or non-uniqueness. Non-uniqueness can be handled appropriately by the homotopy method but only for structures with a small number of degrees of freedom, at present.

When the modeling is incorrect, it is extremely difficult to determine whether the parameter estimates are in a close neighborhood of the "best" physical set of values. It is, indeed, difficult to determine if there is such a thing as a "best" set of values. Good linear structural models are those in which the parameter estimates yield error fits as good as the ones provided by *modal* parameter estimation algorithms, provided the latter are also accurate. Modal models generally provide the best fit that any linear model is capable of giving and should be considered as an important complementary tool in linear structural identification. Generally, if a modal identification algorithm can match the observed data very accurately, the structural identification algorithm should be able to do so too, if the model is appropriately chosen. Errors in the response match which are much larger than those for the modal identification suggest significant structural model error. If the

identified modal model does not perform adequately, then the assumptions made in its development should be reconsidered, e.g., are classical modes acceptable?, viscous damping?, linearity?, etc. Even in the case where the structural identification match is as good as the modal identification match, there can still be model error.

In the case where estimated parameter values are not physically reasonable, these can be constrained in the algorithm procedure by utilizing additional prior knowledge. For damage detection purposes, these types of constraints may not be conducive to an appropriate identification procedure. Constraining parameters influences the estimation of the other parameters since there is generally a trade-off among the parameters in order to retain similar modal properties. For example, to keep a certain modal frequency fixed, one can increase the value of one stiffness parameter while decreasing the values of others. From this example, it is conceivable that constraints on some parameters in the presence of model error may preclude the others from arriving at "damage level" values.

Full confidence in a model is gained only when the optimal set of parameters is unique, produces nearly perfect agreement with the abundant (if possible) observed data, and the parameter values agree with one's physical intuition. There are models, e.g., a chain model, which can accurately match the recorded response of a structure, e.g., a framed structure, and yield physically acceptable parameter estimates, but these estimates may provide the wrong information to the engineer. For example, they might imply a mass or stiffness distribution which is, in reality, incorrect. In general, and especially when suspect parameter estimates are obtained, the identification procedure should be repeated with each *subset* of observed data, separately and in groups. Correct models are more likely to give consistent results for each subset of data while incorrect models are more likely to predict different parameter estimates. The data should include as varied testing conditions as possible in order to make sure many modes of vibration are excited. The model can be used with more confidence if the estimates are consistent in all possible tests.

Section 7.2 - Rules of Thumb

Experience dictates the following steps should be taken for efficient damage detection of structures:

A) Prior to the use of real data:

(1) Choose two FE (or other) models: the first one should be a detailed model whose behavior is to be much closer to that of the real structure than that of the second model. The latter should also be discretized sufficiently well to allow for a representative behavior of the undamaged state of structure (if available) but its main characteristic is that it is computationally efficient for repeated evaluation in an output-error type code or for use with a homotopy technique. It is then important to

determine the maximum number of trustworthy modes that can be expected from the simple model (by comparison with the modal parameters derived from the complex model). Establish, if possible, a model for which the number of parameters is no more than the number of modes available, unless practically all modeshape information is available.

(2) "Calibrate" the simpler computational model with the simulated data employing the equivalent of SUB-ID-Time, SUB-ID-Modal and/or SUB-ID-SS.

(3) Study the ill-conditioning of the problem by performing a check of either the gradient of the J error index for the output-error approaches or the condition number for the successive substitutions algorithm. Add some noise to the simulated data, if the real data is expected to be highly contaminated. Add more modes (by refining the computational model first) or add/reallocate the sensors to reduce any ill-conditioning.

(3) Study non-uniqueness by using the equivalent of SUB-ID-SS, if possible. Otherwise, use SUB-ID-Homotopy if enough computational power is available. Otherwise, start the minimization runs from as many different points as the number of existing sub-structures. In each of the latter runs, start the minimization close to each of the axes, respectively, near the expected observed fundamental frequency. Increasing the number of modes or adding/reallocating the sensors, as mentioned above, should help remove non-uniqueness.

B) Using the real data:

(1) Determine which of the two, time-domain data or modal data, is to be used, or trusted.

(2) If in the time domain, (2a) synchronize the records and (2b) filter the data with a low-pass filter at a frequency above the one corresponding to the last trustworthy mode. Use other filters only if the causes of the noise or interference are well known. (2c) Employ data in the signals until the amplitude of the response decays significantly relative to the data in the large-motion segment (unless the expected values of the estimates are known).

(3) If in the modal domain, determine what weighting should be used according to the amount of data and according to the ultimate use of the data (other than damage detection?).

(4) Perform time-window analyses to check if the structure has undergone considerable non-linear behavior.

(5) Once some damage pattern has been established for a given structure from the available data, refine the model by sub-structuring the potentially damaged region(s). An increase in the number of parameters θ_i , needed for the refinement, should be prevented in order to avoid ill-conditioning and/or non-uniqueness. This can be accomplished by keeping, in the next optimization, the "stable" and "unstable" θ_i (those θ_i which did not change much or increased in the prior optimization,

respectively) fixed at the nominal values.

Section 7.3 - Future Research

For each of the methodologies presented in this study, a number of additions can improve upon what has been done here:

Additions to SUB-ID-Time - (1) Determine a method for finding, or at least bounding, all non-unique solutions within the parameter space. (2) Some attempts have been made to remove the banana valley in situations where ill-conditioning exists. This has been done by mathematically remapping the local topology to one in which the shallow valley is straightened out and made parallel to the transformed axes. In this way, the local topology has been converted to one where the convergence to the local minimum is attained efficiently by most optimization algorithms. (3) A formal measure of the flatness of the banana valleys by means of an evaluation of the gradient of J along the valley direction. In this way, ill-conditioning can be determined more precisely.

Additions to SUB-ID-Modal - (1) Introduce the participation factors into the formulation in the case where the modal identification program provides such information, as is the case for program MODE-ID.

Additions to SUB-ID-SS - (1) Recast the function $f(\theta)$ to prevent the repeated divergence which occurs in the current version whenever the modeshape information is incomplete.

Additions to SUB-ID-Homotopy - (1) Determine, early into the homotopy path, whether the end values will turn out complex (with large imaginary components). If so, then discard solution immediately. Solutions such that the imaginary component is small should be studied more closely since these might indicate that the current model is somewhat close to the system, and it might be reliable enough to detect damage zones. (2) Determine whether the algorithm can be partitioned adequately for implementation in a massively parallel computer (most likely so!).

Section 7.4 - Conclusions

Models with few parameters which possess a clear mechanical interpretation have allowed for more informative damage detection procedures than other more *ad hoc* approaches (such as those in which all components of the stiffness matrix are independently estimated). In the former, it is very likely that a configuration which provides unique parameter estimates can be found. In particular, the addition of the homotopy technique gives a novel method to completely determine all non-unique parameter distributions for the general structural identification problem.

Although methods such as the ones described above are computationally intensive, they can be implemented for use with simple structural models on small computers allowing for the continuous health monitoring of important structural systems. More efficient methods, however, should be developed to make the analysis of large, more complex models feasible. Before long, nevertheless, commercially available computational power will allow the use of the present set of algorithms for such cases.

In summary, experimental errors should be minimized, especially synchronization errors. Model-data interaction problems can be analyzed prior to using data from the experimental or real structure by studying simulated data where the exact parameter values are known. Yet it is clear from the foregoing how difficult it is to determine a model which is (a) computationally efficient, sufficiently refined to allow for (b) good response prediction and (c) damage detection without (d) non-uniqueness or ill-conditioning. Problems arising at this stage, such as non-uniqueness or ill-conditioning, may be resolved with the addition of more data or different placement of the sensors. In this way, better designs for the experimental set-up can be achieved.

Special attention must be paid to the modeling process so that the resulting model can be identifiable. Without a good identifiable model, the parameter estimates may be misleading. In limiting situations where a very simple model is used, however, the estimates may still provide enough information leading to the detection of general areas of damage. The results presented in this study are very encouraging although some efficiency-related difficulties remain.